



Full-Depth Precast Concrete Bridge Deck Panel Systems

DETAILS

115 pages | | PAPERBACK

ISBN 978-0-309-42078-5 | DOI 10.17226/23122

AUTHORS

BUY THIS BOOK

FIND RELATED TITLES

Visit the National Academies Press at NAP.edu and login or register to get:

- Access to free PDF downloads of thousands of scientific reports
- 10% off the price of print titles
- Email or social media notifications of new titles related to your interests
- Special offers and discounts



Distribution, posting, or copying of this PDF is strictly prohibited without written permission of the National Academies Press. (Request Permission) Unless otherwise indicated, all materials in this PDF are copyrighted by the National Academy of Sciences.

NCHRP REPORT 584

**Full-Depth Precast
Concrete Bridge
Deck Panel Systems**

Sameh S. Badie

THE GEORGE WASHINGTON UNIVERSITY
Washington, DC

AND

Maher K. Tadros

UNIVERSITY OF NEBRASKA—LINCOLN
Lincoln, Nebraska

Subject Areas

Bridges, Other Structures, and Hydraulics and Hydrology

Research sponsored by the American Association of State Highway and Transportation Officials
in cooperation with the Federal Highway Administration

TRANSPORTATION RESEARCH BOARD

WASHINGTON, D.C.

2008

www.TRB.org

NATIONAL COOPERATIVE HIGHWAY RESEARCH PROGRAM

Systematic, well-designed research provides the most effective approach to the solution of many problems facing highway administrators and engineers. Often, highway problems are of local interest and can best be studied by highway departments individually or in cooperation with their state universities and others. However, the accelerating growth of highway transportation develops increasingly complex problems of wide interest to highway authorities. These problems are best studied through a coordinated program of cooperative research.

In recognition of these needs, the highway administrators of the American Association of State Highway and Transportation Officials initiated in 1962 an objective national highway research program employing modern scientific techniques. This program is supported on a continuing basis by funds from participating member states of the Association and it receives the full cooperation and support of the Federal Highway Administration, United States Department of Transportation.

The Transportation Research Board of the National Academies was requested by the Association to administer the research program because of the Board's recognized objectivity and understanding of modern research practices. The Board is uniquely suited for this purpose as it maintains an extensive committee structure from which authorities on any highway transportation subject may be drawn; it possesses avenues of communications and cooperation with federal, state and local governmental agencies, universities, and industry; its relationship to the National Research Council is an insurance of objectivity; it maintains a full-time research correlation staff of specialists in highway transportation matters to bring the findings of research directly to those who are in a position to use them.

The program is developed on the basis of research needs identified by chief administrators of the highway and transportation departments and by committees of AASHTO. Each year, specific areas of research needs to be included in the program are proposed to the National Research Council and the Board by the American Association of State Highway and Transportation Officials. Research projects to fulfill these needs are defined by the Board, and qualified research agencies are selected from those that have submitted proposals. Administration and surveillance of research contracts are the responsibilities of the National Research Council and the Transportation Research Board.

The needs for highway research are many, and the National Cooperative Highway Research Program can make significant contributions to the solution of highway transportation problems of mutual concern to many responsible groups. The program, however, is intended to complement rather than to substitute for or duplicate other highway research programs.

NCHRP REPORT 584

Project 12-65
ISSN 0077-5614
ISBN 978-0-309-09914-1
Library of Congress Control Number 2007909932

© 2008 Transportation Research Board

COPYRIGHT PERMISSION

Authors herein are responsible for the authenticity of their materials and for obtaining written permissions from publishers or persons who own the copyright to any previously published or copyrighted material used herein.

Cooperative Research Programs (CRP) grants permission to reproduce material in this publication for classroom and not-for-profit purposes. Permission is given with the understanding that none of the material will be used to imply TRB, AASHTO, FAA, FHWA, FMCSA, FTA, or Transit Development Corporation endorsement of a particular product, method, or practice. It is expected that those reproducing the material in this document for educational and not-for-profit uses will give appropriate acknowledgment of the source of any reprinted or reproduced material. For other uses of the material, request permission from CRP.

NOTICE

The project that is the subject of this report was a part of the National Cooperative Highway Research Program conducted by the Transportation Research Board with the approval of the Governing Board of the National Research Council. Such approval reflects the Governing Board's judgment that the program concerned is of national importance and appropriate with respect to both the purposes and resources of the National Research Council.

The members of the technical committee selected to monitor this project and to review this report were chosen for recognized scholarly competence and with due consideration for the balance of disciplines appropriate to the project. The opinions and conclusions expressed or implied are those of the research agency that performed the research, and, while they have been accepted as appropriate by the technical committee, they are not necessarily those of the Transportation Research Board, the National Research Council, the American Association of State Highway and Transportation Officials, or the Federal Highway Administration, U.S. Department of Transportation.

Each report is reviewed and accepted for publication by the technical committee according to procedures established and monitored by the Transportation Research Board Executive Committee and the Governing Board of the National Research Council.

The Transportation Research Board of the National Academies, the National Research Council, the Federal Highway Administration, the American Association of State Highway and Transportation Officials, and the individual states participating in the National Cooperative Highway Research Program do not endorse products or manufacturers. Trade or manufacturers' names appear herein solely because they are considered essential to the object of this report.

Published reports of the

NATIONAL COOPERATIVE HIGHWAY RESEARCH PROGRAM

are available from:

Transportation Research Board
Business Office
500 Fifth Street, NW
Washington, DC 20001

and can be ordered through the Internet at:

<http://www.national-academies.org/trb/bookstore>

Printed in the United States of America

THE NATIONAL ACADEMIES

Advisers to the Nation on Science, Engineering, and Medicine

The **National Academy of Sciences** is a private, nonprofit, self-perpetuating society of distinguished scholars engaged in scientific and engineering research, dedicated to the furtherance of science and technology and to their use for the general welfare. On the authority of the charter granted to it by the Congress in 1863, the Academy has a mandate that requires it to advise the federal government on scientific and technical matters. Dr. Ralph J. Cicerone is president of the National Academy of Sciences.

The **National Academy of Engineering** was established in 1964, under the charter of the National Academy of Sciences, as a parallel organization of outstanding engineers. It is autonomous in its administration and in the selection of its members, sharing with the National Academy of Sciences the responsibility for advising the federal government. The National Academy of Engineering also sponsors engineering programs aimed at meeting national needs, encourages education and research, and recognizes the superior achievements of engineers. Dr. Charles M. Vest is president of the National Academy of Engineering.

The **Institute of Medicine** was established in 1970 by the National Academy of Sciences to secure the services of eminent members of appropriate professions in the examination of policy matters pertaining to the health of the public. The Institute acts under the responsibility given to the National Academy of Sciences by its congressional charter to be an adviser to the federal government and, on its own initiative, to identify issues of medical care, research, and education. Dr. Harvey V. Fineberg is president of the Institute of Medicine.

The **National Research Council** was organized by the National Academy of Sciences in 1916 to associate the broad community of science and technology with the Academy's purposes of furthering knowledge and advising the federal government. Functioning in accordance with general policies determined by the Academy, the Council has become the principal operating agency of both the National Academy of Sciences and the National Academy of Engineering in providing services to the government, the public, and the scientific and engineering communities. The Council is administered jointly by both the Academies and the Institute of Medicine. Dr. Ralph J. Cicerone and Dr. Charles M. Vest are chair and vice chair, respectively, of the National Research Council.

The **Transportation Research Board** is one of six major divisions of the National Research Council. The mission of the Transportation Research Board is to provide leadership in transportation innovation and progress through research and information exchange, conducted within a setting that is objective, interdisciplinary, and multimodal. The Board's varied activities annually engage about 7,000 engineers, scientists, and other transportation researchers and practitioners from the public and private sectors and academia, all of whom contribute their expertise in the public interest. The program is supported by state transportation departments, federal agencies including the component administrations of the U.S. Department of Transportation, and other organizations and individuals interested in the development of transportation. www.TRB.org

www.national-academies.org

COOPERATIVE RESEARCH PROGRAMS

CRP STAFF FOR NCHRP REPORT 584

Christopher W. Jenks, *Director, Cooperative Research Programs*
Crawford F. Jencks, *Deputy Director, Cooperative Research Programs*
David B. Beal, *Senior Program Officer*
Eileen P. Delaney, *Director of Publications*

NCHRP PROJECT 12-65 **Field of Design—Area of Bridges**

Michael M. Sprinkel, *Virginia DOT, Charlottesville, VA (Chair)*
Michael D. Hyzak, *Texas DOT, Austin, TX*
Ted L. Barber, *New Mexico DOT, Santa Fe, NM*
Shrinivas B. Bhide, *LEAP Software, Inc., Tampa, FL*
Kishor Doshi, *STV Incorporated, New York, NY*
Mark A. Gaines, *Washington State DOT, Olympia, WA*
Majid Madani, *California DOT, Sacramento, CA*
A. Osimboni, *Rhode Island DOT, Providence, RI*
Peter Smith, *Fort Miller Co., Inc., Schuylerville, NY*
Benjamin Graybeal, *FHWA Liaison*
Joey Hartmann, *FHWA Liaison*
Frederick Hejl, *TRB Liaison*

AUTHOR ACKNOWLEDGMENTS

The research reported herein was performed by the Civil and Environmental Engineering Department, The George Washington University, Washington DC; Tadros Associates, LLC, Omaha, Neb.; and the Department of Civil Engineering, University of Nebraska-Lincoln. The George Washington University was the contractor for this study. The work undertaken at Tadros Associates, LLC, and the University of Nebraska-Lincoln was under individual subcontracts with The George Washington University.

Sameh S. Badie, Assistant Professor of Civil Engineering, Civil and Environmental Engineering Department, The George Washington University, was the principal investigator. Coauthors of this report are Maher K. Tadros, The Charles J. Vranek Distinguished Professor of Civil Engineering, and Amgad F. Girgis, Research Assistant Professor, Department of Civil Engineering, University of Nebraska-Lincoln.

The following individuals provided assistance during various phases of the project: Walter Mesia, Nghi Nguyen, Parul Patel, and Krissachai Sriboonma, graduate research students at The George Washington University; Karen A. Bexten, Senior Engineer and partner of Tadros Associates, LLC; and Carlos Encarnacion and Yuri V. Jukarev, graduate research students, and Kelvin J. Lein, Senior Laboratory Technician, at the University of Nebraska-Lincoln.

FOREWORD

By **David B. Beal**

Staff Officer

Transportation Research Board

This report provides recommended guidelines and AASHTO load and resistance factor design (LRFD) specifications language for design, fabrication, and construction of full-depth precast concrete bridge deck panel systems. Durable and rapidly constructed connections between panels were also developed as part of this research. The report details the development of the guidelines, connection details, and recommended specifications. The material in this report will be of immediate interest to bridge designers.

The impact of highway construction projects on the public is considerable. Increased travel times resulting from congested construction work zones and the resultant degradation in traffic safety are the most readily apparent consequences. Development of a totally precast bridge construction system offers one means of significantly reducing construction time, because forming, casting, and curing operations can be carried out at a remote location with less on-site impact on motorists. Considerable time can be saved on bridge construction projects through the use of precast bent caps, columns, parapets, abutments, and other components.

Development of a full-depth precast concrete bridge deck panel system with a ride quality suitable for high-speed, direct traffic contact would be a major achievement, complementing work being done elsewhere in developing a totally precast bridge construction system. Previous research has resulted in implementation of posttensioned and overlaid systems for connection durability and ride quality. Issues that have been addressed include panel casting and placement tolerances, shear connections, vertical alignment, final grade adjustment, drainage, and parapet connections.

The objectives of this research were to develop recommended guidelines and AASHTO LRFD specifications language for design, fabrication, and construction of full-depth precast concrete bridge deck panel systems and to develop durable and rapidly constructed connections between panels. To reduce total deck construction time, full-depth precast concrete bridge deck panels that provide connection durability and ride quality without the use of posttensioning and overlays were developed. Connections suitable for simple and continuous spans and composite and noncomposite design were also developed and other connection details that reduce construction time associated with precast decks were investigated. In addition, applications for steel and prestressed concrete superstructures were investigated and research to extend the 24 in. maximum shear connector spacing to 48 in. was performed.

This research was performed by The George Washington University, the University of Nebraska-Lincoln, and Tadros Associates, LLC. The report fully documents the research leading to the recommended design, fabrication, and construction guidelines; specification language; and connection details. The appendices, available on the TRB website (<http://www.trb.org/TRBNet/ProjectDisplay.asp?ProjectID=354>), contain the recommended guidelines and proposed revisions to LRFD specifications language.

CONTENTS

1	Summary
3	Chapter 1 Introduction
3	Problem Statement
3	Objective and Scope of the Research
4	Research Approach
4	Organization of the Report
4	Applicability of the Results to Highway Practice
5	Chapter 2 Background and Literature Review
5	Panel to Superstructure Connection
7	Transverse Panel to Panel Connection
10	Longitudinal Reinforcement
12	Grout Material
14	History of the Shear Connector Spacing Limits of the AASHTO LRFD Design Specifications
15	Summary of the Literature Review
17	Chapter 3 Research Results
17	Recommended Full-Depth Precast Concrete Bridge Deck Panel Systems
28	Panel to Panel Connection
53	Panel to Concrete Girder Connection
61	Panel to Steel Girder Connection
105	Guidelines for Design, Detailing, Fabrication, and Installation of Full-Depth, Precast Concrete Deck Panel Systems
105	Proposed Revisions to AASHTO LRFD Specifications
106	Chapter 4 Conclusions, Recommendations, and Suggested Future Research
106	Conclusions and Recommendations
107	Suggestions for Future Research
108	References
110	Appendices

S U M M A R Y

Full-Depth Precast Concrete Bridge Deck Panel Systems

Highway construction projects have considerable impact on the public. The most obvious consequences are longer travel times and an increased risk of traffic collisions. Cast-in-place (CIP) bridge deck slabs represent a significant part of construction and rehabilitation schedules for stringer-type bridge superstructures because much of the construction time is consumed in forming, placing, and tying the steel reinforcement, as well as placing and curing the CIP concrete. To shorten the construction time, full-depth precast concrete deck panel systems have increasingly been used to replace CIP decks.

Full-depth precast panel systems have many other advantages in addition to shorter construction times, including high-quality plant production under tight tolerances, low permeability, less variation in volume caused by shrinkage and temperature changes during initial curing, and lower maintenance costs.

Full-depth precast panel systems with no overlays or longitudinal posttensioning are particularly attractive for two reasons. First, eliminating overlays helps get the bridge opened to traffic faster, especially on a deck replacement project, because CIP concrete is needed only at the joints between the prefabricated panels. Rapid-set concrete mixes, which do not require skilled concrete placement and finishing workers, can be used for those joints. Second, eliminating field posttensioning shortens the construction schedule, lowers the cost of the deck, and simplifies the process of partial deck placement and replacement.

The objectives of this project were to develop (a) recommended guidelines for the design, fabrication, and construction of full-depth precast concrete bridge deck panel systems without the use of posttensioning or overlays and (b) connection details for new deck panel systems. To achieve those objectives, the researchers

- Conducted a comprehensive literature review,
- Conducted a national survey of highway and design engineers,
- Developed new details for panel-to-panel and panel-to-superstructure joints, and
- Conducted an experimental and analytical investigation to validate these new connection details.

The outcomes of the research can be summarized as follows:

1. Comprehensive literature review: Information on bridge projects built with full-depth precast concrete panel systems was collected, reviewed, and summarized. For each project, the summary provides information on grouting materials, shear key details, panel-to-panel connections, panel-to-superstructure connections, design, reinforcement details, fabrication, installation of the deck panel system, and other critical issues.

2. Summary of results of the national survey: The national survey helped the researchers document specifications and policies developed by highway agencies that have used full-depth precast panel systems. The material collected from the national survey was instrumental in developing the language for the guidelines and the load and resistance factor design (LRFD) specifications.
 3. Guidelines: Recommended guidelines were developed for design, detailing, fabrication, installation, and construction. The guidelines were developed to promote the use of full-depth precast panel systems among design engineers and highway agencies.
 4. LRFD bridge design specifications language: Proposed LRFD specifications were developed for design, fabrication, installation, and construction. These proposed specifications are intended to replace Article 9.7.5 of the 3rd edition of the *AASHTO LRFD Bridge Design Specifications*.
 5. New connection details:
 - Panel-to-panel connection details: Two panel-to-panel connection details were developed that allowed the longitudinal reinforcing bars to be spliced and the bar yield strength to be fully developed, while minimizing the required embedment length. This was achieved using a new confinement technique.
 - Panel to concrete girder connection detail: A new panel to concrete girder connection detail was developed using a cluster of three 1¼ in. (31.8 mm) studs embedded in the top flange of the concrete girder. The new detail solves the mismatching problem currently encountered between the vertical shear reinforcement of the girder and the shear pockets of the precast panels.
 - Panel to steel girder connection detail: A new panel to steel girder connection detail was developed using 1¼ in. (31.8 mm) studs. The studs are clustered in groups spaced 48 in. (1220 mm) apart. The proposed 48 in. (1220 mm) spacing between clusters exceeds the 24 in. (610 mm) limit in the LRFD specifications.
 6. New full-depth precast concrete deck systems: The new connection details were used to develop two full-depth precast concrete deck systems. The first system is transversely pretensioned, and the second system is transversely conventionally reinforced. Neither system uses overlays or longitudinal posttensioning. These systems can be used for new construction projects or deck replacement projects. Step-by-step design calculations were developed for the first system to educate design engineers on how to best handle issues they may encounter when using full-depth precast concrete deck panel systems.
 7. Experimental and analytical investigation of the new connection details and full-depth precast concrete deck systems: A comprehensive experimental and analytical study was conducted to validate and check the structural behavior of the new connection details and full-depth precast concrete deck systems.
-

CHAPTER 1

Introduction

Problem Statement

Highway construction projects have considerable impact on the public. The most apparent consequences are increased travel times in congested work zones and a degradation in traffic safety. Field assembly of prefabricated bridge systems offers one means of significantly reducing construction time. Bridge elements that can be made of precast portland cement concrete include girders, deck panels, pier columns, pier caps, abutments, and railing systems.

Previous research led to the use of posttensioning and overlays as means of providing connection durability and ride quality (1-6). Issues that have been addressed include panel fabrication and placement tolerances, shear connections, vertical alignment, final grade adjustment, drainage, and parapet connections. A significant body of data is available for development of a guide specification for the design, fabrication, and construction of posttensioned and overlaid full-depth, precast concrete bridge deck systems. Development of a full-depth precast concrete bridge deck panel system that did not require a cast-in-place (CIP) overlay and that had a ride quality suitable for high-speed traffic would be a significant step toward a totally prefabricated bridge construction system. Elimination of deck panel system posttensioning would also mean fewer traffic delays and less reliance on specialty subcontractors.

Objective and Scope of the Research

The objectives of this project were to develop (a) recommended guidelines for the design, fabrication, and construction of full-depth precast concrete bridge deck panel systems without the use of posttensioning or overlays and (b) connection details for new deck panel systems. To accomplish those objectives, six tasks were performed.

Task 1—Relevant literature on bridge projects built with full-depth precast concrete panel systems was collected, reviewed,

and summarized. Information on issues related to these systems, such as grouting materials, shear key details, and connections between precast panels and superstructure, was collected and studied. In addition, relevant practice and other information related to the design, fabrication, and installation of full-depth precast concrete bridge deck panel systems was collected and studied.

Task 2—A survey was prepared and sent to bridge engineers in departments of transportation (DOTs) in the United States and Canada, as well as consulting firms, precast concrete producers, and members of the Precast/Prestressed Concrete Institute (PCI) Committee on Bridges and the TRB Concrete Bridges Committee.

Task 3—Connection details for full-depth precast concrete deck systems, which can be used with steel and prestressed concrete girders, were developed and evaluated experimentally. These details satisfy the following conditions: high durability, fast construction time, good ride quality, and high structural performance. The focus centered on deck systems that needed no longitudinal posttensioning or overlay. The connection details (panel to panel and panel to superstructure) were used to develop two precast deck systems. The first system is transversely pretensioned, and the second system is conventionally reinforced. Both systems are conventionally reinforced in the longitudinal direction, and neither uses an overlay.

Task 4—A detailed experimental research plan, which included pullout specimens, push-off specimens, a full-scale bridge specimen, and two full-scale beam specimens, was developed and conducted to evaluate the structural performance, capacity, and constructability of the connection details.

Task 5—Guidelines for the design, detailing, fabrication, and construction of full-depth precast concrete bridge deck panel systems were developed.

Task 6—Specification language and commentary necessary to implement full-depth precast concrete bridge deck panel systems were developed for the *AASHTO LRFD Bridge Design Specifications* (7).

Research Approach

Various types of full-depth precast concrete bridge panel systems have been developed and used during the past 50 years. The majority of these systems use longitudinal posttensioning and overlays.

Longitudinal posttensioning is typically used to put the panel to panel connection in compression to prevent water leakage and to provide the longitudinal reinforcement required for distribution of live loads. Posttensioning may, however, increase the cost of the deck construction, especially if it means bringing in a qualified subcontractor. Also, a lack of practical quality control procedures related to splicing and grouting the posttensioning ducts may lead to corrosion of the longitudinal posttensioning reinforcement, which could jeopardize its functionality. Because of these concerns, many DOTs have stopped using full-depth precast concrete deck panel systems on bridges.

Overlays on precast concrete deck systems provide added corrosion protection of the deck reinforcement and hide any differences in color between the precast panels and the grouted areas, such as the shear pockets and panel-to-panel joints. Overlays also provide a smooth riding surface. Adding an overlay, however, slows construction time and raises costs.

To encourage bridge designers to use precast concrete deck systems, this project took the following approach:

1. The connection details and the proposed systems satisfy the following conditions:
 - They do not use longitudinal posttensioning.
 - They do not use any proprietary products.
 - The precast panels can be fabricated off the construction site or at a precast yard.
 - The grouted areas are minimized and kept as hidden as possible.
 - No overlay is required.
2. Guidelines for design, detailing, fabrication, and installation were developed.
3. Specification language for the *AASHTO LRFD Bridge Design Specifications* was developed (7).

Organization of the Report

Chapter 1 provides the introduction and research approach and describes the problem statement and research objectives.

Chapter 2 summarizes the findings of the literature review and the national survey related to full-depth precast concrete bridge deck systems, panel to panel and panel to superstructure connection details, and the grouting materials used with these systems.

Chapter 3 provides (a) details of two proposed full-depth precast concrete deck panel systems, where new details of panel to panel and panel to girder connections were developed and used; (b) details of the experimental program used to test for the structural performance and constructability of the developed connection details; (c) design, fabrication, and installation guidelines; and (d) language for the *AASHTO LRFD Bridge Design Specifications* related to design, fabrication, and installation of full-depth precast concrete deck systems (7, 8).

Chapter 4 summarizes the significant conclusions of this project and provides suggestions for future research.

The appendices are not published herein but are available on the TRB website (<http://www.trb.org/TRBNet/ProjectDisplay.asp?ProjectID=354>). Appendix A provides a summary of the information collected from the national survey and literature review. Appendix B provides the design calculations of the proposed full-depth precast concrete bridge deck system CD-1. Appendix C provides proposed guidelines for design, detailing, fabrication, and installation of full-depth precast concrete bridge deck panels. Appendix D provides proposed revisions to Section 9 of the *AASHTO LRFD Bridge Design Specifications*. Appendix E provides information on the specifications of selected commercial grout material. Appendix F provides information on the finite element analysis conducted for the new panel to girder connection details.

Applicability of the Results to Highway Practice

The project was structured to provide design and details that can be directly implemented on highway bridges designed in accordance with the *AASHTO LRFD* specifications. The design, fabrication, and installation guidelines presented in Chapter 3 and in Appendix C of this report can be used by designers in various steps of project design, such as preliminary and final design, production shop detailing, production and installation, and quality control.

Several items presented in Chapter 3 of this report are intended for possible inclusion in the *AASHTO LRFD Bridge Design Specifications*.

CHAPTER 2

Background and Literature Review

The use of full-depth precast concrete deck panels in highway bridges in the United States started as early as 1965. The motive for switching to this construction system was a desire to shorten deck construction time in rehabilitation projects in areas with high traffic volumes, where road closures have high costs and cause major inconvenience to the public. Since then, design engineers have realized that there are significant advantages to this construction system not only for rehabilitation projects, but also for new construction, due to the relatively fast construction speed and because the higher quality of precast decks reduces maintenance costs and increases service life.

This chapter summarizes the information gleaned from a review of the literature and a national survey. The survey was sent to highway agencies in the United States and Canada and to members of the PCI Committee on Bridges and the TRB Concrete Bridges Committee. The goal of this summary is not to report on all of the bridges built with full-depth precast panels, but to show the diversity of the connections between panels and between panels and superstructure. The survey and results are provided in Appendix A, which also provides information collected from the literature review.

Several bridges were constructed using full-depth precast panels prior to 1973 (9, 10). Among them were the Pintala Creek Bridge, Montgomery County, Alabama; the Kosciuszko Bridge, Brooklyn–Queens Expressway, New York; the Big Blue River Bridge, Kingstown, Indiana; and the Bean Blossom Creek Bridge, Bloomington, Indiana. Biswas reports that these structures have generally performed well; however, some structures have exhibited partial failures at panel to panel joints (10). These bridges have the following common features: (a) the deck-girder systems are primarily noncomposite, (b) the spans do not have skewers or superelevations, (c) most projects involved new construction rather than rehabilitation, (d) fewer geometric fit-up problems have been experienced with new construction than with replacement decks, and (e) a full-depth precast panel deck system was used for both temporary and permanent bridges.

Since 1974, significant advances have been made in the construction of bridge decks built with full-depth precast concrete deck panels. The following sections provide information on the connection details and grout material used in these bridges. More information can be found in Appendix A and in reports by Anderson and others (9–26).

Panel to Superstructure Connection

Most of the bridges built during this period were made composite with the superstructure. This was achieved by extending steel shear studs or structural steel channels into the precast deck through prefabricated pockets. The spacing between pockets ranged from 18 in. to 24 in. (457 to 610 mm), and the number of studs per pocket ranged from 4 to 12. In some cases, one stud per row was used, as in the three-span bridge over the Delaware River between Sullivan County, New York, and Wayne County, Pennsylvania (Figure 1). In other cases, as many as four studs per row were used, as in the I-80 overpass project in Oakland, California (Figure 2).

As an alternative to steel shear studs, standard channel sections welded to the top flange of the stringer beam were used, such as in the experimental bridge in Amsterdam, New York (13), shown in Figure 3. Although the experimental study showed that the channel welded sections performed well, their use was limited because of the relatively high labor cost. On the same experimental bridge, a bolted connection was also used, as shown in Figure 4; in this connection, the panels were first placed using steel shims for leveling. After the holes for the bolts were drilled in the top flange of the steel girder through the sleeves in the panels, high-strength bolts were fastened. Full tension in the bolts could not, however, be achieved because of concerns the precast slab would break as a result of the excessive tensioning. This connection detail was not used on any subsequent projects.

In most of the projects built during this period, the panels were supported on the girders using steel shims, and a 1 in. to

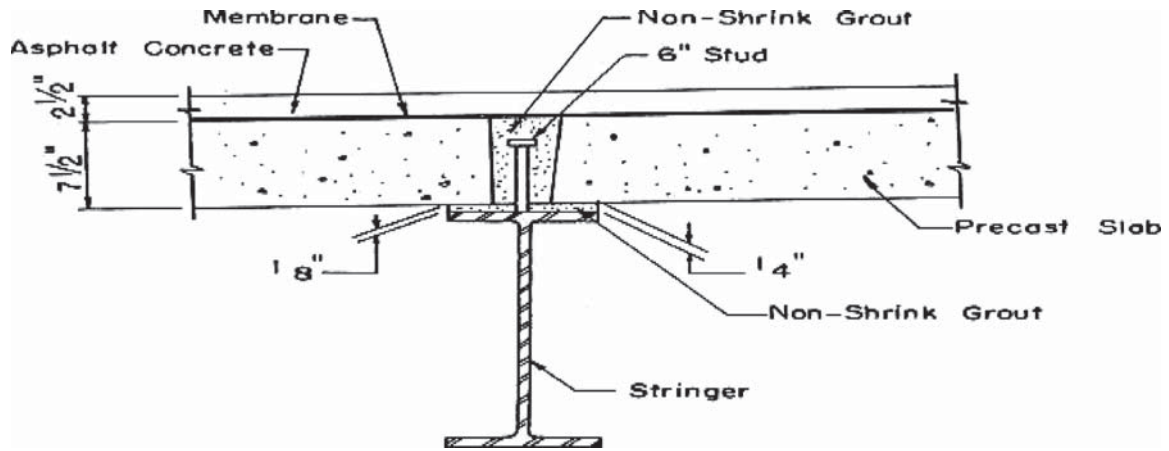


Figure 1. Deck/superstructure connection details of the Delaware River bridge.

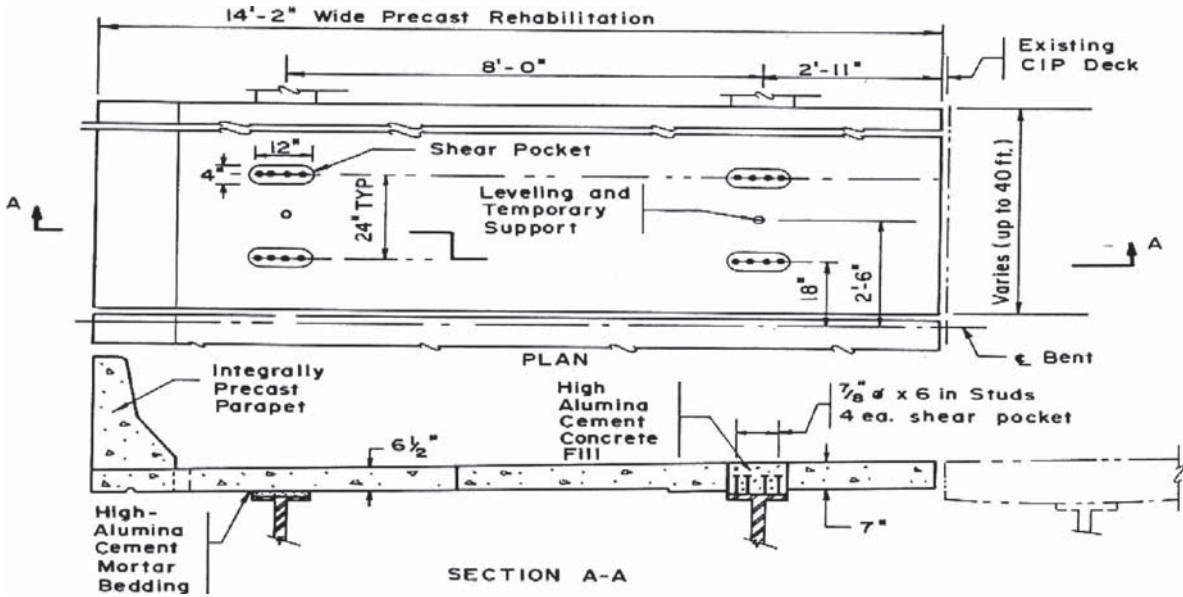


Figure 2. Panel dimensions and cross section of the I-80 overpass project, Oakland, California.

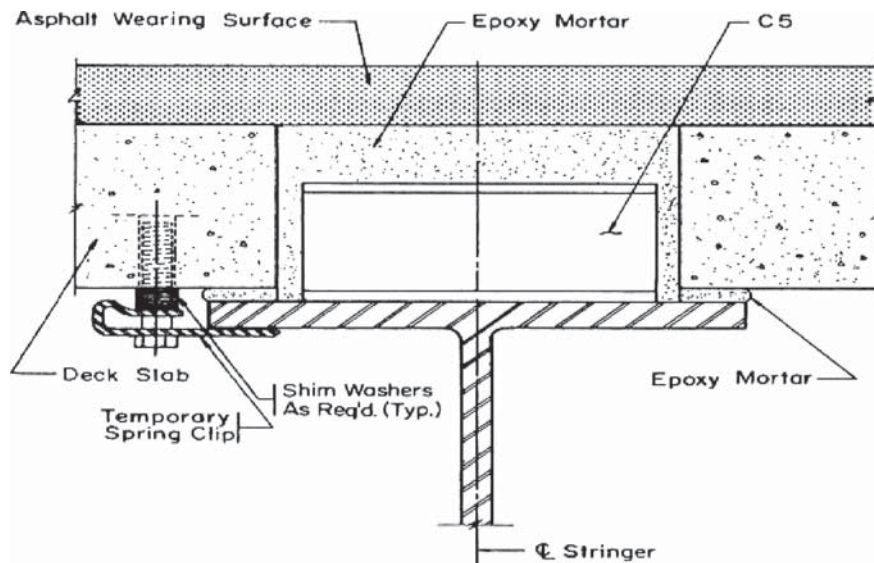


Figure 3. Welded channel section detail used in the New York Thruway experimental bridge.

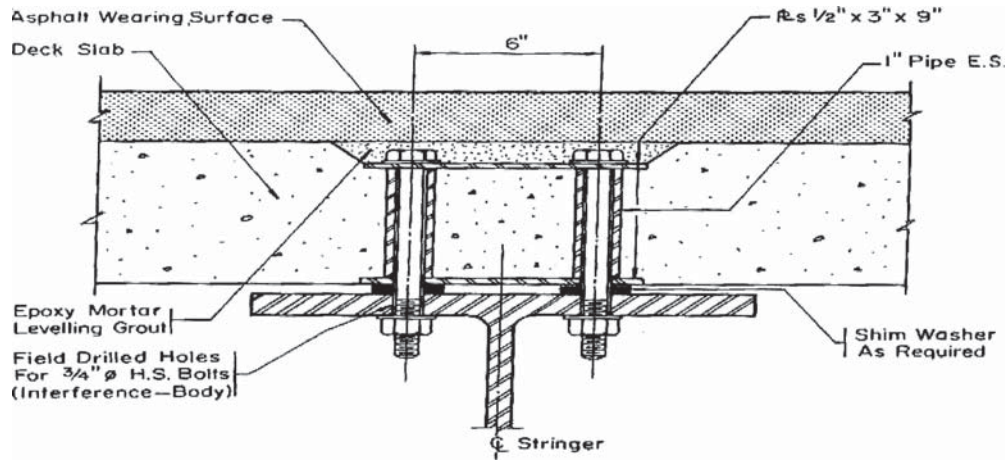


Figure 4. Bolted detail used in the New York Thruway experimental bridge.

2 in. (25 mm to 50 mm) high haunch was provided between the precast panel and the girders. Once the grout filling the haunch achieved design strength, full bearing of the precast panels on the supporting girders could be expected, eliminating any possible stress concentrations in the panels. Many details were used to form dams for the grout, such as the light-gauge side forms that were used on the Queen Elizabeth Way–Welland River Bridge in Ontario, Canada, as shown in Figure 5, and the elastomeric strips used on the Clark's Summit Bridge on the Pennsylvania Turnpike, as shown in Figure 6. In both cases, tie anchors, bolted on the bottom surface of the panels, were used to secure the grout dam against leakage.

As shown in Figure 7, leveling screws were used to adjust the panel elevation. Two screws per panel were typically used at every girderline. These screws were designed to support the panel weight and expected construction loads. After the grout that filled the haunches and pockets gained strength, the screws were removed or were flame cut.

Transverse Panel to Panel Connection

The transverse edges of the precast panels were usually provided with shear keys, which play an important role in the

service performance of the finished deck. The shear key must be designed to protect adjacent panels from relative vertical movement and to transfer the traffic load from one panel to the next without failure of the panel to panel joint. Under traffic load, a panel to panel joint experiences two types of forces: (a) a vertical shear force that tries to break the bond between the panel and the grout filling the joint, and (b) a bending moment that puts the top half of the joint in compression and the bottom half in tension. The following two types of shear keys have typically been used with full-depth precast concrete panels:

- NongROUTED match-cast shear key (see Figure 8). This type of shear key was used with longitudinal posttensioning on the Bloomington Bridge in Indiana. Thin Neoprene sheets were installed between adjacent panels to avoid high stress concentrations. Although match casting can be achieved in a controlled fabrication environment, such as in a precast concrete plant, it was difficult to achieve a perfect match in the field as a result of construction tolerances and the necessary elevation adjustment of the panels. After 5 years of service, cracking and spalling was observed in the concrete at the panel joints, which eventually led to leakage problems at the joints (17).

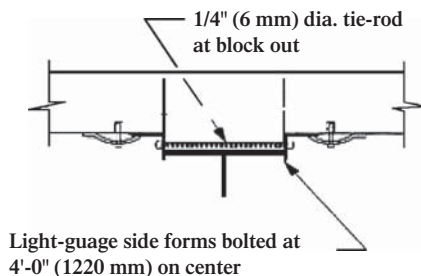


Figure 5. Grout dam built using light-gauge side forms (Queen Elizabeth Way–Welland River bridge, Ontario, Canada).

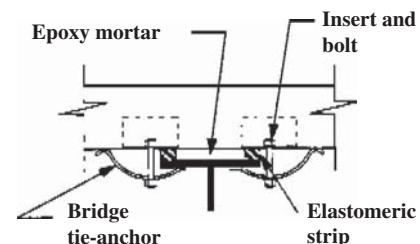


Figure 6. Grout dam built using elastomeric strips (Clark's Summit bridge, Pennsylvania Turnpike)

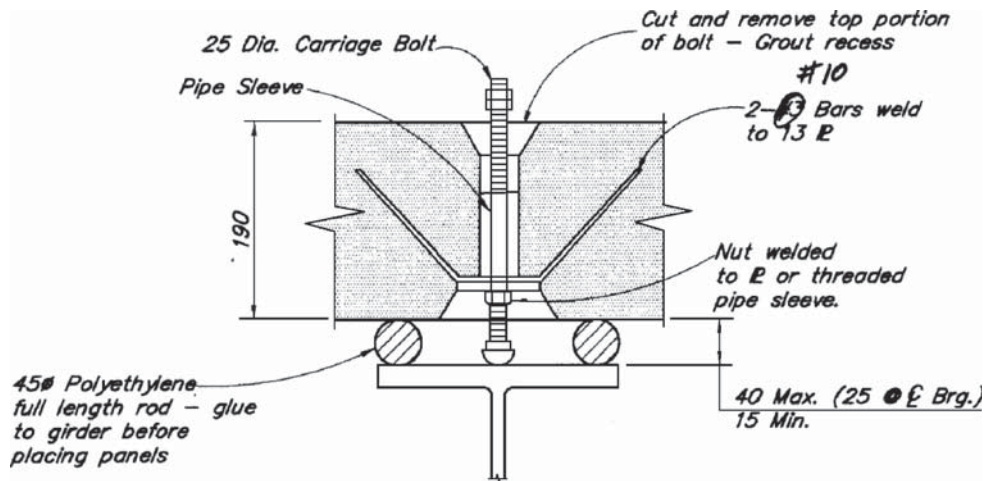


Figure 7. Leveling screw detail.

- Grouted female-to-female joints. With this type of joint, grout was used to fill the joint between adjacent panels. Inclined surfaces were provided in the shear key detail to enhance the vertical shear strength of the joint. Vertical shear forces applied at the joint were thus resisted by bearing and bond between the grout and the panel. The shear key was recessed at the top to create a relatively wide gap that allowed casting the grout in the joint. Figure 9 shows some of the shear key details for bridge decks built since 1973.

With grouted joints, a form must be provided at the bottom surface of the panels to protect the grout from leaking during casting. The following two methods of forming have been used:

- Polyethylene backer rods are placed in the tight space between panels at the bottom of the joint, as shown in Figure 10. This detail has been used for a very long time by many highway authorities. Although this detail does not require any construction work to be done from below, it has been reported that, as a result of fabrication and construction tolerances, joints in some cases ended up partially full, as shown in Figure 10 (21, 22, 23). Partially filled grouted joints cause high stress concentrations at the panel edges, especially if longitudinal posttensioning is applied, and initiate cracking close to the bottom surface of the panels.
- Wood forming is installed from under the panel, as shown in Figure 11. In this detail, a gap of 1 to 3 in. (25 to 76 mm)

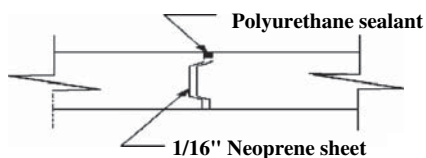


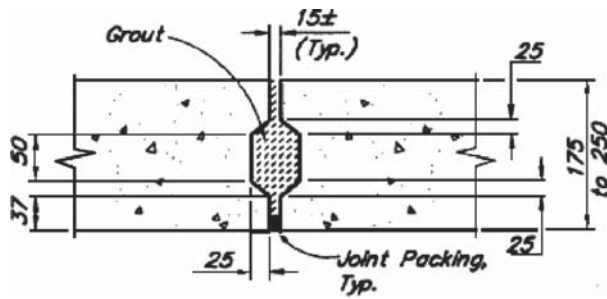
Figure 8. Nongrouted match-cast joint.

is maintained between adjacent panels, and wood forms are installed from under the panel. The forms are hung from the top surface of the precast panels using threaded rods and nuts. This detail usually results in a full-height grouted joint with excellent performance (21, 22). This technique allows the joint to be completely filled with grout, but it requires access from below for form erection and removal.

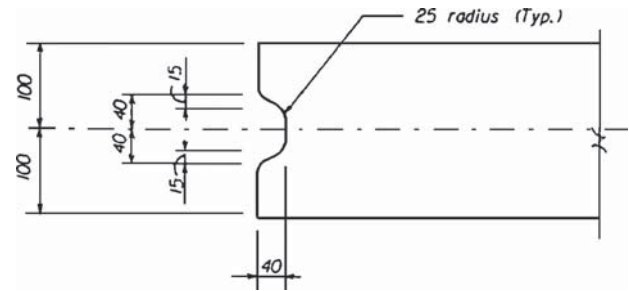
The bond between the grout and the shear key surface can be significantly enhanced by roughening the surface of the shear key (23). This has been found to be extremely important when connecting precast panels that have no longitudinal posttensioning. The roughening can be achieved by sandblasting, followed by a thorough washing. This operation can be done either in the precast plant before the panels are shipped or at the bridge site before the panels are installed. Roughening can also be achieved during panel fabrication by painting the side forms with a retarding agent. After removing the side forms, the shear key is washed with water under high pressure so that the aggregate in the concrete will be exposed, creating a uniformly roughened surface. This concept was used by Texas DOT on precast concrete panels for tied-arch bridges, as shown in Figure 12.

The findings from the literature review of the performance of the transverse panel to panel connection can be summarized as follows:

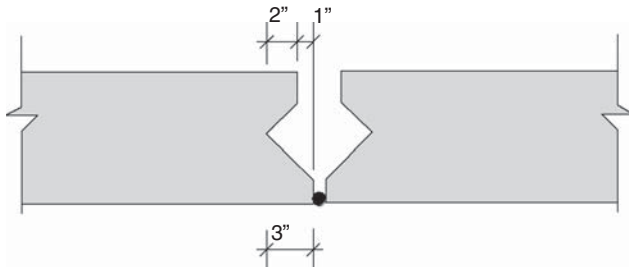
- The nongrouted match-cast shear key joint detail was used on a small number of projects and had unsatisfactory performance; cracking and spalling of the concrete was noticed after a bridge was in service for a short period of time.
- Joints made with polyethylene backer rods have performed satisfactorily in most cases, especially when longitudinal posttensioning is provided on the deck.
- The use of wood forming has recently become more common than the use of polyethylene backer rods.



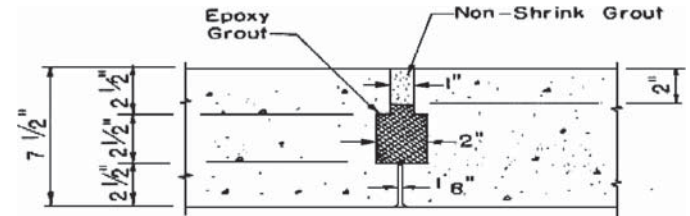
(a) Trapezoidal-shape shear key detail used in the Pedro Creek Bridge, Alaska



(b) Semi-circle shear key detail used in the George Washington Memorial Parkway Bridges, Washington DC



(c) V-Shape shear key detail used in the Skyline Drive Bridge, Omaha, Nebraska



(d) Rectangular shear key detail used in the Delaware River Bridge, New York

Figure 9. Shear key details for various grouted female-to-female joints.

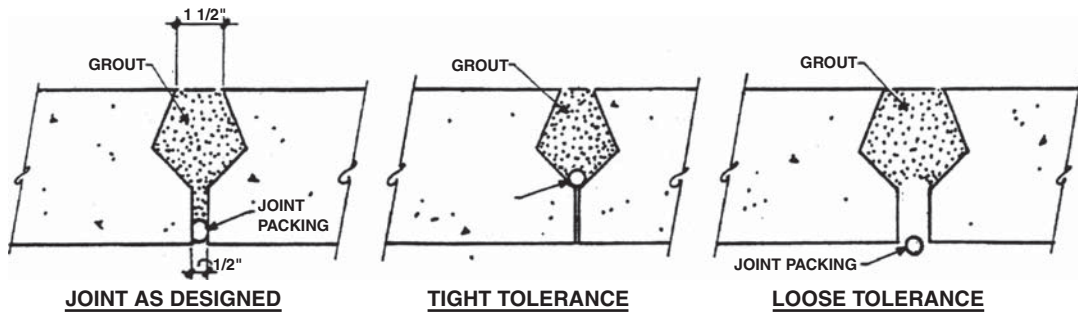


Figure 10. Effect of tight and loose tolerances on panel-to-panel joints.

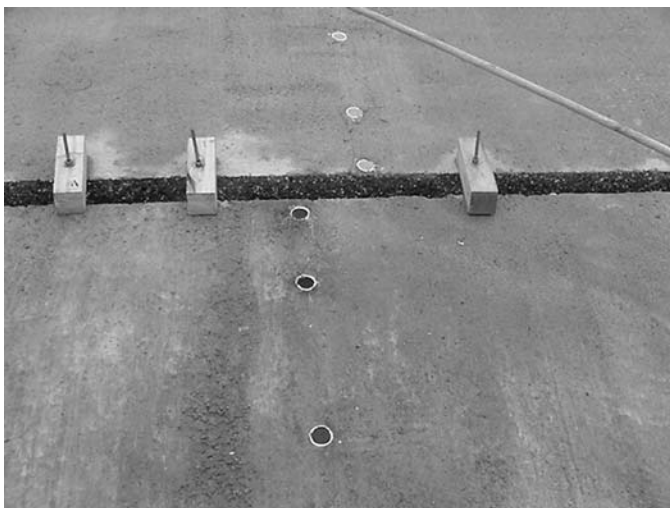


Figure 11. Wood forming of the panel-to-panel joint used in the tied-arch bridges, Texas.



Figure 12. Exposed aggregate roughened surface used on the tied-arch bridges, Texas.

Longitudinal Reinforcement

Longitudinal reinforcement in deck slabs is used to distribute the concentrated live load in the longitudinal direction. It is also used to resist the negative bending moment due to superimposed dead and live loads at the intermediate supports of continuous span bridges. For deck slabs made with full-depth precast panels, splicing this reinforcement at the transverse joint between panels is a challenge for design engineers for the following reasons:

- The panels are relatively narrow, measuring 8 to 10 ft. Therefore, a wide concrete closure joint (2 to 3 ft) is needed if the longitudinal reinforcement splices are to be lapped. This would require wood forming under the panels and an extended period of time for curing.
- The longitudinal reinforcement is spliced at the transverse grouted joint between panels that is considered the weakest

link in the system. Great care thus has to be taken in detailing the splice connection to maintain the construction feasibility and avoid leakage at the joint during the service life of the deck.

- Splicing the longitudinal reinforcement requires a high level of quality control during fabrication to guarantee that the spliced bars will match within a very small tolerance.
- Splicing the longitudinal reinforcement requires creating pockets and/or modifying the side form of the panels, which increases the fabrication cost.

As a result, a few highway agencies, such as the Alaska DOT and the New Hampshire DOT, have opted not to splice the longitudinal reinforcement on simply supported span bridges. Figure 13 shows the transverse joint of the precast deck system that has recently been used on the Dalton and Pedro Creek bridges on Route FAP 65 in Alaska. Although Alaska DOT design engineers have reported that there is no significant cracking or leakage at the joints, the reader should note that the average daily traffic on these bridges is very low compared with bridges in metropolitan areas.

Most highway agencies prefer to provide some type of reinforcement across the transverse joints. Various methods have been used in the past to provide and splice the longitudinal reinforcement, including the following four methods:

- A lap splice was used in the full-depth precast concrete deck panel system on the rehabilitation project involving structure C-437 of the county road over I-80 to Wanship, Utah, as shown in Figure 14. In this project, the design engineer allowed the use of threaded couplers at the face of the transverse joints to simplify the side forms used in fabrication.
- U-shaped pin bars were used on the Castlewood Canyon Bridge in Colorado. Figure 15 shows the U-shaped pin bars where they are overlapped and confined with rectangular stirrups.

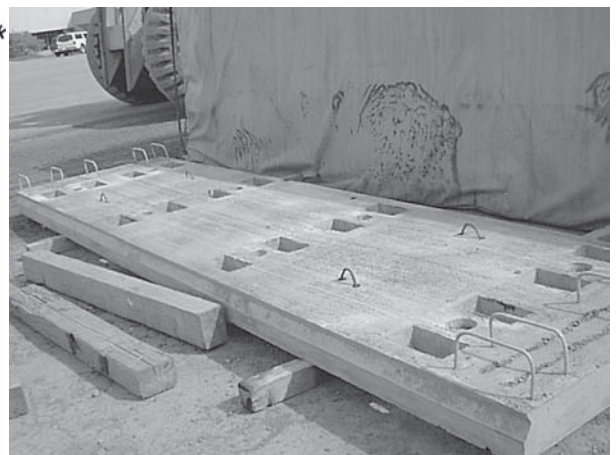
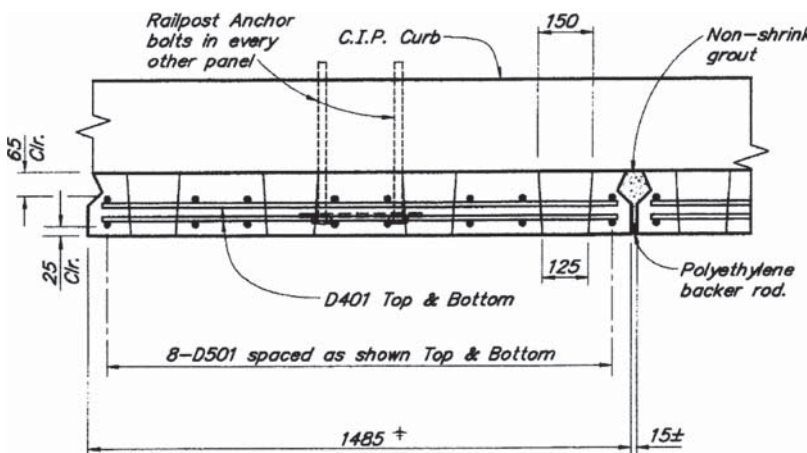


Figure 13. Nonreinforced panel-to-panel connection used on bridges by Alaska DOT.

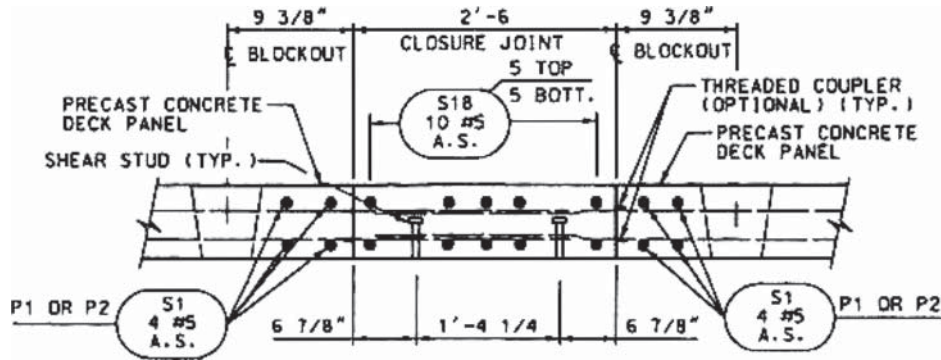


Figure 14. Lap splicing of longitudinal reinforcement used on Structure C-437, Wanship, Utah.

- Spiral confinement has been developed to reduce the lap splice length and give higher construction flexibility for the spliced connection (2, 3, and 5). Figure 16 shows the spliced connection where a loose bar confined with high-strength spiral is used. This detail reduces the lap splice length by about 40% to 50% and helps in simplifying the fabrication of the panel because no bars extend outside the transverse edges of the panel.
- Longitudinal posttensioning has been used on the majority of bridges built with full-depth precast panels during the past 30 years. It puts the transverse panel-to-panel joints under compression, which eliminates the tensile stresses resulting from a live load. The amount of posttensioning stress on the concrete after seating losses used in bridge decks ranges from 150 to 250 psi (1.03 to 1.72 MPa).

Longitudinal posttensioning is typically conducted after the transverse panel-to-panel joints are grouted and cured, but before the deck-girder connection is locked. This procedure guarantees that all of the posttensioning force is applied to the precast deck.

In most cases, high-strength threaded rods uniformly distributed between girderlines are used. The threaded rods are fed through galvanized or polyethylene ducts that are provided in the panels during fabrication. Figure 17 shows the posttensioning details that were used on Bridge 4 on Route 75 in Sangamon County, Illinois. Longitudinal posttensioning can be provided in stages and coupled as shown in Figure 17. After the threaded rods are posttensioned and secured, the ducts are grouted with nonshrink grout to protect the threaded rods from corrosion.

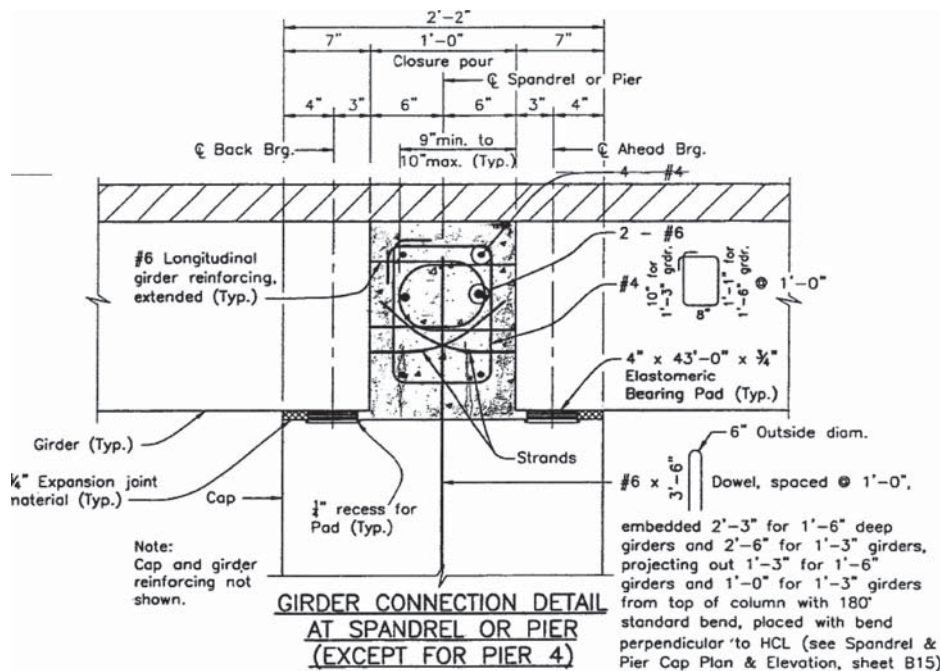


Figure 15. Continuity detail over the cross piers used on Castlewood Canyon bridge, Colorado.

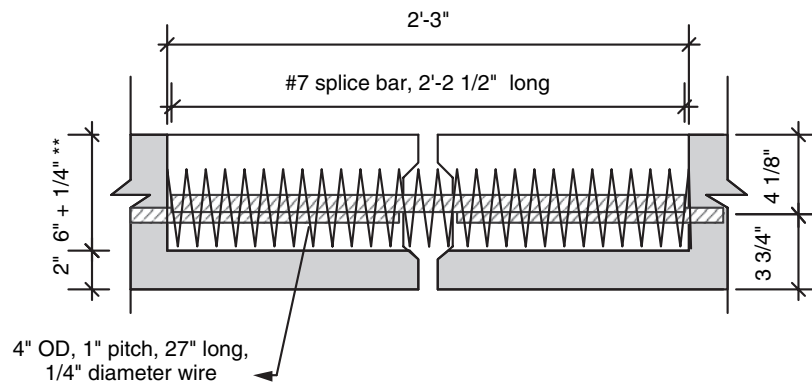


Figure 16. Panel-to-panel connection using spiral confinement.

Recently, longitudinal posttensioning concentrated at the girderlines has been used on the Skyline Drive Bridge in Omaha, Nebraska. Figure 18 shows a cross section of the bridge at a girderline. The posttensioning consists of 16.5 in. (12.7 mm) diameter, 270 ksi (1.86 GPa) low-relaxation strands. The strands are fed into open channels created over the girderlines, and a special end panel that houses the anchorage device is used, as shown in Figure 18.

Grout Material

Several grout materials have been used to fill the shear pockets and the transverse joints between adjacent panels. Some of these materials are commercial products, while others have been developed by state highway agencies. The properties common to all types of grout are: (a) relatively high strength (2,000 to 4,000 psi) at young age (1 to 24 hours), (b) very small shrinkage

deformation, (c) superior bonding with hardened concrete surfaces, and (d) low permeability. In conducting the literature review, the researchers noticed that most state highway agencies specify the properties required for the grout material, rather than a certain type of grout material. The contractor therefore has to assume responsibility for choosing the type of grout material and then secure the approval of the highway agency.

The following sections provide a summary of the most common types of grout that have been used with full-depth precast panels. Information is also included about some of the recent research that has compared the performance of various types of grout.

Commercial Products

Various commercial types of grout material have been used with full-depth precast concrete deck, such as: Set 45,

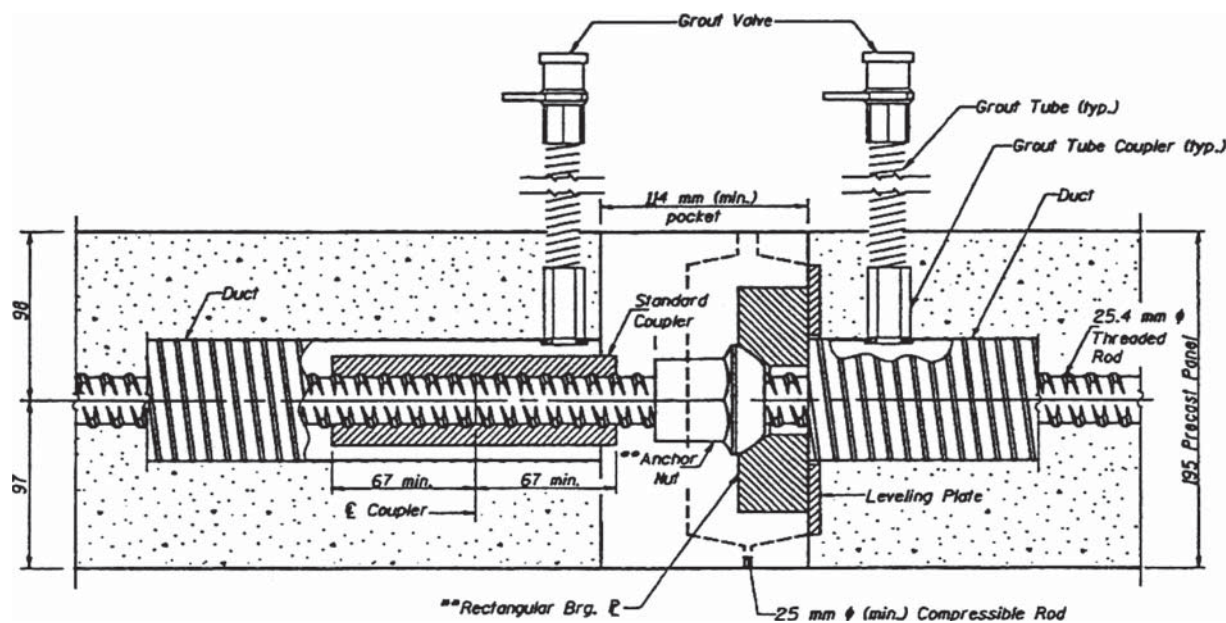


Figure 17. Posttensioning detail used on Bridge-4 constructed on Route 75, Sangamon County, Illinois.

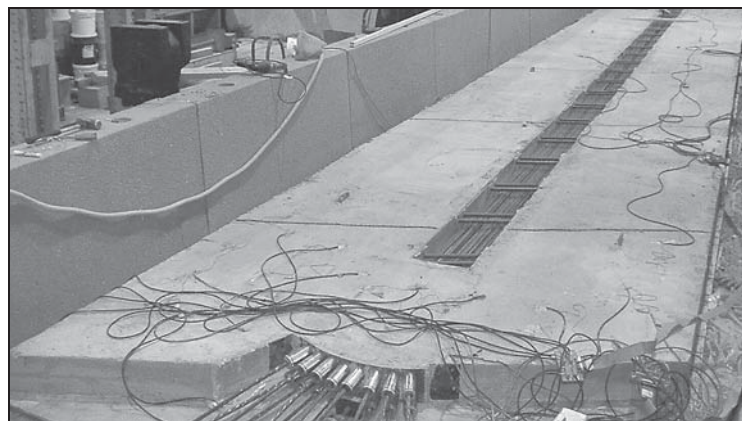
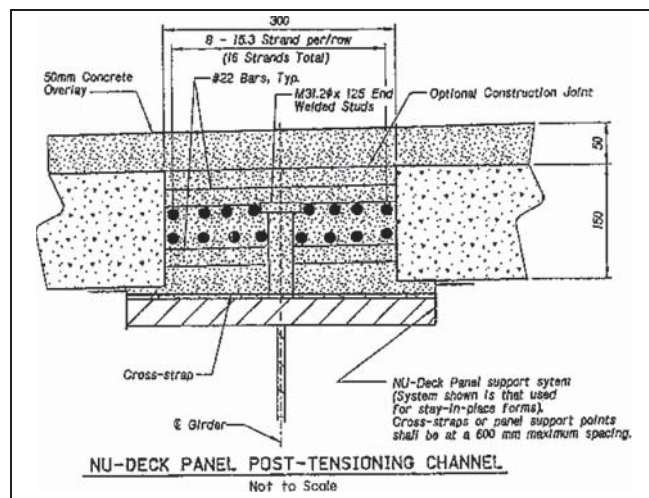


Figure 18. Longitudinal posttensioning concentrated at girder lines used on the Skyline Drive bridge, Omaha, Nebraska.

Set 45 Hot Weather (HW), Set Grout, EMACO 2020, SS Mortar, Masterflow 928, 747 Rapid Setting Grout, S Grout, and SonogROUT 10K. A comparison of the physical and mechanical properties of some of these products is given in Chapter 3.

In a recent study by Issa et al. (23), the researchers studied the behavior of female-to-female joint details using Set 45, Set 45 HW, Set Grout, and EMACO 2020. The joint was tested for direct vertical shear, direct tension, and flexure. A total of 36 specimens were tested. The compressive strength of the elements that represented the precast panels was about 6,250 to 6,500 psi (43 to 45 MPa). For all specimens, the joint surfaces were sandblasted and thoroughly cleaned. There was no reinforcement crossing the interface between the joint and the precast panel. In addition to the full-scale testing of the joint, the permeability and shrinkage properties of the grouting material were determined in accordance with ASTM C1202-97 and ASTM C157, respectively.

The findings of that experimental program can be summarized as follows:

- The shear, tensile, and flexural strength of joints made with EMACO 2020 were the highest among all types of grouting material.
- The shear, tensile, and flexural strength of joints made with Set Grout were higher than those made with Set 45 and Set 45 HW.
- Failure of specimens made with EMACO 2020 occurred away from the joint in the precast panels, while failure of the specimens made with Set Grout occurred simultaneously through the joint and in the precast panels. For specimens made with Set 45 and Set 45 HW, failure occurred through the joint.

- Moisture and carbonation at the joint surface adversely affected the bond and strength of joints made with Set 45.
- EMACO 2020 and Set 45 set very quickly, which necessitates fast mixing and installation.
- EMACO 2020 was significantly less permeable and showed much lower shrinkage deformation compared with other grout materials.

Noncommercial Grout Material

The noncommercial grout materials presented in this section were used for projects with regular construction schedules, where the bridge was closed for an extended period of time, and where the grout needed an extended period of continuous curing (at least 7 days).

Hydraulic Cement Concrete

Hydraulic cement concrete (HCC) mixes were used on some of the bridges built before 1972. The specifications for these mixes contained a minimum concrete strength of 4,000 psi (27.6 MPa), relatively high slump (about 6 in., or 153 mm), and a maximum aggregate size of 0.5 in. (12.7 mm).

Latex-Modified Concrete

Latex-modified concrete (LMC) mixes are different from HCC mixes in that a latex admixture is added to the mix. The latex forms a thin film on the aggregate surface, which enhances the bond between the paste and the aggregate and results in high compressive strength and a less permeable concrete mix.

Many state highway agencies have developed their own LMC mix. The following are the specifications for the LMC mix that has been developed and used by the Virginia DOT (24, 25).

Portland cement III (minimum):	7 bags, 658 lb/yd ³ (388 kg/m ³)
Water (maximum):	2.5 gal/bag of cement
Water/cement ratio:	0.35 to 0.40
Styrene butadiene latex admixture:	3.5 gal/bag of cement
Air content:	3 to 7%
Slump (measured 4.5 minutes after discharge):	4 to 6 in. (100 to 200 mm)
Cement/sand/aggregate by weight:	1.0/2.5/2.0

Menkulasi and Roberts-Wollman (26) conducted an experimental investigation using two types of grout material—LMC and Set 45 HW; angular pea gravel filler was added to both types. The test included only direct shear specimens that simulated precast concrete panels supported on prestressed concrete girders, as shown in Figure 19. Three specimens with different amounts of reinforcement crossing the interface were used: no reinforcement, reinforcement with No. 4 (No. 13 metric) bar, and reinforcement with No. 5 (16) bar. The height of the haunch used in all specimens was 1.0 in. (25.4 mm). The investigation revealed that specimens made with Set 45 HW and LMC had almost the same shear capacity when no or only a small amount of shear reinforcement was present. However, at high amounts of shear reinforcement, the specimens made with Set 45 HW showed higher strength than those made with LMC. The researchers were in favor of using Set 45 HW over LMC as the recommended grout

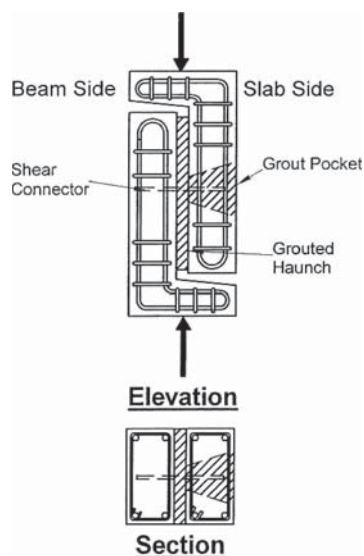


Figure 19. Push-off test specimen from Salvis (19).

material. The investigation also showed that changing the height of the haunch from 1.0 to 3.0 in. (25.4 to 76 mm) had almost no effect on the shear capacity of the specimens made with Set 45 HW grout.

Type K Cement Concrete Mix

Type K cement concrete mix was used on the Skyline Bridge in Omaha, Nebraska, to fill the longitudinal open channels that house the posttensioned cables (6). The concrete mix had a specified concrete strength of 4,000 psi (27.6 MPa), and only Type K cement was used in the mix. The concrete mix had no fly ash, and the maximum aggregate size was $\frac{3}{8}$ in. (9.5 mm). Type K cement is an expansive cement that contains anhydrous calcium aluminate, which when mixed with water forms a paste that increases in volume significantly more than portland cement paste does during the early hydrating period that occurs after setting.

History of the Shear Connector Spacing Limits of the AASHTO LRFD Design Specifications

Creating a composite action between the precast deck and the supporting girders has been one of the challenges facing the engineers designing precast concrete panel decks. Intermediate pockets over the girderlines have to be created in the panel to accommodate the shear connectors extending from the supporting girders into the precast deck. In addition, the shear connectors have to be clustered in groups lined up with these pockets.

Forming the shear pocket typically slows the panel fabrication process and eventually raises the fabrication cost. Therefore, design engineers try to space the shear connectors as far as the specifications allow them. The *AASHTO Standard Specifications for Highway Bridges* (27) and the *AASHTO LRFD Bridge Construction Specifications* (8) state that the spacing between the shear connectors for steel or concrete girders should not exceed 24 in. (610 mm). The following discussion provides a brief summary of the history of this limit in the specifications.

The first composite concrete slab on a steel I-beam bridge in the United States was constructed in the early to mid 1930s in Iowa. A composite bridge design example, prepared as part of a paper by Newmark and Siess in accordance with the third (1941) edition of the American Association of State Highway Officials (AASHTO) *Standard Specifications for Highway Bridges*, states “the spacing of the shear connectors shall be not more than 3 to 4 times the depth of the slab” (28). While this limit did not appear in the AASHTO provisions, it appears to have been used as a convention or rule of thumb. Newmark and Siess recognized that while these connectors are generally

only designed to transfer horizontal shear, they also play a role in preventing the separation of the beam and the slab.

The 2 ft maximum limit on shear connector spacing, or pitch, first appeared in the fourth edition of the AASHTO *Standard Specifications for Highway Bridges* (1944). This requirement appears without commentary, which was typical of that era, and the source of this change was not given.

A 1953 paper by Viest and Siess contains a discussion of why mechanical connectors are needed (29). Their arguments include (a) to prevent relative movement (either horizontal or vertical) between the beam and the slab during all loading levels up to ultimate, and (b) to transfer horizontal shear from the slab to the beam. The discussion that supports these roles for shear connectors is primarily directed at ensuring linear-elastic behavior of the composite system.

Viest and Siess returned to this subject in a 1954 paper that reports conclusions based on their experimental results and includes design recommendations (30). It should be noted that these experiments were carried out using the channel-type shear connectors that were conventional at the time. Although they did not comment on the origin of the 24 in. (610 mm) maximum connector spacing in the AASHTO provisions, the experimental results support retaining the limit. The testing considered connector spacing of 18 in. (457 mm) and 36 in. (914 mm). While the 18 in. (457 mm) spaced connectors performed as necessary, the 36 in. spaced connector specimens experienced lift-off between connectors under load in the experiments. This result motivated the authors to recommend that “the maximum spacing of channel shear connectors be not greater than four times the thickness of the slab, but in no case greater than 24 inches.”

Further investigation has revealed that when the headed stud shear connector became available to the steel bridge construction industry in the late 1950s, the steel industry people relied on Viest and Siess to help formulate the design provisions for these connectors that were eventually incorporated into the AASHTO specifications in the early 1960s. Based on their previous work, Viest and Siess again recommended a limit of 24 in. (610 mm) maximum spacing for these provisions. This timeframe also coincides with industry acceptance of precast/prestressed concrete girders as an alternative to steel girders for highway bridge construction.

The effect of the number of studs per cluster and the number of clusters per specimen was studied by Issa et al. in 2003 (31). In that research, quarter- and full-scale push-off specimens were made with various configurations. The researchers concluded that the increase in ultimate strength of a cluster of studs was not linearly proportional to the number of studs. The researchers stated that, for all specimens, an initial slippage of about 0.02 in. was noticed before the studs started to initiate the composite action, and that shear failure was recorded at the stud base. The failure was accompanied by

local cracking and crushing of the concrete close to the stud base. Once the concrete at the stud base was crushed, the stud lost its bearing support and started to act as a partial cantilever, which led to shear failure at the base. It was also reported that the ultimate capacity of a cluster of studs determined by Equation 6.10.10.4.3-1 of the AASHTO LRFD specifications was overestimated by as much as 22% in some specimens. This conclusion was drawn based on testing of push-off specimens and was not confirmed by any full-scale beam test.

On the Interstate 39/90 Door Creek project, the Wisconsin DOT has used a precast deck panel system, where a 48 in. (1220 mm) spacing of clustered studs was used (32). The decision to violate the maximum spacing limit given by the AASHTO LRFD specifications was based on the experimental investigation conducted by Markowski, where a half-scale composite beam was tested (32). One-half of the beam length had studs at 24 in. (610 mm) spacing, and the other half had studs at 48 in. (1220 mm) spacing. The test results have shown that full composite action was achieved under full service load, and no signs of stiffness deterioration were noticed after applying 2,000,000 cycles of repeated loading. The beam continued to show full composite action when it was overloaded beyond the service load level; however, Markowski could not test the beam at ultimate because of the limited capacity of the loading frame.

Summary of the Literature Review

Panel to Panel Connection

- Female-to-female joints (i.e., shear key details) filled with cast-in-place nonshrink grout provide superior performance compared with match-cast, male-to-female joints. Sharp corners of the shear key enhance the shear transfer across the joint.
- The design criteria for a successful joint detail include no cracks under repeated service loads and no water leakage.
- Various methods were used in the past to provide and splice the panel-to-panel longitudinal reinforcement:
- Although longitudinal posttensioning, which puts the joint in compression and secures it against leakage, increases the cost of the deck system, it was used with the majority of full-depth precast concrete deck panel systems.
- U-shaped pin bars and/or lap splice details require a wide joint and/or a thick precast panel to provide for the required lap splice length and concrete cover.

Panel to Girder Connection

- The majority of full-depth precast concrete deck panel systems were used on steel girders.
 - Typically, headed steel studs are used to compositely connect the girder with the deck.

- Two sizes of steel studs are typically used— $\frac{3}{4}$ in. and $\frac{7}{8}$ in. (19 mm and 22 mm).
 - Recently, one successful attempt was made to extend the shear pocket spacing to 48 in. (1220 mm).
 - A very limited amount of research was conducted on the panel to concrete girder connection.
 - Practically, it is very difficult to cluster the vertical shear reinforcement of the concrete girder to match the shear pockets of the deck panel.
 - Some attempts have recently been made to separate the vertical shear reinforcement from the horizontal shear reinforcement.
-

CHAPTER 3

Research Results

This chapter presents the results and findings of Tasks 3 through 6 listed in Chapter 1. Additional information is provided in Appendices B through F. The following issues are discussed in this chapter:

- Recommendations for full-depth precast concrete bridge deck panel systems. Two systems were developed, a transversely pretensioned system and a transversely conventionally reinforced system. Neither system uses longitudinal posttensioning or an overlay. New panel-to-panel and panel-to-girder connection details were developed and used in these systems, as follows:
 - Panel to panel connection. Four connection details were initially developed and tested in direct tension. Based on the structural performance of these details, two details were selected and used in the recommended systems.
 - Panel to concrete girder connection. A new connection detail that uses clusters of three 1¼ in. (31.8 mm) diameter double-headed steel studs was developed. The clusters are spaced at 48 in. (1220 mm).
 - Panel to steel girder connection. A new connection detail that uses clusters of eight 1¼ in. (31.8 mm) diameter steel studs was developed. The clusters are spaced at 48 in. (1220 mm).
- Analytical and experimental investigation of selected details:
 - Panel to panel connection
 - Direct tension test using pullout specimens
 - Full-scale bridge specimen
 - Precast panel to concrete girder connection: full-scale direct tension test
 - Precast panel to steel girder connection
 - Push-off (direct shear) specimens tested for ultimate capacity
 - Push-off (direct shear) specimens exposed to fatigue loading and then tested for ultimate capacity
 - Full-scale beam test (two composite beams)

- Guidelines for design, detailing, fabrication, and installation of full-depth precast concrete bridge deck panel systems.
- Proposed revisions to the *AASHTO LRFD Bridge Design Specifications*.

Recommended Full-Depth Precast Concrete Bridge Deck Panel Systems

Design Criteria

The following criteria were set in advance to pave the way for the development of the deck systems. The criteria were decided after a careful study of the bridges covered in the literature review and national survey. The criteria were also discussed with a panel of experts on this type of construction.

- Type of superstructure—The slab/I-girder bridge type was used. This decision was made based on the fact that 50% to 60% of the bridges in United States are of this type (33).
- Construction material—The deck slab is made from conventionally or prestressed reinforced concrete. The supporting I-girder can be made of prestressed concrete or steel.
- Composite versus noncomposite superstructure—It was evident from the literature review that the superstructure of the majority of bridges built with precast deck panels is made composite with the deck. Composite systems typically have many advantages over noncomposite systems, such as shallower depth of the superstructure, longer spans, smaller deflection and less vibration caused by moving traffic, and larger clearance.
- New construction projects versus deck replacement projects—The details of the precast deck systems presented in this chapter were developed to fit new construction projects, as well as deck replacement projects. This decision was made because of the almost 50/50 split between new construction and deck replacement projects nationwide.

- No longitudinal posttensioning was used—This criterion was set by the research problem statement.
- No overlay was used—This criterion was set by the research problem statement.

Two systems were developed. The general features of these systems are listed in Table 1. Although these systems were developed without utilizing longitudinal posttensioning or an overlay, the systems can be easily modified to accept those features.

The following model bridge was considered to develop the recommended systems:

Total width:	44 ft (13.41 m)
Superstructure:	Four steel girders spaced at 12 ft (3.66 m) with a top flange width of 12 to 14 in. (300 to 356 mm), or four BT-72 or NU1800 prestressed, precast concrete girders spaced at 12 ft (3.66 m). The 12 ft (3.66 m) girder spacing was chosen to provide extreme straining actions in the deck and, consequently, the highest amount of reinforcement.
Concrete deck panels:	Total thickness = 8¼ in. (210 mm) Structural slab thickness = 8 in. (200 mm) Normal weight concrete, unit weight = 150 lb/ft ³ = 23.6 kN/m ³ Compressive strength at 28 days = 6.0 ksi (41.37 MPa)

Grout material:	Compressive strength at time of opening the bridge for traffic = 6.0 ksi (41.37 MPa)
Live load:	HL-93 (AASHTO LRFD specifications)
Side barriers:	Jersey barrier, 600 plf (2.19 kN/m) per side

The design was carried out in accordance with the AASHTO LRFD specifications (7).

Recommended System CD-1

Figures 20 to 29 show the details of recommended system CD-1. The panel is 8 ft (2.44 m) long and covers the full width of the bridge (44 ft, or 13.41 m). Although the panel has a structural thickness of 8 in., it is made 8¼ in. (210 mm) thick because no overlay is used. The top ¼ in. (6 mm) of the panel is used as a sacrificial layer that allows for texturing the top surface of the slab. After the panels are installed and grouted, the texture is applied by machine grinding. The texturing process helps ensure a uniform elevation of the finished deck slab and provides a high-quality riding surface.

The panel is transversely reinforced with eight ½ in. (12.7 mm) diameter pretensioned strands and 12 No. 5 (16) bars distributed on two levels. A 2 in. (50 mm) top and bottom clear concrete cover is provided for the two layers of reinforcement. This amount of reinforcement is sufficient to cover the required flexural capacity at positive and negative moment area. Step-by-step design calculations of the system are given in Appendix B.

The longitudinal reinforcement of the panel is made of No. 6 (19) bars at 13.3 in. (338 mm). In order to splice these

Table 1. General features of the conceptual designs of CD-1 and CD-2.

System Designation	CD-1	CD-2
Reinforcement Type: Transverse Longitudinal	Pretensioned Conventional	Conventional Conventional
Supporting girder and construction type: New construction projects Deck replacement projects Alteration to existing shear connectors	Steel or concrete girders Steel girders High	Steel or concrete girders Steel or concrete girders Minimum
Made composite with the girder	Yes	Yes
Longitudinal posttensioning	No	No
Use of overlay	No	No
Panel can be crowned to match the bridge profile	No	Yes
Notes	Two panel-to-panel connection details were developed for this system (CD-1A and CD-1B). A full-scale bridge mockup using this system was constructed and tested in this project.	This system was not tested in this project.

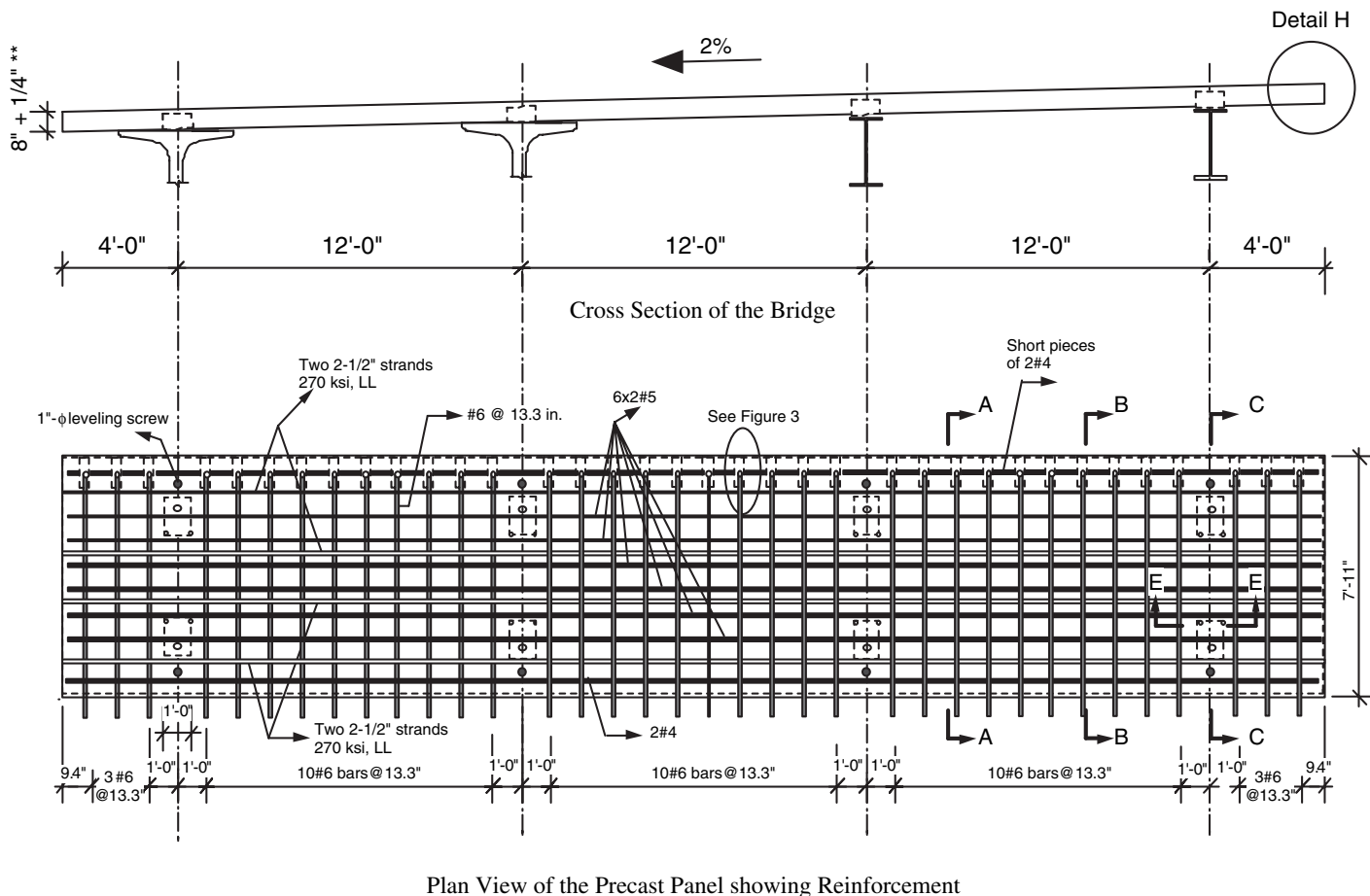


Figure 20. Cross section and plan view of CD-1A ($\frac{1}{4}$ in. is used as a sacrificial layer for texturing).**

bars across the transverse panel-to-panel joints, two connection details were developed—CD-1A and CD-1B.

- *CD-1A* (Figures 20 to 23). On one side of the panel, the No. 6 bar is embedded 6 in. (152 mm) in a galvanized bulged hollow structural steel (HSS) tube (HSS $4 \times 12 \times \frac{3}{8}$ in., or $102 \times 305 \times 10$ mm). On the other side of the panel, the No. 6 bar extends $7\frac{1}{2}$ in. (190 mm) outside the panel. The HSS tube is a 4 in. (102 mm) cut and is installed on its side. It is bulged in the middle to a total height of 5 in. (127 mm). To keep the HSS tube empty during casting of the panel's concrete, its sides are covered with thin cardboard sheets. A 1 in. (25 mm) diameter plastic pipe is attached to the top surface of the HSS tube and is used to fill the tube with flowable grout. The HSS tube has an oversize $1\frac{3}{4}$ in. (45 mm) diameter hole on the free side of the panel to help in installing the new panel without interference with the shear connectors. The panel is installed so that the HSS tubes are ready to receive the No. 6 bars of the next panel, as shown in Figure 23. As the next panel is being installed, it will be tilted to avoid interference with the shear connectors of the superstructure.

- *CD-1B* (Figures 24 to 26). On both sides of the panel, the No. 6 bar is embedded 12 in. (305 mm) in an HSS tube ($4 \times 12 \times \frac{3}{8}$ in.). The dimensions of the HSS tube are exactly the same as those for the HSS tube in CD-1A. In this case, however, the HSS tube is not bulged, and it is provided with a 1.5 in. (38 mm) wide top slot. The slot extends all the way to the top surface of the panel. The new panel is installed vertically, and then a $24\frac{1}{2}$ in. (622 mm) long splice bar is dropped from the top surface of the panel through the slot.

The goal of using the HSS tube is to confine the grout surrounding the No. 6 bar, which enables the bar to develop its yield strength in a shorter distance than required for unconfined bars. According to the LRFD specifications, an unconfined No. 6 bar requires at least 18 in. (457 mm) to develop its full yield strength (7). The No. 6 bar has only about 6 in. (152 mm) of embedment length and 12 in. (305 mm) of lap splice length in CD-1A and CD-1B, respectively. These new details were tested for direct tension due to static load and for flexure due to repeated loading; the test results found full development of the No. 6 bar yield strength. A similar technique that uses a

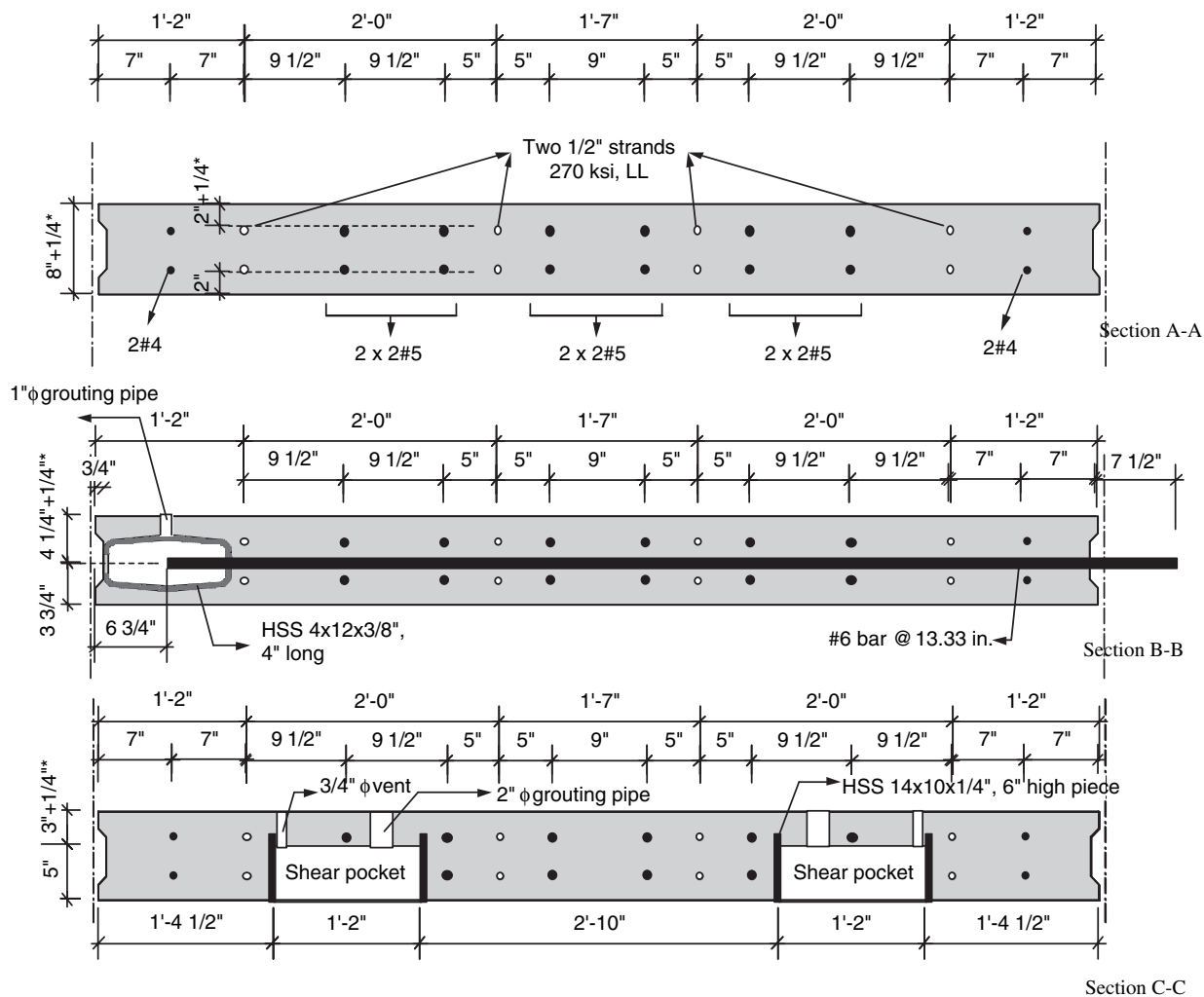


Figure 21. CD-1A, Sections A-A, B-B, and C-C ($1/4$ in. is used as a sacrificial layer for texturing).

high-strength spiral wire was successfully used with the NUDECK precast system (2, 3).

Forms needed for grouting the transverse joints can be built by attaching strips of plywood to the top surface of the panel, as discussed in Chapter 2. This method is recommended to ensure the shear key is completely filled with grout.

The panel is made composite with the supporting girder through hidden shear pockets. The shear pockets are 12 in. (305 mm) wide, 14 in. (356 mm) long, and 5 in. (127 mm) high, and they are spaced at 48 in. (1220 mm). The dimensions of the pockets are optimized to minimize the volume of grout needed to fill a pocket, which will make the system more economical. The 48 in. (1220 mm) spacing of the pockets was chosen to simplify the fabrication process of the panels by minimizing the number of shear pockets to be formed, which will reduce the fabrication cost. An experimental validation was conducted using push-off specimens and full-scale beam testing because the 48 in. (1220 mm) spacing was in violation of the LRFD specifications that limit the spacing

to 24 in. (610 mm) (7). After the panels are installed and their elevation is adjusted using the leveling screws, the shear pockets and transverse joints between panels, including the HSS tubes, are filled with flowable grout.

Two panel-to-girder connection details were developed. The first detail is used for steel girders, where $1\frac{1}{4}$ in. (31.8 mm) diameter steel studs are used. The reason for using the $1\frac{1}{4}$ in. studs, rather than the $\frac{7}{8}$ in. (22 mm) diameter studs commonly used, is to minimize the dimensions of the shear pockets; two $\frac{7}{8}$ in. studs are replaced with one $1\frac{1}{4}$ in. stud (34). The studs are set in groups at 48 in. (1220 mm), and each group has eight studs, as shown in Figure 27. A 3 in. (76 mm) spacing between studs in the longitudinal direction is proposed, which violates the LRFD specifications that stipulate a minimum spacing of four times the stud diameter to be used (4×1.25 in. = 6 in. [152 mm]). The intent of the LRFD limit has been to guarantee that the compressive stresses in concrete or grout in front of the stud will not exceed the allowable bearing strength due to overlapping stress

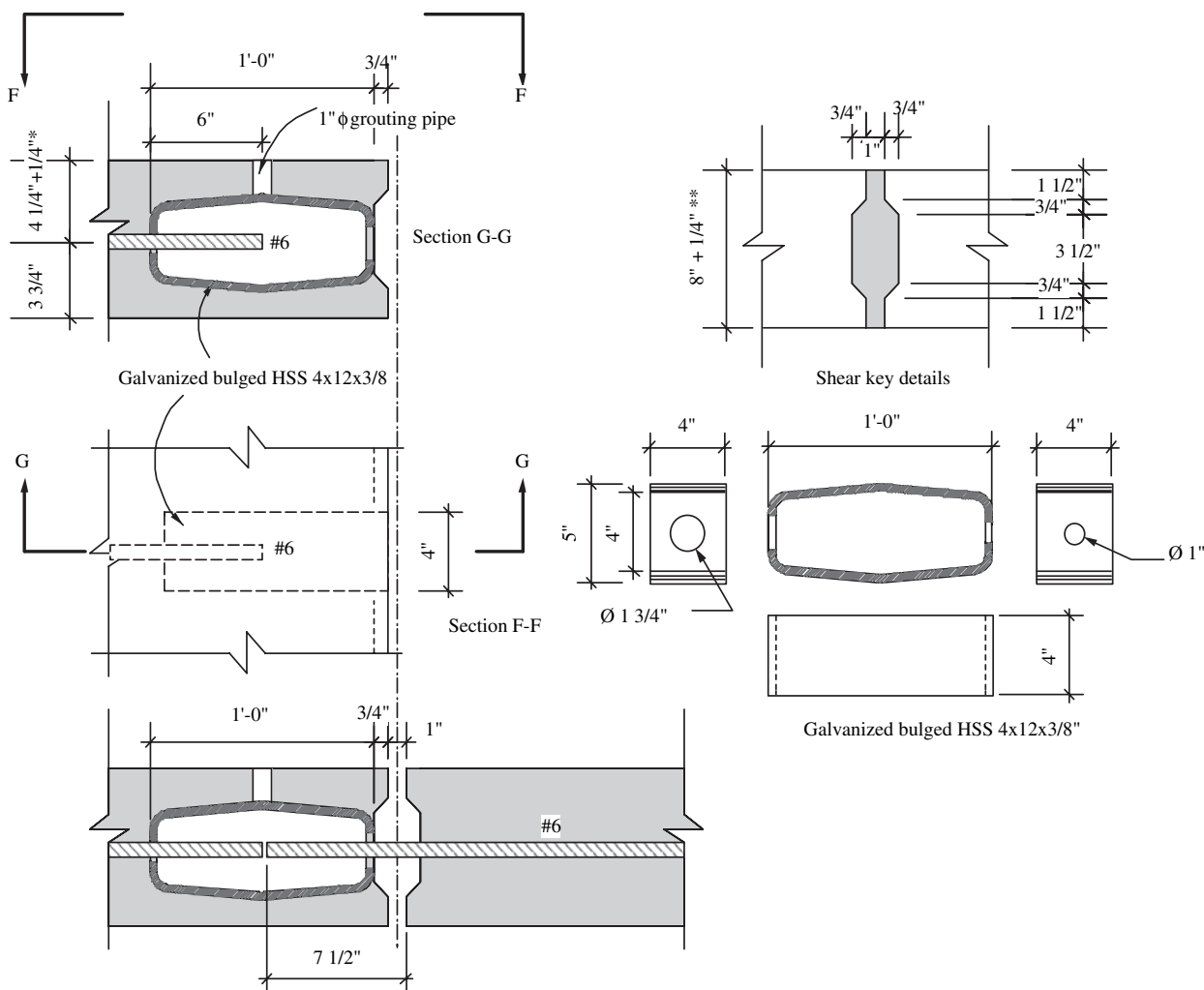


Figure 22. CD-1A, panel-to-panel connection detail, Detail D (* $\frac{1}{4}$ in. is used as a sacrificial layer for texturing).

distributions of adjacent studs. The shear pocket is confined with an HSS tube in order to increase the compressive strength of the grout. Another alternative is to confine the shear pocket using three No. 6 closed ties. Both alternatives were experimentally investigated.

The number of studs per pocket was determined based on a parametric study by Tadros and Baishya on a wide range of steel bridges with spans between 60 and 130 ft (18 and 40 m) and girder spacing between 6 and 12 ft (1.82 and 3.66 m) (2). The study concluded that one $1\frac{1}{4}$ in. (31.8 mm) stud at 6 in. (152 mm) would be sufficient to maintain full composite action between the deck and the steel girder. It is recommended that the designer run the analysis for the horizontal shear and determine the required number of studs for the bridge under consideration.

Figure 28 shows the recommended detail for concrete girders, where clusters of three $1\frac{1}{4}$ in. (31.8 mm) diameter double-headed studs are set at 48 in. (1220 mm). The studs are embedded in the top flange of the prestressed concrete

girder. The reason for using double-headed studs as horizontal shear reinforcement, rather than the commonly used vertical web shear reinforcement of the girder, is to minimize the shear pocket dimensions. If vertical web shear reinforcement were used for this model bridge, 12 legs of No. 5 bars would be needed per cluster. In addition, the stud's head provides full anchorage without consuming a large amount of space compared with the No. 5 bars that need to be bent to an L-shape or an inverted U-shape. The number of studs per cluster was determined based on information collected from the design examples given in Chapter 9 of the *PCI Bridge Design Manual* (35) and from bridge designers in the DOTs. However, it is recommended that the designer run the analysis for the horizontal shear and determine the required number of studs for the bridge under consideration because the amount of horizontal shear reinforcement required depends on many variables, such as the width and surface condition of the interface, span length, girder spacing, and girder depth.

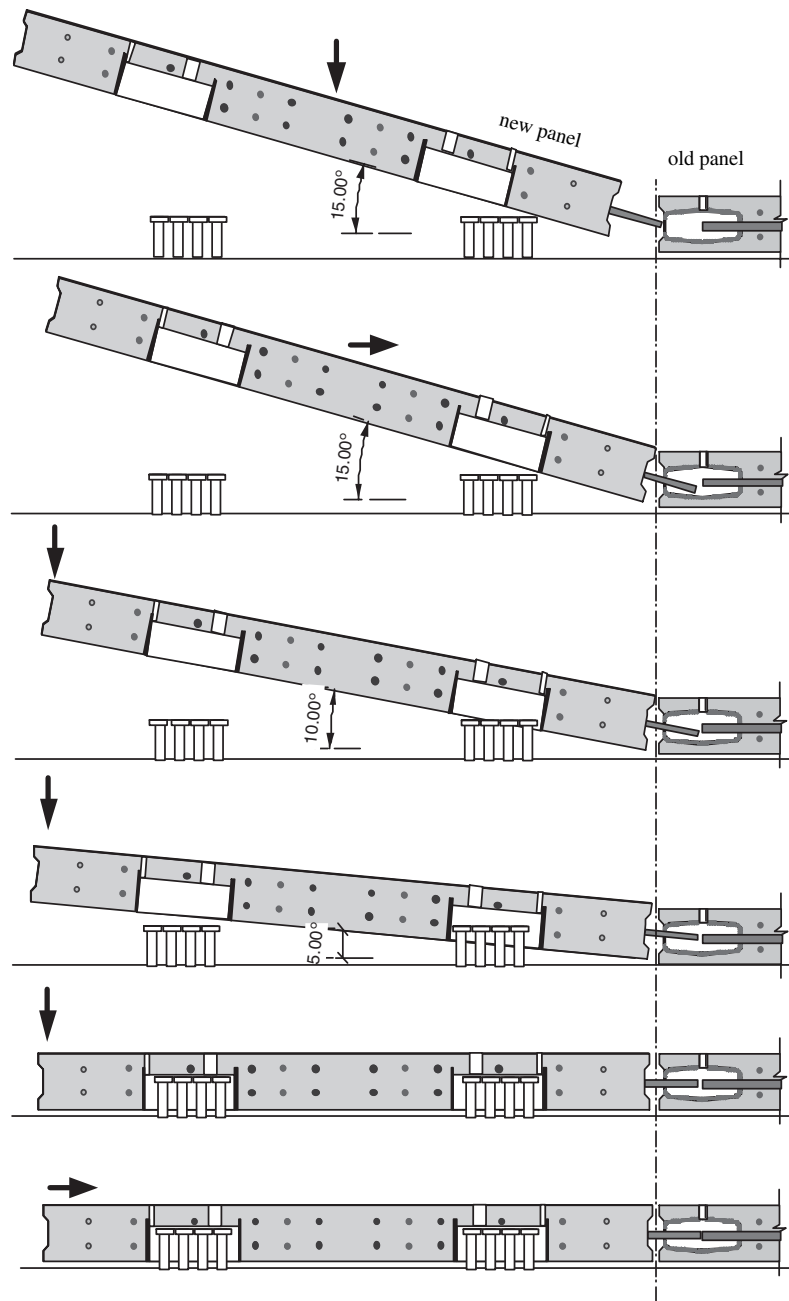


Figure 23. CD-1A, installation of a new panel.

Figure 29 shows the recommended detail for the panel-to-barrier connection. A closed pin bar is cast in the panel and extended outside the top surface of the panel. The bar's size and spacing depend on the barrier's design. The top surface of the panel at the interface between the barrier and the panel is intentionally roughened to enhance the bond capacity.

The transverse edges of the panel are provided with a vertical shear key. The dimensions of the shear key are designed to guarantee full transfer of wheel loads from one side of the joint to the other. The modified shear friction theory (36) is used to determine the vertical shear strength of the shear key

joint. The theory depends on depicting possible modes of failure of the joint. The failure modes are shown in Figure 30 and are described below.

Bearing failure at side *bc* of the shear key

$$P_u \leq \phi(0.85f'_c)(12 * L_{bc}) \text{ kip/ft} \quad (1)$$

where

ϕ = strength reduction factor for bearing = 0.7 (Section 5.5.4.2.1, AASHTO LRFD Bridge Design Specifications [7]),

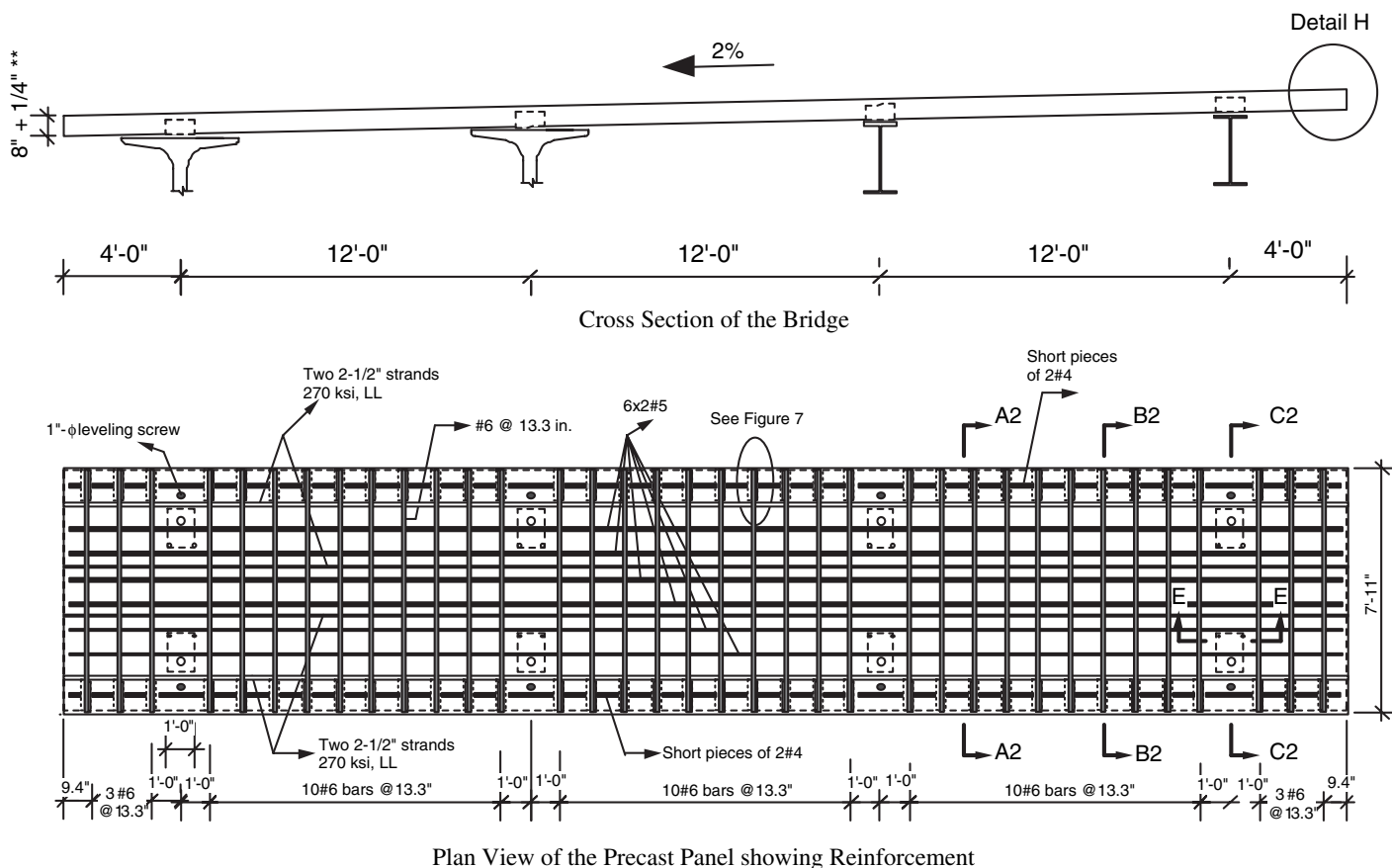


Figure 24. Cross section and plan view of CD-1B (1/4 in. is used a sacrificial layer for texturing).**

f'_c = specified concrete strength of the precast panel or the grout material, whichever is smaller, = 6.0 ksi.

L_{bc} = length of the side bc of the shear key = 1.06 in., and

P_u = factored wheel load with dynamic allowance, calculated in kip per linear foot in the transverse direction.

$$P_u \leq (0.7 \times 0.85 \times 6.0 \times 12 \times 1.06) = 45.4 \text{ kip/ft}$$

Shear failure along line be inside the grout filling the shear key

$$P_u \leq \phi (c * 12 * L_{be} + \mu A_v f_y) \text{ kip/ft} \quad (2)$$

where

ϕ = strength reduction factor for shear = 0.9 (Section 5.5.4.2.1, *AASHTO LRFD Bridge Design Specifications*),

c = cohesion strength of the grout material = 0.15 ksi for concrete cast monolithically (Section 5.8.4.2, *AASHTO LRFD Bridge Design Specifications*),

L_{be} = length of the distance from b to e = 5.0 in.,

μ = friction coefficient of the grout material = 1.4 for concrete cast monolithically (Section 5.8.4.2, *AASHTO LRFD Bridge Design Specifications*),

A_v = longitudinal reinforcement crossing the shear interface per foot = $0.44 \times 12 / 13.3 = 0.397 \text{ in}^2/\text{ft}$,

f_y = yield strength of the longitudinal reinforcement = 60 ksi, and

P_u = factored wheel load with dynamic allowance, calculated in kip per linear foot in the transverse direction.

$$P_u \leq 0.9 (0.15 \times 12 \times 5 + 1.4 \times 0.397 \times 60) = 38.1 \text{ kip/ft}$$

Therefore, $P_u = 38.1 \text{ kip/ft}$ (556 kN/m).

According to Section C3.6.1.2.5 of the LRFD specifications (7), which provides guidelines for determining the tire contact area of the design truck of the HL-93 live load, the width of the contact area in inches = $P/0.8$, where P = design wheel load in kip = 16 kip.

Therefore, the width of the contact area = $(16/0.8) = 20 \text{ in.}$

The applied factored wheel load = P (load factor for live loads) (dynamic load allowance, IM)

$$= 16 \times 1.75 \times 1.33 = 37.24 \text{ kip/20 in.}$$

$$= 22.3 \text{ kip/ft} (325 \text{ kN/m}) < 38.1 \text{ kip/ft} (556 \text{ kN/m})$$

Recommended System CD-2

The empirical design method given in Section 9.7.2.4 of the LRFD specifications (7) was used to design the required reinforcement. The LRFD specifications limit the use of the

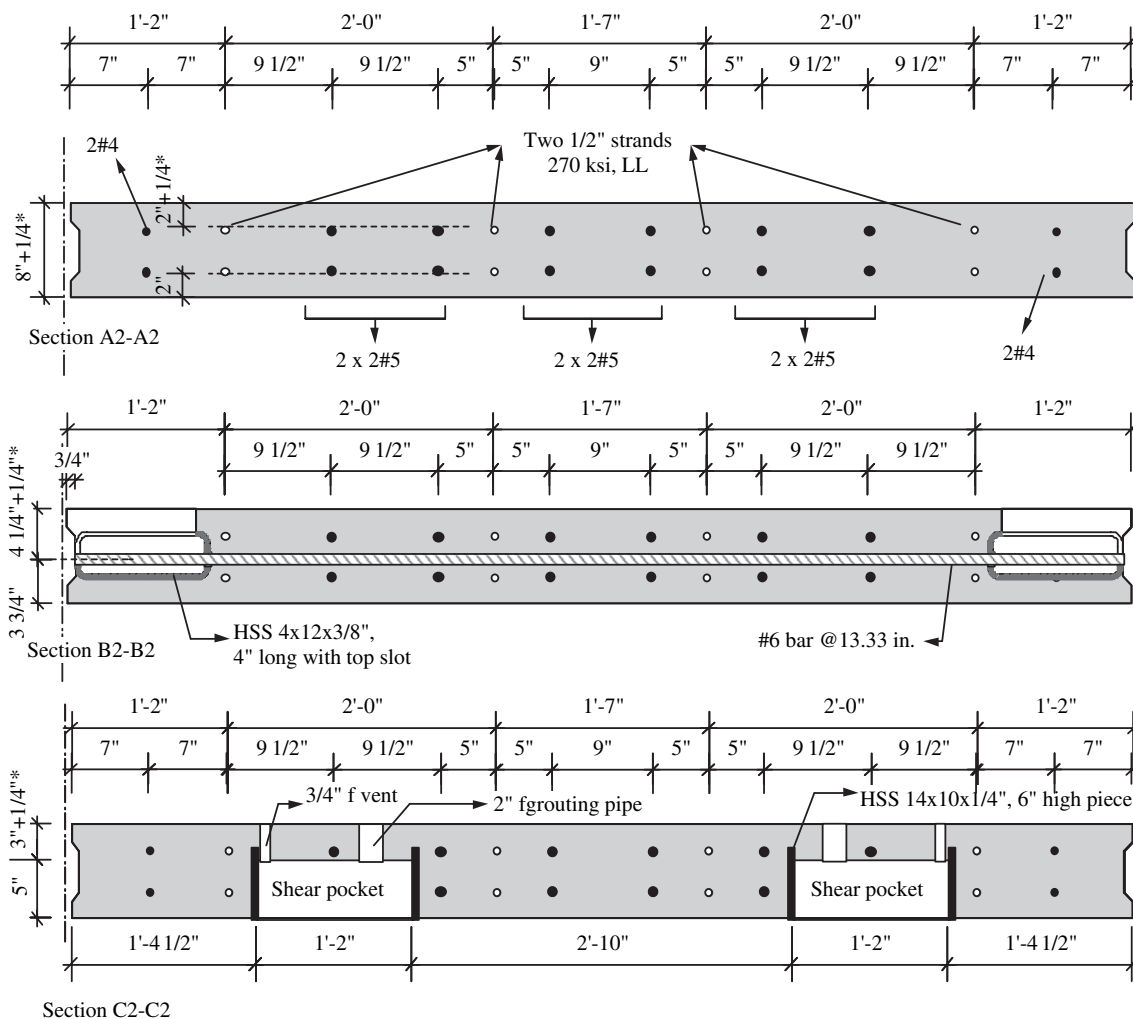


Figure 25. CD-1B, Sections A2-A2, B2-B2, and C2-C2 (* $\frac{1}{4}$ in. is used as a sacrificial layer for texturing).

empirical method to CIP slabs because all the validation tests for this design method were conducted on CIP slabs. The empirical method depends on the arching effect, where the bottom layer of transverse reinforcement acts as a tension tie to the concrete arch that is developed between adjacent girderlines.

The research team believes that this method can be equally applied to precast panel deck systems if the following conditions are satisfied: first, the arching effect is successfully developed by anchoring the bottom layer of transverse reinforcement at the girderlines to make it able to fully develop its yield strength, and second, the transverse panel-to-panel joints are constructed to simulate monolithic CIP slabs by splicing the longitudinal reinforcement of the precast panels.

The empirical design method requires any section of the slab between the exterior girders to have a top and bottom mesh. Each mesh is made of two layers of reinforcement. The amount of reinforcement required for each layer of the top

mesh = $0.18 \text{ in}^2/\text{ft}$ ($381 \text{ mm}^2/\text{m}$), and the amount of reinforcement required for each layer of the bottom mesh = $0.27 \text{ in}^2/\text{ft}$ ($572 \text{ mm}^2/\text{m}$). Maximum spacing of reinforcement in any layer = 18 in. (457 mm), and the minimum thickness of the slab = 7.0 in. (178 mm).

The recommended system CD-2 is made of an $8\frac{1}{4}$ in. (210 mm) thick solid panel. The top $\frac{1}{4}$ in. (6 mm) of the panel thickness is used as a sacrificial layer for texturing the top surface of slab. Texturing is executed by machine grinding after the panels are installed and grouted. The texturing process helps to maintain a uniform elevation of the finished deck slab and provides a high-quality riding surface. Figures 31 to 35 provide details of the recommended system.

The precast panel has a partial depth continuous channel at the girderlines. The channel is covered with a 3 in. (76 mm) thick slab that houses the transverse top layer of reinforcement. After the precast panels are installed and their elevation is adjusted using leveling screws, the continuous channels are

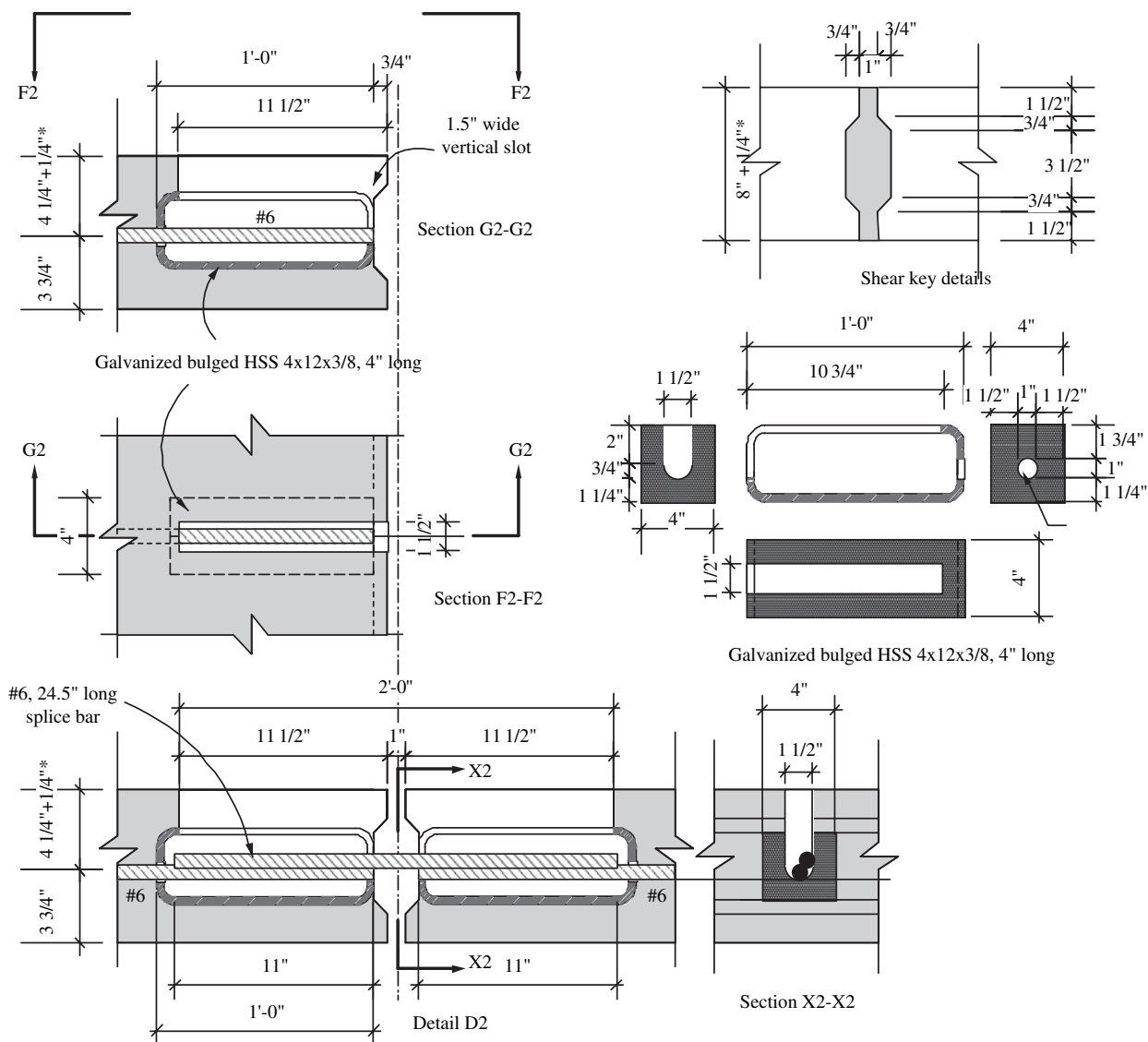


Figure 26. CD-1B, panel-to-panel connection detail, Detail D2 (* $\frac{1}{4}$ in. is used as a sacrificial layer for texturing).

filled with nonshrink grout through grouting pipes provided in the 3 in. slab.

The panel is reinforced with three layers of reinforcement—transverse top and bottom reinforcement layers and one longitudinal reinforcement layer provided near the mid height of the panel. The longitudinal layer combines the two longitudinal layers of reinforcement required by the empirical design method. The amount of reinforcement for these layers satisfies the reinforcement requirements of the empirical design method, as follows:

Top transverse layer between the exterior girders = 1 No. 6 @ 18 in. = $0.293 \text{ in}^2/\text{ft} > 0.18 \text{ in}^2/\text{ft}$

Bottom transverse layer between the exterior girders = 1 No. 6 @ 18 in. = $0.293 \text{ in}^2/\text{ft} > 0.27 \text{ in}^2/\text{ft}$

To fit the 18 in. spacing between the transverse bars, the panel is made 9 ft long.

Longitudinal layer of reinforcement = 1 No. 8 Grade 60 steel with 4 in. long threaded ends @ 15 in. = $0.601 \times 12/15 = 0.481 \text{ in}^2/\text{ft} > (0.18 + 0.27) = 0.45 \text{ in}^2/\text{ft}$

The longitudinal No. 8 (25) bars are spliced using HSS $8 \times 4 \times \frac{3}{16}$ in. ($203 \times 102 \times 5$ mm), $3\frac{1}{2}$ in. (89 mm) long cut, Grade 36 tubes, and heavy-duty nuts, as shown in Figure 33. The HSS tube is installed in 10×6 in. (254×152 mm) prefabricated pockets located on one transverse edge of the panel. The No. 8 bars extend about 4 in. (102 mm) inside the pocket and about 4 in. outside the other transverse edge of the panel. The panel to be installed is vertically lowered and then it is moved horizontally until the No. 8 bars are inserted

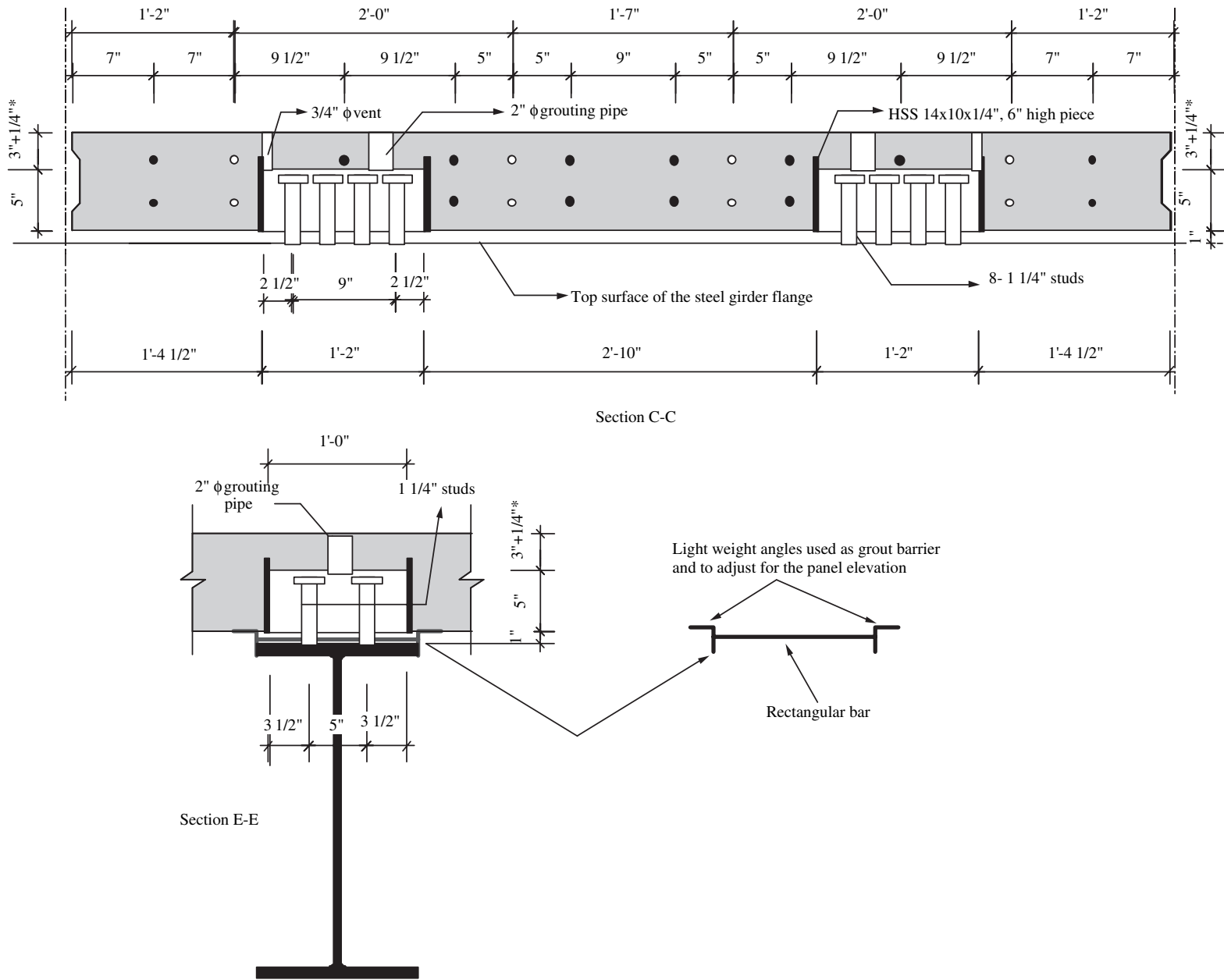


Figure 27. Sections C-C and E-E for steel girders (*1/4 in. is used as a sacrificial layer for texturing).

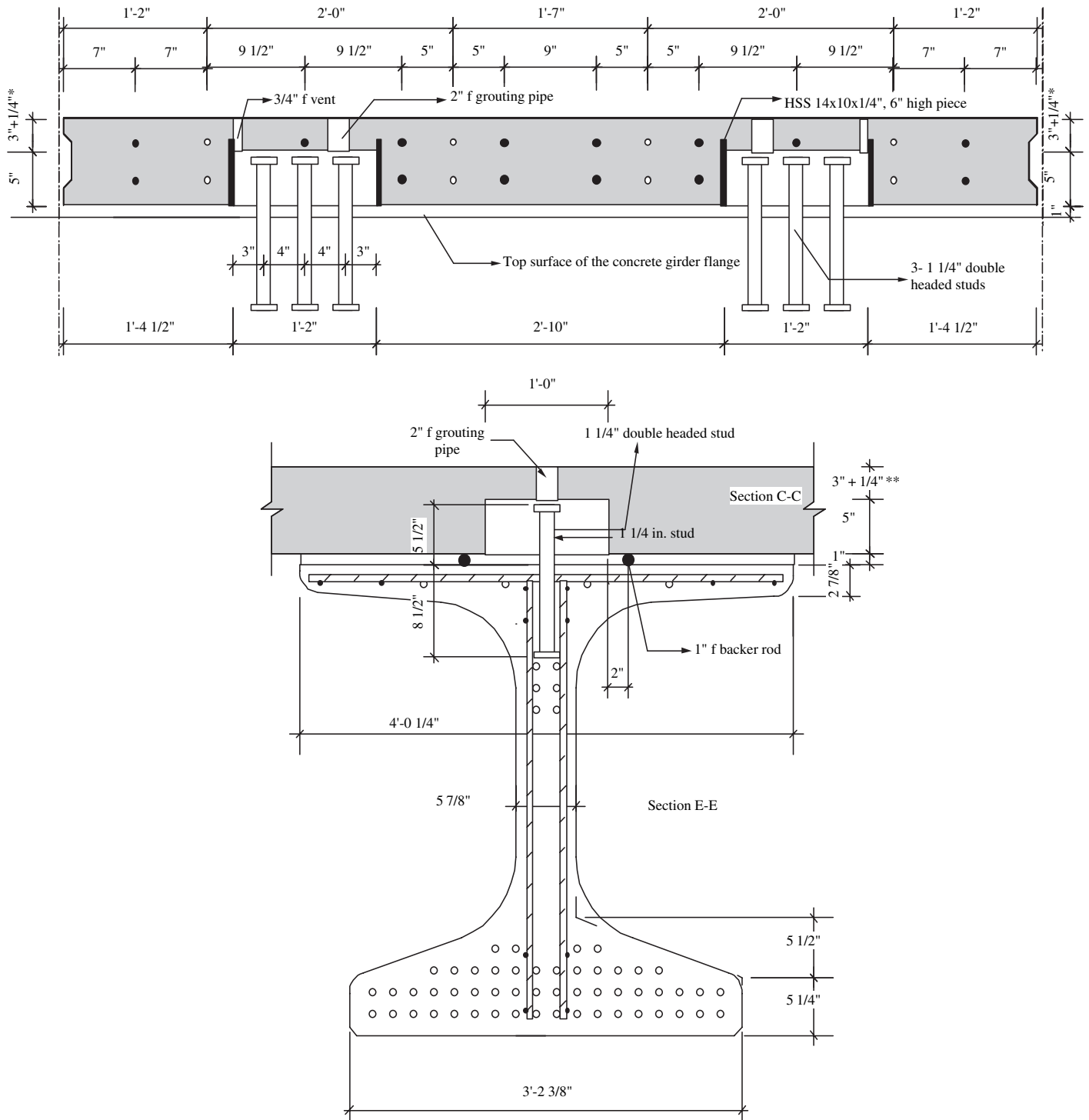


Figure 28. Sections C-C and E-E for concrete girders (*1/4-in. is used as a sacrificial layer for texturing).

in the HSS tubes. The thickness of the HSS tube is designed to provide 125% or more of the yield capacity of the No. 8 bar, as follows:

Yield capacity of the No. 8, Grade 60, with threaded ends = $0.601 \times 60 = 36.1 \text{ kip (161 kN)}$
 Yield capacity of the 3/16 in. thick HSS

$$= 2 \times \frac{3}{16} \times 3 \frac{1}{2} \times 36 = 47.5 \text{ kip} > 125\%(36.1) = 45.1 \text{ kip}$$

$$(201 \text{ kN}) > 36.1 \text{ kip (161 kN)}$$

If the bridge owner requires corrosion protection measures to be used for the deck reinforcement, the top and bottom transverse reinforcement layers can be made of epoxy-coated

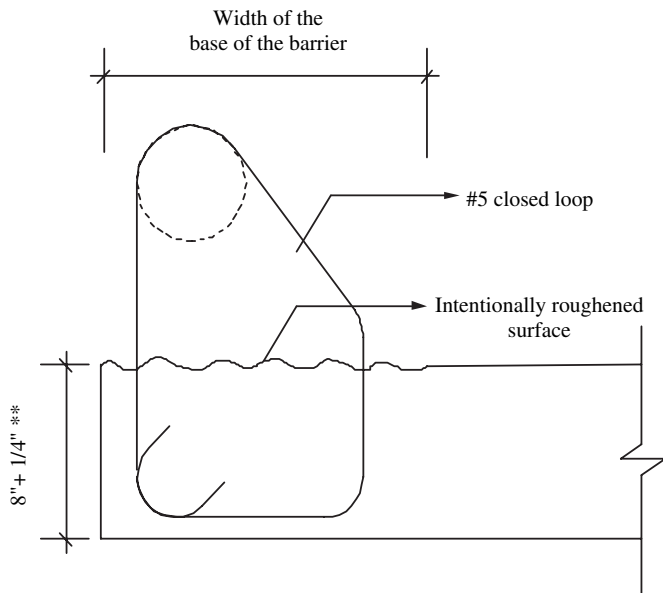


Figure 29. Detail H, panel-to-barrier connection detail (1/4-in. is used as a sacrificial layer for texturing).**

reinforcement, while the longitudinal reinforcement layer with the coupling accessories can be made of galvanized steel.

The transverse edges of the precast panels are provided with a female shear key. The dimensions of the shear key are identical to those with CD-1. Using the modified shear friction theory (36) shown in CD-1, it can be seen that the shear key detail with No. 8 bars at 15 in. (381 mm) has enough capacity to transfer the weight of the HL-93 design load.

The empirical design method does not apply to the overhanging part of the slab. It is thus necessary to design the overhang for collision effects. The design calculations of the overhang are provided in Appendix B of this report.

It is also important to check the stresses in the bottom layer of reinforcement—six No. 6 (19) bars at the girderline locations—during shipping and handling. If the panel is lifted at the girderline locations (the continuous blockout channels),

this area will be in negative moment. The compression force of this moment will be carried by the bottom six No. 6 bars, and the tension force will be carried by the top six No. 6 and top 12 No. 8 bars. The bottom six No. 6 bars need to be checked against buckling, as follows:

$$\begin{aligned} \text{Panel weight} &= (8/12)(0.150)(9) = 0.9 \text{ kip/ft} \\ \text{Negative moment} &= (0.9)(12^2)/(10) = 12.96 \text{ kip/ft} \\ \text{Tension force} &= (12.96 \times 12)/(4.25) = 36.6 \text{ kip (distributed} \\ &\quad \text{on six No. 6 bars)} \\ &= 36.6/6 = 6.1 \text{ kip/bar} = 6.1/0.44 = 13.9 \text{ ksi} \end{aligned}$$

Allowable stress of No. 6 bar, $F_a =$

$$F_y \frac{\left[1 - \frac{1}{2} \left(\frac{Kl/r}{C_c} \right)^2 \right]}{\left[\frac{5}{3} + \frac{3}{8} \left(\frac{Kl/r}{C_c} \right) - \frac{1}{8} \left(\frac{Kl/r}{C_c} \right)^3 \right]}, \frac{Kl/r}{C_c} \leq 1.0, C_c = \sqrt{\frac{2\pi^2 E_s}{F_y}}$$

where

- E_s = modulus of elasticity of the bar = 29,000 ksi
- F_y = yield strength of the bar = 60 ksi
- Kl = effective buckling length of the bar = 1.0×12 in. = 12 in.
- r = radius of gyration of the bar = $0.25 \times$ the bar diameter

$$C_c = \sqrt{\frac{2\pi^2(29,000)}{60}} = 97.67$$

$$(Kl/r) = (12)/(0.25 \times 0.75) = 64.00$$

$$\left(\frac{Kl/r}{C_c} \right) = 0.655 < 1.0$$

$$F_a = 25.1 \text{ ksi} > 13.9 \text{ ksi (safe)}$$

Panel to Panel Connection

Development of the panel-to-panel connection details, which were used in the recommended systems CD-1A and CD-1B, was achieved using the following approach:

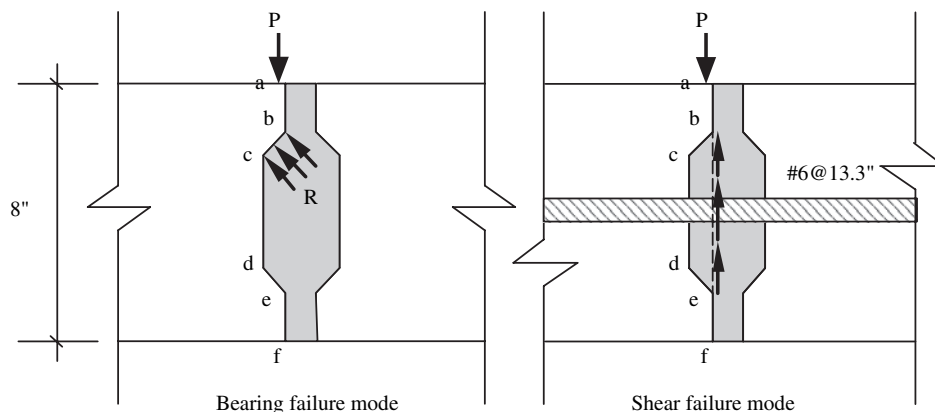


Figure 30. Design parameters of the shear key.

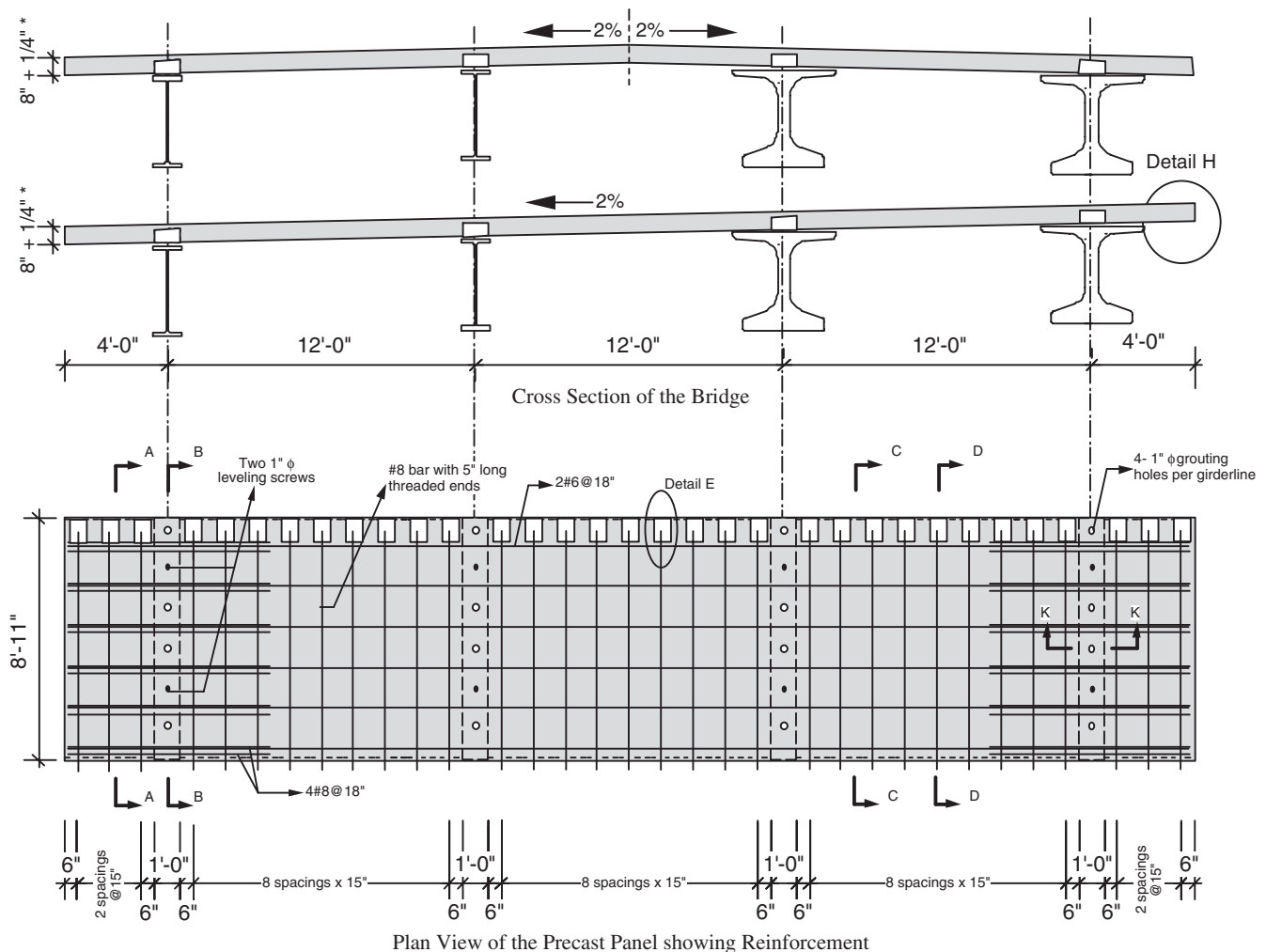


Figure 31. Cross section and plan view of CD-2 (* $\frac{1}{4}$ in. is used as a sacrificial layer for texturing).

- Investigation and Review of Grout Materials Available in the Market—This investigation was conducted to decide on the type of grout material to be used in the experimental investigation.
- Group 1 Specimens—Initially, four connection details were developed and tested in direct tension using 16 pull-out specimens. In these details, an HSS tube is used to confine the grout surrounding the spliced bars. Confinement typically increases the grout strength, resulting in a significant reduction in the length required to fully develop the yield strength of the bar. Based on the experimental results of these specimens, the top three successful connection details were considered in the next step.
- Group 2 Specimens—Nine pullout specimens, representing the top three successful details of Group 1, were fabricated and tested in direct tension to confirm the experimental results obtained in Group 1. Based on the experimental results, two connection details were chosen as the final connection details used in the development of the recommended systems CD-1A and CD-1B.
- Full-Scale Bridge Specimen—After the recommended systems CD-1A and CD-1B were developed, a full-scale bridge specimen made of three precast panels and utilizing the candidate connection details was fabricated and tested for 2,000,000 cycles of fatigue load.

Investigation of Various Grout Materials

To determine what type of grout material should be used in the experimental investigation, the research team reviewed the specifications of many grout materials commercially available in the market. The products chosen in the review process were selected based on the results of the literature review and national survey. Table 2 compares some of the products that were considered in the review process. To choose the grout material that will be used in the entire experimental program, the research team set the following criteria: (a) nonshrink grout, (b) 6 ksi (41.4MPa) compressive strength at 1 day, (c) not reactive with steel, (d) high flowability, and (e) can be mixed with pea gravel to increase the yield volume.

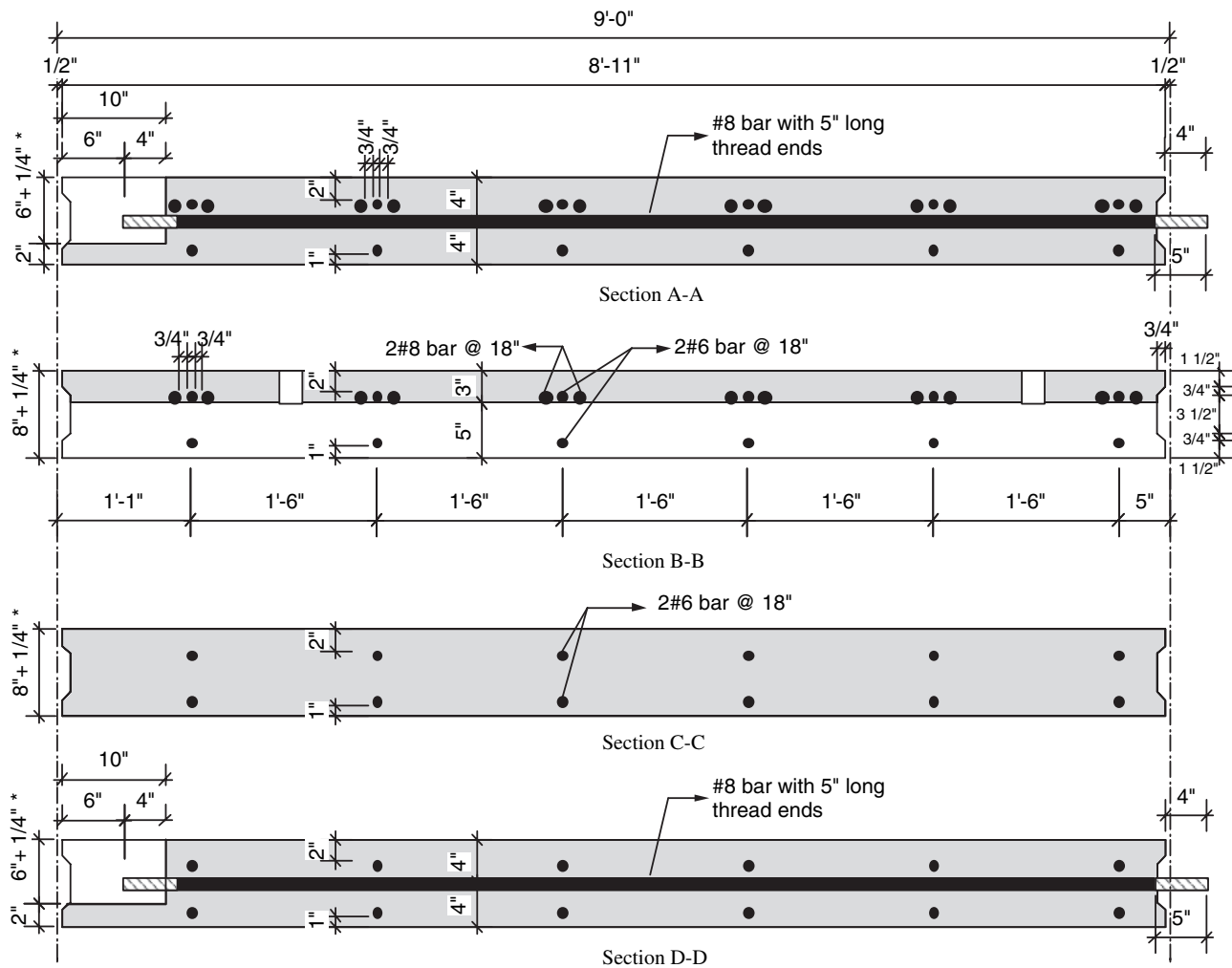


Figure 32. CD-2, Sections A-A and B-B (* $\frac{1}{4}$ in. is used as a sacrificial layer for texturing).

The research team decided to use SS Mortar for the experimental investigation of the connection details. This decision was based on the fact that SS Mortar is exclusively designed for splice connections where steel tubes are used to confine reinforcing bars, which is the case with the new connection details developed for CD-1A and CD-1B, where HSS tubes are used. In addition, SS Mortar has a relatively high flowability, which helps in filling tight connection details.

The research team monitored the compressive strength gain of $2 \times 2 \times 2$ in. ($51 \times 51 \times 51$ mm) SS Mortar cubes over a period of 28 days. It was found that the early-age compressive strength measured by the research team was higher than that given by the manufacturer. The SS Mortar was able to reach a compressive strength of 6.0 ksi in less than 1 day, which makes this type of grout suitable for use in weekend construction projects. However, the 28-day compressive strength measured by the research team was less than that specified by the manufacturer, as shown in Figure 36, but it was higher than the target compressive strength specified by the research team for use with the recommended systems (6.0 ksi [41 MPa]). No shrink-

age cracks were observed in either the SS Mortar filling the tubes of the pullout specimens or the $2 \times 2 \times 2$ in. cubes.

Based on a discussion with the SS Mortar manufacturer on how to increase the yield volume of the mortar, a trial mix of SS Mortar and $\frac{1}{4}$ in. diameter pea gravel was made. The ratio of pea gravel to SS Mortar was 1 to 2 by weight. The trial mix was placed in 4×8 in. cylinders to monitor the compressive strength gain with time, as shown in Figure 36. SS Mortar with 50% pea gravel showed slightly slower gain of compressive strength than the SS Mortar without pea gravel. However, both mixes reached almost the same compressive strength at 28 days. Pure SS Mortar, with no pea gravel, was used for the pullout specimens.

Group 1: Direct Tensile Test of Four Connection Details

Sixteen pullout specimens were fabricated and tested. The following variables were considered in making the 16 specimens:

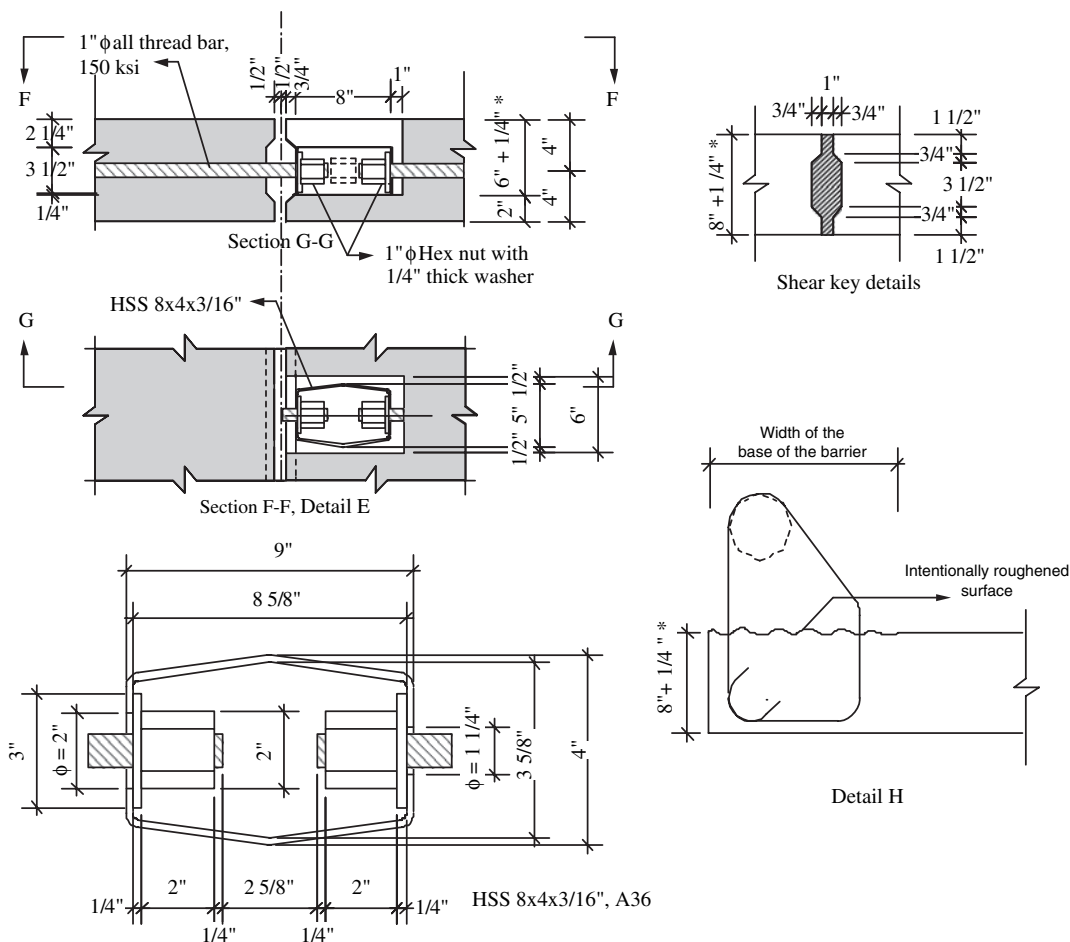


Figure 33. CD-2, Details E and H (* $\frac{1}{4}$ in. is used as a sacrificial layer for texturing).

- Size of the HSS Tube. Two sizes were used—HSS $3 \times 12 \times \frac{1}{4}$ in. ($76 \times 305 \times 6$ mm) and HSS $4 \times 12 \times \frac{3}{8}$ in. ($102 \times 305 \times 10$ mm). For both sizes, a 4 in. (102 mm) long strip was used. These sizes were chosen because they fit the 8 in. (203 mm) thickness of the panel, while satisfying the minimum top and bottom concrete cover for reinforcement in deck slabs as specified by the AASHTO LRFD specifications (7), and because they are commercially available from many producers.
- Size of Spliced Bar. Two bar sizes were considered—No. 6 (Metric No. 19) and No. 7 (22), Grade 60 (414 MPa) uncoated.
- Connection Details.
 - Detail A—A bulged HSS tube with two side holes. The spliced bars were embedded for 6 in. (152 mm) inside the tube, but they were not overlapped. The purpose of bulging the tube was to increase the volume of grout that is confined within the tube and optimize the required development length.
 - Detail B—A straight HSS tube with a 12 in. (305 mm) long slot located on the top surface of the tube. The developed bars were embedded 11 in. (279 mm) inside the tube, and they overlapped each other.
 - Detail C—A straight HSS tube with a side slot. The developed bars were embedded for 6 in. (152 mm) inside the tube, but set head to head. This detail was similar to Detail A except that the tube had no bulge.
 - Detail D—A bulged HSS tube with a 6 in. (152 mm) long slot on the top surface of the tube. The spliced bars were embedded for 6 in. (152 mm) inside the tubes and set head to head.

Table 3 shows the design criteria of the 16 pullout specimens, and Figure 37 shows the details of the test specimens. Each HSS tube was embedded in an $8 \times 12 \times 24$ in. ($203 \times 305 \times 610$ mm) concrete prism, and the concrete prism was reinforced with two No. 4 (13) top bars and two No. 5 (16) bottom bars. This amount of reinforcement was chosen to simulate the reinforcement required by the empirical design method given by the AASHTO LRFD specifications (7). The tube was set flush with one face of the concrete prism, and one of the two developed bars was embedded in the prism and extended inside the HSS tube to represent the longitudinal reinforcement of the panel. This bar was extended outside the concrete prism from the other side so it could be hooked

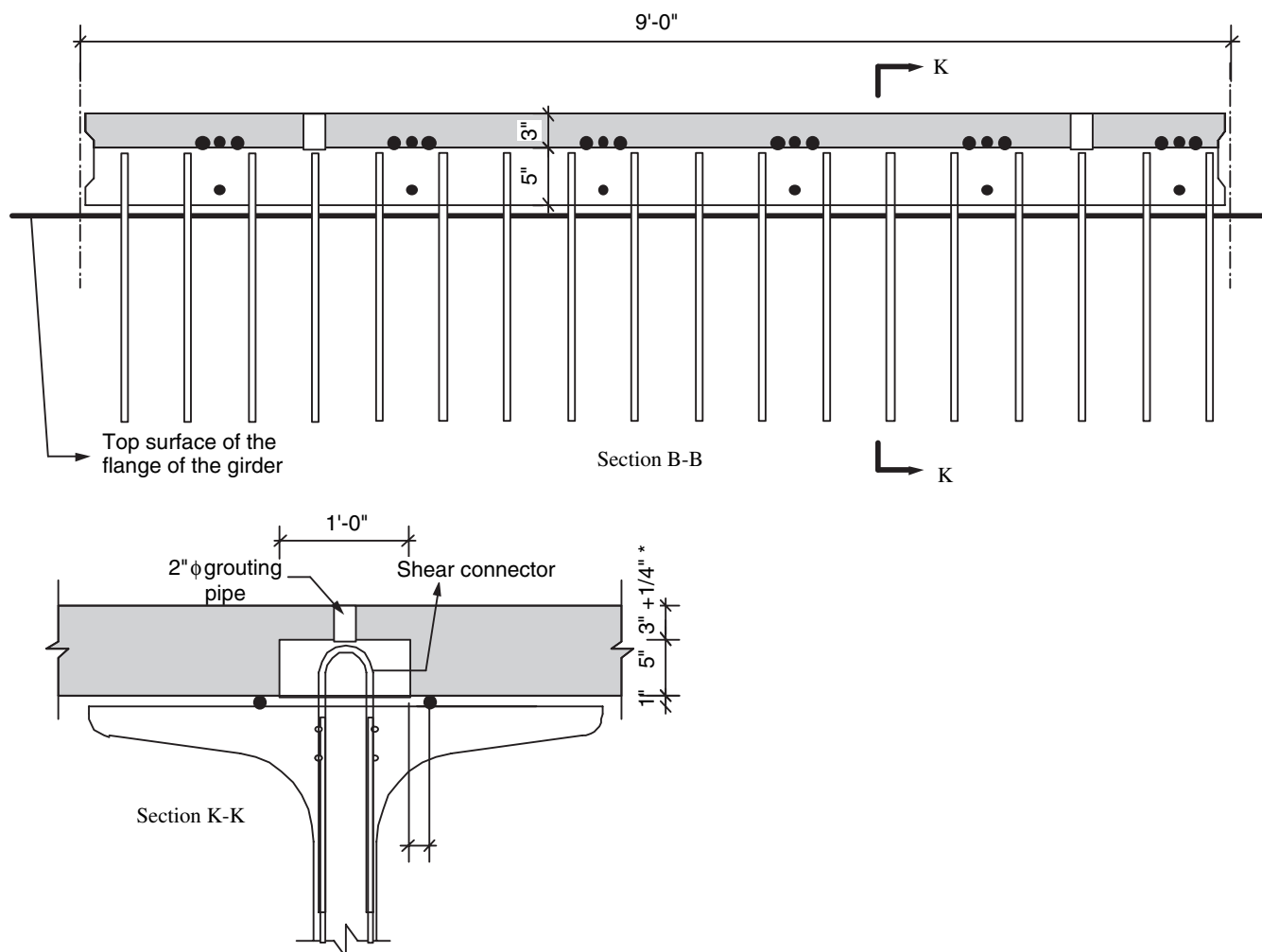


Figure 35. CD-2, Sections B-B and K-K for precast concrete girders (* $\frac{1}{4}$ in. is used as a sacrificial layer for texturing).

tube in the next step of investigation. Although the small-size HSS $3 \times 12 \times \frac{1}{4}$ in. ($76 \times 305 \times 6$ mm) tube showed almost the same structural behavior as, and developed a bar strength similar to that developed with, the HSS $4 \times 12 \times \frac{3}{8}$ in. ($102 \times 305 \times 10$ mm) tubes were used. The connection details considered in this group were as follows (see Figure 37):

Group 2: Direct Tensile Test of Selected Connection Details

In this group, nine pullout specimens were tested, representing three connection details and three specimens per detail. In all specimens, No. 6 (19) bars and HSS $4 \times 12 \times \frac{3}{8}$ in. ($102 \times 305 \times 10$ mm) tubes were used. The connection details considered in this group were as follows (see Figure 37):

- Detail A—Same as Detail A of Group 1.
- Detail BB—Same as Detail B of Group 1 except that the slot on the top surface of the HSS tube was open all the way

to the top surface of the concrete prism. This change was made to simulate the connection detail that would be used later on the recommended system CD-1B.

- Detail AA—Same as Detail A of Group 1 except that the HSS tube was not bulged. This detail was added to check the effect of bulging the HSS tube on the developed bar strength.

Table 4 shows the design criteria of the nine pullout specimens, and Figure 40 shows details of the specimens during fabrication. The concrete mix and grout material used for the specimens of Group 1 were used for the specimens of Group 2 (see Figure 36 for the compressive strength gain with age). The specimens were tested in direct tension when the concrete strength of the grout was about 6.5 ksi (44.82 MPa). At that time, the concrete strength of the prism was about 6.1 ksi (42.06 MPa).

Bar slippage failure occurred in all of the specimens, where the failure load is measured at the moment when the bar

Table 2. Comparison between various types of commercial grout material.

		Set 45	Set 45 HW	Construction Grout	SS Mortar	Masterflow 928	747 Rapid Setting Grout	S Grout	SonogROUT 10K
Description		Magnesium phosphate patching and repair mortar. It sets in 15 minutes.	Hot weather, magnesium phosphate patching and repair mortar	Noncatalyzed multi-purpose, mineral aggregate grout.	High-precision, high-strength, cement-based, metallic aggregate mortar. It is used for NMB splice sleeve splicing system.	High-precision, hydraulic-cement-based, mineral aggregate grout. Ideal for grouting machines or plates with precision load bearing support.	Nonmetallic cement-based grout. It is used wherever a rapid setting material is needed.	Shrinkage compensated, nonmetallic, cement-based grout. It is used for applications requiring strength and durability.	Shrinkage compensated, portland-cement-based, high-strength grout.
Composite strength (ksi)	1 hour	2.0 @ 72 ° F	–	–	–	–	–	–	–
	3 hours	5.0 @ 72 ° F	3.0 @ 95 ° F	–	–	–	–	–	–
	6 hours	5.0 @ 72 ° F 1.2 @ 36 ° F	5.0 @ 95 ° F	–	–	–	–	–	–
	1 day	6.0 @ 72 ° F 5.0 @ 36 ° F	6.0 @ 95 ° F	1.5	4.0 @ 70 ° F	7.5 @ 77 ° F	4.0	3.5 @ 77 ° F	1.6 @ 70 ° F
	3 days	7.0 @ 72 ° F 7.0 @ 36 ° F	7.0 @ 95 ° F	5.0	5.4 @ 70 ° F	8.2 @ 77 ° F	5.0	5.0 @ 77 ° F	3.8 @ 70 ° F
	7 days	–	–	6.0	7.0 @ 70 ° F	10.5 @ 77 ° F	–	6.0 @ 77 ° F	5.1 @ 70 ° F
	28 days	8.5 @ 72 ° F 8.5 @ 36 ° F	8.5 @ 95 ° F	7.0	11.0 @ 70 ° F	12.6 @ 77 ° F	8.0	8.0 @ 77 ° F	6.2 @ 70 ° F
Features		- High early strength at 1 hour - Superior bonding - Very low drying shrinkage - Resistant to freeze/thaw, sulfate and deicing chemicals	- Superior bonding - Very low drying shrinkage - Resistant to freeze/thaw, sulfate and deicing chemicals	- Can be extended with pea gravel - Designed for the 50 °F to 90 °F range - Non rusting	- Nonshrink grout - High flowability, suitable for pumping in tight spaces - Can be used over wide range of temperature - Design for use with splice sleeve system	- Nonshrink grout - Resistant to freeze/thaw & sulfates - High flowability, suitable for pumping in tight spaces - Designed for the 40 °F to 90 °F range	- Nonshrink grout - High early strength at 1 day - Chloride free - Nonrusting - Not recommended for placing below 35 °F	- Recommended for shear key grouting - Can be extended by adding pea gravel - High flowability	- Cannot be extended by adding gravel - Shrinkage compensated grout
Yield (ft ³ /bag)		0.39 w/o gravel 0.58 w 60% gravel	0.39 w/o gravel 0.58 w 60% gravel	0.45 w/o gravel	0.42 w/o pea gravel	0.50 w/o pea gravel	–	0.5 w/o gravel 0.6 w 27% gravel 0.69 w 55% gravel	0.40

Source: manufacturers' literature.

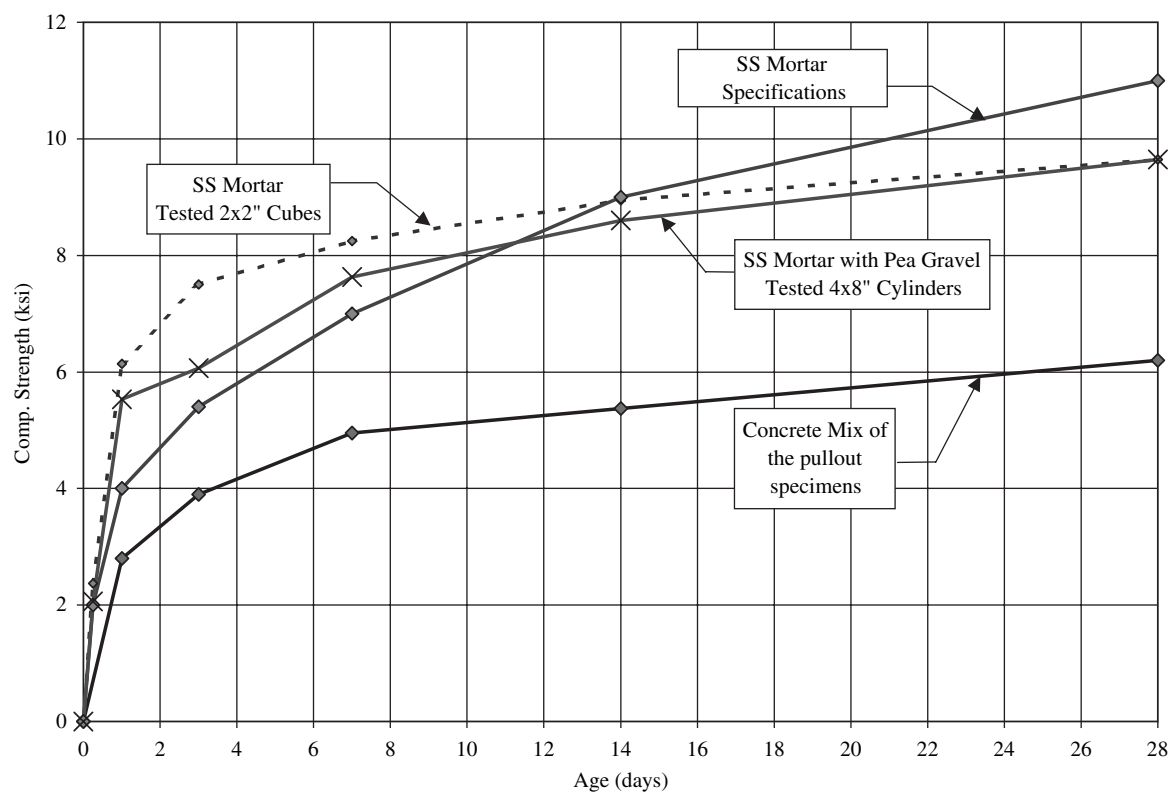


Figure 36. Compressive strength versus time for SS Mortar and concrete mix.

started to slip away from the concrete prism, as shown in Figure 41 Specimen A. This moment was identified when a sudden drop of the applied load is observed on the load gauge of the testing machine. For the specimens made with Detail BB (i.e., specimens with a top slot), cracks between the grout filling the slot and the specimen were observed very close to the failure load, as shown in Figure 41 Specimen BB. The failure load and the equivalent developed bar strength are given in Table 4. The following conclusions were drawn from the experimental program of the pullout specimens.

- All of the connection details tested with No. 6 (19) spliced bars were able to develop a bar strength equal to or greater than 125% of the 60 ksi (413.7 MPa) yield design strength, which is consistent with the requirement of Section 5.11.5.2.2 of the AASHTO LRFD specifications (7).
- Connection Detail AA made with straight tubes and no slots showed about a 5% increase in developed strength compared with connection details made with slotted tubes (Detail BB).
- Connection details made with bulged tubes and no slots (Detail A) showed about a 10% increase in developed strength compared with connection details made with straight tubes (Detail AA).

Based on the test results of this group, connection Details A and BB were considered in the development of the recommended systems CD-1A and CD-1B.

Full-Scale Bridge Specimen

After connection Details A and BB were used to develop the recommended systems CD-1A and CD-1B, respectively, the structural behavior of these connections as a result of fatigue flexural loading was investigated. The experimental investigation was conducted by building a full-scale bridge specimen. The bridge was made of a concrete deck measuring 20 ft (6.1 m) wide, 24 ft (7.31 m) long, and 8 in. (203 mm) thick and supported by two W18 × 119 steel beams. The steel beams were set 12 ft (3.66 m) on center. The concrete deck was made of three precast concrete panels, each 20 ft (6.10 m) wide by 8 ft (2.44 m) long. The design and details of these panels were according to the recommended system CD-1. The panel-to-panel connection details, Details A and BB, were used on these panels as follows:

- Panel P1—Detail A was used on the north and south transverse joints.
- Panel P2—Detail A was used on the north transverse joint, and Detail BB was used on the south transverse joint.
- Panel P3—Detail BB was used on the north and south transverse joints.

Table 3. Design criteria and test results of the pullout specimens (Group 1).

Connection Detail	Size of HSS Tube (in.)	Type of Slot NS = No Slot TS = Top Slot SS = Side Slot	Straight (S) or Bulged (B) Tube	Size of Bar	Embedment Length (in.)	Mode of Failure	Failure Load (kip)	Developed Bar Strength, f_d (ksi)	$\frac{f_d}{60}$ %	
A	1	HSS 4x12x3/8	NS	B	No. 6	6" head-to-head	Prism	37.7	85.3	142% ✓
	2	HSS 4x12x3/8	NS	B	No. 7	6" head-to-head	Bar Slip	43.4	72.2	120% ✓
	3	HSS 3x12x¼	NS	B	No. 6	6" head-to-head	Bar Slip	32.8	74.2	124%
	4	HSS 3x12x¼	NS	B	No. 7	6" head-to-head	Bar Slip	45.2	75.2	125%
B	1	HSS 4x12x3/8	12"-TS	S	No. 6	12" overlapped	Prism	36.0	81.5	136% ✓
	2	HSS 4x12x3/8	12"-TS	S	No. 7	12" overlapped	Prism	40.9	68.0	113% ✓
	3	HSS 3x12x¼	12"-TS	S	No. 6	12" overlapped	Prism	37.0	83.8	140%
	4	HSS 3x12x¼	12"-TS	S	No. 7	12" overlapped	Prism	40.3	67.0	112%
C	1	HSS 4x12x3/8	SS	S	No. 6	6" head-to-head	Bar slip	23.3	52.7	88%
	2	HSS 4x12x3/8	SS	S	No. 7	6" head-to-head	Bar slip	34.6	57.5	87%
	3	HSS 3x12x¼	SS	S	No. 6	6" head-to-head	Bar slip	34.4	77.8	130%
	4	HSS 3x12x¼	SS	S	No. 7	6" head-to-head	Bar slip	30.0	49.9	83%
D	1	HSS 4x12x3/8	6"-TS	B	No. 6	6" head-to-head	Bar slip	35.5	80.4	134%
	2	HSS 4x12x3/8	6"-TS	B	No. 7	6" head-to-head	Prism	24.1	40.0	67%
	3	HSS 3x12x¼	6"-TS	B	No. 6	6" head-to-head	Bar slip	28.5	64.5	108%
	4	HSS 3x12x¼	6"-TS	B	No. 7	6" head-to-head	Bar slip	30.5	50.7	85%

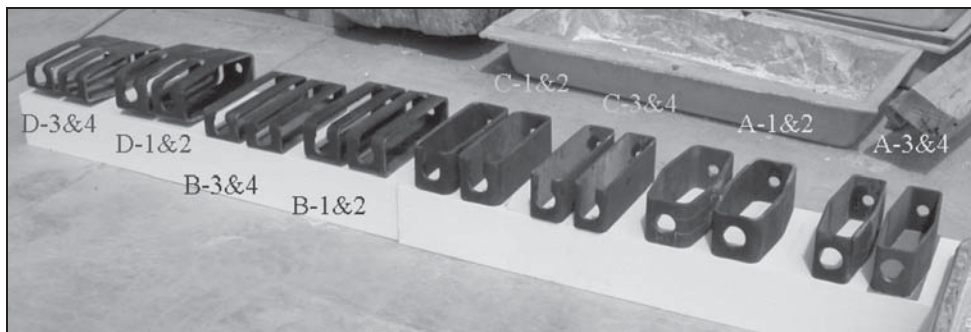
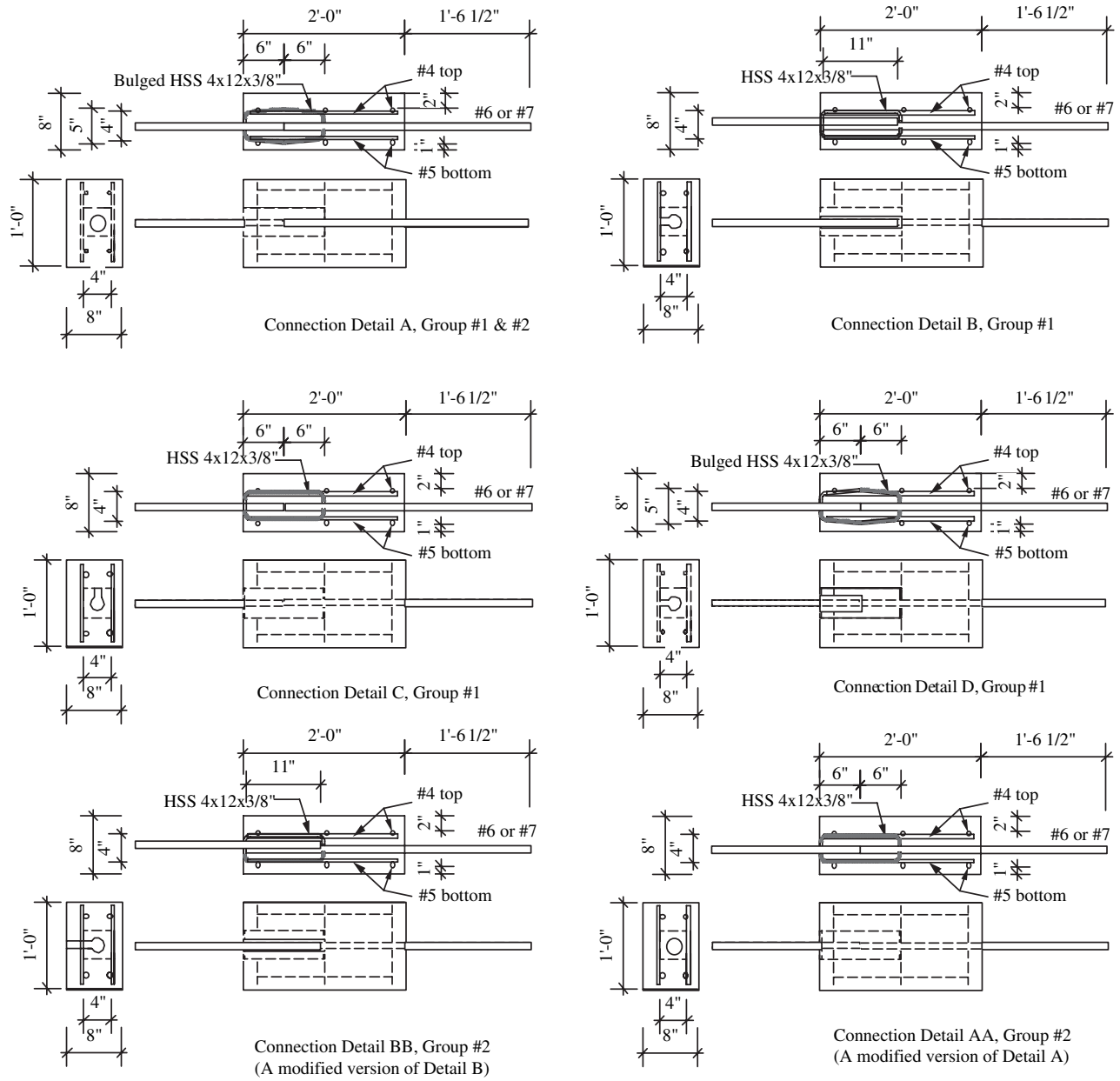


Figure 37. Details of the pullout specimens of Groups 1 and 2.

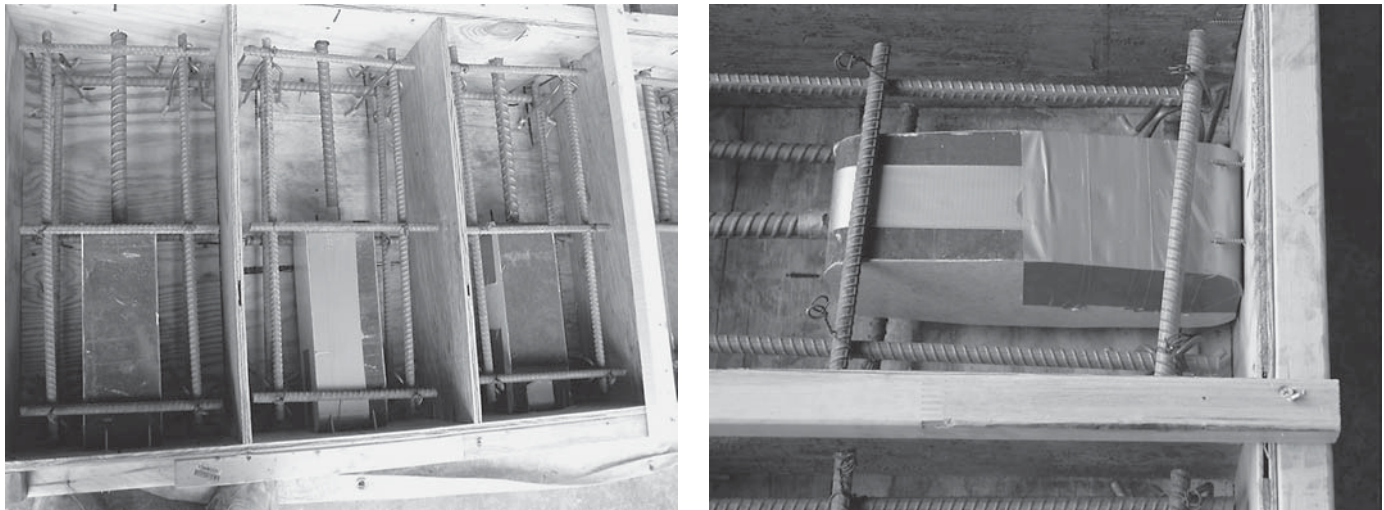
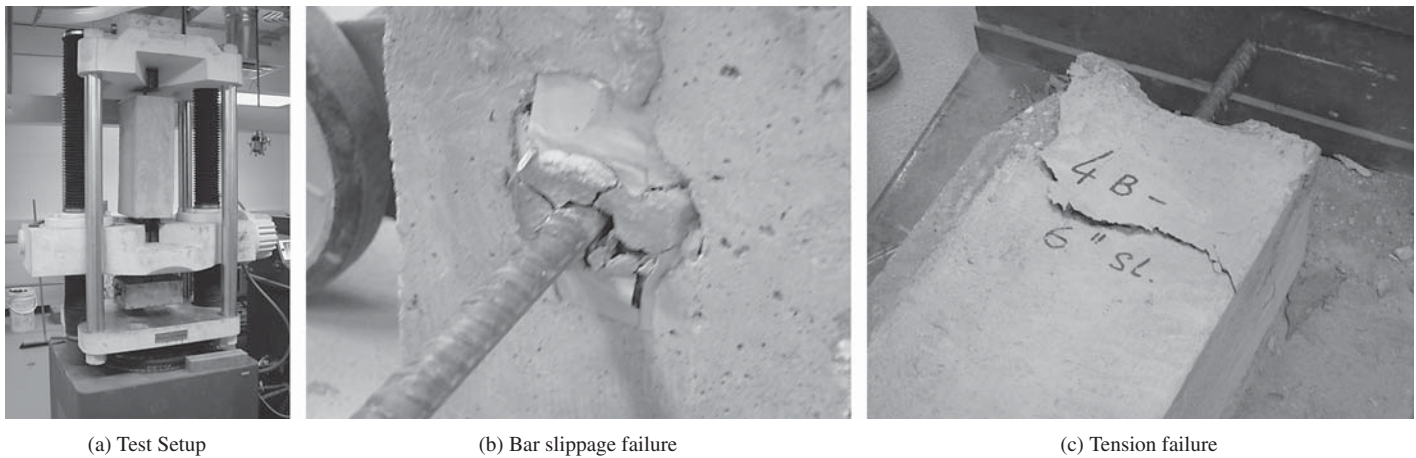


Figure 38. Specimens used in Group 1 during fabrication.



(a) Test Setup

(b) Bar slippage failure

(c) Tension failure

Figure 39. Test setup and failure modes of Group 1 specimens.

Table 4. Design criteria and test results of the pullout specimens (Group 2).

Connection Detail	Size of HSS Tube (in.)	Type of Slot	Straight (S) or Bulged (B) Tube	Size of Bar	Embedment Length (in.)	Mode of Failure	Failure Load (kip)	Developed Bar Strength, f_d (ksi)	$\frac{f_d}{60}$ %	
A	1 2 3	HSS 4x12x3/8	No slot	B	No. 6	6 in. head-to-head	Bar Slip	37.6	85.5	
							Bar Slip	34.2	77.8	
							Bar Slip	38.7	88.0	
	Average							83.8	139.7%	
BB	1 2 3	HSS 4x12x3/8	12 in. Top slot	S	No. 6	12 in. overlapped	Bar Slip	32.9	74.8	
							Bar Slip	32.9	74.8	
							Bar Slip	33.8	76.8	
	Average							75.5	125.8%	
AA	1 2 3	HSS 4x12x3/8	No slot	S	No. 6	6 in. head-to-head	Bar Slip	34.7	78.9	
							Bar Slip	32.9	74.8	
							Bar Slip	35.4	80.5	
	Average							78.0	130.0%	

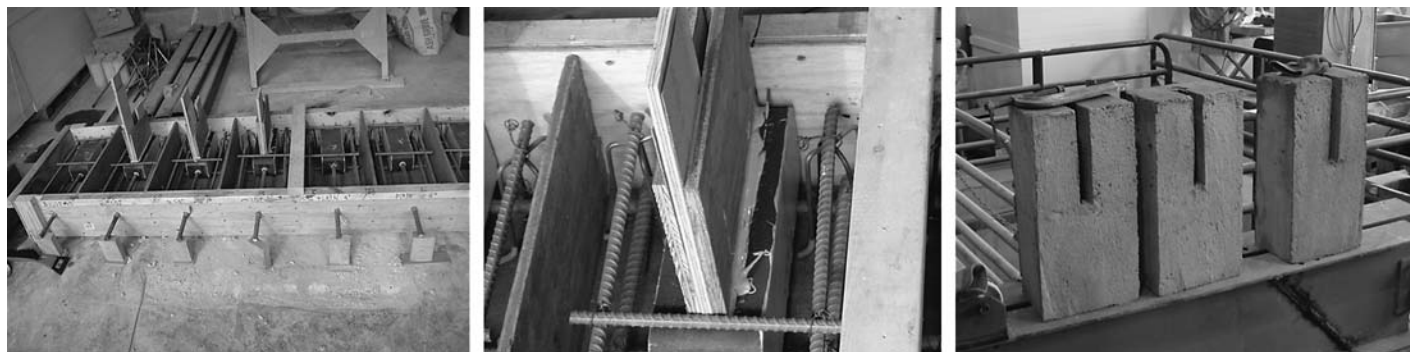


Figure 40. Specimens used in Group 2 during fabrication.

Figures 42 and 43 show details of the bridge specimen. Figures 44 and 45 show the precast panels during fabrication and after 7 days of moist curing. Top and bottom layers of the strands were initially tensioned to 205 ksi ($0.76 f_{pu}$), and concrete was cast on the next day of tensioning the strands. A normal weight concrete mix of 6.0 ksi specified compressive strength was used.

After the concrete was cast and consolidated, the panels were continuously moist cured for 7 days using wet burlap. Three days after the concrete was cast, the strands were released using a mechanical hydraulic system that allows gradual release of the tension force of the strands at one end of the bed. This technique of prestress release was used to protect the panels against cracking that could result from sudden release of the prestress force. The research team also used this technique during fabrication of similar precast panels (2, 3, 5, 6). No cracks were observed at the panel edges during or after the prestress release. No shrinkage cracking was observed on the top surface of the panel. Figure 46 shows the strength gain of the concrete mix with age. The curing process continued for 4 days after the strands were released, and the panels were kept exposed to the laboratory environment afterward, where the average temperature was about 80 °F in the morning and 70 °F at night and the average rela-

tive humidity was about 40% to 50%. Regular checking of the top and bottom surfaces of the panels at different ages did not reveal any shrinkage cracks.

Figure 47 shows the test setup, where a self-equilibrium frame was built at the transverse joint. The self-equilibrium frame consisted of a top and bottom beam connected together with four 2.0 in. diameter high-strength threaded rods. A 110 kip (489 kN) hydraulic actuator and a load spreader beam were used to apply the fatigue load. The spreader beam was supported by the precast panel at two points spaced at 6 ft (1.82 m) using two Neoprene pads measuring 9 × 22 in. (229 × 559 mm) each. The dimensions of the Neoprene pads were determined according to the LRFD specifications (7). The supports were positioned on one side of the transverse joint. This load arrangement simulated the center axle of an HS20 truck. The applied load fluctuated between 4.00 kip (17.8 kN) and 46.56 kip (207.1 kN). The 4 kip (17.8 kN) load was determined in order to maintain stability of the test setup, while the 42.56 kip (189.3 kN) difference between high and low loads was determined based on the weight of the center axle of the HS20 truck plus dynamic allowance, 32 kip × 1.33 = 42.56 kip (189.3 kN). The fatigue load was applied for 2,000,000 cycles at 2 cycles per second, as recommended by ASTM D6275 (37).



Specimen A

Specimen BB

Figure 41. Failure modes of Group 2 specimens.

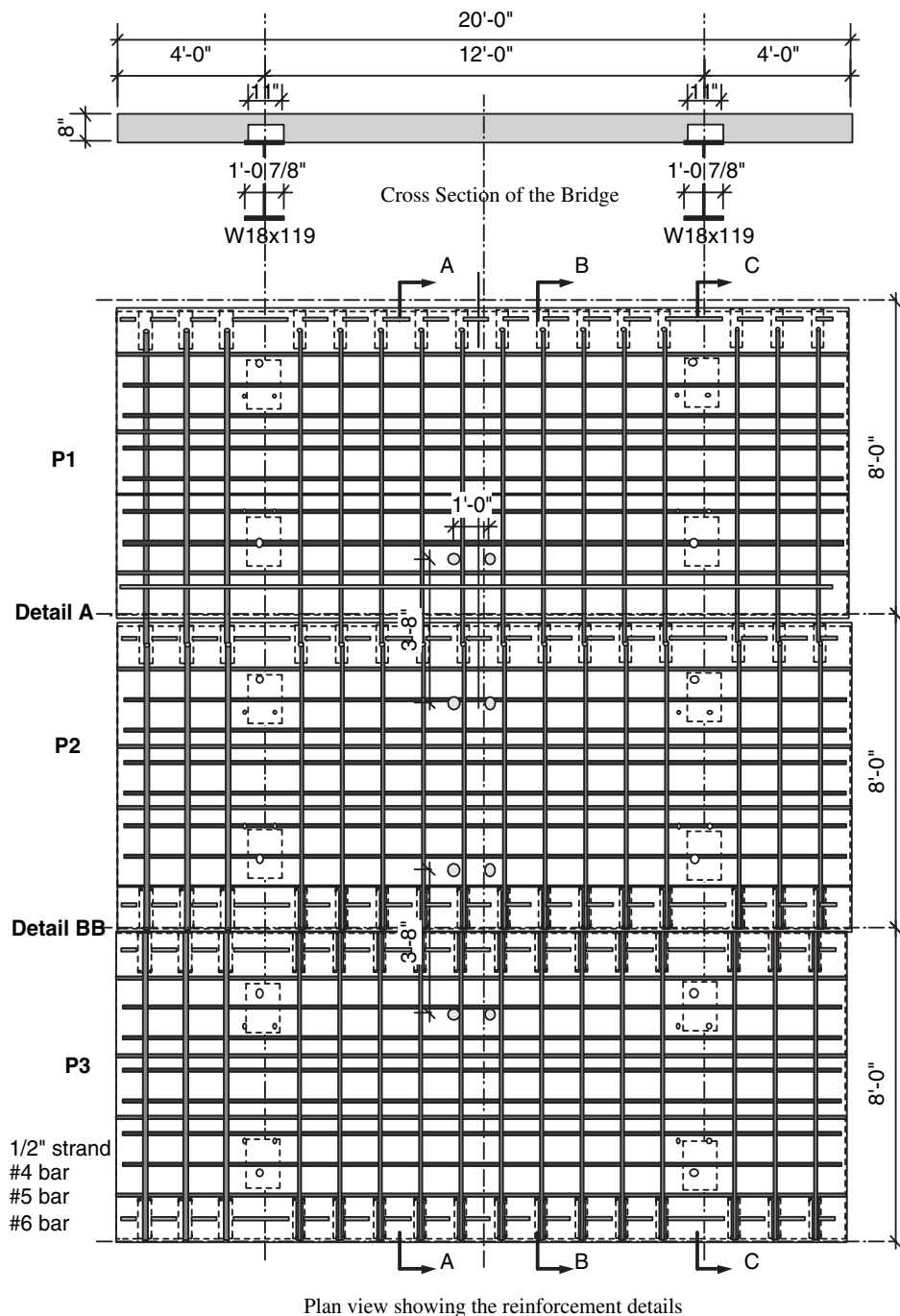


Figure 42. Cross section and plan view of the full-scale bridge specimen.

The research team used the chance of building a full-scale bridge specimen to address several questions that were raised about the construction feasibility of the recommended system CD-1, as follows:

- Would panels made with connection Detail A be installed without interfering with the shear stud cluster? This issue was addressed by welding steel pipes, 2½ in. (63.5 mm) diameter and 5½ in. (140 mm) high, on the top surface of the steel beams to simulate the footprint of eight 1¼ in.

(31.8 mm) diameter studs. The pipes were set in clusters at 48 in., four pipes per cluster. The four pipes in each cluster were welded at the corners of the perimeter of the stud cluster, as shown in Figure 48.

- Would the 1 in. gap in the shear key be wide enough to allow efficient filling and consolidation of the grout? This issue was addressed by attaching 6 in. (152 mm) wide strips of plywood to the bottom surface of the precast panels at the transverse joints. The plywood strips were hung from the top surface using short pieces of threaded rods.

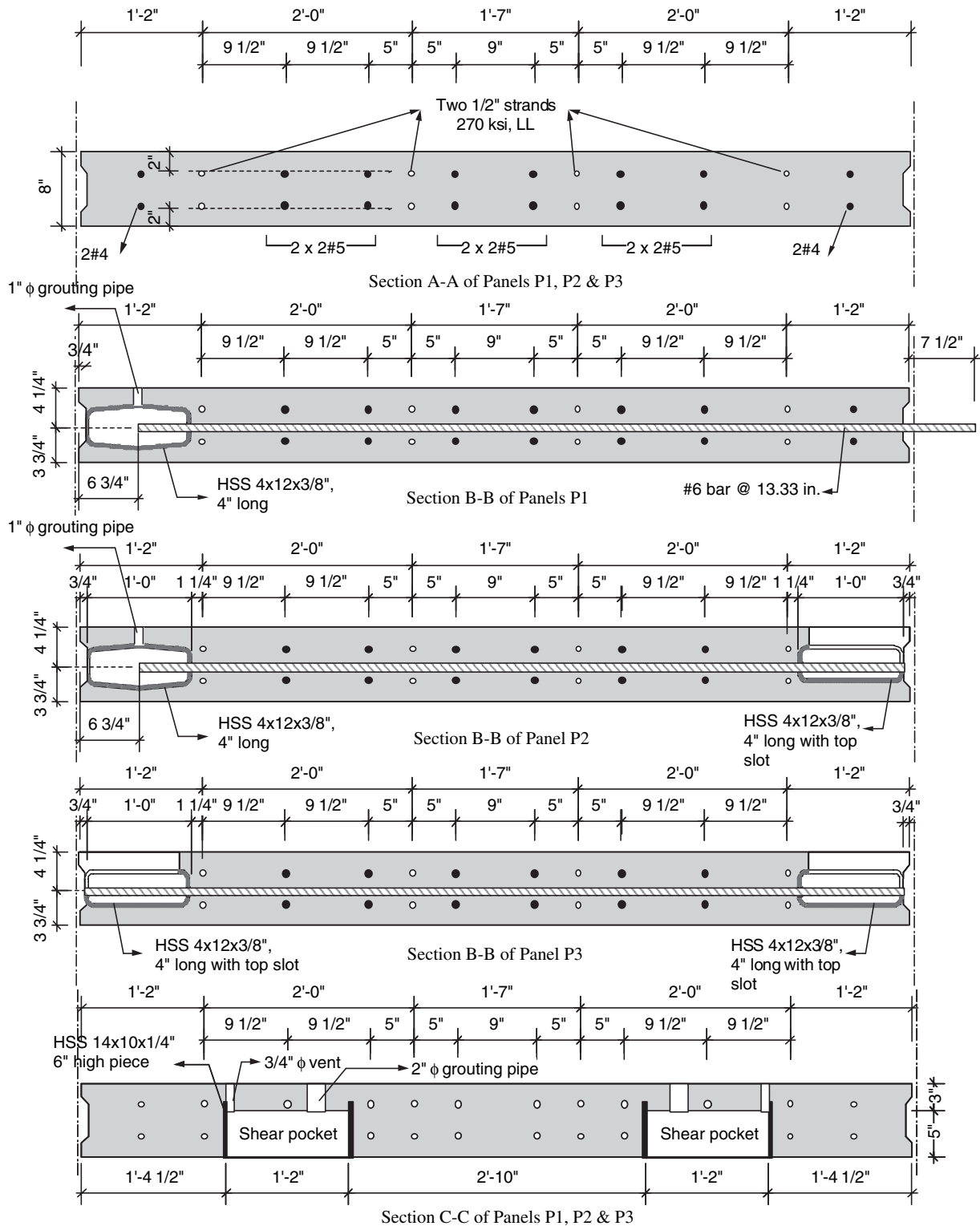
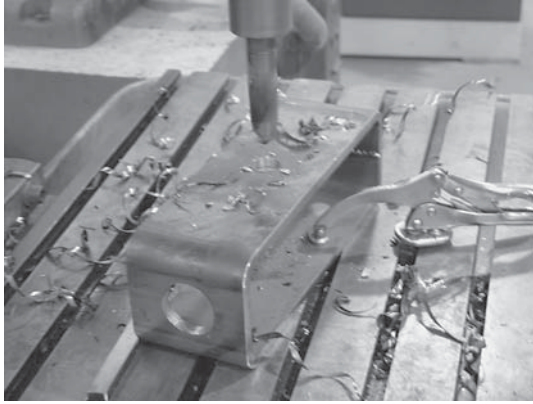
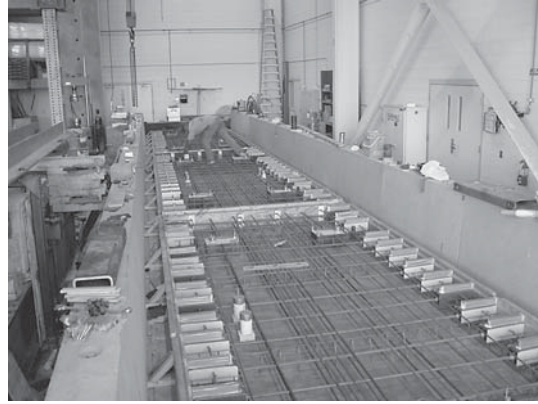


Figure 43. Sections A-A, B-B, and C-C of Panels P1, P2, and P3.



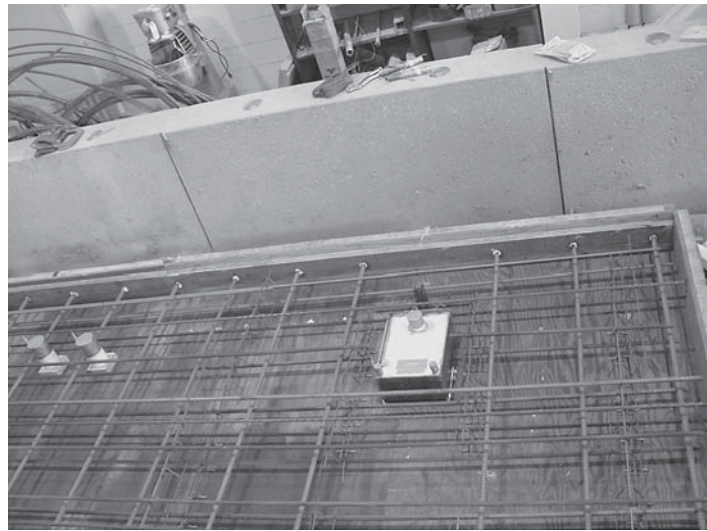
HSS 12x4x3/8 in.



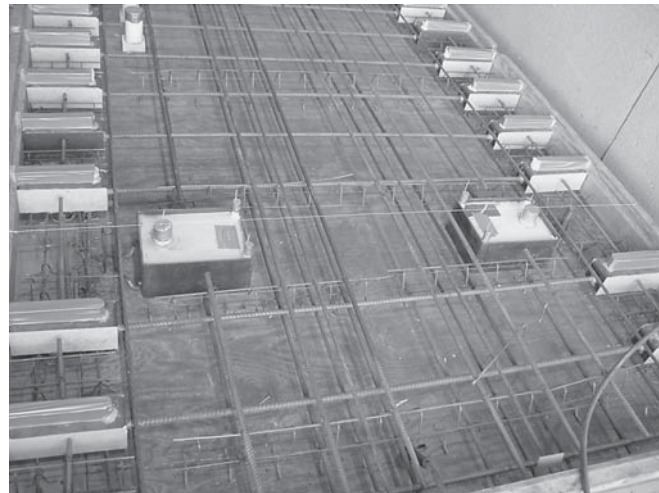
Precast panels ready to receive concrete



Panel P1: Detail A, North side

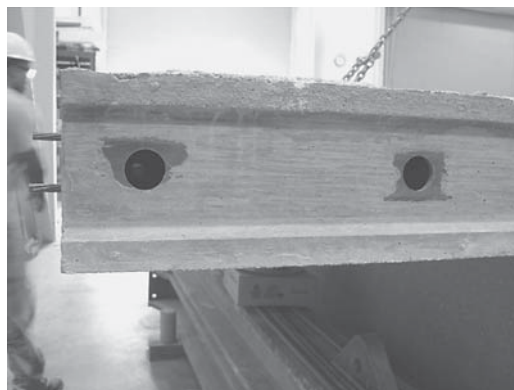


Panel P1: Detail A, South side



Panel P3: Detail BB, North and South sides

Figure 44. Panels P1, P2, and P3 during fabrication.



Panel P1



Panel P2



Panel P3

Figure 45. Panel P1, P2, and P3 after 7 days of moist curing.

- Would the grout be able to travel the 48 in. distance between the shear pockets to completely fill the haunch between the precast panels and the steel beam? This issue could not be addressed in this part of the experimental investigation because no 1¼ in. (31.8 mm) studs were welded on the steel beams in order to save the beams for the full-scale beam specimens. This issue was, however, addressed during the construction of the full-scale beams.

The following steps were taken to build the full-scale bridge specimen:

- Backer rods measuring 1 in. in diameter were glued to the top surface of the steel beams to form the haunch between the panels and the steel beams.
- Panel P2 was installed vertically and set on the steel beams using 1.0 in. high steel shims.
- Panel P1 was lifted from the prestressing bed. The panel was tilted about 15 degrees by shortening the length of the chains on one side of the panel. The No. 6 bars were inserted into the oversize holes provided on the transverse side of Panel P2; the panel was then lowered and moved horizontally. The installation process took about 120 seconds and went smoothly, with no need to change the tilting angle of the panel during installation.
- Panel P3, which had connection Detail BB, was installed vertically.
- Plywood strips were used for wood forms on the bottom side of the panel-to-panel joints. The plywood strips were hung from the top surface of the panels using threaded rods.

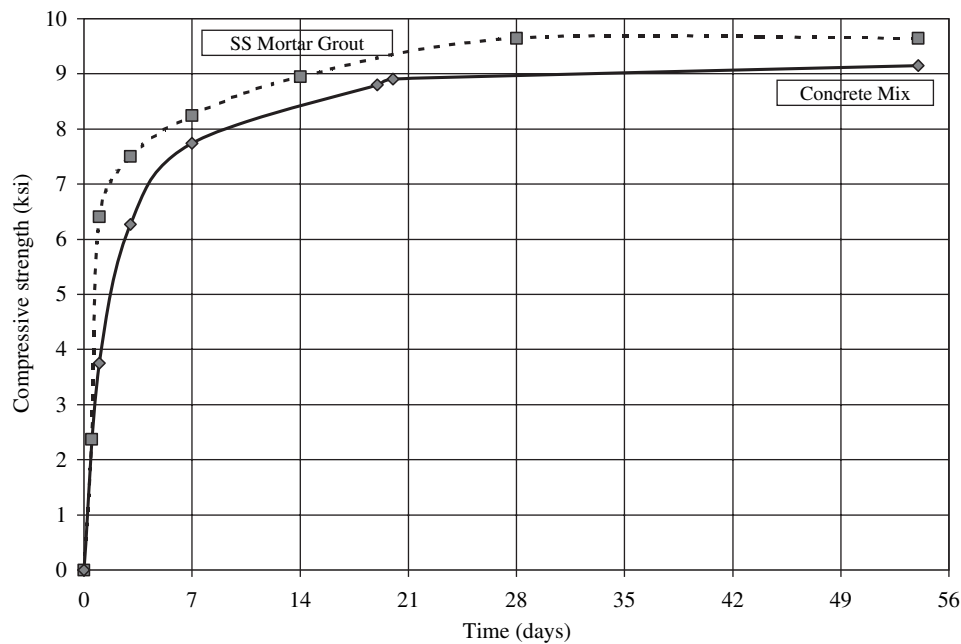


Figure 46. Concrete strength gain versus time for the concrete mix and SS Mortar grout.

- The shear pockets were filled with SS Mortar through the 2 in. (50 mm) diameter tubes until the grout came out from the 1 in. (25 mm) diameter vent tubes on the far side of the pockets (7). The transverse shear key joints were filled with the SS Mortar grout. The grout had sufficient flowability to set without the need for any external vibrators. Figures 49 and 50 show some of the construction steps.

When the grouting material reached the minimum required strength of 6.0 ksi (41.37 MPa), the test setup was built around the north transverse joint P1–P2, between Panel P1 and P2. The load was positioned in the transverse direction between the steel beams to produce the highest flexural effects, as shown in Figures 47, 51, and 52, where each of the two Neoprene pads that support the load spreader beam were set 3 ft (0.914 m) from the centerline of the supporting steel beam. This arrangement provided a 6 ft (1.828 m) spacing between the Neoprene pads to simulate the LRFD HS20 truck.

To investigate the effect of the fatigue load on the structural behavior of the joint, the following actions were taken:

- A series of strain gauges and displacement devices were installed around the joint on the top and bottom surface of the precast panels, as shown in Figure 52. First, the full fatigue load, 42.56 kip (189 kN), was applied as a static load, and the strain and displacement measurements were recorded with a data acquisition system.
- The fatigue load, varying from 4.00 to 42.56 kip (17.8 to 189.3 kN), was applied for 2,000,000 cycles at 2 cycles per second.
- A $\frac{3}{4}$ in. (19 mm) deep water pool was built around the joint covering the full width of the bridge, as shown in Figure 51. The pool was kept full of water before and while the fatigue load was applied. Every 12 hours the bottom surface of the joint was checked for water leakage.
- The full fatigue load, 42.56 kip (189 kN), was then applied as a static load, and the strain and displacement measurements were collected.
- These steps were repeated at south transverse joint P2–P3, between Panel P2 and P3.

Test Results

The clustered stud shear connectors did not obstruct the installation of Panel P1 that was made with connection Detail A.

The idea of building the grout forms of the transverse joints on the bottom surface of the panels worked very well. No leakage was observed as the joints were filled with grout, and no air voids were noticed on the top or bottom surface of the joints.

The size and number of the grouting and venting ports of the shear pockets was sufficient to provide complete filling of the shear pockets and the haunch.

No water leakage was detected before, while, or after the 2,000,000-cycle fatigue load was applied.

No tension cracks were observed on the bottom surface of the transverse joints or the panels after the 2,000,000-cycle fatigue load was applied. This observation showed that no slippage occurred to the spliced No. 6 (19) bar of Detail A and Detail BB.

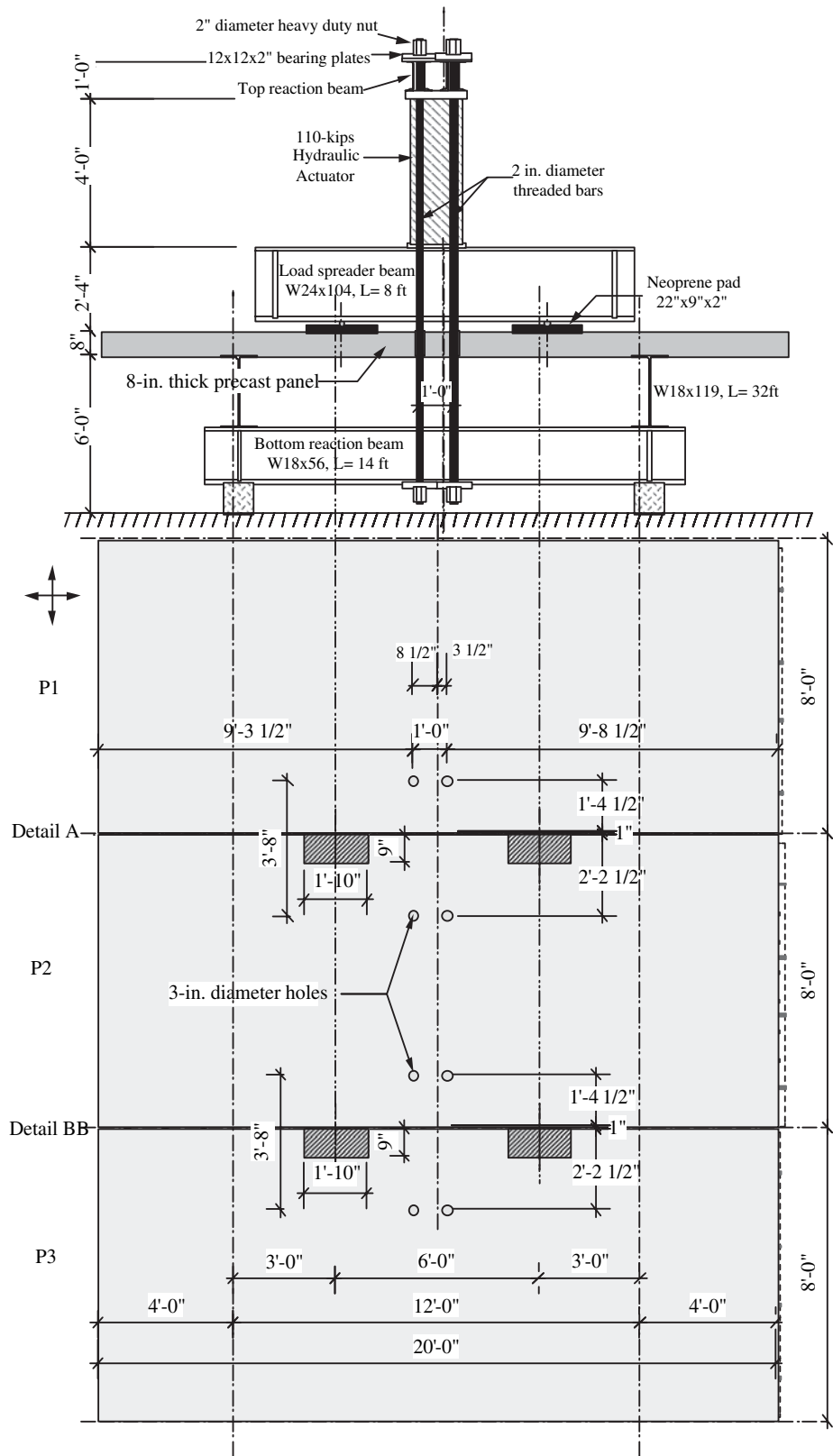


Figure 47. Test setup.

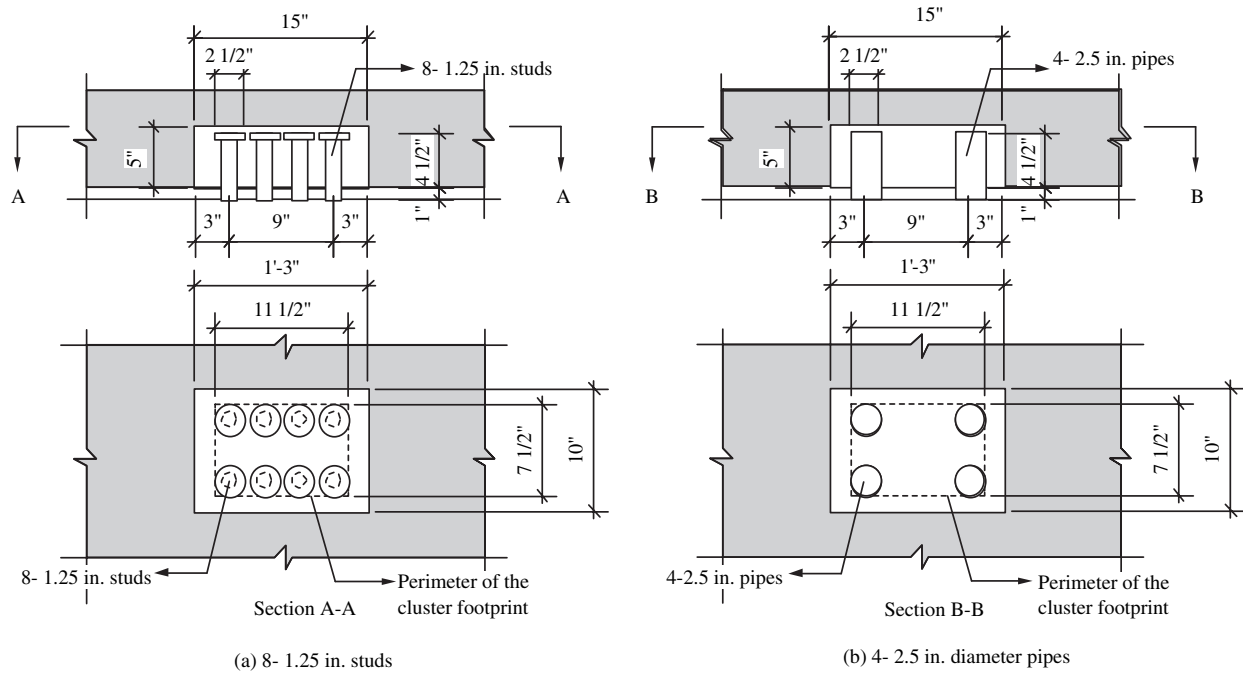


Figure 48. Arrangement of the four 2 1/2-in.-diameter pipes.

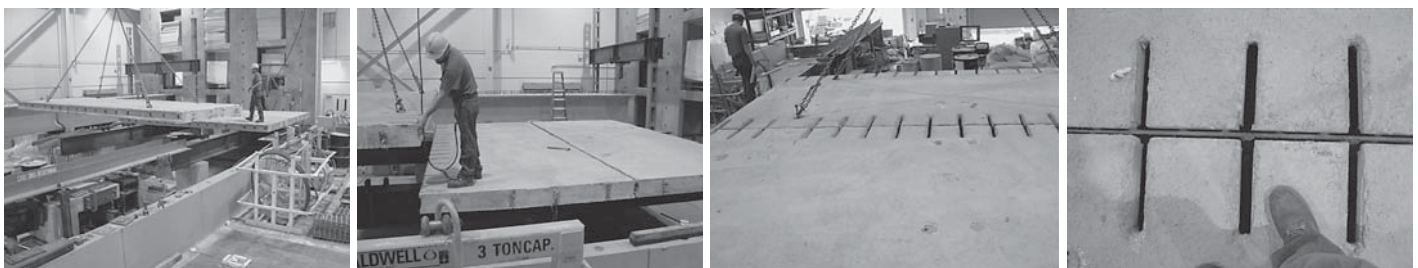


(a) Panel P2 being lifted from the prestressing bed

(b) Vertical installation of Panel P2



(c) Installation of Panel P1



(d) Installation of Panel P1

Figure 49. Installation of the precast panels.



Figure 50. Grouting of the shear pockets and shear keys.

No signs of concrete crushing were observed at the top surface of the joint or the panels after the 2,000,000-cycle fatigue load was applied.

No separation between the grout and the vertical surface of the shear key was observed.

The strain measurements at the P1–P2 and P2–P3 transverse joints are summarized in Figures 52, 53, and 54. Table 5 summarizes the displacement measurement at both joints. Studying the strain and displacement measurements revealed the following:

- The strain gauges oriented in the transverse direction (1uE, 8uE, 3uE, 6uE, 9uE, and 12uE) showed high stresses compared with the strain gauges oriented in the longitudinal direction (2uE, 7uE, 4uE, 5uE, 10uE, and 11uE). This observation confirms the logic that is used by the equivalent strip method of the LRFD specifications (7), where the deck slab is assumed to act as a one-way slab in the transverse direction.
- Comparable gauges on the sides of each joint showed almost the same amount of transverse strains (compare

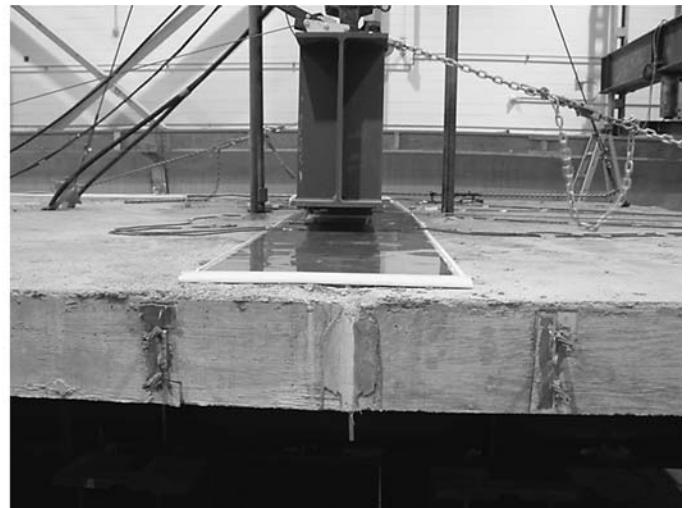


Figure 51. Test setup at the north transverse joint (left) and the water pool around the joint (right).

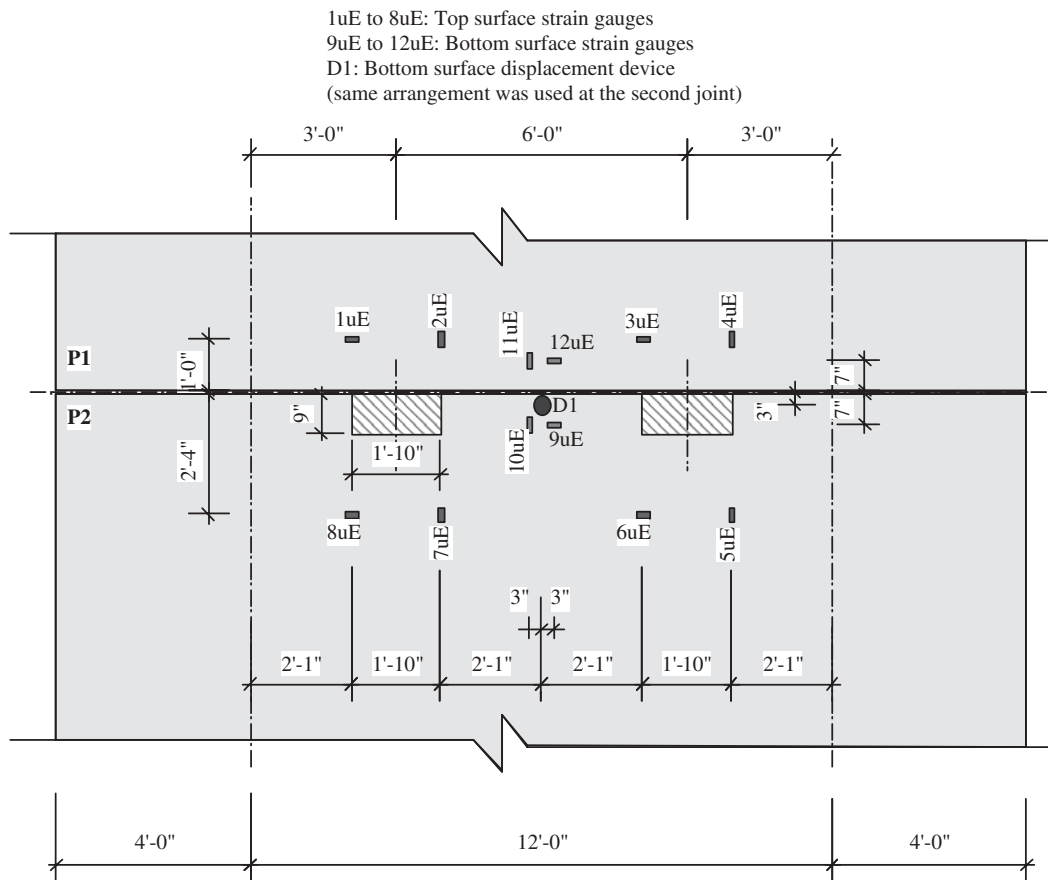


Figure 52. Locations of the measuring devices (uE = strain gauges, D = vertical displacement device).

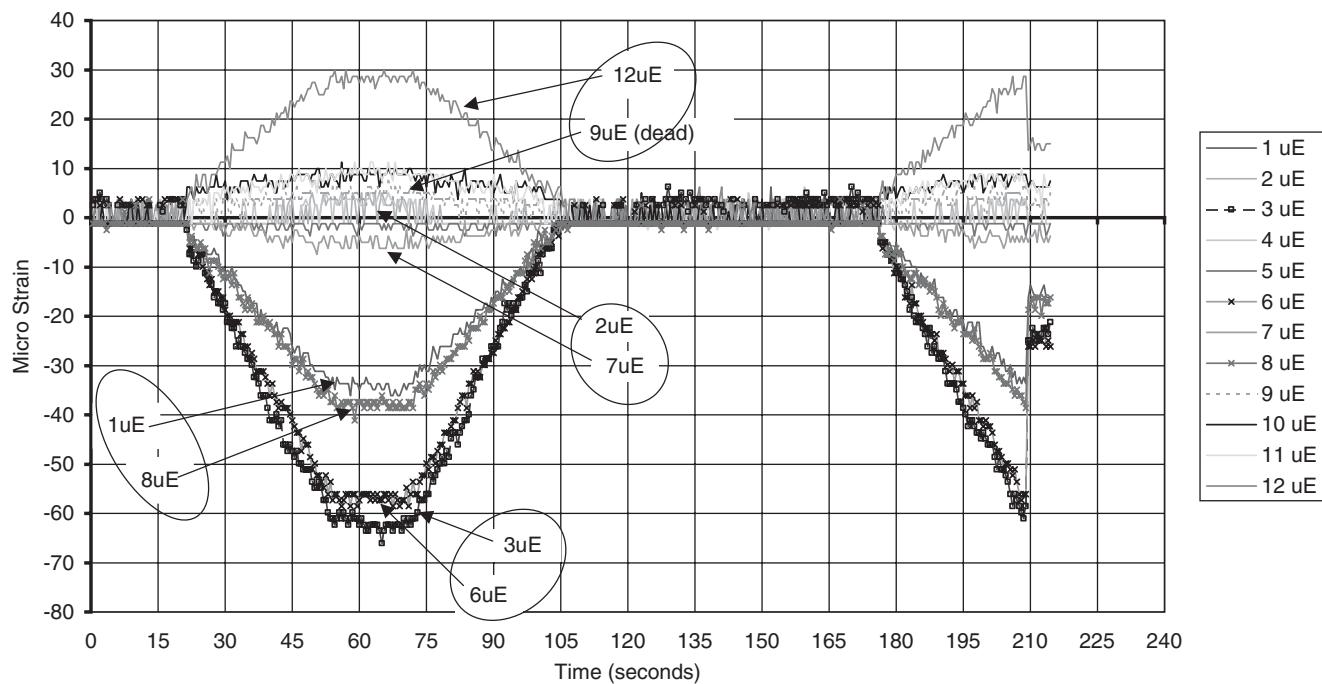
1uE with 8uE, 3uE with 6uE, and 9uE with 12uE). This indicates that both joints (Detail A and BB) were able to transfer the full applied load.

- The strain measurements on the north and south sides of the P1–P2 and P2–P3 joints were almost identical. This indicates that the structural behavior of the deck system was not affected by type of panel-to-panel connection, as long as the connection is capable of transferring the full load.
- The stress and displacement measurements of both joints before and after the 2,000,000 cycles of fatigue load were almost the same, which indicates that no stiffness deterioration occurred as a result of the fatigue load.
- Comparing the strain and displacement measurements of this test with those calculated using the equivalent strip method of the LRFD specifications (7) showed that the LRFD equation used to calculate the width of the equivalent strip leads to a conservative design, as it distributes the wheel load on a smaller distance than it should be, which results in higher flexural stresses. This observation may be due to the fact that the panels used in this test were transversely pretensioned. Transverse pretension-

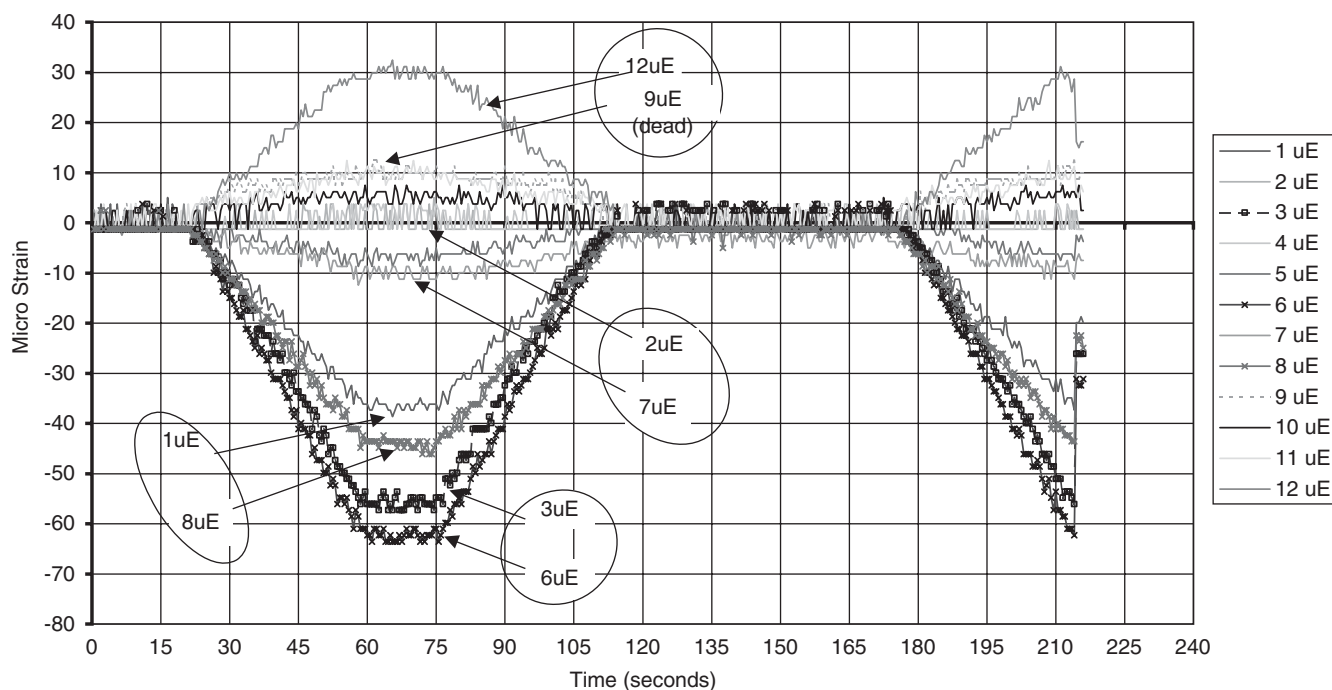
ing increases the panel stiffness, which causes the wheel load to be distributed on a wider strip. The effect of transverse pretensioning is not recognized by the LRFD specifications, as the same equation is used to calculate the equivalent width of the strip for CIP and precast concrete slabs.

Demolition of the Precast Panels

To demolish the bridge, the transverse joints between Panels P1 and P2 and Panels P2 and P3 were saw cut. The small diameter of the blade did not allow for cutting through the full 8 in. thickness of the panel; therefore, only the top 6 in. (152 mm) of the joint was cut. This was sufficient to cut the No. 6 (19) spliced bars inside the joints. The center panel, P2, was then lifted by an overhead crane, which caused the bottom 2 in. (51 mm) of the joint to break. Investigation of the cut joints showed: (a) complete filling of the joint with grout, with no air voids, (b) no grout crushing, (c) no bond failure between the grout and the shear key of the panels, and (d) no bond failure between the grout and the No. 6 (19) spliced bars, as shown in Figure 55.



(a) Before applying the 2,000,000-cycle Fatigue Load



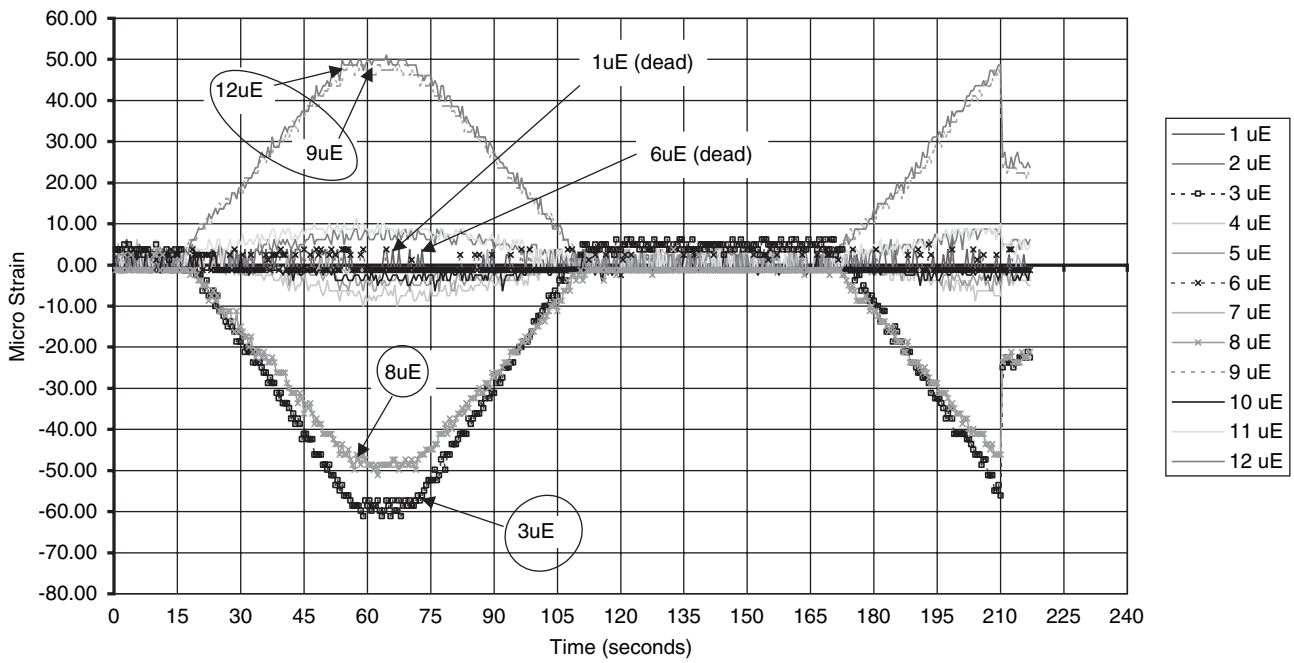
(B) After applying the 2,000,000-cycle Fatigue Load

Figure 53. P1-P2 joint, connection Detail A.

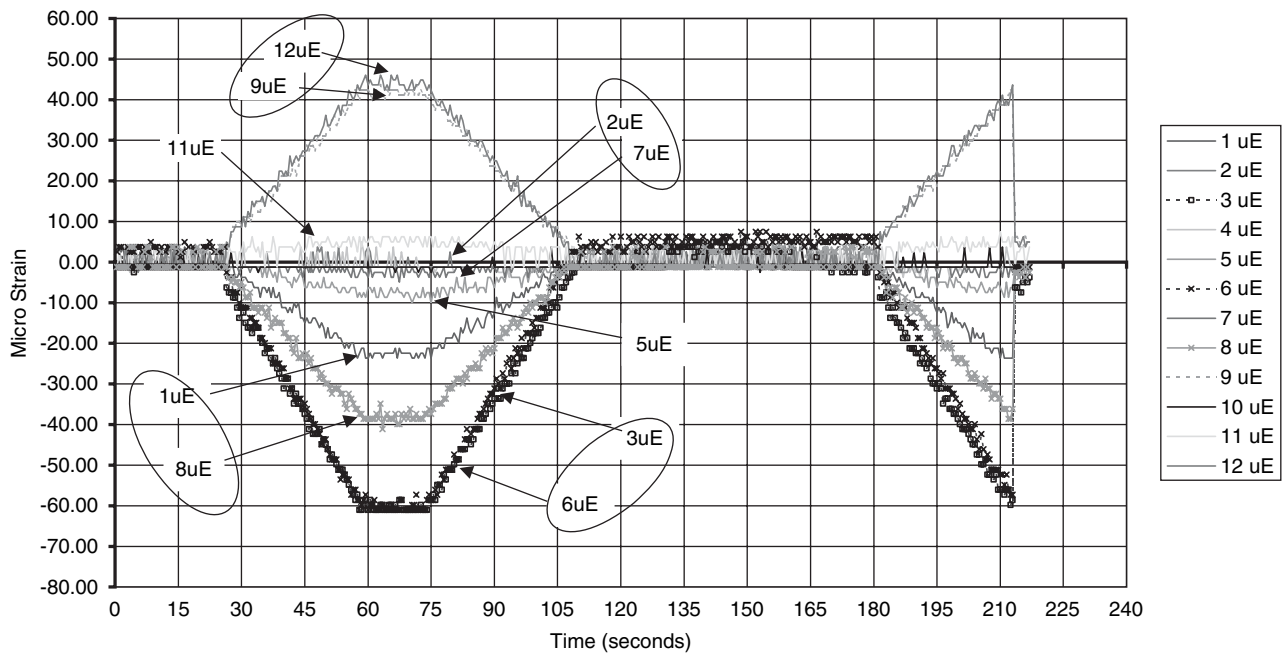
Analytical Investigation of the Development Length of Confined Reinforcing Bars

A concrete member's strength can be significantly increased with the use of lateral confinement. Many researchers have investigated this technique over the past two decades.

Saatcioglu et al. and Sun et al. provide a summary of various research activities conducted in this area (38, 39). Lateral confinement can be provided by spiral reinforcement, as in the case of circular columns; circular steel tubes, as in the case of concrete-filled tube structures; or other shapes of structural steel, such as the HSS tubes that were used in this project. Lateral reinforcement produces lateral confining pressure on



(a) Before applying the 2,000,000-cycle Fatigue Load



(B) After applying the 2,000,000-cycle Fatigue Load

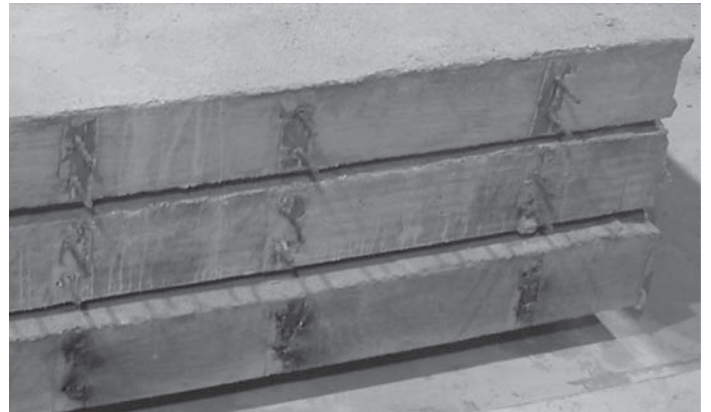
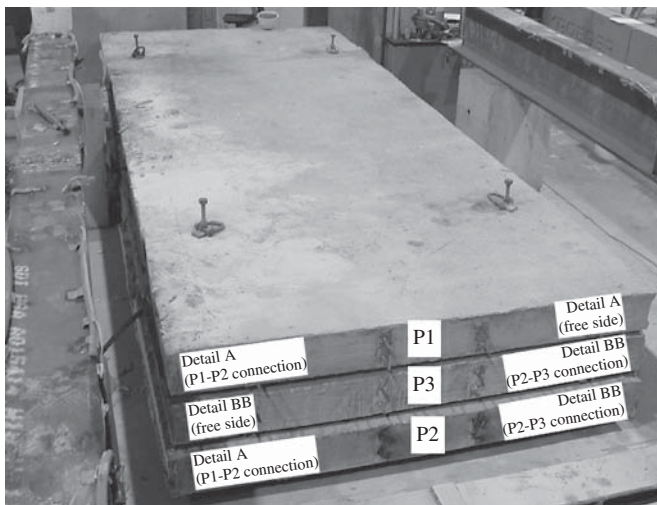
Figure 54. P2-P3 joint, connection Detail BB.

Table 5. Displacement measurements at P1-P2 and P2-P3 joints.

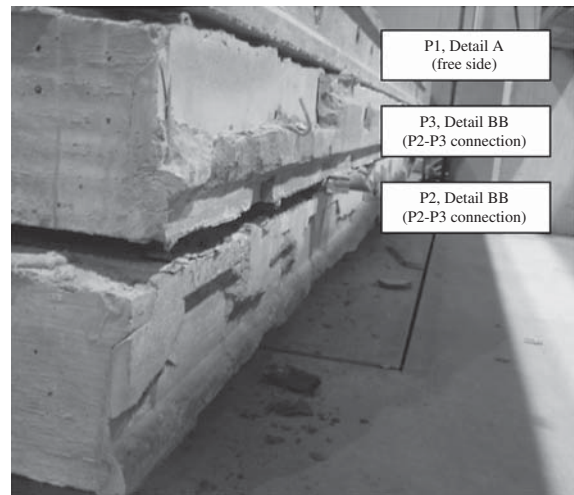
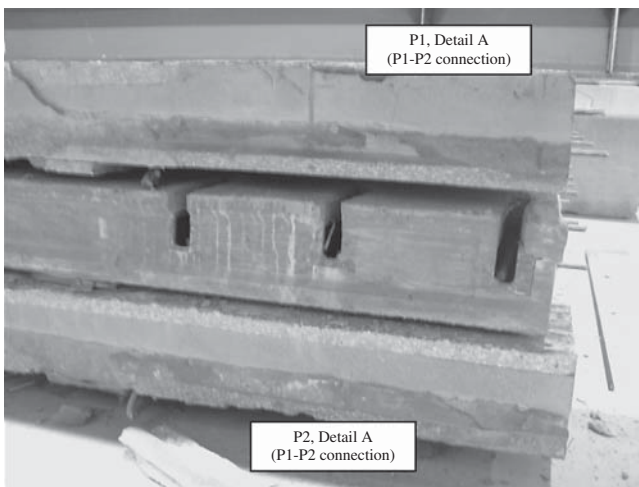
Joint	Displacement (in.)	
	Before Applying the Fatigue Load	After 2,000,000 Cycles of Fatigue Load
P1-P2	0.0401	0.0390
P2-P3	0.0379	0.0388



(a) The Haunch fully filled with Grout with no Air Voids



(b) Panels Stacked after Demolition



(c) Condition of the Transverse Edges after Saw Cutting

Figure 55. Precast panels after demolition.

the concrete core, which significantly reduces the core tendency for internal cracking and increases the concrete compressive strength and ductility.

Many mathematical models that describe the stress-strain relationship of confined concrete have been developed (38). Among the latest models is the one presented by Sun et al. (39) that can be used for noncircular lateral confinement:

$$f_{c0} = f_0 + 4.1kf_l \quad (3)$$

where

f_{c0} = confined concrete strength,

f_0 = unconfined concrete strength (i.e., f'_c for concrete cylinders),

k = a factor that relates the average lateral pressure f_l to the equivalent uniform pressure (k can be taken = 1.0 for the case of using HSS tubes),

f_l = effective lateral confining pressure,

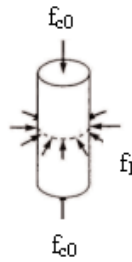
$$= \frac{\sum A_s f_{yh}}{sb_c} \quad (4)$$

A_s = area of lateral confinement steel,

f_{yh} = confinement steel strength,

s = pitch of lateral confinement, and

b_c = core dimension, center-to-center of perimeter of lateral confinement.



Providing lateral confinement to the concrete core surrounding a reinforcing bar can significantly reduce its development length. As the reinforcing bar, which is in tension, tries to slip away from the concrete surrounding it, high longitudinal compressive stresses are created in the concrete. Because concrete is a semielastic material, the longitudinal compressive stresses force the concrete surrounding the bar to expand laterally, which may cause the concrete to split along the bar and the bar to then slip away from the concrete. The lateral confinement resists the lateral expansion of concrete and protects it against splitting.

Two approaches can be used to calculate the development length of steel reinforcement bars embedded in laterally confined concrete.

The first approach is to develop a mathematical model through an experimental program. This method can be used for a specific type of lateral confinement, where a large number of pullout specimens are tested for various variables that may affect the development length, such as bar size and concrete strength. The mathematical model uses the unconfined concrete, f'_c , as a base for calculating the development length. This method provides an accurate estimate of the development length and a flexible model that can be easily adjusted for a wide range of variables. However, a large number of specimens need to be tested to get a reliable model.

The second approach is to use the development equation that is given by a code or specification for bars confined by regular stirrups, but replacing the unconfined concrete strength f'_c with the confined concrete strength, f_{c0} , given in Equation 3. Then the reduced development length can be verified through a limited number of pullout specimens. This method gives conservative estimates of the development length.

The second approach was used in this project because the development length of reinforcing bars confined with HSS tubes had not been experimentally investigated before. The development length of the No. 6 (19) bars confined by an HSS $4 \times 12 \times \frac{3}{8}$ in. tube was estimated as follows:

Step 1

Determine the confined concrete strength, f_{c0}

$$f_l = \frac{\sum A_s f_{yh}}{sb_c} = \frac{(2 \times 12 \times \frac{3}{8})(36,000)}{(12 \times 4)} = 6,750 \text{ psi}$$

$$f_{c0} = f_0 + 4.1kf_l = 6,000 + 4.1 \times 1.0 \times 6,750 = 33,675 \text{ psi} \quad (232.2 \text{ MPa})$$

Step 2

Determine the development length of the No. 6 (19) bar using:

Article 5.11.2.1.1 of the LRFD specifications (7)

$$l_d = \frac{1.25 A_b f_y}{\sqrt{f_{c0}}} \quad (5)$$

where

A_b = cross-sectional area of the bar = 0.44 in²,

f_y = bar yield strength = 60 ksi, and

$$l_d = \frac{1.25 \times 0.44 \times 60}{\sqrt{33,675}} = 5.68 \text{ in. (144 mm)}$$

Equation 12-1 of the ACI318-05 (40)

$$l_d = \frac{3 f_y \psi_t \psi_e \psi_s \lambda}{40 \sqrt{f_{c0}} \left[\frac{c + k_{tr}}{d_b} \right]} d_b \quad (6)$$

where

f_y = bar yield strength = 60,000 psi,

ψ_t = reinforcement location factor = 1.0, and

ψ_e = reinforcement coating factor = 1.0.

Check $\psi_t \psi_e = 1.0 < 1.7$

ψ_s = reinforcement size factor = 0.8,

λ = light weight concrete factor = 1.0, and

$$\left[\frac{c + k_{tr}}{d_b} \right] = 2.5 \text{ (this is the upper limit specified by ACI318-05).}$$

The ACI318-05 upper limit was recommended for this case because calculations of this term yielded a much higher value than 2.5

$$d_b = \text{bar diameter} = 0.75 \text{ in.}$$

$$l_d = \frac{3 \times 60,000 \times 1.0 \times 1.0 \times 1.0 \times 0.8}{40\sqrt{33,675} \times 2.5} \times 0.75 = 5.88 \text{ in. (149 mm)}$$

Therefore, 6.0 in. (152 mm) development length of the No. 6 (19) bar in Detail A was used for the recommended system CD-1A.

Step 3

Determine the lap splice length of the No. 6 (19) using:

Article 5.11.5.3.1, LRFD specifications, (7)

$$\text{Lap splice length} = 1.7l_d = 1.7 \times 5.88 = 9.66 \text{ in. (245 mm)}$$

Section 12.15, ACI318-05 (40)

$$\text{Lap splice length} = 1.3l_d = 1.3 \times 5.88 = 7.65 \text{ in. (194 mm)}$$

Therefore, an 11.0 in. (279 mm) lap splice length of the No. 6 (19) bar was used in Detail BB, which was used in recommended system CD-1B.

Panel to Concrete Girder Connection

Description of the Connection Detail

Typically, the girder web reinforcement is extended outside the top surface of the girder and is embedded in the concrete slab to create full composite action. The maximum size of the girder web reinforcement is No. 5 (16) bar, and these bars are made of an L- or inverted U-shape to develop their yield strength at the interface. As a result of extending the maximum spacing between shear connectors to 48 in. (1220 mm), a large number of No. 5 (16) bars need to cluster and be made to fit into the shear pocket dimensions, which cannot be practically done. Also, the minimum bending diameter of the No. 5 (16) bar will require (a) increasing the girder web thickness if the inverted U-bars are set in the transverse direction, (b) increasing the length of the shear pocket if the inverted U-bars are set in the longitudinal direction, or (c) significantly increasing the width of the shear pocket if the L-shaped bar is used (Figure 56).

A new connection detail for creating full composite action for slab/concrete girders systems, such as system CD-1, was developed. The new connection detail minimizes the interference between the horizontal shear reinforcement of the girder and the shear pockets of the panel. The new detail uses clusters of 1¼ in. (31.8 mm) diameter double-headed studs spaced at 4 ft (1220 mm). The studs in each cluster are spaced at 3 in. and embedded 8½ in. (216 mm) in the concrete girder. The studs are made from SAE 1018 steel that is used

to make the 1¼ in. (31.8 mm) studs for steel girders (34). The top surface of the concrete girder is intentionally roughened to ¼ in. (6 mm) amplitude. (The details of the connection are shown in Figure 28.) A precast NU I-girder is used in developing this detail, for the following reasons:

- The NU girder represents the most critical conditions encountered with thin top flanges and webs. Web thickness of the NU girder is 5.9 in. (150 mm), and the top flange thickness is 2 7/8 in. (73 mm).
- Most of the new series of I-girders developed in the United States, such as the Washington State Super Girder, the New England Bulb Tee, and the Iowa Bulb Tee, have almost the same features as the NU girders.

To determine the amount of horizontal shear reinforcement, the design examples given by the PCI *Bridge Design Manual* were considered (35). Four design examples of slab/I-girder bridge systems are given in the design manual; the bridge structures range from a simply supported span to three continuous span structures, with a span length up to 120 ft and girder spacing from 9 to 12 ft. Studying these examples revealed that the maximum horizontal factored shear force at the interface between the deck slab and the precast concrete girders is about 3.7 kip/in. (0.65 kN/mm) of the longitudinal direction of the girder. Therefore, the required horizontal nominal shear strength for a precast panel measuring 8 ft (2.44 m) long is

$$V_n = (3.71 \text{ kip/in.}) (8 \times 12 \text{ in.}) / (\phi = 0.9) = 396 \text{ kip/panel}$$

$$(1761 \text{ kN/panel})$$

For example, try three 1¼ in. (31.8 mm) diameter double-headed studs per pocket, with a cluster spacing of 48 in. (1220 mm) and with one stud per row. The studs are made from SAE 1018, 54 ksi (372 MPa) yield strength, 64 ksi (441 MPa) ultimate tensile strength steel. The pocket dimensions are 14 in. wide and 14 in. (356 mm) long.

The shear friction theory (7) was used to design for the required reinforcement. The nominal shear resistance of the interface plane according to Equation 5.8.4.1-1 of the LRFD specifications (7) is

$$V_n = c A_{cv} + \mu A_{vf} f_y \quad (7)$$

where

c = cohesion factor, 0.1 ksi for concrete placed against clean, hardened concrete with surface intentionally roughened (LRFD specifications, Article 5.8.4.2),

μ = friction factor, 1.0 for concrete placed against clean, hardened concrete with surface intentionally roughened (LRFD specifications, Article 5.8.4.2),

A_{cv} = area of concrete engaged in shear transfer = (12 in. × 14 in.) (2 pockets) = 336 in²,

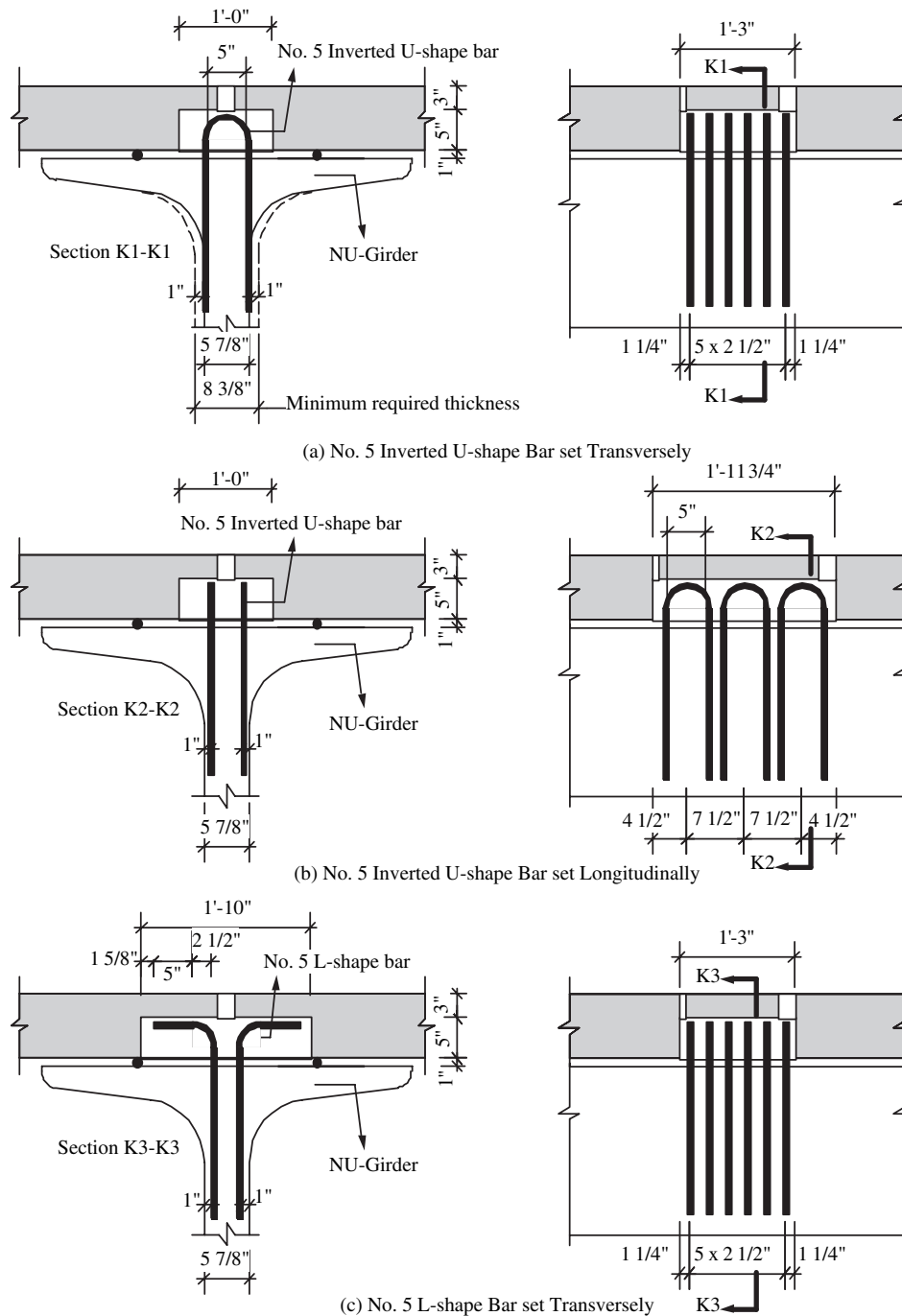


Figure 56. Various options for setting the No. 5 bar.

A_{vf} = area of shear reinforcement crossing the shear plane

$$= \left(3.14 \times \frac{1.25^2}{4} \right) (3 \text{ studs per pocket})(2 \text{ pockets})$$

$$= 7.38 \text{ in}^2/\text{panel}, \text{ and}$$

f_y = yield strength of the horizontal shear reinforcement,

$$54.0 \text{ ksi for SAE 1018 steel.}$$

$$V_n = (0.1 \text{ ksi})(336 \text{ in}^2) + 1.0(7.38 \text{ in}^2)(54 \text{ ksi})$$

$$= 432.1 \text{ kip/panel (1922 kN/panel)} > 396 \text{ kip/panel (1761 kN/panel)}$$

Limits on V_n given by Equations 5.8.4.1-2 and 5.8.4.1.3 of the LRFD specifications (7) are not used here, as the shear pockets are confined with HSS tubes or closed ties that protect the grout surrounding the studs from crushing at the limits given by these equations.

Experimental Investigation

The shear friction theory depends on the assumption that the shear connectors will be able to develop their tensile yield strength. The axial tension force will be provided in the studs

once the deck slab starts to slide horizontally on the concrete girder. Due to the roughness of the top surface of the girder, the horizontal sliding of the deck slab will be accompanied by vertical separation at the interface. The head of the stud will resist the vertical separation, causing axial tension force in the studs and compression force in the concrete around the stud.

The double-headed stud that is used in the new connection detail should be fully developed on both sides of the interface. On the girder side of the interface, the studs are embedded in thin elements with light reinforcement (i.e., the top flange and the web of the girder), which may not provide enough confinement to fully develop them. It was thus important to test this connection detail on the girder side to make sure that enough confinement is provided and that the studs can develop their tensile strength. Anchorage of the headed stud on the slab side was checked with the panel to steel girder connection discussed later in this chapter.

Figures 57 and 58 provide details of the test specimens. The specimens were full-size top parts of an NU I-girder, and each specimen was made with one cluster of three 1¼ in. (31.8 mm) studs. Two groups of specimens were designed, with three specimens in each group. The first group of specimens was made with the exact amount of web reinforcement that is usually used with NU girders, which is No. 4 @ 4 in. (13 @ 102 mm) on each side of the web, as shown in Figure 57, while the second group of specimens was made with a higher amount of reinforcement in the web, as shown in Figure 58. The amount of web rein-

forcement provided in the second group was determined based on matching the yield strength of the studs, as follows:

Ultimate tensile force of three studs = (3 studs)

$$\left(\frac{\pi}{4} \times 1.25^2 \text{ in}^2 \right) (54 \text{ ksi}) = 200.0 \text{ kip}$$

Yield strength of No. 4 @ 4 in., which is the typical web reinforcement of the NU girder,

$$= (0.20 \text{ in}^2 \text{ per leg})(2 \text{ legs})(4 \text{ rows of reinforcement})(60 \text{ ksi}) = 96.0 \text{ kip}$$

Use an additional two No. 4 (13) inverted U-shaped bars per stud

$$= (0.20 \text{ in}^2 \text{ per leg})(2 \text{ legs})(6 \text{ rows of reinforcement})(60 \text{ ksi}) = 144.0 \text{ kip}$$

Total yield strength of the web reinforcement in the vicinity of the three studs

$$= 96.0 + 144.0 = 240.0 \text{ kip} (1067 \text{ kN}) > 200.0 \text{ kip} (890 \text{ kN})$$

Figure 59 shows the test setup, where one cluster of three studs was embedded in a full-size top part of an NU girder. The studs were tested in direct tension by anchoring them with a top reaction beam that was supported by two hydraulic jacks. The specimen was tied to the strong floor using high-strength threaded rods.

Two steel side forms, which are used in fabricating the NU I-girders, were borrowed from a precast concrete producer and used to fabricate the six specimens, as shown in Figure 60.

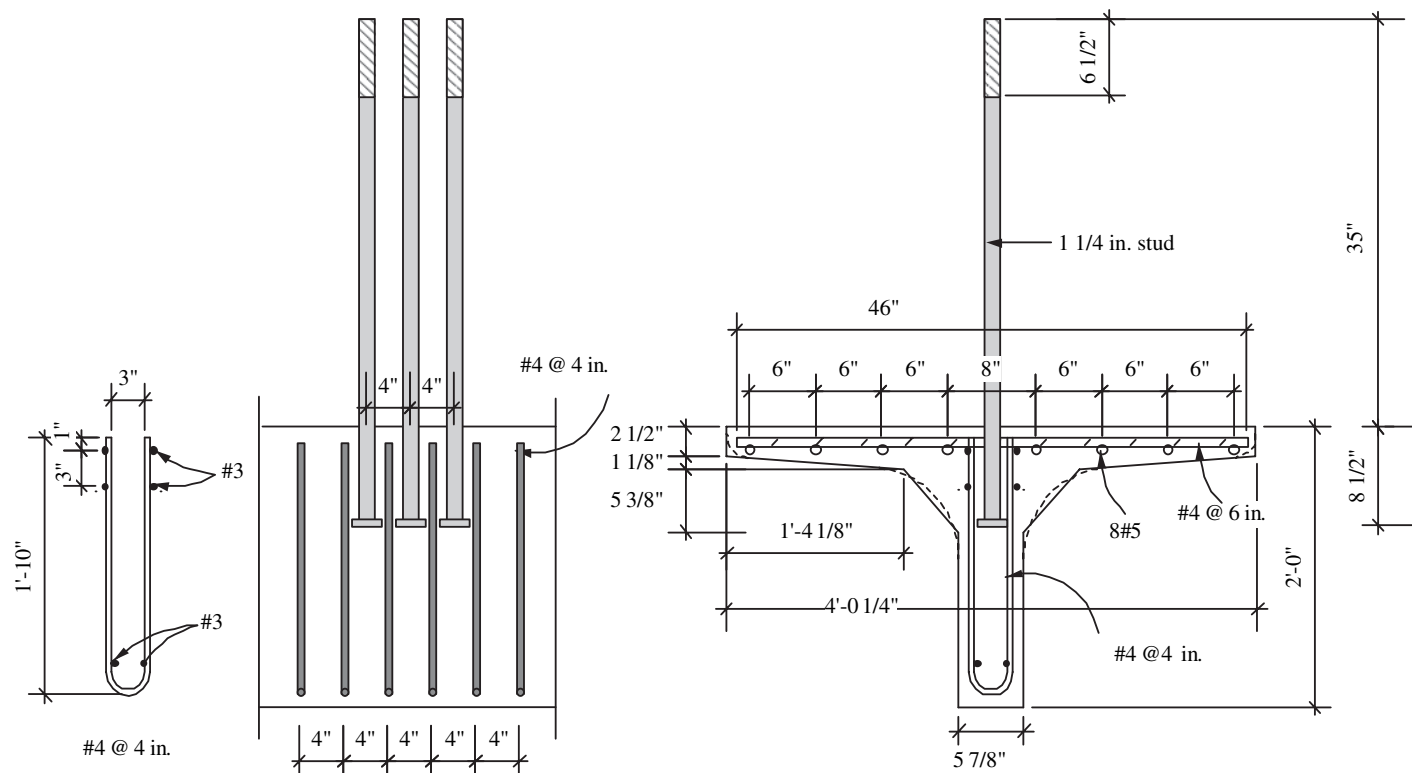


Figure 57. Group 1 of the slab/concrete girder specimens.

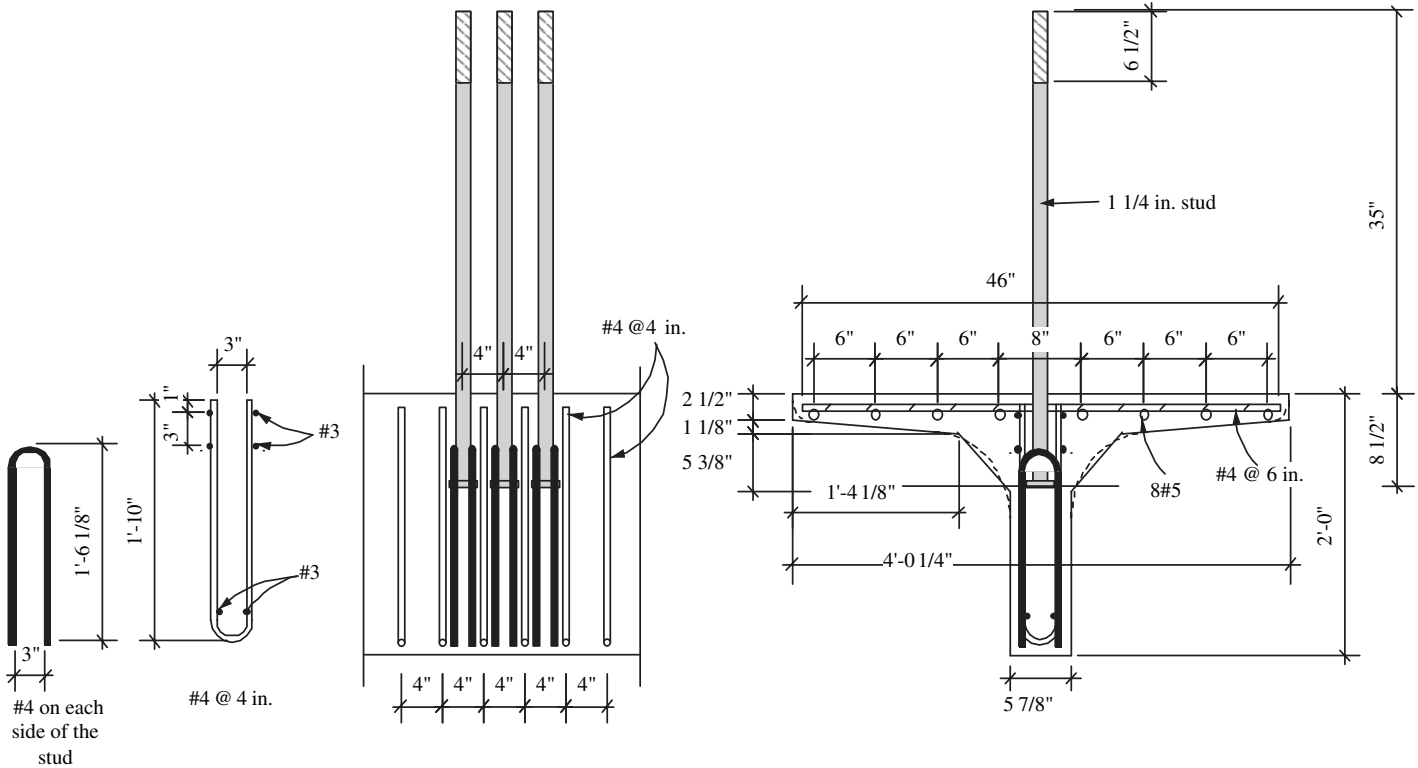


Figure 58. Group 2 of the slab/concrete girder specimens.

A steel beam was used to temporarily support the $1\frac{1}{4}$ in. (31.8 mm) long studs and keep them perfectly vertical until the concrete gained sufficient strength to support the studs. A high-performance concrete mix with 8.0 ksi (55 MPa) specified concrete strength at 28 days was used for all the specimens, as shown in Part b of Figure 60. The specimens were moist cured using wet burlap for 7 days. Concrete cylinders were made and cured by the specimens to monitor the strength gain with age. Figure 60 also shows the compressive strength gain with time.

The specimens were anchored to the strong floor using 2 in. (51 mm) diameter high-strength threaded bars, as shown in Part d of Figure 60. Two synchronized hydraulic jacks, 300 kip (1334 kN) capacity each, and a stiff reaction beam were used to apply load on the studs. The load was applied at a rate of 300 kip/sec (1334 kN/second) until failure occurred.

Test Results and Discussion

Group 1 Specimens with Regular Web Reinforcement.

At a relatively low load of about 90 kip, two horizontal hair cracks developed on the side surfaces of the specimen. These cracks were at the junction between the top flange and the vertical web of the specimen and were very close to the level of the head of the studs embedded in the flange. During this stage, no signs of failure were observed, and the top reaction beam was perfectly horizontal. Also, the recorded load from

the two hydraulic jacks was almost identical. These signs gave a clear indication that the applied load was uniformly distributed between the three studs, and no stud slippage occurred.

When the total applied load approached about 90 to 98 kip (400 to 436 kN), the side cracks started to widen and could be easily observed from a distance, as shown in Figure 61. Also, the recorded load from the two hydraulic jacks started to show a small difference, and the reaction beam started to lose its perfect horizontal alignment. These signs showed that the applied load was not perfectly distributed between the three studs. Note that the 90 kip (400 kN) applied load is about the maximum tensile capacity of web reinforcement provided in the specimen.

When the applied load reached about 105 kip (467 kN), some cracks started to form on the top surface of the specimen close to the exterior studs. The three studs with the concrete surrounding them started to pull out of the concrete specimen. The top surface cracks continued to widen until failure occurred, as shown in Figure 61. The recorded failure loads of the three specimens were 116.4, 131.4, and 116.2 kip (517, 584 and 517 kN), with an average value of 121.0 kip (538 kN), which was about 61% of the yield capacity of the stud group. Failure occurred when the studs pulled out of the concrete specimen and a sudden drop in the recorded load was reported. The amount of stud slippage at failure ranged from 1.5 to 2.0 in. (38 to 51 mm).

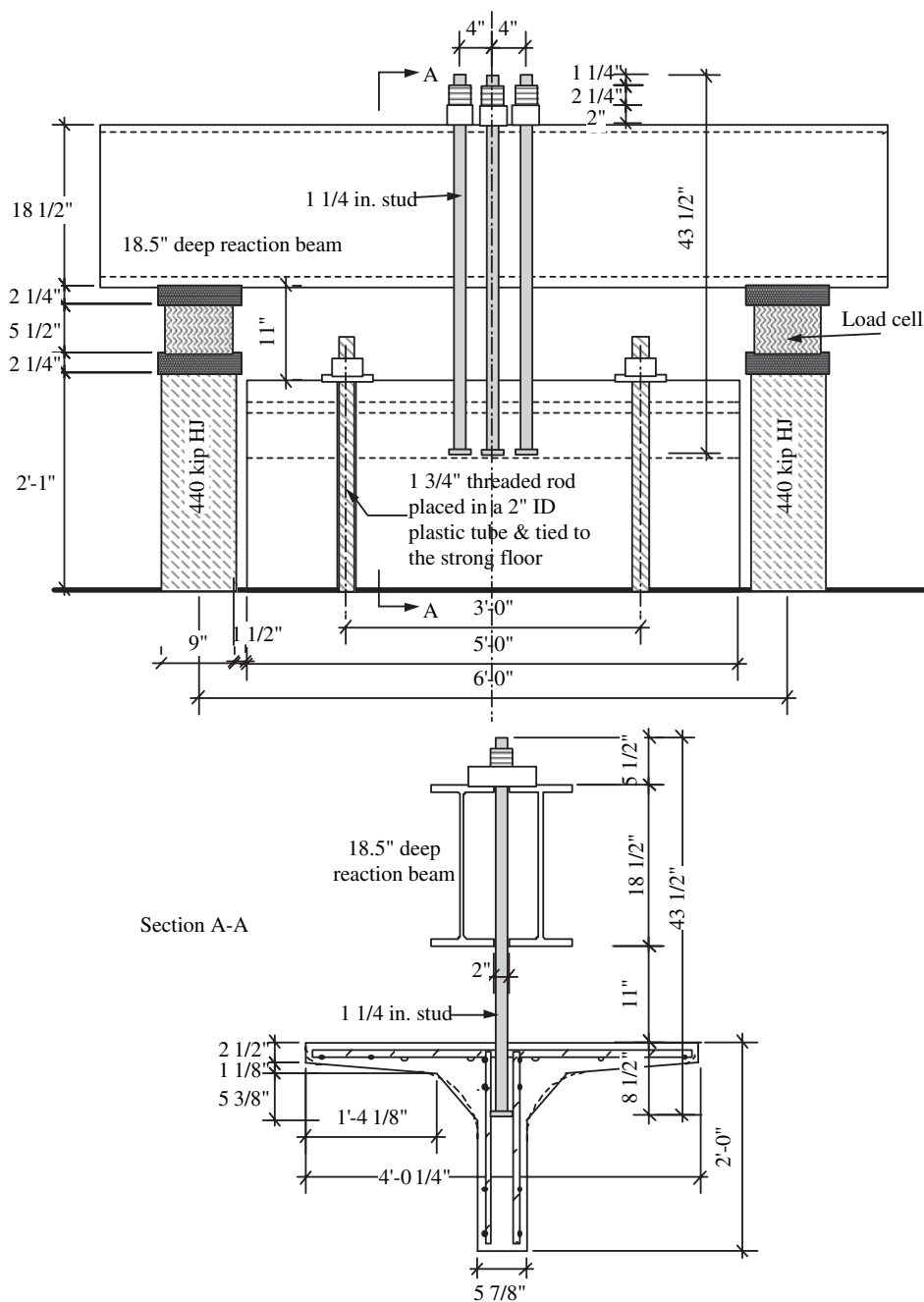


Figure 59. Test setup of the slab/concrete girder specimens.

It was clear that failure started when the tensile stresses generated at the junction between the top flange and the vertical web exceeded the tensile strength of the provided web reinforcement of 90 kip (400 kN). However, the heads of the studs protected them from pulling out of the concrete specimen by applying compressive stresses on the concrete surrounding the stud stems. The compressive stresses confined the stud stems and made the studs and the concrete around them act as a unit that took the shape of an inverted pyramid. When the applied load reached 105 kip (467 kN), the web reinforcement of the girder yielded and started to show

plastic deformation. This behavior was evident by the sudden widening of the horizontal cracks on the sides of the specimen. Failure finally occurred when the concrete at the junction between the top flange and the web could not resist the tensile stresses generated.

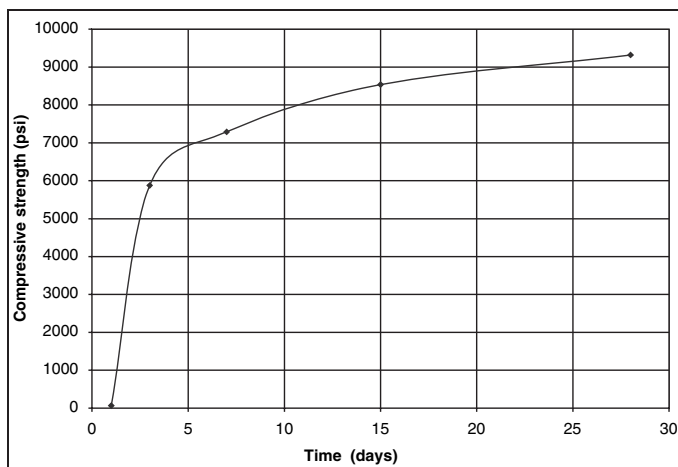
In one of the three tested specimens, the studs were completely pulled out from the specimen by jackhammering the concrete around them, as shown in Figure 61. Inspection of the concrete around the studs found no air pockets were observed in the concrete specimen in the area around the studs, which indicated that although this area was congested



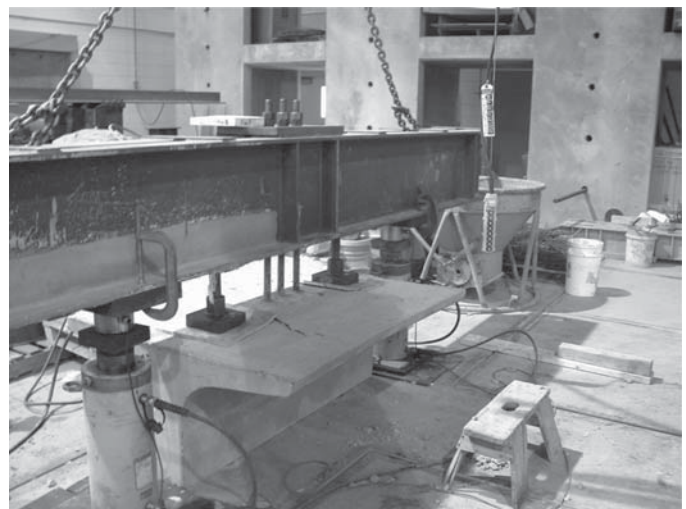
(a) The test specimens ready to receive concrete



(b) Casting of concrete



(c) Compressive Strength Gain versus Time of the Concrete Mix



(d) Test Setup

Figure 60. Fabrication and test setup of the slab/concrete girder specimen.

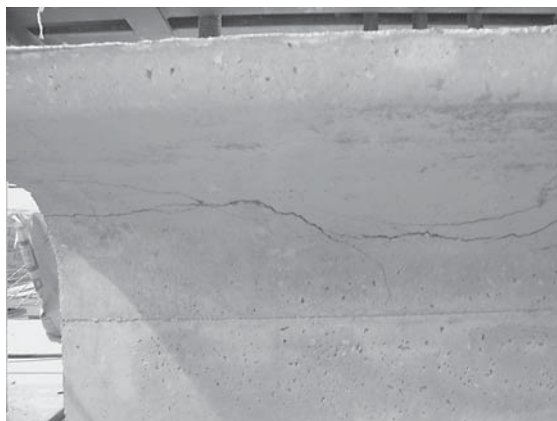
with heavy reinforcement, standard consolidation practices were able to remove air voids from the concrete. The inspection also detected no crushing of the concrete in the vicinity of the studs and no permanent deformation on the stud head that was buried in the concrete.

Group 2 Specimens with Additional Web Reinforcement. In general, the structural behavior of the specimens with additional web reinforcement was superior to that of specimens without additional reinforcement. The number and size of cracks was smaller, and the failure capacity was almost doubled.

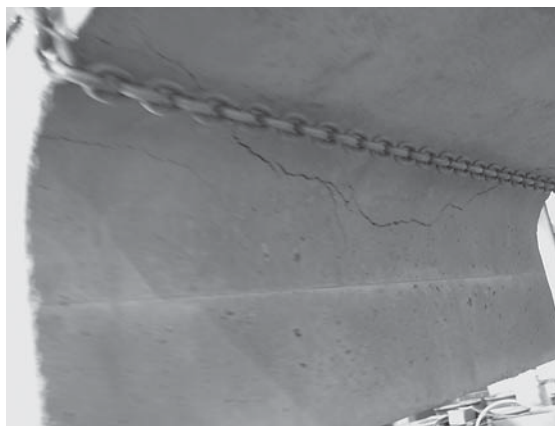
The first sign of cracking started to appear when the applied load was about 150 kip (667 kN), where one hair crack was formed on each side of the specimen. These cracks were at the junction between the top flange and vertical web of the

specimen, and very close to the level of the stud heads embedded in the flange. At this stage, no cracks were observed on the top surface of the specimen, and the reaction beam was in perfect horizontal alignment. Also, the recorded loads from the two hydraulic jacks were almost identical. These signs gave an indication that no slippage of any of the three studs occurred and that the applied load was uniformly distributed between the studs.

When the applied was about 190 kip, some minor hair cracks started to form on the top surface, and the hair cracks on the side surface started to open and became visible. It was clear that the inverted pyramid, made of the studs with the concrete surrounding them, was trying to pull out of the concrete specimen. The top surface cracks continued to widen until failure occurred, as shown in Figure 62. The recorded failure loads for the three specimens were 215.4, 213.9, and



(a) Location of the horizontal side surface cracks that started at about 105 kip



(b) Top surface cracks at failure



(c) Side surface cracks at failure

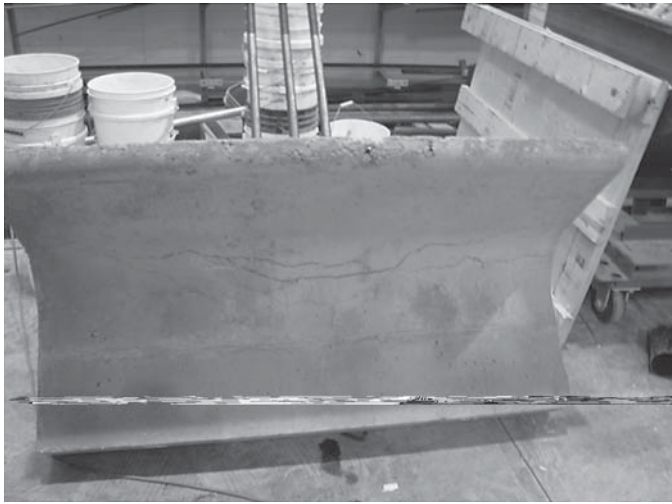


(d) Studs after being pulled away from the specimen

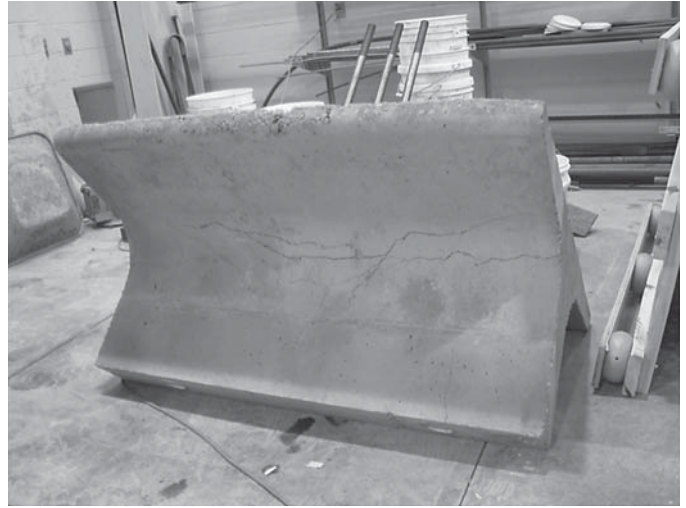
**Figure 61. Structural behavior of Group 1 specimen of the slab/concrete girder.**

203.6 kip (958, 952 and 907 kN), with an average value of 211.0 kip (938 kN), which is about 107% of the yield capacity of the stud group. Failure occurred when the studs pulled out of the concrete specimen and a sudden drop in the recorded load was reported. The amount of stud slippage at failure was about 1.0 in. (25 mm). The failure load was higher than the yield capacity of the studs and smaller than the ultimate strength capacity.

It was clear that the additional web reinforcement significantly helped in anchoring the studs to the concrete specimen and fully developed their yield strength. Also, the number and size of side cracks was significantly reduced, compared with specimens of Group 1. Based on the test results, it is recommended to use stud yield strength of 54 ksi (372 MPa) to determine the number of shear connectors and to provide



(a) Side surface cracks at failure



(b) Top surface cracks at failure



Figure 62. Structural behavior of Group 2 specimen of the slab/concrete girder.

additional web reinforcement in the vicinity of the stud clusters to achieve full composite action.

As a result of the test setup, the top flange of the tested specimens in Group 1 and Group 2 was under longitudinal tensile flexural stresses that expedited failure. In real bridges, the top flange at the strength limit state is typically under compressive flexural stresses, which will help to confine the concrete around the studs and increase the failure load. Therefore, the results obtained from this test would be considered conservative if compared with real bridge behavior.

Analytical Investigation

Finite element analysis was used to investigate the behavior of the slab/concrete girder pullout specimens. A commercial program, Nastran, was used in the analysis. The concrete specimen was modeled using the eight-node, cubic, three-

dimensional element. Each node has three displacement degrees of freedom, in the x, y, and z directions. The x direction is transverse to the girder longitudinal axis, the y direction is parallel to the girder longitudinal axis, and the z direction is parallel to the girder height. The following mechanical properties were assigned to the concrete specimen: compressive concrete strength = 8 ksi (55 MPa), unit weight = 150 lb/ft³ (23.6 kN/m³), and Poisson ratio = 0.15.

The 1¼ in. (31.8 mm) studs and web reinforcement bars were also modeled using the 20-node cubic element. The circular cross-sectional area of the stud's stem and head and the web reinforcement bars were replaced with the equivalent square cross-sectional area, as shown in Table 6. This simplification helped to refine the mesh in the vicinity of the 1¼ in. (31.8 mm) studs.

The following mechanical properties were assigned to the stud: tensile strength = 64 ksi (441 MPa), yield strength = 54 ksi

Table 6. Dimensions of the equivalent square area used for finite element analysis.

	Actual Diameter (in.)	Cross Sectional Area (in. ²)	Equivalent Square Area (in. x in.)
Stud Stem	1.25	1.227	1.108 x 1.108
Stud Head	2.5	4.909	2.216 x 2.216
No. 4 Bar	0.5	0.200	0.447 x 0.477

(372 MPa), unit weight = 490 lb/ft³ (76.9 kN/m³), and Poisson ratio = 0.30.

The following mechanical properties were assigned to the vertical web reinforcement: yield strength = 60 ksi (414 MPa), unit weight = 490 lb/ft³ (76.9 kN/m³), and Poisson ratio = 0.3.

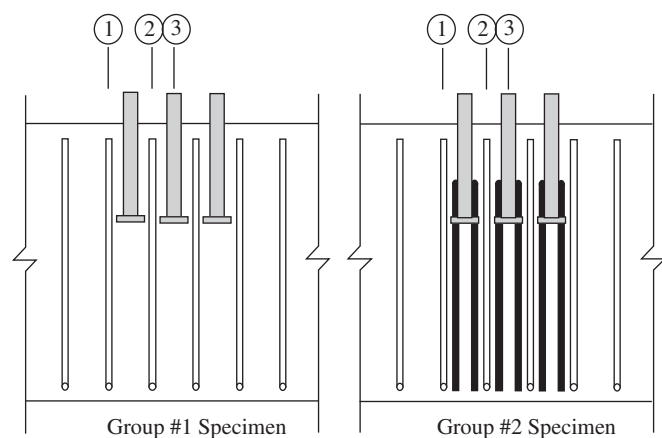
Details of the finite element model are given in Appendix F. Each stud was loaded with a tensile axial force equivalent to the stud yield capacity—66.4 kip (295 kN). This load was applied as a surface load uniformly distributed on the stud cross-sectional area—54 ksi (372 MPa).

To study the internal stress concentration around the studs, three sections were chosen, as shown in Figure 63. Section 1-1 is at the free side of the external stud, Section 2-2 is at the mid distance between two adjacent studs, and Section 3-3 is at the centerline of the center stud. Appendix F gives the *z* direction and principal stress distributions for these three sections, as well as the principal stress distribution on the top and side surfaces of the specimens. Studying these figures reveals the following:

- For Group 2 specimens, the additional web reinforcement helped in widening the base area of the inverted pyramid, which resulted in a lower stress concentration at the junction between the top flange and the web. This observation is consistent with the experimental program results, where the size of the side crack at failure was wider for the Group 1 specimens than for Group 2 specimens.
- The additional web reinforcement helped to distribute the tension force provided by the studs on a wider and deeper

volume, resulting in reduced stress concentrations around the studs. This can be seen from the following observations:

- Stress concentration at the flange-to-web junction in the Group 1 specimens is higher than that of the Group 2 specimens.
- The concrete stress in the vicinity of the stud's stem in the Group 1 specimens is higher and extends deeper than that of the Group 2 specimens
- The stress distribution at Section 3-3 (in the *z* direction or principal stress) shows that the proposed 18 in. (457 mm) embedment of the additional web reinforcement is quite enough to develop its yield strength. The high tensile stresses generated in concrete between adjacent rows of additional web reinforcement do not extend to the bottom surface of the concrete specimen. This finding is consistent with the experimental test results, where no signs of slip-page or vertical side-surface cracking parallel to the additional web reinforcement were observed.
- The principal stresses at all sections are higher than the *z*-direction stresses due to the specimen setup that puts the top flange of the specimen in tension.
- The compressive stress at the flange-web junction is about 2.0 ksi (14 MPa), which is less than the concrete bearing strength, $0.85 \times 8 \text{ ksi} = 6.8 \text{ ksi}$ (47 MPa). This observation is consistent with the test result as no concrete crushing in this location was observed at failure. It is believed that the web reinforcement helped to confine the concrete and consequently protected it from premature cracking.

**Figure 63. Location of Sections 1, 2, and 3.**

Panel to Steel Girder Connection

Steel studs welded to the top surface of steel girders and embedded in the concrete slab have been the typical technique used to create full composite action for slab/steel girder construction (2, 34). The $\frac{3}{4}$ in. (19 mm) and $\frac{7}{8}$ in. (22 mm) diameter studs have been the common sizes used in bridges. Recently, a $1\frac{1}{4}$ in. (31.8 mm) diameter stud was developed by a group of researchers at the University of Nebraska (34). The stem of the $1\frac{1}{4}$ in. (31.8 mm) diameter stud has double the cross-sectional area of a $\frac{7}{8}$ in. (22 mm) diameter stud. Therefore, one $1\frac{1}{4}$ in. (31.8 mm) stud replaces two $\frac{7}{8}$ in. (22 mm) studs.

There are many advantages to using the $1\frac{1}{4}$ in. (31.8 mm) stud, including (a) higher speed of construction, as a smaller

number of studs are welded; (b) less congestion of the girder top flange, especially in areas of high horizontal shear stresses; (c) easier deck removal; and (d) less damage to the girder top flange during deck removal. The 1¼ in. (31.8 mm) stud has been successfully used in bridges in some of the Midwest states (36, 41, 42). The use of the 1¼ in. (31.8 mm) studs with precast concrete panels adds another advantage, as the shear pocket dimensions are reduced by about 40%, resulting in a smaller volume of grout to be used and a more economical system.

As discussed in Chapter 2 of this report, the maximum spacing between shear connectors is 24 in. (610 mm) in the LRFD specifications (7). Investigation of the background of this limit revealed that a very limited amount of testing was conducted with stud spacing greater than 24 in. (610 mm). In addition, the majority of these tests were made for CIP slabs, where the studs are uniformly spaced across the specimen and not clustered in groups, as is the case with precast panel construction.

Recently, two attempts have been made to address the issues of clustering the studs in groups for precast panels and extending the 24 in. (610 mm) maximum spacing to 48 in. (1220 mm) (31, 32). (A brief summary of those attempts is given in Chapter 2 of this report.) The first attempt (31) focused only on the effect of the number of studs and their orientation per cluster on the ultimate capacity, while the second attempt focused only on the effect of extending the maximum spacing limit to 48 in. (1220 mm) on the fatigue capacity (32). Study of these attempts revealed the following:

- Extending the maximum spacing to 48 in. (1220 mm) has no negative effect on the fatigue capacity of clustered ⅞ in. (22 mm) studs.
- Clustered studs may not be able to produce their ultimate capacity as a result of premature crushing failure of the grout surrounding the studs or premature failure of the concrete slab surrounding the shear pocket.
- None of these attempts was able to simultaneously investigate fatigue and ultimate capacity of clustered studs.
- Both attempts used ¾ in. (19 mm) and ⅞ in. (22 mm) diameter studs.

A review of the literature found that the fatigue and ultimate capacities of shear studs were studied individually, which means that the effect of the fatigue load on the ultimate stud capacity was not investigated. In a real bridge, there is a fair chance that the studs will be exposed to a large number of live load cycles before the bridge is overloaded and the studs are loaded up to their maximum strength.

Description of the Connection Detail

As discussed earlier in this chapter, recommended system CD-1 uses clusters of eight 1¼ in. (31.8 mm) studs spaced

at 48 in. (1220 mm). The number of studs per cluster was determined based on the parametric study conducted by Tadros and Baishya, in which a large number of slab/steel girder bridges, with spans ranging from 60 to 130 ft (18.2 to 39.6 m) and girder spacing ranging from 6 to 12 ft (1.82 to 3.66 m), were analyzed (2). The study revealed that the maximum horizontal shear stress at the interface required one 1¼ in. (31.8 mm) stud set at 6.0 in. (152 mm) spacing. To prevent the grout surrounding the studs from premature cracking due to the high compressive stresses generated by the stud group, the shear pocket was confined with an HSS tube, as shown in Figures 20 to 30. Another alternative for confining the grout that was considered in the experimental investigation was using three individual No. 6 (19) closed ties. A 2 in. (50 mm) clear concrete cover was maintained on the lower tie, and a 1 in. (25 mm) clear spacing was maintained between the ties. This arrangement resulted in setting the tie group as close as possible to the bottom surface of the panel, where the bearing stresses of the studs on the grout reach their highest value close to the base of the stud. This finding was revealed by the finite element analysis of the push-off specimens that will be discussed later in this chapter, and it was also confirmed by other researchers (43, 44).

Two options for manufacturing the 1¼ in. (31.8 mm) stud were investigated: (a) produce a headed stud where the head is made integral with the stud stem, and (b) produce a headless stud with a heavy-duty nut and washer to form the stud head. The two options were investigated with three stud manufacturers located in different states; it was found that the first option would reduce the cost of making the stud and save time and effort required to install the heavy nut. But producing the headed stud requires a special forging machine that may not be available at every stud manufacturer. The headed stud was used for the push-off specimens, while the headless stud with a heavy-duty nut and washer was used for the full-scale beams. Figure 64 shows the dimensions of the headed and headless 1¼ in. (31.8 mm) diameter studs. The weight of the 1¼ in. (31.8 mm) headed stud was 2.37 lb, compared with 1.10 lb for a ⅞ in. (22 mm) stud. SAE 1018 steel was used to make both the headed and the headless studs.

To validate the proposed concept of extending the maximum stud spacing to 48 in. (1220 mm) and to study the effect of fatigue load on ultimate capacity, the following activities were conducted:

- Push-off specimens: Group 1 was tested directly for ultimate capacity and Group 2 was exposed to 2,000,000 cycles of fatigue load and then tested for ultimate capacity.
- Full-scale beam testing: Two full-scale beams were tested. The first beam was made with clusters of four 1¼ in. studs

spaced at 24 in., and the second beam was made with clusters of eight $1\frac{1}{4}$ in. studs spaced at 48 in.

Push-Off Specimens

Description of the Push-Off Specimens

Two groups of push-off specimens were fabricated and tested. Group 1 consisted of eight specimens tested for ultimate capacity. Group 2 consisted of eight specimens exposed to 2,000,000 cycles of fatigue load and then tested for ultimate capacity. Table 7 gives the design criteria for these specimens. Figures 64 to 73 show the details of the specimens. Figure 74 shows the specimens during fabrication.

The specimen details of both groups are identical, with the following exceptions:

- The specimens of Group 1 were made with a $1\frac{1}{4}$ in. (31.8 mm) thick haunch between the concrete specimen and the steel plate, while the specimens of Group 2 were made without a haunch. The haunch was eliminated in the second group of specimens in order to compare the test results with the ultimate capacity as given by the LRFD specifications (7) and other sources, such as Ollgaard et al. (45), Oehlers and Bradford (43), and Viest (46), where the equations were developed using a symmetric specimen with no haunch provided in the push-off specimens. Symmetric specimens are typically made with a steel beam with studs welded on both flanges and with a concrete prism on each side of the steel beam. The symmetric specimen could not be used in this research because a very high load would be required to break a specimen with sixteen $1\frac{1}{4}$ in. (31.8 mm) studs, which was beyond the capability of the testing facility.
- External confinement was added to the specimens of Group 2 by two side plates attached to the specimens. The plates were anchored by $\frac{1}{2}$ in. (12.7 mm) diameter threaded bars and nuts. The threaded bars were embedded in the specimens and extended 3 in. (76 mm) outside the specimen on each side, as shown in Figure 73. The external confinement was added to simulate real bridge deck sys-

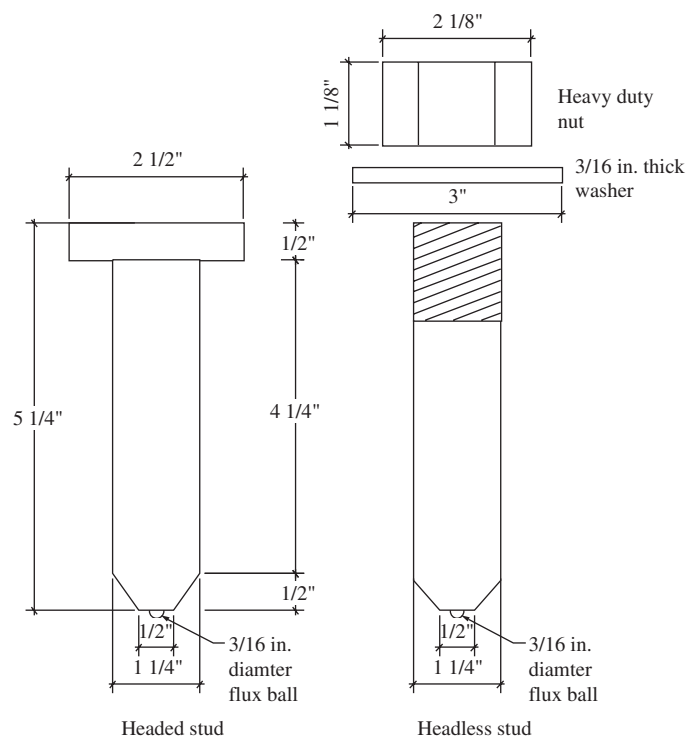


Figure 64. Dimensions of the $1\frac{1}{4}$ -in.-diameter stud.

tems where the slab has extended length on both sides of the girderline to help confine the shear pockets. This technique was successfully used during the development of the $1\frac{1}{4}$ in. (31.8 mm) diameter studs (42, 47).

The standard welding gun used to weld the $\frac{7}{8}$ in. (22 mm) studs was also used to weld the headed $1\frac{1}{4}$ in. (31.8 mm) studs. A special chuck that can fit the headed $1\frac{1}{4}$ in. (31.8 mm) stud was fabricated and used, as shown in Figure 75. The studs of first and second specimens of Group 1 were welded using a tri-legged support to adjust the verticality of the studs, as shown in Figure 75. Once the technician gained enough confidence in the welding process, however, he shot

Table 7. Design criteria of the push-off specimens.

Push-Off Specimen	Number of Specimens	Number of Studs per Specimen	Type of Grout Confinement	Test Type
Group 1				
P-4-CT-U	2	4	3 No. 6 closed ties (CT)	Ultimate (U)
P-4-ST-U	2	4	Steel tubes (ST)	
P-8-CT-U	2	8	3 No. 6 closed ties (CT)	
P-8-ST-U	2	8	Steel tubes (ST)	
Group 2				
P-4-CT-F/U	2	4	3 No. 6 closed ties (CT)	Fatigue/Ultimate (F/U)
P-4-ST-F/U	2	4	Steel tubes (ST)	
P-8-CT-F/U	2	8	3 No. 6 closed ties (CT)	
P-8-ST-F/U	2	8	Steel tubes (ST)	

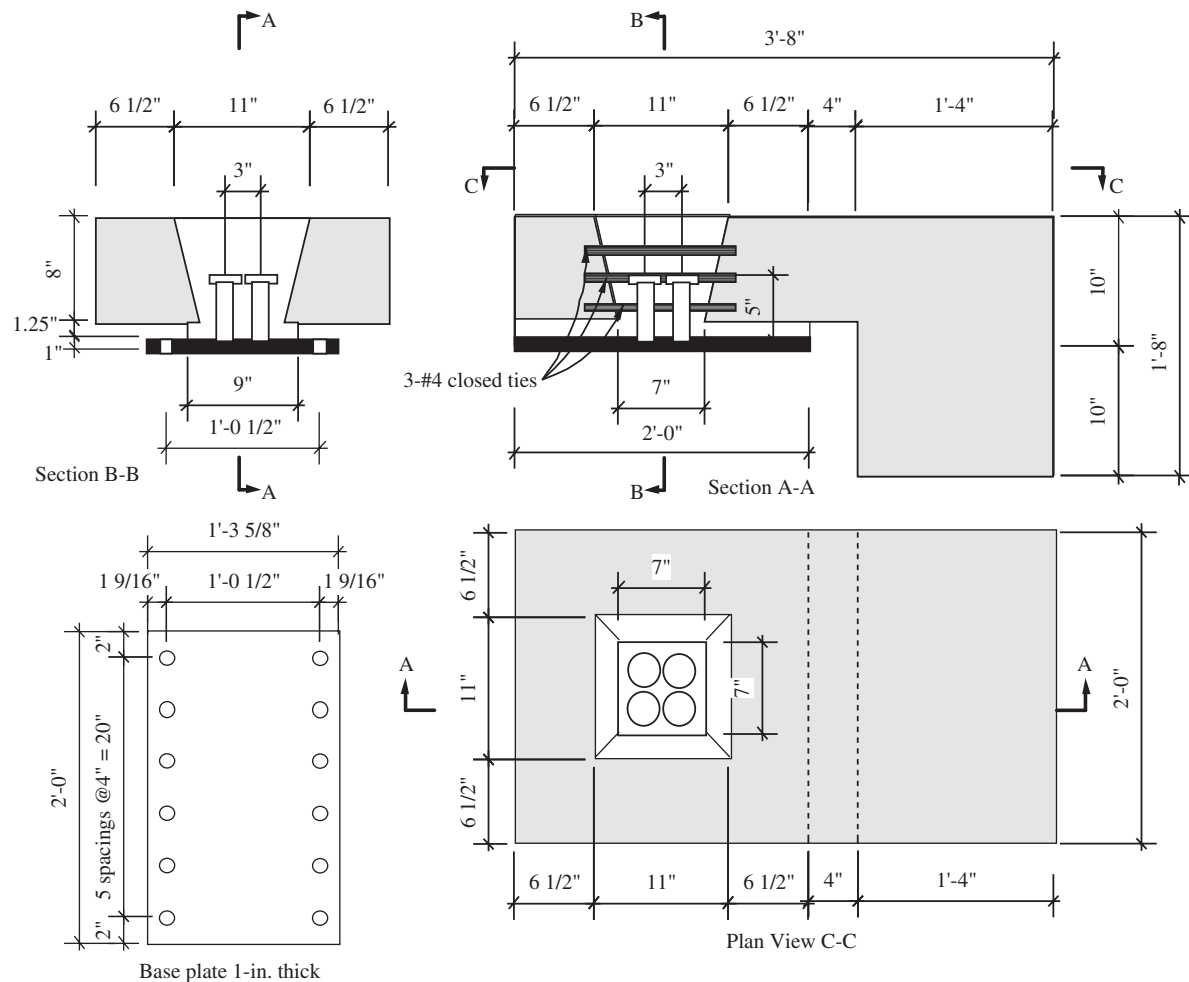


Figure 65. Concrete dimensions of P-4-CT-U.

the rest of the studs without using the tri-legged support. The studs were welded using a direct current power supply of 2,600 A. The welding was successful at an average rate of 1.8 sec/stud. The quality of the stud welding was checked using the following three measures:

- Visual inspection. The weld was visually inspected to make sure that the melted material formed a complete and uniform flash (i.e., dam or weld collar) at the base of the stud with no flaws, as shown in Figure 75. Also, the bottom surface of the 1 in. (25 mm) thick steel plate was inspected to make sure that the generated heat did not melt the full thickness of the plate.
- Bending the stud to 45 degrees. Most of the state agency specifications require that a stud be bent 45 degrees without failure. Figure 75 shows the 1¼ in. (31.8 mm) stud was successfully bent to 45 degrees with no sign of failure at the base.
- Using a portable hydraulic jacking device. A portable hydraulic jacking device that could be used in the field or in

the shop was developed (34, 42). The device consists of two collars placed around two adjacent studs, a small hydraulic jack, and a top tie, as shown in Figure 75. The collar consists of two steel blocks tied together with four screws. By tightening the four screws, the collar is placed in full contact with the 1¼ in. (31.8 mm) stud. The base of the collar is recessed to accommodate the weld at the stud base. A compact 100 kip (445 kN) hydraulic jack is placed between the collars to provide lateral shearing force at the stud base. The top tie, which consists of two plates and two threaded rods, is used to protect the studs from bending and to protect the technicians during the test. The quality control test is conducted by applying a horizontal force that would cause an axial tension failure in the stud. This force can be calculated by analyzing the studs with the top tie as a closed frame action, where the studs are fixed at their base and hinged at the top. The device was successfully used to test studs used in the experimental program. An 85 kip (378 kN) force was applied on two adjacent studs, and no signs of failure were observed at the stud base.

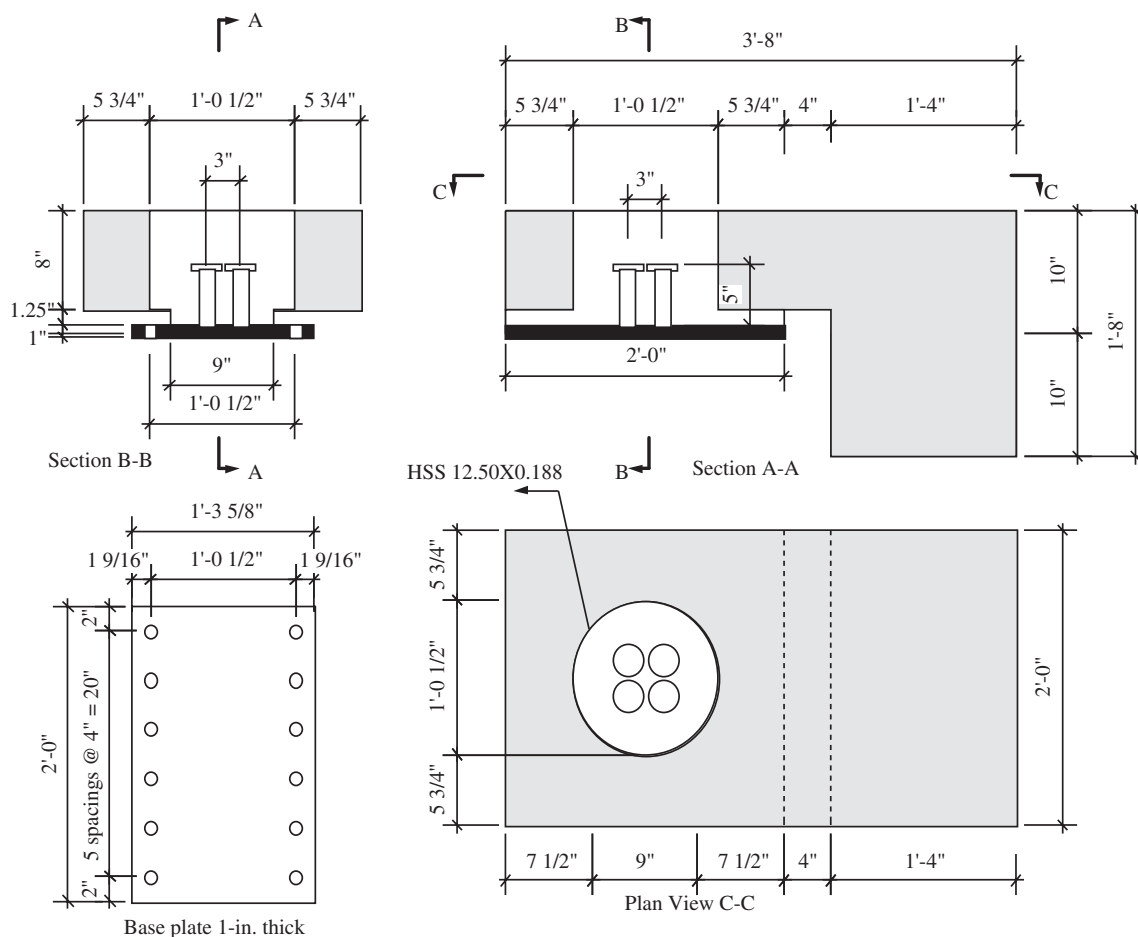


Figure 66. Concrete dimensions of P-4-ST-U.

A normal weight concrete mix with 6 ksi (41 MPa) specified concrete strength was used to make the specimens. The shear pockets of the specimens were filled with an SS Mortar mix containing 50% pea gravel ($\frac{1}{4}$ in., 6 mm, diameter). Figure 76 shows the compressive strength gain with age of the concrete and grout mixes.

The specimens were tested using a horizontal self-equilibrium frame, as shown in Figure 77. Because a nonsymmetric specimen was used, it was expected that the specimen would move upward at the bearing end of the specimen where the load was applied, which would lead to a premature and unrealistic failure. Therefore, a steel frame was built around the bearing area of the specimen, as shown in Figure 77. The steel frame was provided with roller supports to allow for horizontal sliding of the specimen. All specimens were tested when the grout was 28 days or older.

The specimens of Group 1 were tested by applying the load at mid height of the 8 in. (203 mm) thick slab at a rate of about 5 kip (22 kN) per second. The relative horizontal movement between the steel plate and the concrete specimen was recorded with a linear variable displacement transducer (LVDT).

The specimens of Group 2 were tested using the following steps: (a) the specimen was loaded with a static load equal to the fatigue capacity of the stud group as determined by the LRFD specifications (7), and the relative horizontal movement between the steel plate and the concrete specimen was recorded; (b) the specimen was exposed to 2,000,000 cycles of fatigue load, and the upper limit of the fatigue load was the fatigue capacity of the stud group as determined by the LRFD specifications (7), and the lower limit was 5 kip (22 kN) to maintain equilibrium of the specimen; and (c) the upper limit of the fatigue load was applied as a static load, and relative horizontal movement was recorded. At all steps, the load was applied at mid height of the 8 in. (203 mm) thick slab.

Fatigue and Ultimate Capacities of Steel Studs

Fatigue Capacity. The fatigue capacity was estimated in accordance with Equation 6.10.10.2-1 of the LRFD specifications (7). No other model of the of the fatigue capacity was considered in this study because the literature review revealed

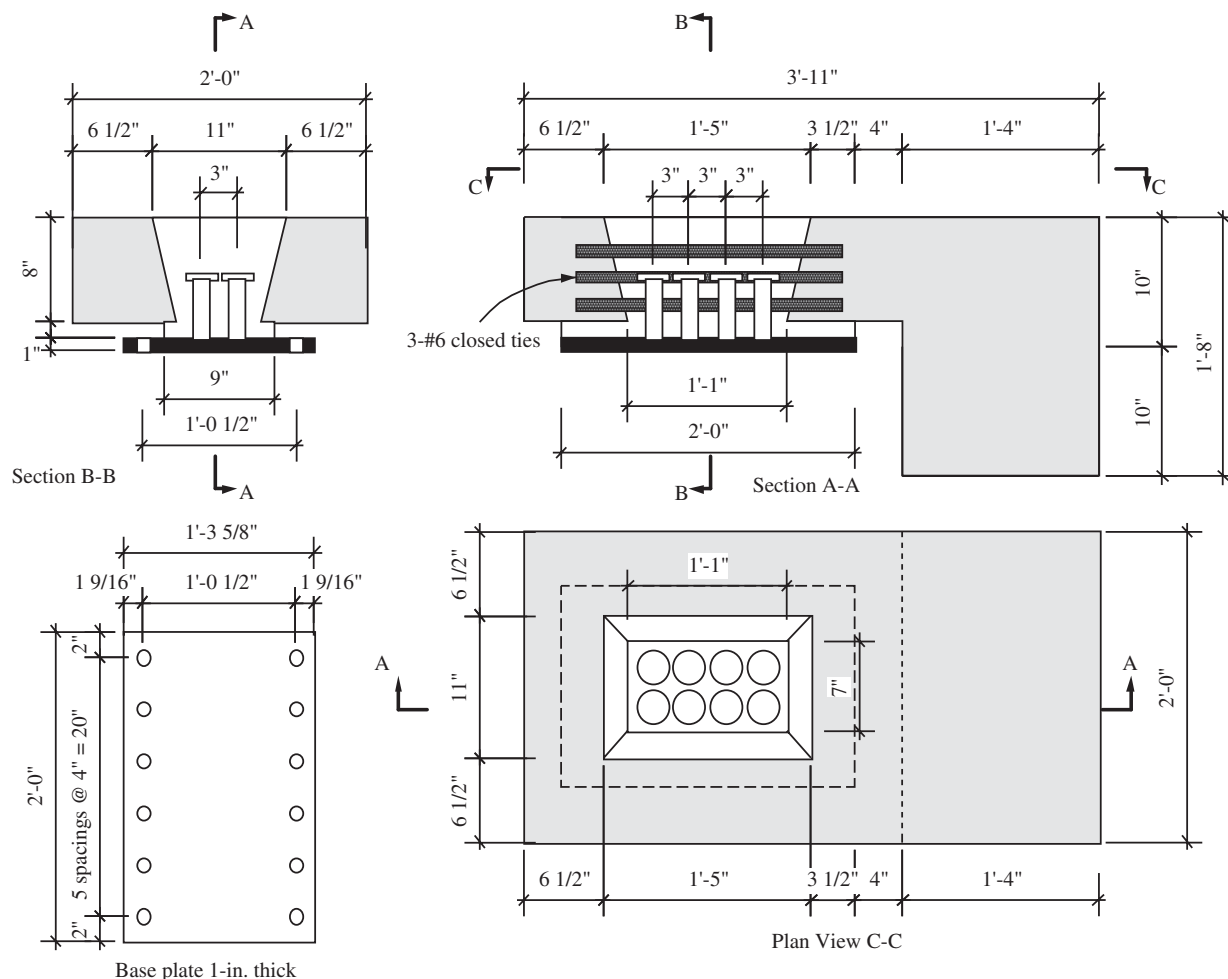


Figure 67. Concrete dimensions of P-8-CT-U.

that this equation gives a fair estimate for all sizes of studs used on bridges, including the 1¼ in. (31.8 MPa) stud.

$$Z_r = \alpha d^2 \geq \frac{5.5}{2} d^2 \quad (8) \quad (\text{English Units})$$

$$\alpha \text{ (ksi)} = 34.5 - 4.28 \log (N) \quad (9) \quad (\text{English Units})$$

where

Z_r = fatigue resistance force of shear connector (kip),

d = stud diameter (in.) = 1.23 in., and

N = number of cycles.

For 2,000,000 cycles and 1¼ in. stud:

$$\alpha = 7.53 \text{ ksi} > \frac{5.5}{2} \text{ ksi}, \text{ and } Z_r = 7.53 \times 1.25^2 = 11.77$$

kip/stud

Four-stud cluster: $Z_r = 4 \times 11.77 = 47.08$ kip (209 kN)

Eight-stud cluster: $Z_r = 8 \times 11.77 = 94.16$ kip (418 kN)

Ultimate Capacity. The following sources were used to estimate the ultimate capacity of the stud group.

- The design equation developed by Viest (46) for studs with diameter greater than 1.0 in. (25 mm):

$$Q_{cr} = 5d_s^2 f'_c \sqrt{4.0 / f'_c} \quad (10) \quad (\text{English Units})$$

where

Q_{cr} = critical load (lb)

d_s = stud diameter (in) = 1.25 in.

f'_c = compressive strength of the grout mix surrounding the stud (ksi) = 9.6 ksi

$$Q_{cr} = 5 \times 1.25^2 \times 9.6 \sqrt{4.0 / 9.6} = 48.4 \text{ kip.}$$

Four-stud cluster: $Q_{cr} = 4 \times 48.4 = 193.6$ kip (861.1 kN)

Eight-stud cluster: $Q_{cr} = 8 \times 48.4 = 387.2$ kip (1722.2 kN)

This equation was considered in this research because it was the only equation that was found in the literature that was developed for studs with a diameter greater than 1.0 in. (25 mm). It was also reported by Issa et al. (31) that this equation correlates well with test results when it was used to determine the ultimate capacity of studs clustered in groups.

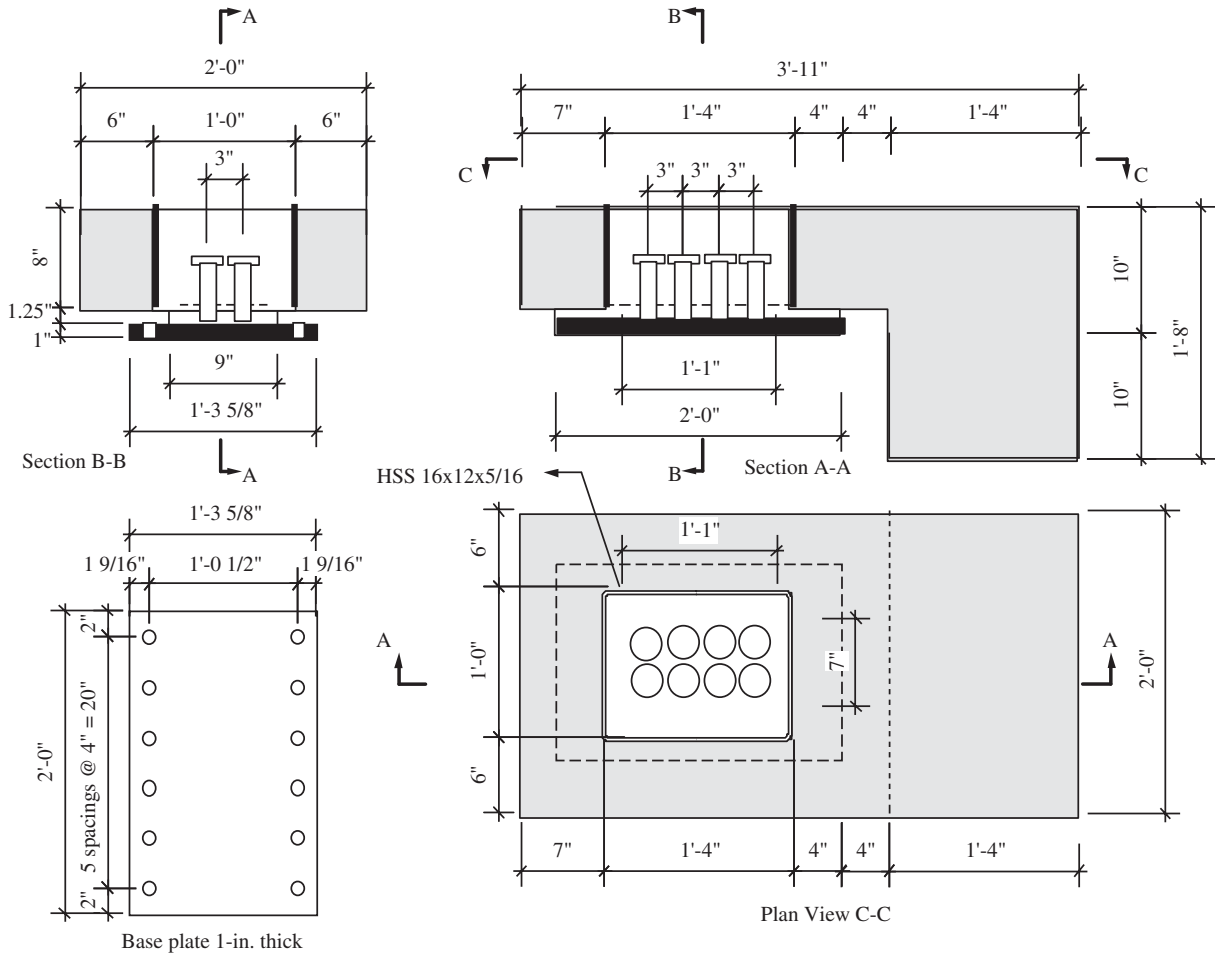


Figure 68. Concrete dimensions of P-8-ST-U.

- The design equation developed by Ollgaard et al. (45): This equation was developed using statistical analysis of push-off specimens, where the slab had not failed prematurely through splitting.

$$D_{max} = 1.1 A_{sh} (f'_c)^{0.3} (E_c)^{0.44} \quad (11) \quad (\text{English Units})$$

where

D_{max} = critical load (kip)

A_{sh} = cross-sectional area of $1\frac{1}{4}$ in. stud (in^2) = 1.23 in^2

f'_c = compressive strength of the grout mix surrounding the stud (ksi) = 9.6 ksi

E_c = modulus of elasticity of the grout mix surrounding the stud (ksi)

$$= 33,000 w_c^{1.5} \sqrt{f'_c} \quad (12) \quad (\text{English Units})$$

where w_c = unit weight of grout mix surrounding the studs (kcf) = 0.145 kcf

$$= 33,000(0.145)^{1.5} \sqrt{9.6} = 5,646 \text{ ksi}$$

$$D_{max} = 1.1 \times 1.23(9.6)^{0.3}(4,463)^{0.44} = 119.3 \text{ kip/stud}$$

Four-stud specimens: $D_{max} = 4 \times 119.3 = 477.2 \text{ kip}$ (2122.6 kN)

Eight-stud specimens: $D_{max} = 8 \times 119.3 = 954.4 \text{ kip}$ (4245.2 kN)

In the four- and eight-stud specimens, the estimated shear capacity is greater than the ultimate tensile capacity.

- The design equation developed by Oehlers and Johnson (48): Using an approach similar to that used by Ollgaard et al., Oehlers and Johnson developed the following equation for the maximum shear capacity of steel studs:

$$D_{max} = \left(5.3 - \frac{1.3}{\sqrt{n}} \right) A_{sh} f_u \left(\frac{f'_c}{f_u} \right)^{0.35} \left(\frac{E_c}{E_s} \right)^{0.40} \quad (13) \quad (\text{English Units})$$

where

D_{max} = critical load for push-off specimens per stud (kip)

A_{sh} = cross-sectional area of $1\frac{1}{4}$ in. studs per group (in^2) = 4×1.23 or $8 \times 1.23 \text{ in}^2$

f_u = ultimate tensile strength of the stud material (ksi) = 64 ksi

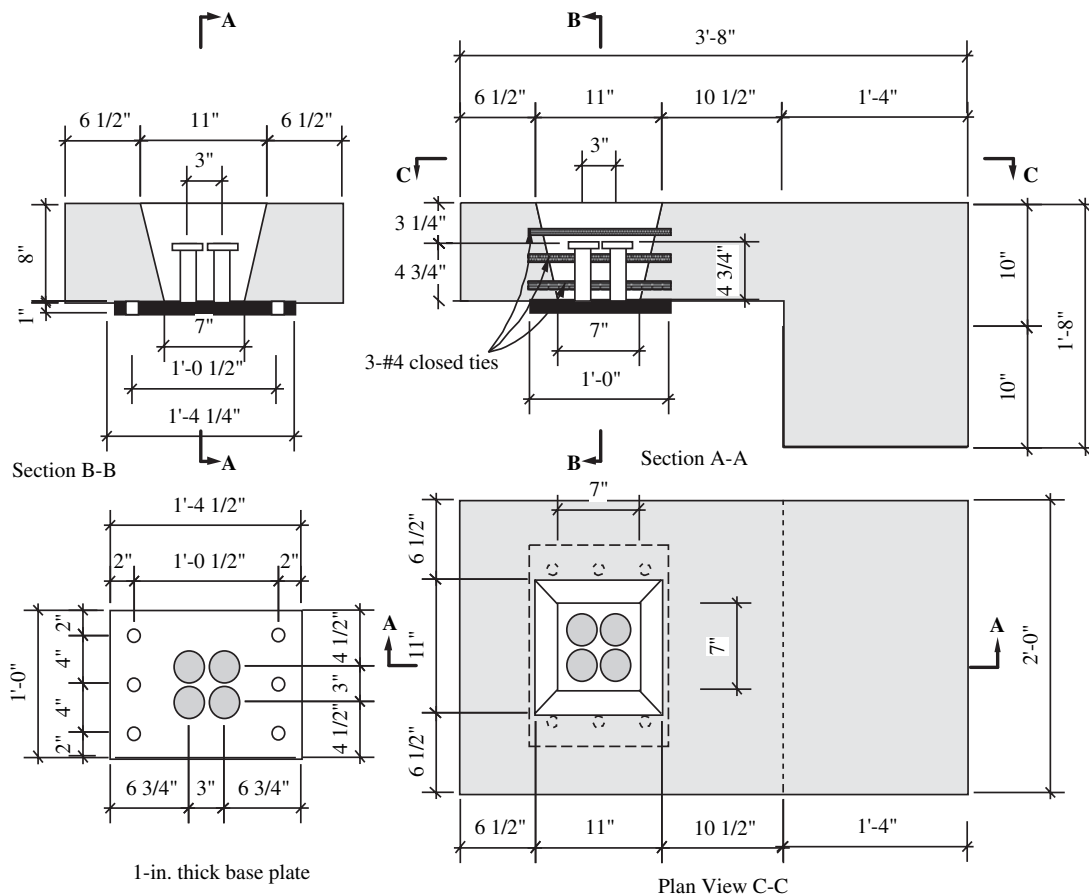


Figure 69. Concrete dimensions of P-4-CT-F/U.

f'_c = compressive strength of the concrete surrounding the stud (ksi) = 9.6 ksi

E_c = modulus of elasticity of the concrete (ksi) = 5,645 ksi

E_s = modulus of elasticity of the stud material (ksi) = 29,000 ksi

n = number of studs per group = 4 or 8.

Four-stud specimens

$$D_{max} = \left(5.3 - \frac{1.3}{\sqrt{4}} \right) (4 \times 1.23) (64) \left(\frac{9.6}{64} \right)^{0.35} \left(\frac{5,645}{29,000} \right)^{0.40}$$

$$= 391.7 \text{ kip (1742.3 kN)}$$

Eight-stud specimens

$$D_{max} = \left(5.3 - \frac{1.3}{\sqrt{8}} \right) (8 \times 1.23) (64) \left(\frac{9.6}{64} \right)^{0.35} \left(\frac{5,645}{29,000} \right)^{0.40}$$

$$= 815.4 \text{ kip (3626.9 kN)}$$

In both the four- and eight-stud specimens, the estimated shear capacity is greater than the ultimate tensile capacity.

- Equation 6.10.10.4.3-1 of the AASHTO LRFD specifications (7): This equation was derived from the equation developed by Ollgaard et al. (45) after changing the exponents of f'_c , E_c

to make the equation dimensionally correct and limiting the shear capacity by the ultimate tensile capacity of the stud.

$$Q_n = 0.5 A_{sc} \sqrt{f'_c E_c} \leq A_{sc} F_u \quad (14) \quad (\text{English Units})$$

where

Q_n = nominal capacity (kip)

A_{sc} = cross-sectional area of 1/4 in. stud (in²) = 1.23 in²

f'_c = compressive strength of the concrete surrounding the stud (ksi) = 9.6 ksi

E_c = modulus of elasticity of the concrete surrounding the stud (ksi) = 5,645 ksi

F_u = ultimate tensile strength of the stud material (ksi) = 64 ksi.

$$Q_n = \text{least} \left\{ \begin{array}{l} 0.5 \times 1.23 \sqrt{9.6 \times 5,645} = 143.2 \text{ kips} \\ 1.23 \times 64 = 78.7 \text{ kips} \end{array} \right\} = 78.7 \text{ kip/stud}$$

Four-stud cluster: $Q_n = 4 \times 78.7 = 314.8 \text{ kip (1400.2 kN)}$

Eight-stud cluster: $Q_n = 8 \times 78.7 = 629.6 \text{ kip (2800.4 kN)}$

- Equation 5.8.4.1-1 of the LRFD specifications (7): This equation is derived from the shear friction theory and is commonly used for the design of horizontal shear reinforcement for slab/concrete girder composite beams.

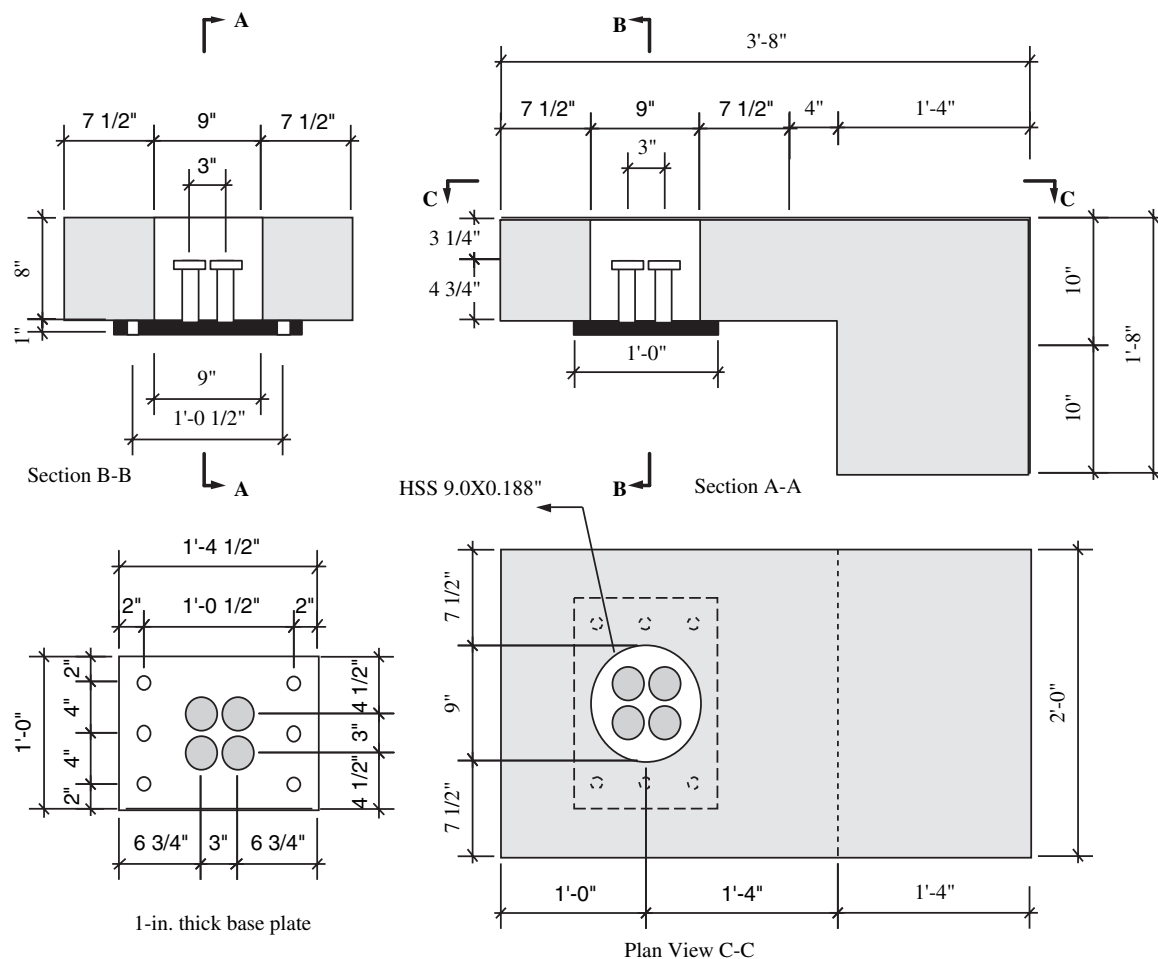


Figure 70. Concrete dimensions of P-4-ST-F/U.

However, the LRFD specifications (7) give values for c and μ if steel beams are used. Using Equation 7 gives

$$V_n = (0.025 \text{ ksi})(113 \text{ in}^2) + 0.7(4.92 \text{ in}^2)(54 \text{ ksi}) \\ = 188.8 \text{ kip (839.8 kN) (four-stud specimens)}$$

$$V_n = (0.025 \text{ ksi})(192 \text{ in}^2) + 0.7(9.84 \text{ in}^2)(54 \text{ ksi}) \\ = 376.8 \text{ kip (1676.0 kN) (eight-stud specimens)}$$

Limits on V_n given by Equations 5.8.4.1-2 and 5.8.4.1-3 of the LRFD specifications (7) are not used here as the shear pockets are confined with HSS tubes or closed ties, which protect the grout surrounding the studs from crushing at the limits given by these equations.

Table 8 summarizes the ultimate capacity using various sources.

Test Results and Discussion

The test results of Groups 1 and 2 are summarized in Table 9 and Figures 78 to 81.

Table 9 gives the failure load and the mode of failure for all the specimens. This table also gives the failure load, F_f , as a percentage of estimated ultimate capacity according to Viest (46), Ollgaard et al. (45), Oehlers and Johnson (48), and Equations 6.10.10.4.3-1 and 5.8.4.1-1 of the LRFD specifications (7).

Figure 78 shows the failure modes of Group 1 specimens.

Figure 79 shows the load-displacement relationship of Group 1 specimens when they were tested for ultimate capacity.

Figure 80 gives the load-displacement relationship of Group 2 specimens due to fatigue load before and after applying the 2,000,000 cycles of fatigue load.

Figure 81 shows the failure mode of Group 2 specimens.

Fatigue Capacity of Clustered Studs. No signs of concrete/grout crushing, weld failure, or local distress around or inside the shear pockets were observed when the push-off specimens, with four and eight $1\frac{1}{4}$ in. studs, were exposed to 2,000,000 cycles of fatigue load. Also, as shown in Figure 80, there was almost no change in the load-displacement relationship of the push-off specimens after applying the

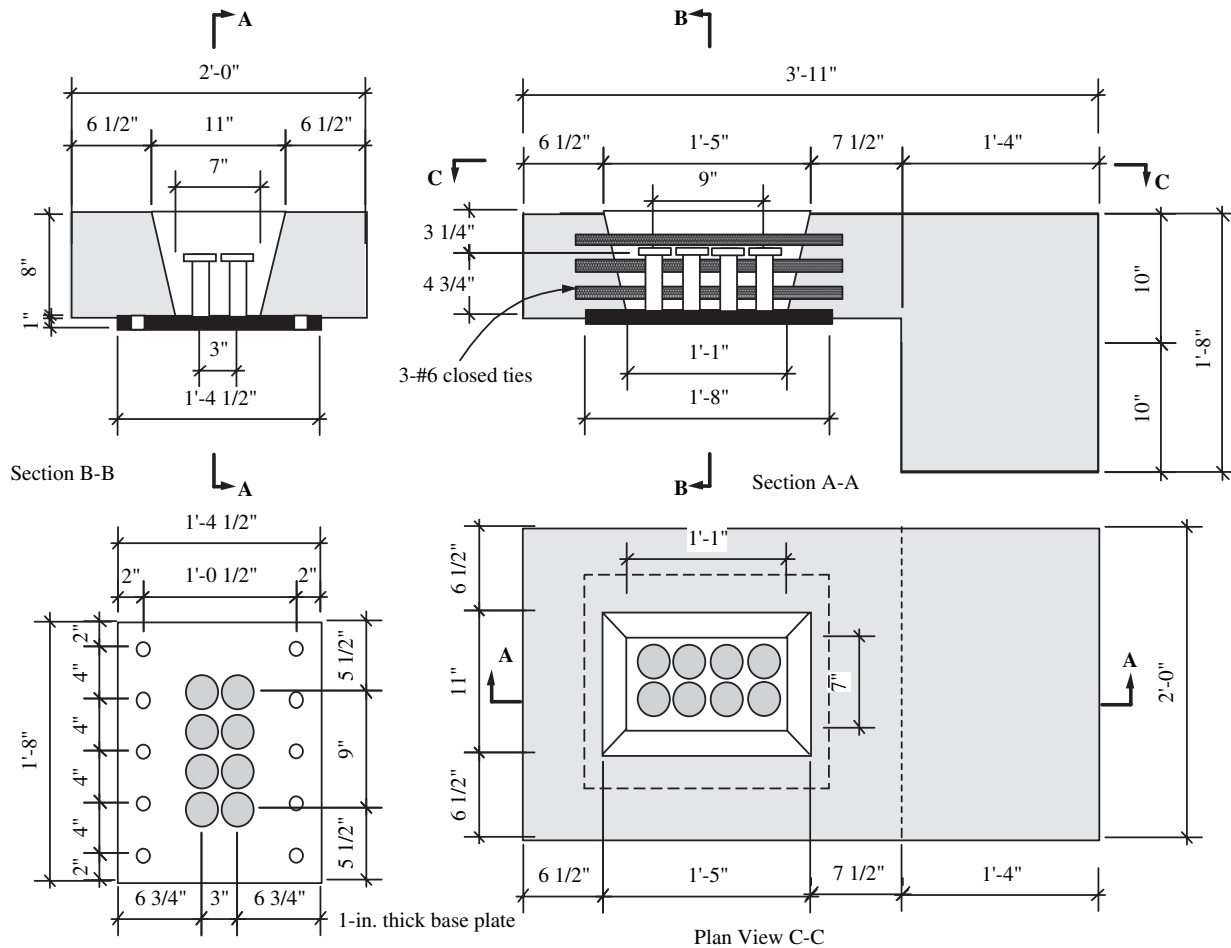


Figure 71. Concrete dimensions of P-8-CT-F/U.

2,000,000 cycles. This observation is consistent with the fatigue test that was conducted on full-scale beams tested later in this research, and the fatigue test results of a half-scale beam tested by Markowski et al. (32). The research team strongly believes that this equation can be satisfactorily used for the design of composite beams made with clusters of eight $1\frac{1}{4}$ in. (31.8 mm) studs spaced as much as 48 in. (1220 mm) apart.

Ultimate Capacity of Clustered Studs. Comparing the test results of the four-stud and eight-stud specimens shows that, regardless of the type of confinement used around the stud group, the ultimate capacity did not proportionally increase when the number of studs was doubled.

Regardless of the number of studs, the ultimate capacity of a stud group confined with the steel tube is about 5% to 15% higher than the ultimate capacity of the same stud group confined with individual closed ties. The difference is more pronounced with the four-stud group than with the eight-stud group.

Regardless of the number of studs per group and the type of stud confinement, Equation 6.10.10.4.3-1 of the AASHTO LRFD specifications (7) overestimated the ultimate capacity

by as much as 50%. The same observation applies to the equations developed by Ollgaard et al. (45) and Oehlers and Johnson (48), where the ultimate capacity is overestimated by as much as 60%.

For push-off specimens tested directly for ultimate capacity, Equation 6.10.10.4.3-1 of the AASHTO LRFD specifications (7) and the equation developed by Viest (46) correlate very well with the test results. This observation is consistent with the findings of Issa et al. (31) that were obtained from testing of quarter-scale symmetric specimens made with two, three, and four $\frac{7}{8}$ in. (22 mm) stud groups.

Comparison between the test results of Group 1 and Group 2 in Table 9 shows that the 2,000,000 cycles of fatigue load reduced the ultimate capacity by about 5% to 18%. The reduction is more pronounced with (a) stud groups confined with closed ties than those confined with steel tubes, (b) specimens made with eight studs than those made with four studs, and (c) Equation 6.10.10.4.3-1 of the AASHTO LRFD specifications (7) and the equation developed by Viest (46) than the other three equations.

A bond failure between the lower tie and the concrete slab was observed in most of the specimens made with closed in-

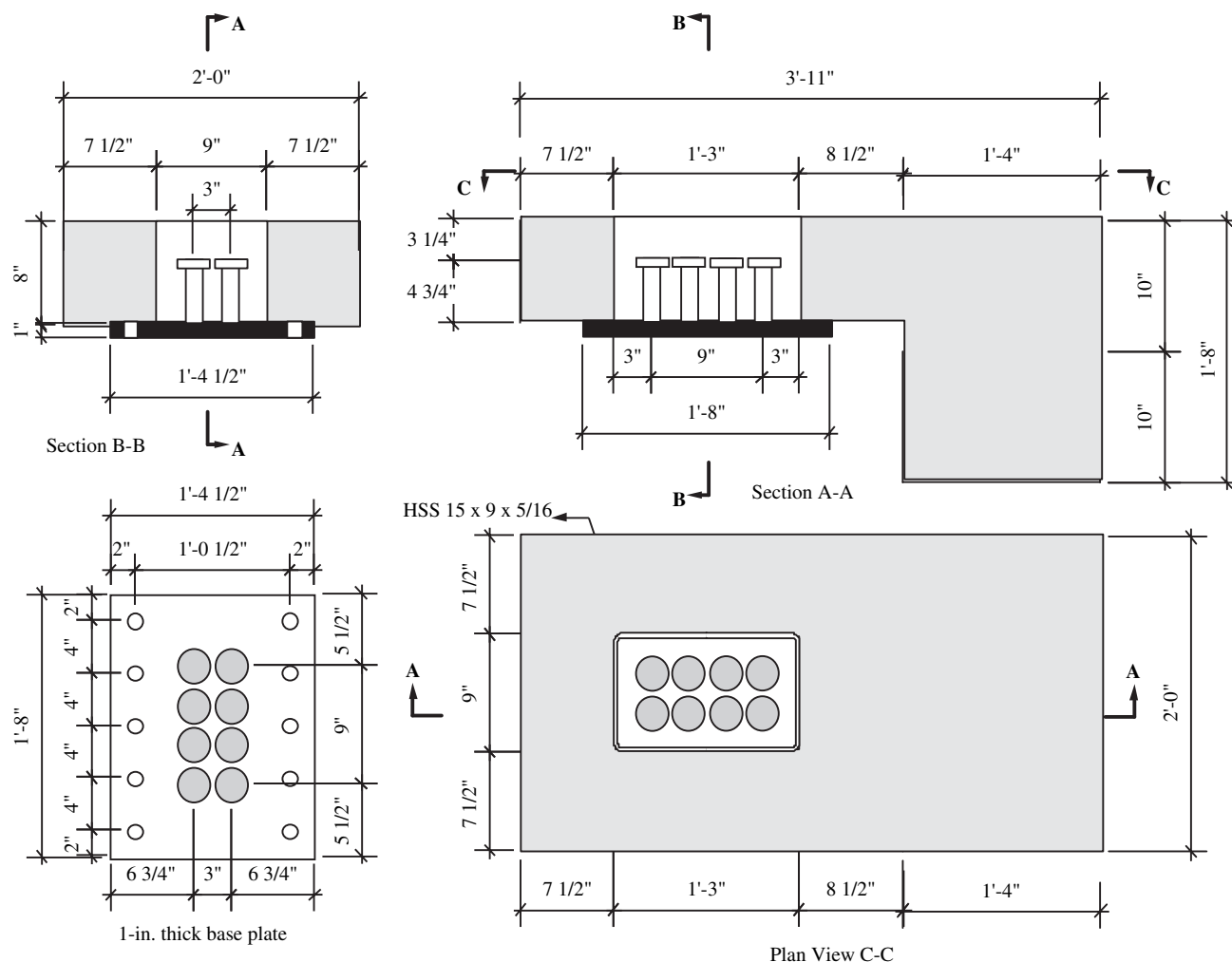


Figure 72. Concrete dimensions of P-8-ST-F/U.

dividual ties and subjected to the 2,000,000 cycles of fatigue load. It is believed that this failure occurred because of the large size of the bar used in this detail, which led to high stress concentration in this area. Using No. 4 or No. 5 closed ties might help avoid this failure.

Shape of the Push-Off Specimens. In future investigations, it is recommended to use symmetric push-off specimens instead of the L-shaped specimen that was used in this research. However, due to the expected high load that is required to break the symmetric specimen, half- or quarter-scale specimens should be used.

Comparing the failure modes of Group 1 and Group 2 shows that the side external confinement of the specimen is very important to overcome the limited-width problem of the push-off specimens. All the specimens of Group 1 had slab failure, while almost all of the specimens of Group 2 had stud failure. Unfortunately, no mathematical models are available to quantify the amount of the side confinement needed to simulate a real bridge.

Finite Element Investigation of the Push-Off Specimens

The finite element method was used to investigate the behavior of the push-off specimens. A commercial finite element package (Nastran) was used in the analysis. The push-off concrete specimen and the grout filling the shear pocket were modeled using a eight-node cube element. Each node has three translational degrees of freedom (x, y, and z direction). The confining tube and the individual closed ties were modeled using the thin shell element. The circular cross section of the studs was replaced with a square cross section with equivalent area. The studs were modeled using the 20-node cube element.

The following mechanical properties were assigned to the concrete mix of the specimen: compressive strength = 6.2 ksi (42.7 MPa), unit weight = 150 lb/ft³ (23.6 kN/m³), and Poisson ratio = 0.15.

The following mechanical properties were assigned to the grout mix: compressive strength = 9.6 ksi (66.2 MPa), unit weight = 145 lb/ft³ (22.8 kN/m³), and Poisson ratio = 0.15.

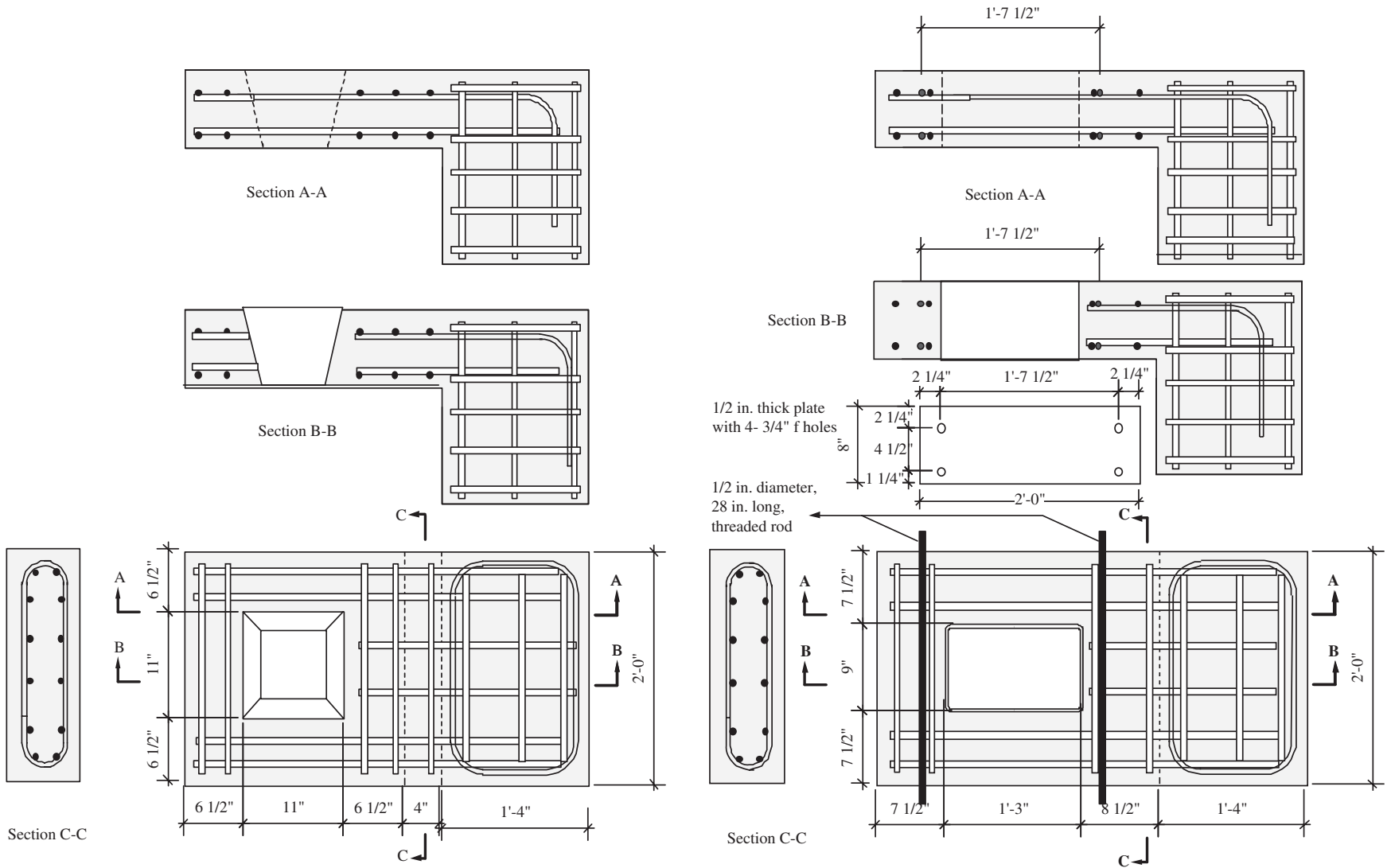
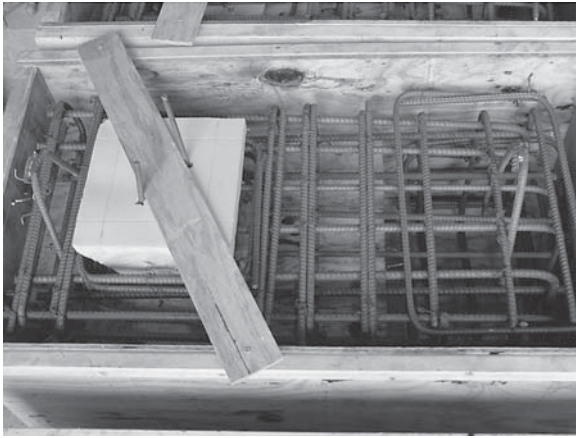
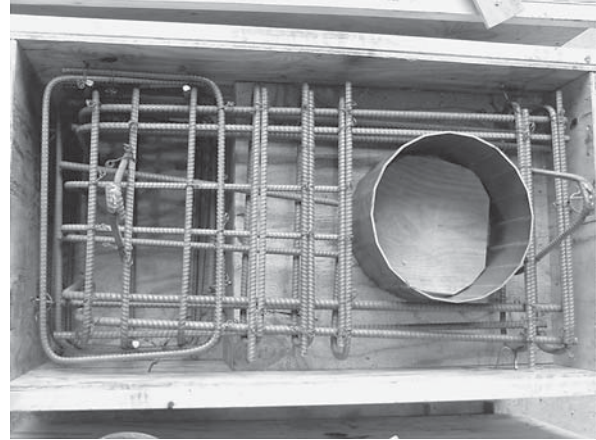


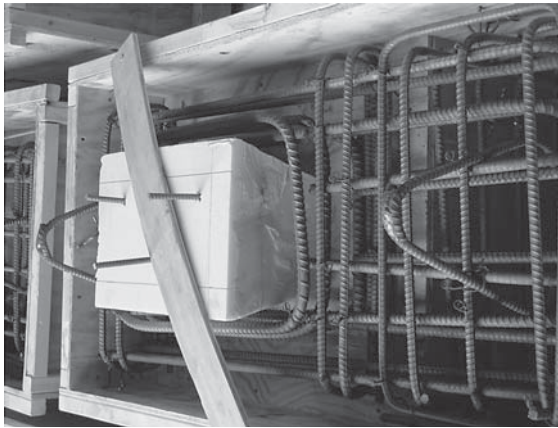
Figure 73. Typical reinforcement of the push-off specimens. Group 1 specimens on left, Group 2 specimens on right.



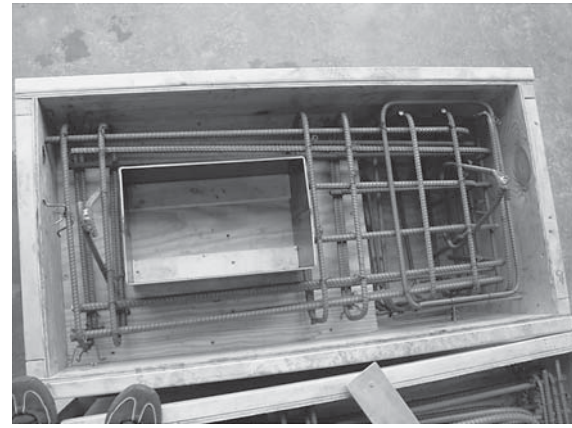
Specimen P-4-CT-U



Specimen P-4-ST-U



Specimen P-8-CT-U



Specimen P-8-ST-U



Figure 74. Fabrication of the push-off specimens.

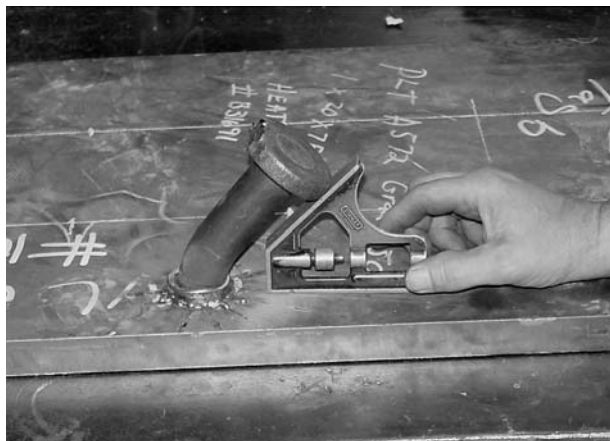


Figure 75. Welding of the 1¼-in. studs and the quality control tests.

The following mechanical properties were assigned to the stud: tensile strength = 64 ksi (441 MPa), yield strength = 54 ksi (372 MPa), unit weight = 490 lb/ft³ (76.9 kN/m³), and Poisson ratio = 0.30.

Details of the finite element model are given in Appendix F. To check the validity of Equation 6.10.10.4.3-1 of the AASHTO LRFD specifications (7) for studs clustered in groups, each spec-

imen was loaded with a horizontal load equal to the ultimate horizontal shear capacity determined by this equation. The load was surface loaded on a 10 × 10 in. (254 × 254 mm) area on the bearing block of the specimen to simulate the test setup. The result of the surface load was at mid height of the 8 in. (203 mm) thick slab. Appendix F gives the results of the finite element
(continued text on page 86)

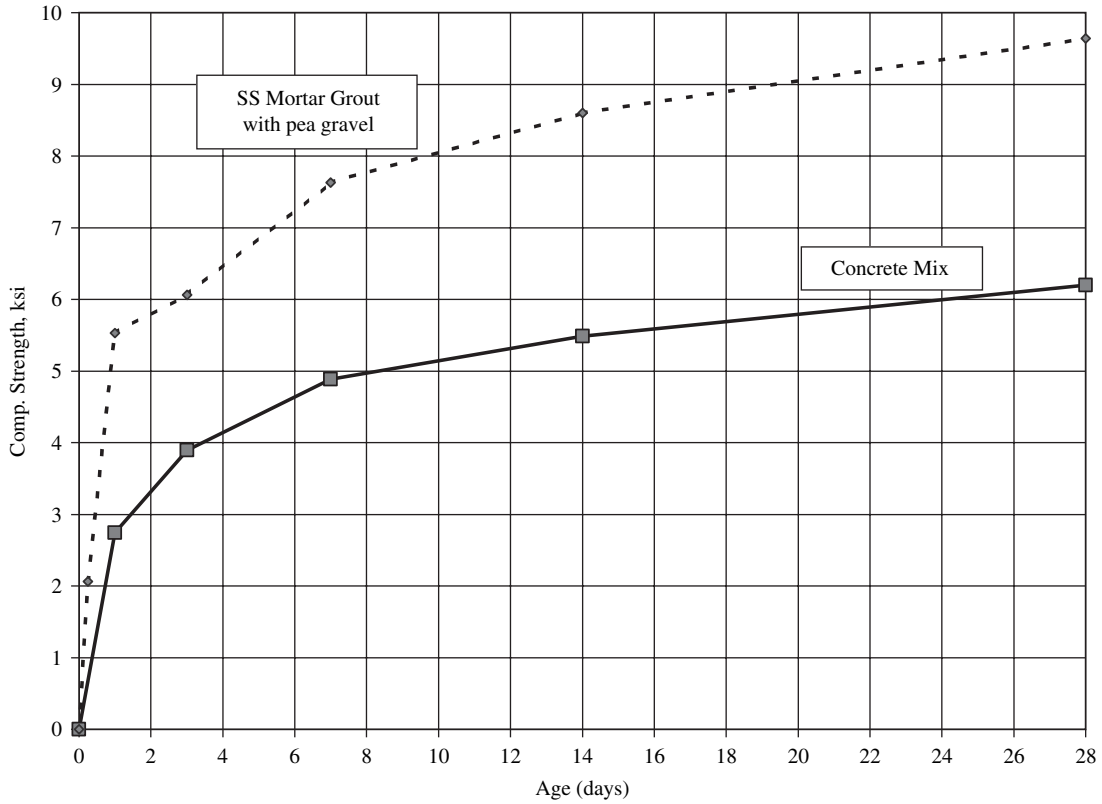


Figure 76. Compressive strength versus age of the concrete mix and grout.

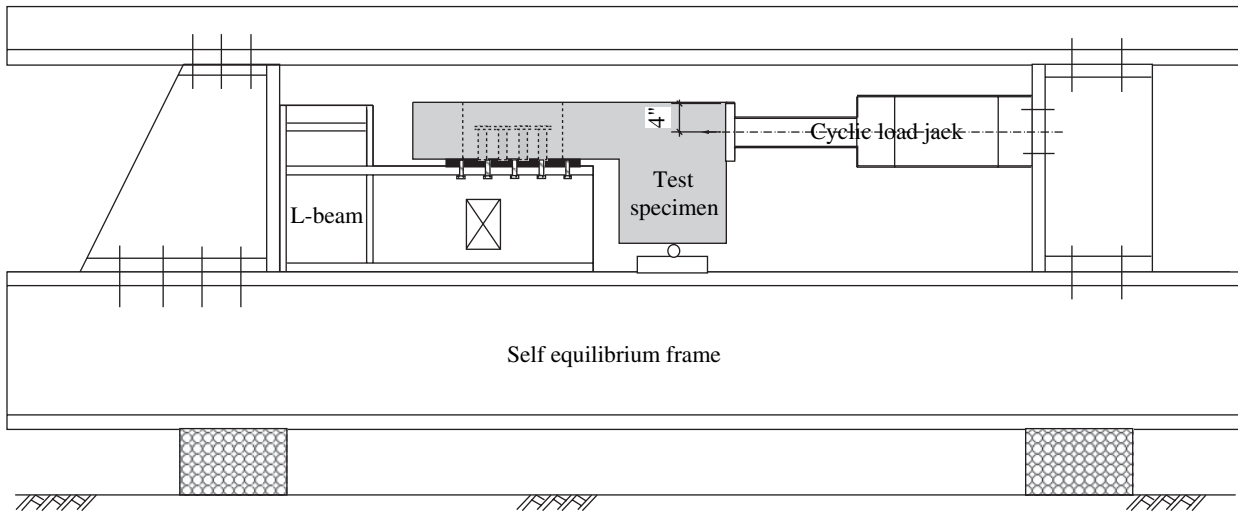


Figure 77. Test setup.

Table 8. Ultimate capacity of the stud cluster using various models.

Source	Ultimate Capacity, kip (kN)	
	Four Studs	Eight Studs
Viest (46)	193.6 (861.1)	387.2 (1722.3)
Ollgaard et al. (45)	477.2 (2122.6)*	954.4 (4245.2)*
Oehlers and Johnson (48)	391.7 (1742.3)*	815.4 (3626.9)*
LRFD Specifications (7), Equation 6.10.10.4.3-1	314.8 (1400.2)**	629.6 (2800.5)**
LRFD Specifications (7), Equation 5.8.4.1-1	188.8 (839.8)	376.8

* Shear capacity is greater than the tensile ultimate capacity.
 ** Shear capacity is controlled by the tensile ultimate capacity.

Table 9. Test results of the push-off panel-to-steel specimens.

	Test Failure Load, F_f kip	Failure Mode	Viest (46)	Ollgaard et al. (45)	Oehlers and Johnson (48)	LRFD Specs. (7) Equation 6.10.10.4.3-1	LRFD Specs. (7) Equation 5.8.4.1-1	See Figure
			$\frac{F_f}{Q_{cr}}$	$\frac{F_f}{D_{max}}$	$\frac{F_f}{D_{max}}$	$\frac{F_f}{Q_n}$	$\frac{F_f}{V_n}$	
Group 1: Ultimate test, 1.25-in. haunch, no external confinement on the specimen, four studs per specimen.								
P-4-ST-U	237	The load was applied by mistake at the interface level Slab failure: 1. Inclined crack on the side of the concrete specimens. 2. No grout crushing 3. All studs bent to about 5 degrees	122%	50%	61%	75%	126%	78-a
	313	Slab failure: 1. Vertical crack on the side of the concrete specimens. 2. No grout crushing 3. All studs bent to about 10 degrees	162%	66%	80%	99%	166%	78-b
Average for P-4-ST-U (four studs and steel tubes)			142%	58%	71%	87%	146%	
P-4-CT-U	241	Slab failure: 1. Horizontal crack on the side of the concrete specimen 2. The slab lifted away from the steel plate and the specimen could not take any more load	124%	51%	62%	77%	128%	78-c
	259	Slab failure: 1. Horizontal crack on the side of the concrete specimen 2. The slab lifted up from the steel plate and the specimen could not take any more load	134%	54%	66%	82%	137%	78-d
Average for P-4-CT-U (four studs and closed ties)			129%	53%	64%	80%	133%	
Average for P-4-ST-U and P-4-CT-U (all four-stud ultimate specimens)			136%	56%	68%	84%	140%	

Table 9. (Continued).

	Test Failure Load, F_f kip	Failure Mode	Viest (46)	Ollgaard et al. (45)	Oehlers and Johnson (48)	LRFD Specs. (7) Equation 6.10.10.4.3-1	LRFD Specs. (7) Equation 5.8.4.1-1	See Figure
			$\frac{F_f}{Q_{cr}}$	$\frac{F_f}{D_{max}}$	$\frac{F_f}{D_{max}}$	$\frac{F_f}{Q_n}$	$\frac{F_f}{V_n}$	
Group 1: Ultimate test, 1.25-in. haunch, no external confinement on the specimen, eight studs per specimen.								
P-8-ST-U	400	Slab failure: 1. Concrete bearing failure at the bearing block of the specimen 2. No grout crushing 3. Studs remained almost vertical	103%	42%	49%	64%	106%	78-e
	346	Slab failure: 1. Concrete bearing failure at the bearing block of the specimen 2. No grout crushing	89%	36%	42%	55%	92%	78-f
Average for P-8-ST-U (eight studs and steel tubes)			96%	39%	46%	60%	99%	
P-8-CT-U	376	Slab failure: 1. Horizontal crack on the side of the concrete specimen	97%	39%	46%	60%	100%	78-g
	318	Slab failure: 1. Horizontal crack on the side of the concrete specimen	82%	33%	39%	51%	85%	78-h
Average for P-8-CT-U (eight studs and closed ties)			90%	36%	43%	56%	92%	
Average P-8-ST-U and P-8-CT-U (all eight-stud ultimate specimens)			93%	38%	45%	58%	96%	
Average of all specimens in Group 1 (ultimate testing)			115%	47%	57%	71%	118%	

Table 9. (Continued).

	Test Failure Load, F_f , kip	Failure Mode	Viest (46)	Ollgaard et al. (45)	Oehlers and Johnson (48)	LRFD Specs. (7) Equation 6.10.10.4.3-1	LRFD Specs. (7) Equation 5.8.4.1-1	See Figure
			$\frac{F_f}{Q_{cr}}$	$\frac{F_f}{D_{max}}$	$\frac{F_f}{D_{max}}$	$\frac{F_f}{Q_n}$	$\frac{F_f}{V_n}$	
Group 2: Fatigue/ultimate test, no haunch, with side external confinement, four studs per specimen.								
P-4-ST-F/U	–	Could not be tested because the specimen rotated in the horizontal plan due to improper setup Test failed.	–	–	–	–	–	81-a
	231	Stud failure: 1. All studs failed at the welding area. 2. The grout around the studs did not crush. 3. Some of the concrete outside the confinement tube failed. 4. At failure load, some cracks around the confinement tube were observed on top of the specimen.	119%	48%	59%	73%	122%	81-b
	Average for P-4-ST-F/U (four studs and steel tubes)		119%	48%	59%	73%	122%	
P-4-CT-F/U	308	Stud/grout failure: 1. Two of the studs failed at the welding area. The other two bent about 30 degrees. 2. No cracks were observed on top of the specimen. 3. Grout inside the confinement area was crushed. 4. Concrete outside the confined grout area was crushed. 5. Bond failure between the bottom tie and the surrounding concrete.	159%	65%	79%	98%	163%	81-c
	220	Stud/concrete failure: 1. One stud failed at the welding area. The remaining studs bent about 25 degrees. 2. A cone-shape failure was observed in the grout around the studs. 3. Bond failure between the bottom tie and the surrounding concrete 4. A pronounced crack was observed on top of the specimen.	114%	46%	56%	70%	117%	81-d
	Average for P-4-CT-F/U (four studs and closed ties)		137%	56%	68%	84%	140%	
Average for P-4-ST-F/U and P-4-CT-F/U (all four-stud fatigue/ultimate specimens)			128%	52%	64%	79%	131%	

Table 9. (Continued).

	Test Failure Load, F_f , kip	Failure Mode	Viest (46)	Ollgaard et al. (45)	Oehlers and Johnson (48)	LRFD Specs. (7) Equation 6.10.10.4.3-1	LRFD Specs. (7) Equation 5.8.4.1-1	See Figure
			$\frac{F_f}{Q_{cr}}$	$\frac{F_f}{D_{max}}$	$\frac{F_f}{D_{max}}$	$\frac{F_f}{Q_n}$	$\frac{F_f}{V_n}$	
Group 2: Fatigue/ultimate test, no haunch, with side external confinement, eight studs per specimen.								
P-8-ST-F/U	379	The slab lifted off from the steel plate at the far edge and the specimen could not take any more load. 1. Plate did not come off the specimen. 2. No grout failure was detected 3. No cracks were observed on top or around the specimen.	98%	40%	46%	60%	101%	81-e
	300	Stud failure: 1. All studs failed. Two studs failed at the base material, four studs failed at the weld location, and the remaining two sheared off. 2. Grout crashed around the studs. 3. Concrete outside the steel tube confinement did not crack. 4. Slippage occurred between the steel tube and the grout inside 5. At failure load, there was a two-crack V shape at the side of the specimen. 6. At failure load, there was a very fine crack around the steel tube on top of the specimen.	77%	31%	37%	48%	80%	81-f
Average for P-8-ST-F/U (eight studs and steel tubes)			88%	36%	42%	54%	91%	
P-8-CT-F/U	245	Stud failure: 1. Two of the studs sheared off, the following two failed at the base material, and the remaining four bent about 20 degrees. 2. A cone-shaped failure was observed in the grout around the studs. 3. Bond failure between the bottom tie and the surrounding concrete	63%	26%	30%	39%	65%	81-g
	245	Bond failure of the lower closed tie: 1. The first four studs were bent about 15 degrees. The remaining four studs were slightly bent. 2. The failure was cone-shaped and formed around the group of studs. 3. Bond failure between the bottom tie and the surrounding concrete.	63%	26%	30%	39%	65%	81-h
Average for P-8-CT-F/U (eight studs and closed ties)			63%	26%	30%	39%	65%	
Average for P-4-ST-F/U and P-4-CT-F/U (all eight-stud fatigue/ultimate specimens)			76%	31%	36%	47%	78%	
Average of all specimens in Group 2 (fatigue/ultimate testing)			102%	42%	50%	63%	105%	

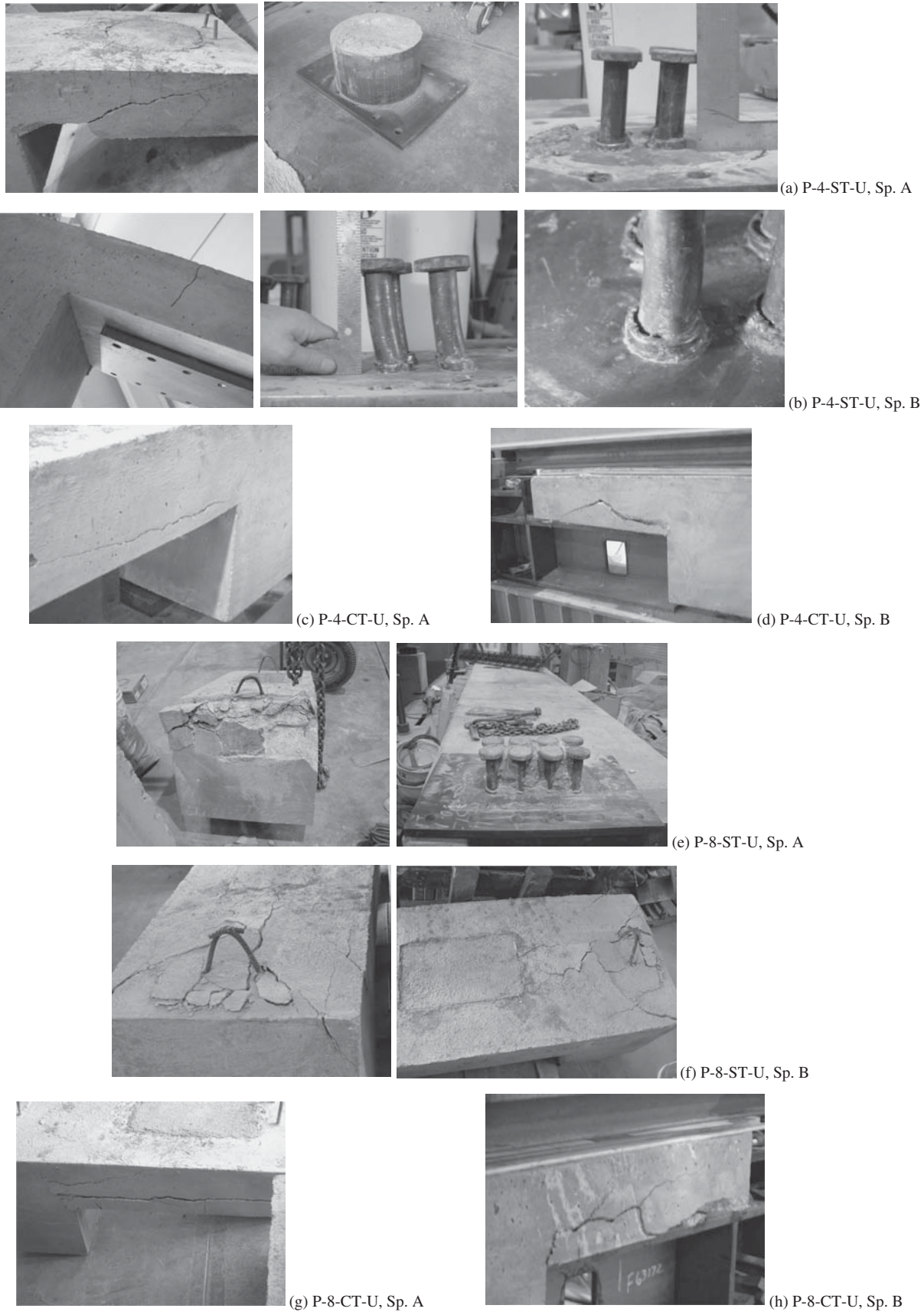


Figure 78. Failure modes of Group 1 push-off specimens.

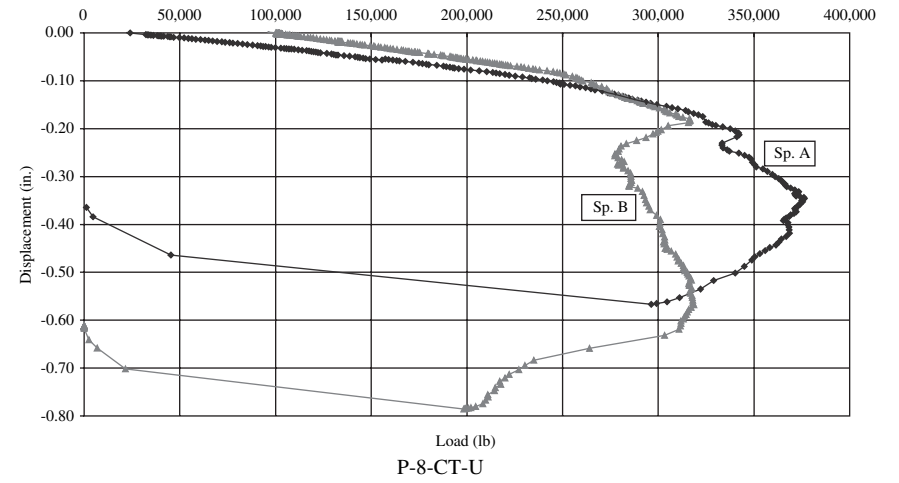
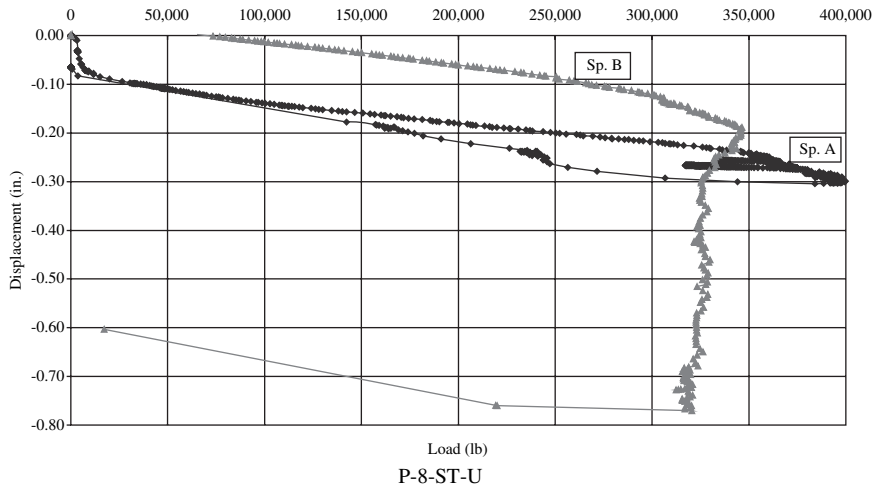
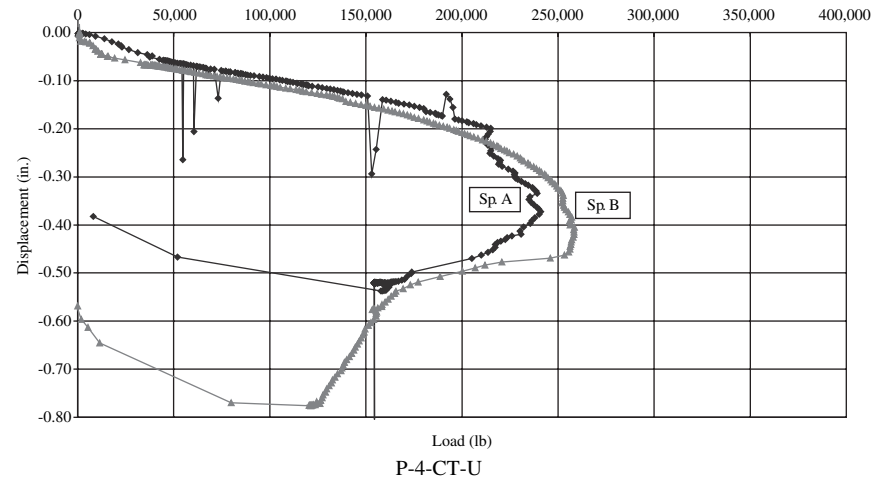
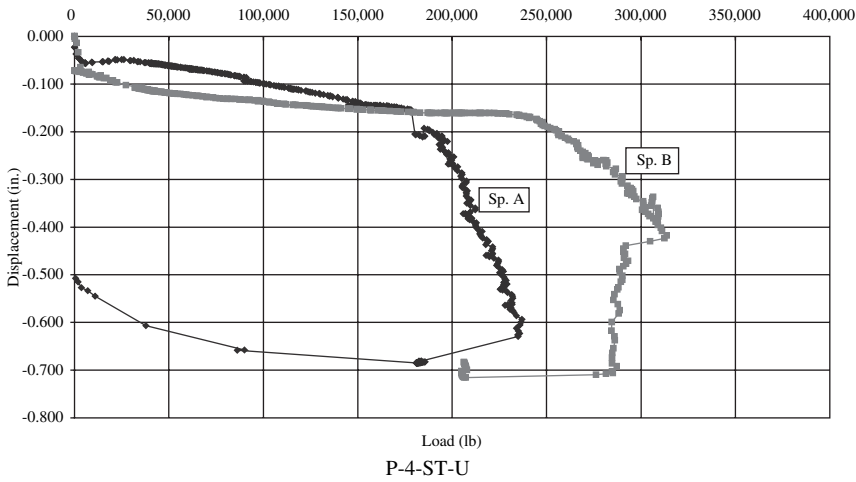


Figure 79. Load-displacement relationship of Group 1 push-off specimens.

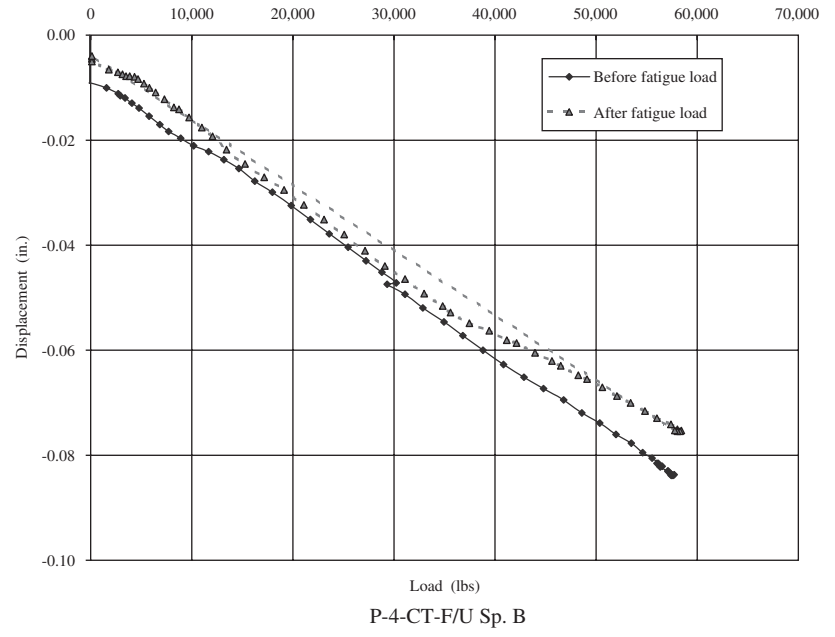
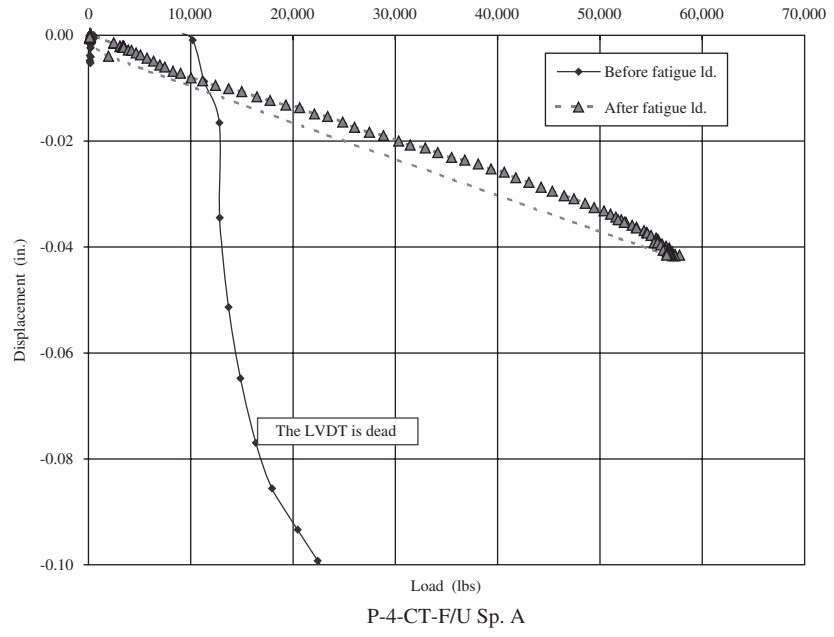
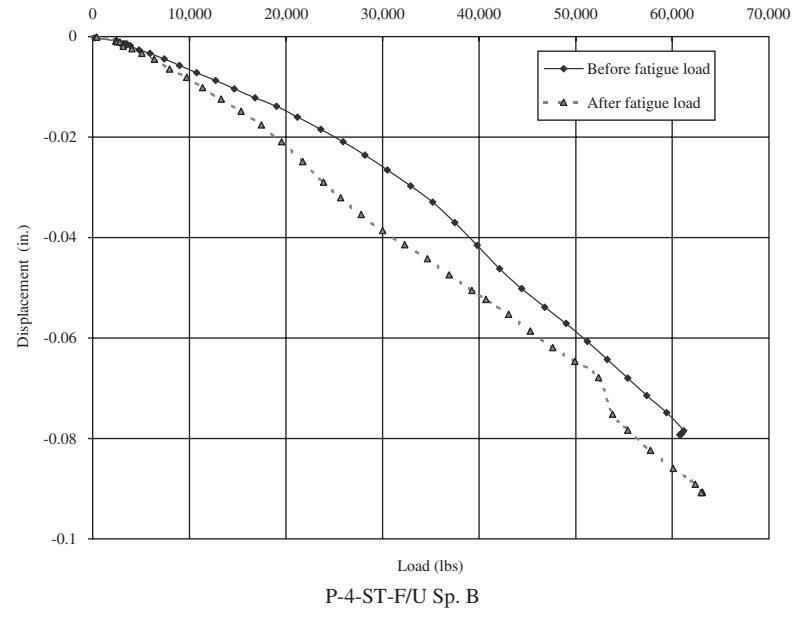
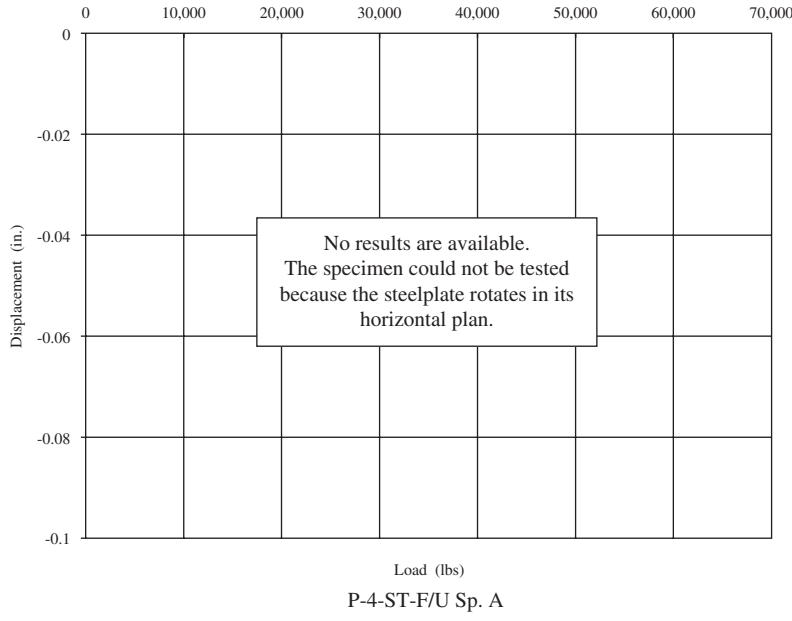


Figure 80. Load-displacement relationship of Group 2 push-off specimens due to fatigue load before and after the 2E+6 cycles.

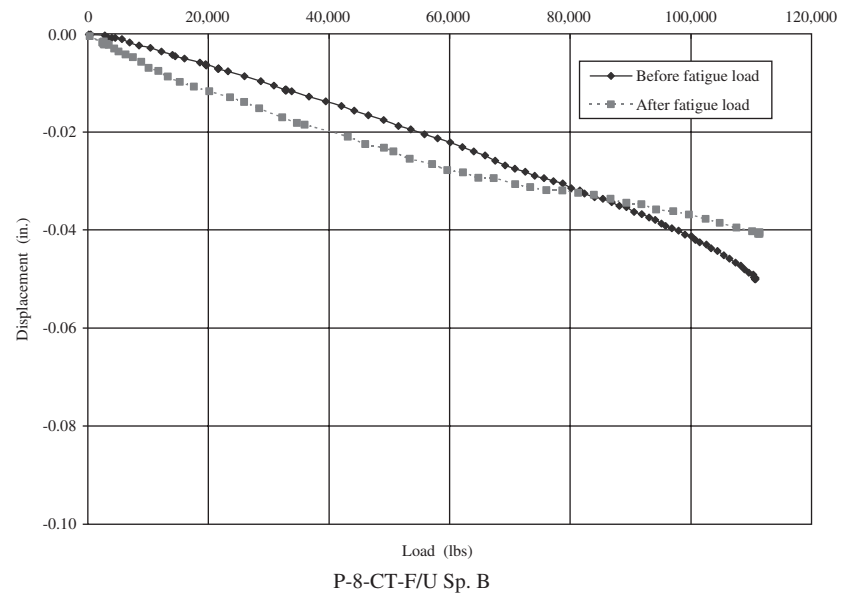
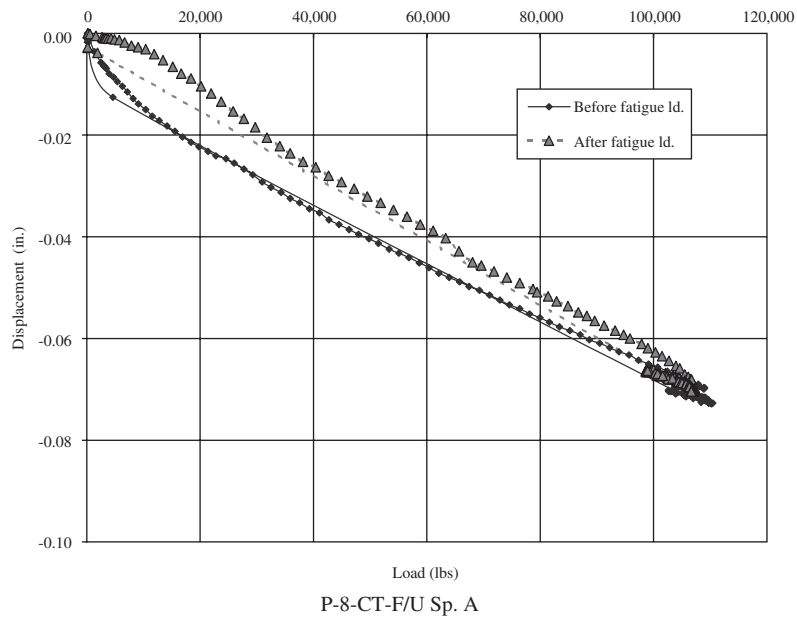
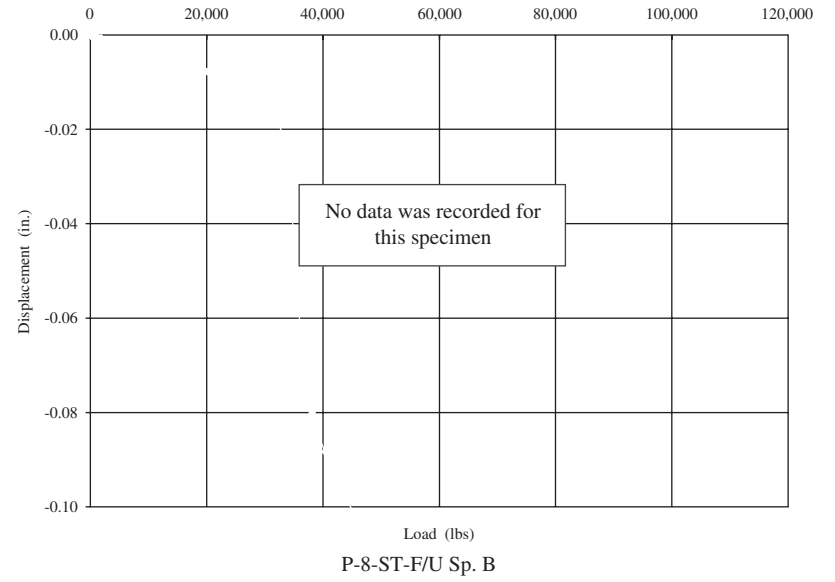
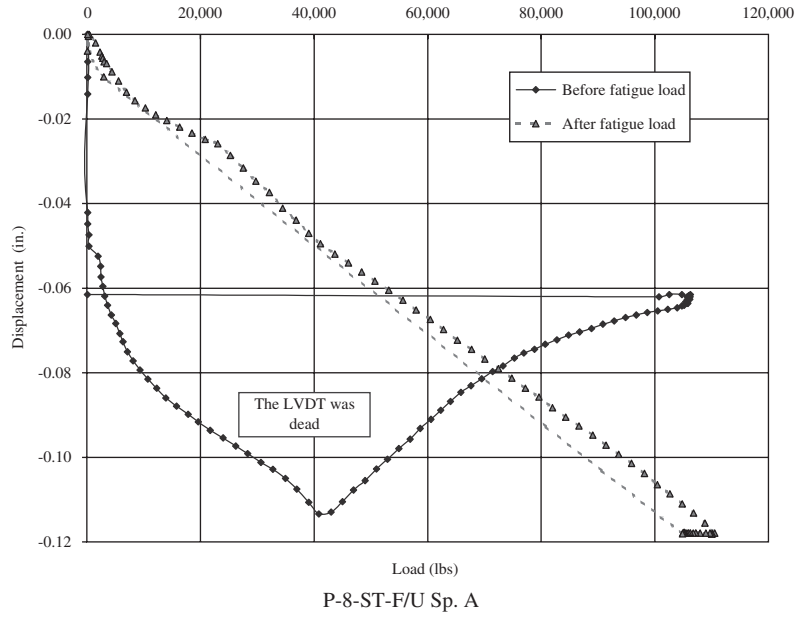
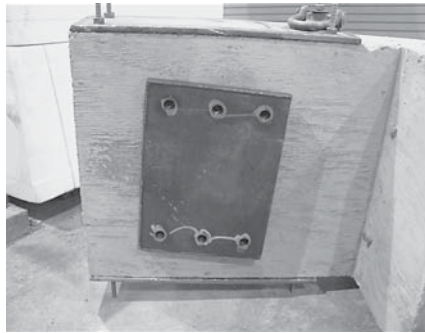


Figure 80. (Continued).



(a) P-4-ST-F/U Sp. A



(b) P-4-ST-F/U Sp. B

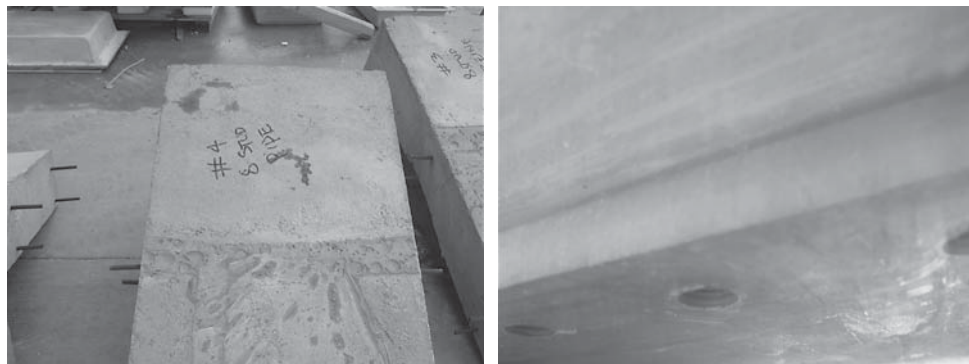


(c) P-4-CT-F/U Sp. A



(d) P-4-CT-F/U Sp. B

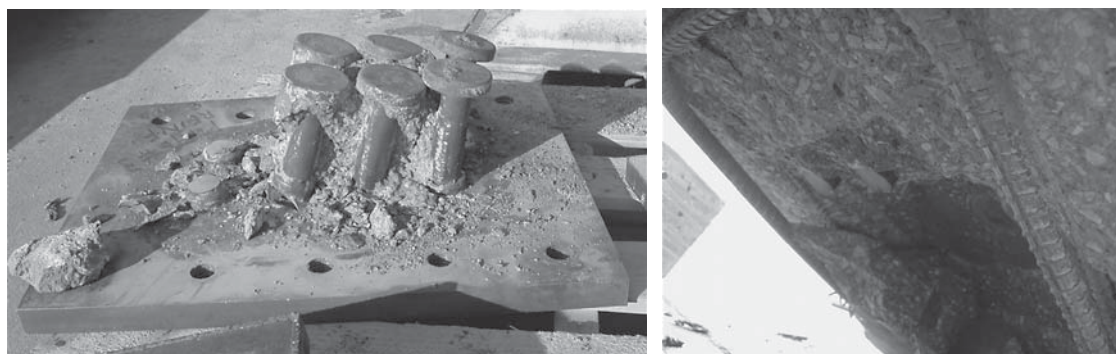
Figure 81. Failure modes of Group 2 push-off specimens.



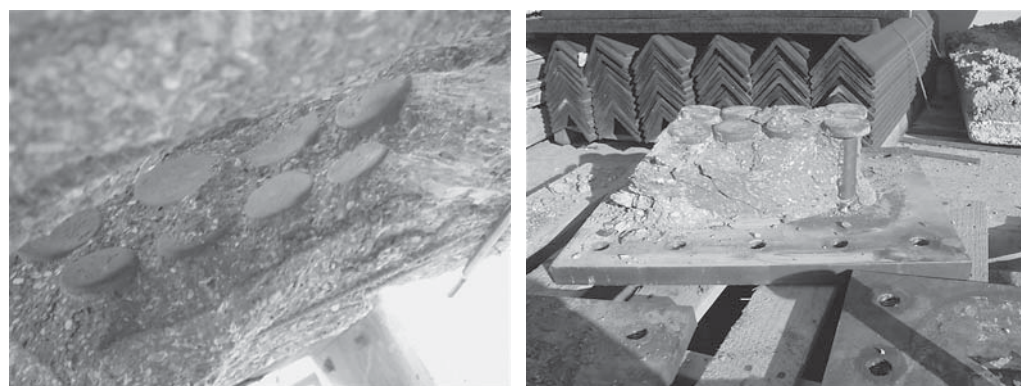
(e) P-8-ST-F/U Sp. A



(f) P-8-ST-F/U Sp. B



(g) P-8-CT-F/U Sp. A



(h) P-8-CT-F/U Sp. B

Figure 81. (Continued).

Table 10. Summary of the finite element analysis results for the push-off specimens.

	Four-Stud Specimens			Eight-Stud Specimens		
	P-4-ST-U (Steel Tube)	P-4-CT-U (Closed Ties)	Average	P-8-ST-U (Steel Tube)	P-8-CT-U (Closed Ties)	Average
Applied horizontal load (kip)*	314.8			629.6		
Maximum axial tensile stress at base of the stud (ksi)	58.4	99.1	78.8	99.9	74.9	87.4
Maximum tensile principal stress at base of the stud (ksi)	92.5	157.0	124.8	162.0	117.0	139.5
Maximum longitudinal movement of the stud head (in.)	0.0075	0.0103	0.0089	0.0109	0.00954	0.01022
Maximum axial tensile stress in confinement material in the transverse direction of the specimen (ksi)	21.0	3.7	NA	30.7	5.3	NA
Maximum bearing stress in grout in front of the stud (ksi)	29.1	31.8	30.5	27.1	31.6	29.4
Maximum bearing stress in the concrete in front of the grout volume (ksi)	2.31	2.31	2.31	2.30	2.30	2.30

* Determined using Equation 6.10.10.4.3-1 of the AASHTO LRFD Specifications (7).

analysis of various specimens, and Table 10 gives a summary of the maximum stresses in the stud, grout, and confinement tool.

The four- and eight-stud specimens are not able to deliver the horizontal ultimate shear capacity as given by Equation 6.10.10.4.3-1 of the AASHTO LRFD specifications (7). This can be seen from the average axial tensile stress at the stud base, which is higher than the ultimate tensile strength of the SAE 1018 stud material (64 ksi, or 441.3 MPa).

The upper limit of Equation 6.10.10.4.3-1 of the AASHTO LRFD specifications (7), $A_{sc}F_{ut}$, does not recognize the fact that the stud close to failure is subjected to a combination of axial tensile and normal flexural stresses. This can be seen by checking the average principal tensile stress at the stud base, which is about 155% of the axial tensile stress, as shown in Table 10. This means that the upper limit of Equation 6.10.10.4.3-1 overestimates the stud's shear capacity. This finding was confirmed by the push-off test, where almost none of the specimens were able to reach the capacity determined by Equation 6.10.10.4.3-1 of the AASHTO LRFD specifications (7).

Maximum bearing stress in the grout is located in front of each stud close to the stud base. It extends vertically for a distance approximately equal to the stud diameter. The maximum bearing stress is about 30 ksi (206.9 MPa), which is about 310% of the compressive strength of unconfined grout mix (9.6 ksi, or 66.2 MPa). However, if confinement is provided around the shear pocket, the compressive strength of the grout can be significantly increased, as follows:

$$\begin{aligned} \text{Effective lateral confining pressure, } f_b &= \frac{\sum A_s f_{yh}}{sb_c} \\ &= \frac{\left(2 \text{ sides} \times 1 \text{ in.} \times \frac{5}{16} \text{ in.}\right)(36 \text{ ksi})}{(1 \text{ in.})(12 \text{ in.})} = 1.875 \text{ ksi} \\ &\quad \text{(for steel tube confinement)} \\ &= \frac{(2 \text{ legs} \times 0.44 \text{ in}^2 \text{ per leg} \times 3 \text{ bars})(60 \text{ ksi})}{(1.75 \text{ in.})(15 \text{ in.})} = 6.034 \\ &\quad \text{(for closed ties confinement)} \end{aligned}$$

$$\text{Confined grout strength, } f_{co} = f_0 + 4.1kf_l$$

$$= 9.6 + 4.1 \times 1 \times 1.875 = 17.3 \text{ ksi (119.3 MPa)} \\ \text{(for steel tube confinement)}$$

$$= 9.6 + 4.1 \times 1 \times 6.034 = 34.3 \text{ ksi (236.8 MPa)} \\ \text{(for closed ties confinement)}$$

The confinement around the stud group helps to distribute the bearing stresses of the grout volume on the concrete slab in front of the grout volume. The highest bearing stress is about 2.30 ksi (15.9 MPa), and the average bearing stress over the slab height is about 2.0 ksi (13.8 MPa).

The confinement provided by the steel tube helps to distribute the bearing stresses on a wider part of the slab, resulting in a reduction in the compression in the slab compared with when closed ties are used.

The truncated shape of the shear pocket and grout volume helps in distributing the bearing stresses more uniformly across the slab height.

Full-Scale Beam Test

The objective of the full-scale beam testing was to investigate the feasibility of extending the AASHTO maximum stud spacing from 2 to 4 ft (610 to 1220 mm) by checking differences in structural performance of two composite beams due to fatigue and ultimate loads.

Two full-scale composite beams, each 32 ft (9.75 m) long, were fabricated. The beams were identical except that the spacing between the stud clusters was 2 ft (610 mm) for the first beam and 4 ft (1220 mm) for the second beam. Each composite beam was made of an 8 in. (203 mm) thick precast slab supported by a W18 × 119 steel beam. The slab and the steel beam were made composite using sixty-four 1¼ in. (31.8 mm) studs over the full-span length. The studs on Beam 1 were clustered in 16 groups spaced at 24 in. (610 mm), with four studs per group. The 24 in. (610 mm) spacing is the current limit according to the AASHTO LRFD specifications (7).

The studs on Beam 2 were clustered in eight groups, spaced at 48 in. (1220 mm), with eight studs per group, as shown in Figures 82 to 84. The spacing between the studs in each group was 3 in. (76 mm) in the longitudinal direction. Two studs per row spaced at 5 in. (127 mm) in the transverse direction were used. In each beam, the stud clusters on the south half of the beam were confined with HSS 9 × 7 × 0.188 in. (229 × 178 × 5 mm) and 13 × 9 × $\frac{5}{16}$ in. (330 × 229 × 8 mm) tubes, and the stud clusters on the north half were confined with individual No. 4 (13) and No. 6 (19) closed ties for the 2 ft (610 mm) and 4 ft (1220 mm) clusters, respectively.

The concrete slab of each beam was made of one precast panel, which was reinforced with two welded wire reinforcement (WWR) meshes. The top mesh was made of 6 × 6 – D10 × D10 (152 × 152 – MD65 × MD65), and the bottom mesh was made of 6 × 6 – D14 × D14 (152 × 152 – MD90 × MD90). This amount of reinforcement was provided in accordance with the minimum reinforcement requirements of the empirical design method given in Article 9.7.2 of the AASHTO LRFD specifications (7). Figures 82 to 84 show the details of the full-scale beams.

Wood forming and a normal weight, 7 in. (178 mm) slump, 6 ksi (41.4 MPa) concrete mix were used in making the

panels, as shown in Figure 85. The panels were moist cured for 7 days and then stored in the laboratory until they were installed on the steel beams. No shrinkage cracks were observed on the panels. On both beams, $\frac{1}{4}$ in. (31.8 mm) headless studs with heavy-duty nuts and washers were used. Due to the lack of a high-voltage source at the testing facility, the studs were manually welded, as shown in Figure 86. The welding quality was checked by visual inspection, bending the stud to 45 degrees, and using the hydraulic push-off device discussed earlier in this chapter. Foam rods were glued at the edges of the top flange of the steel beam to build a dam for the 1 in. (25 mm) thick concrete haunch. Each panel was installed by carrying it with a spreader beam that supported the panel at 7 points spaced uniformly at 4 ft (1220 mm) and located in the mid distance between adjacent shear pockets. Finally, the shear pockets were filled with SS Mortar mix with no pea gravel, as shown in Figure 86. The grouting of each pocket continued until grout came out from the venting ports.

Grouting of Beam 1 went smoothly, with complete filling of the haunch and no recorded problems. For Beam 2, however, after the grout was cured and the foam rods were removed, it was noticed that about a 2 ft (610 mm) long distance between two shear pockets was not completely filled with grout. This

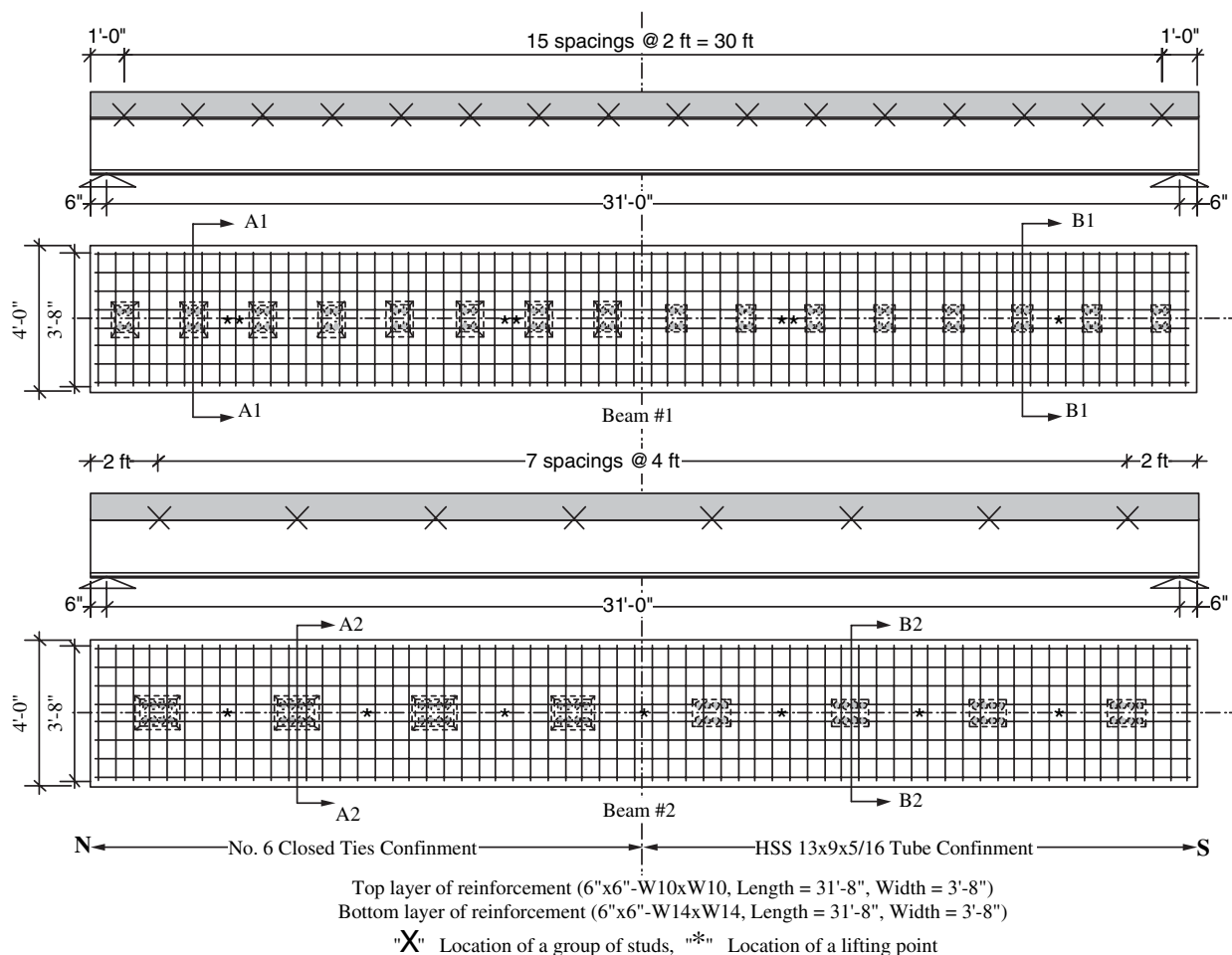


Figure 82. Arrangement of stud clusters of Beam 1 and Beam 2.

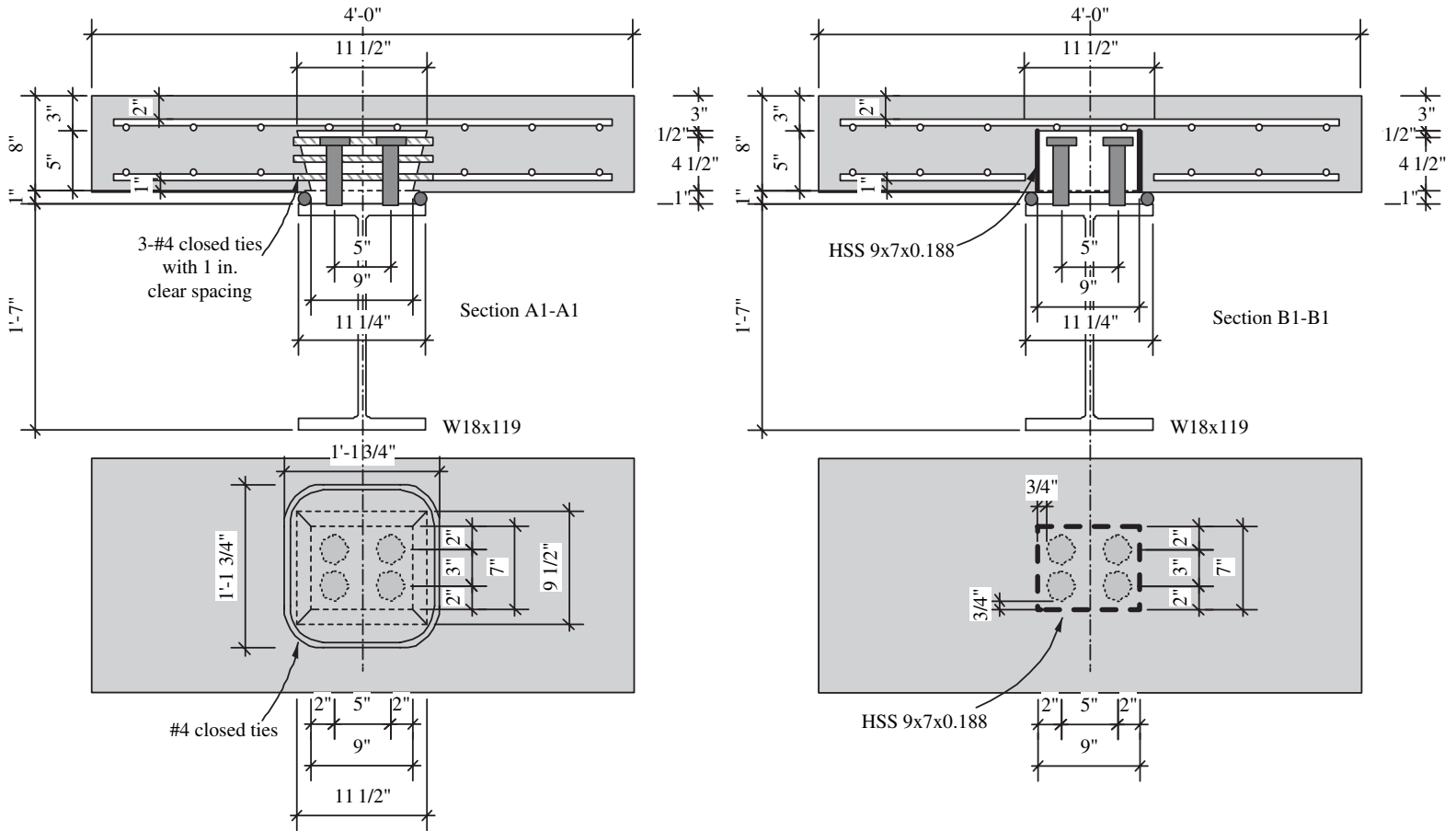


Figure 83. Sections A1-A1 and B1-B1.

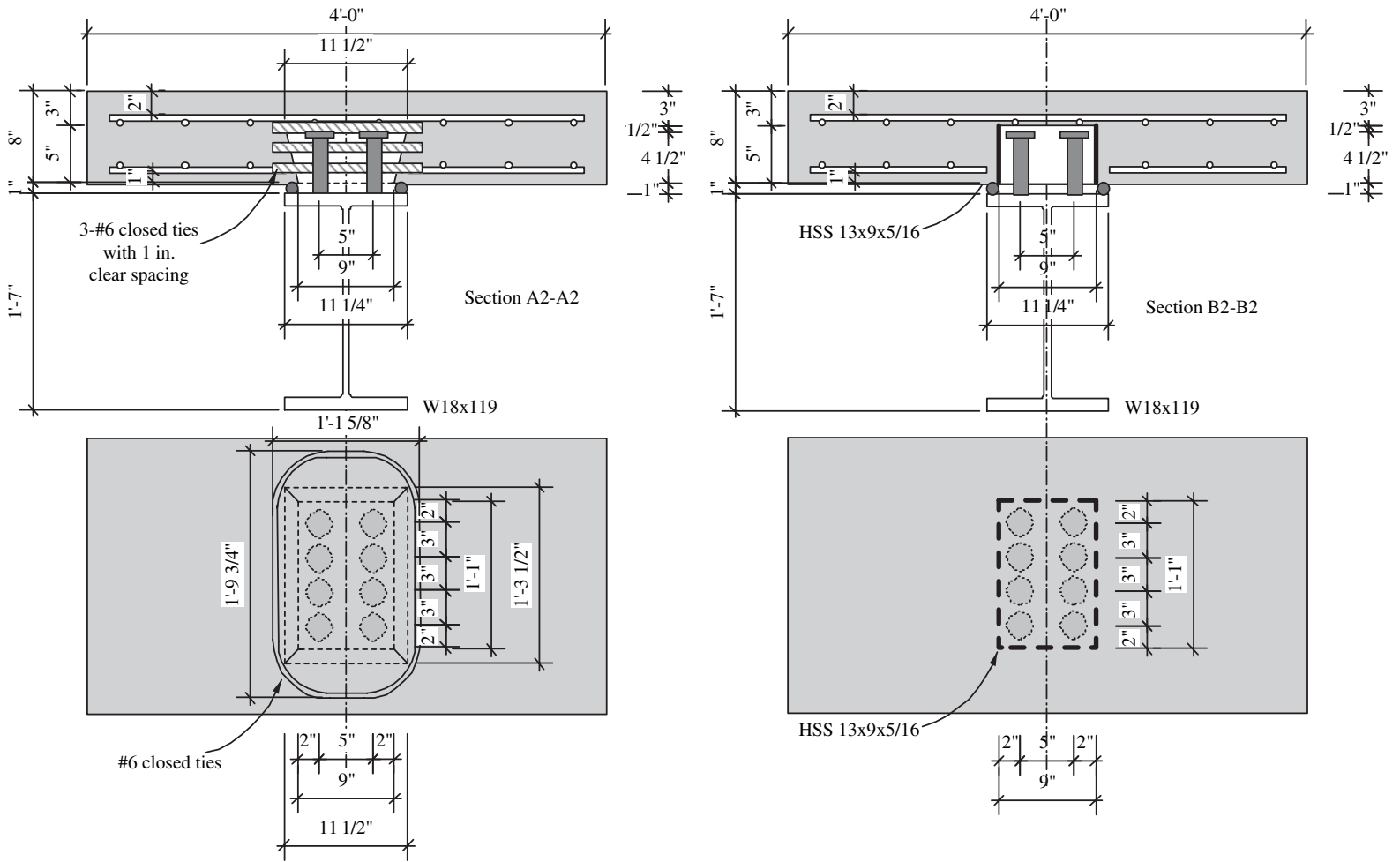


Figure 84. Sections A2-A2 and B2-B2.

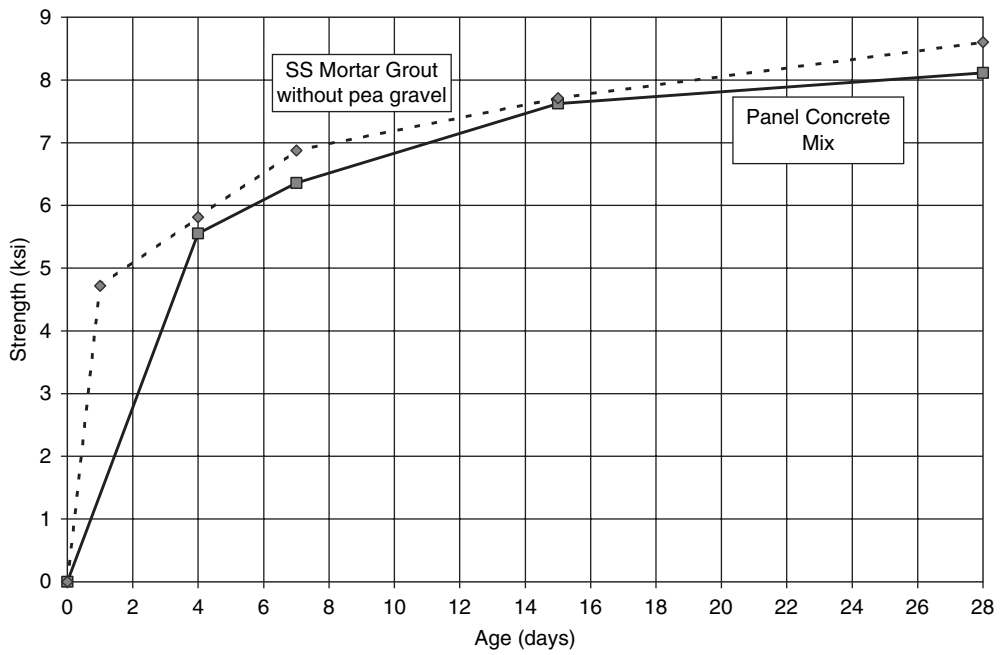
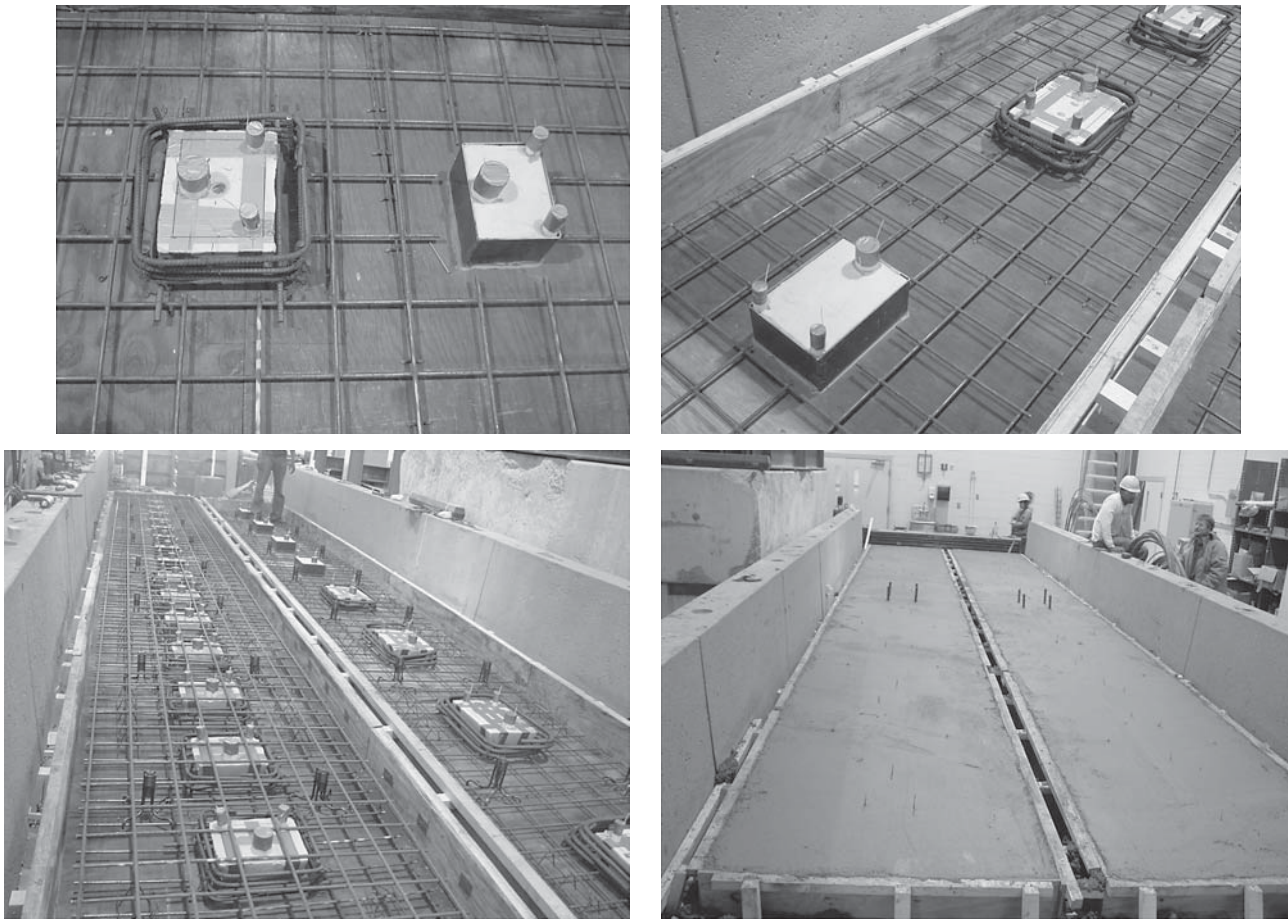


Figure 85. Forming and casting of the precast concrete panels.

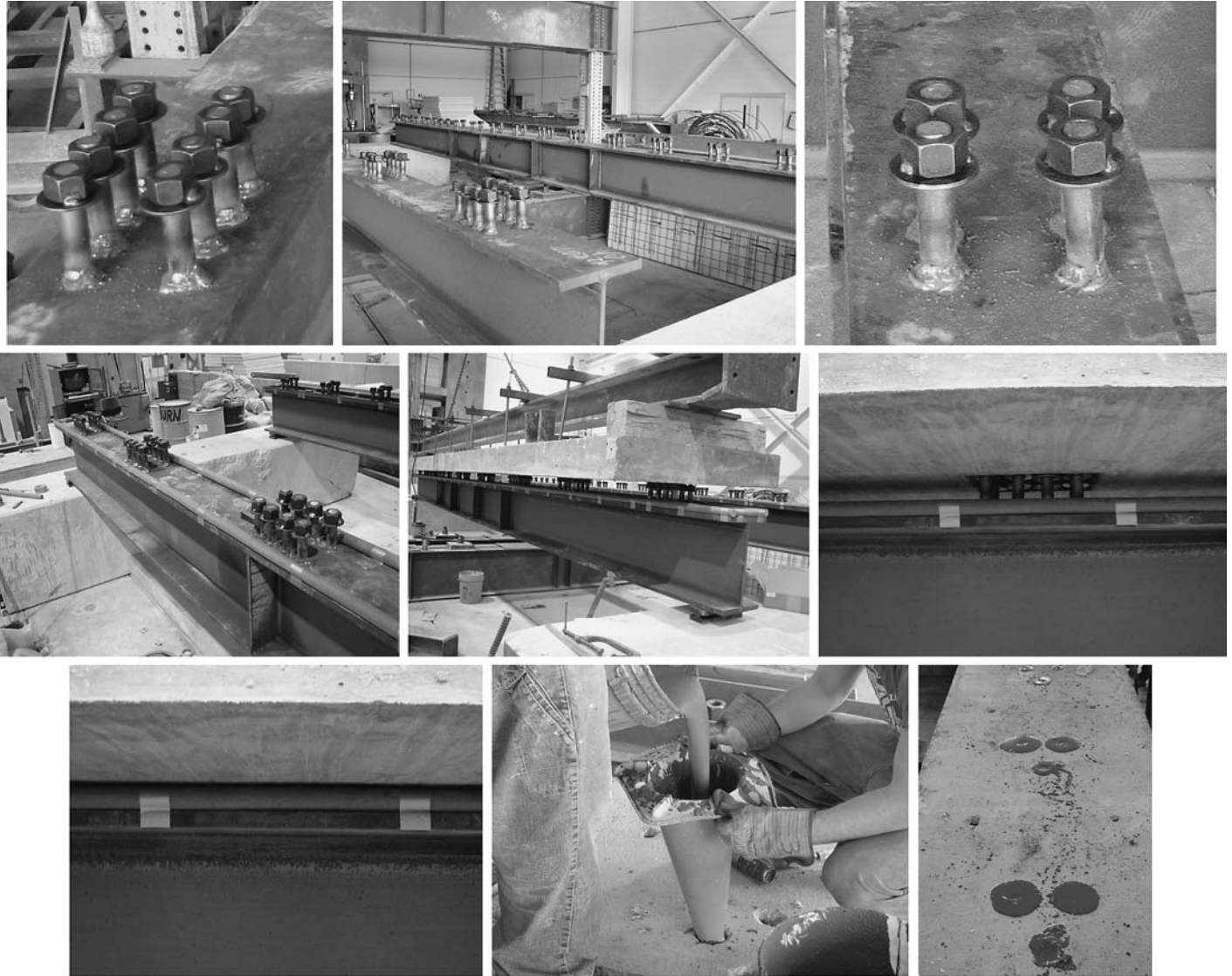


Figure 86. Building the composite beams.

was due to the excessive time that elapsed between when the grout was mixed with water and when this area of the beam was grouted. This area was batched by injecting grout directly at the haunch level.

Fatigue Testing of the Beam

Each beam was loaded with one concentrated load at midspan and subjected to 2,000,000 cycles of fatigue load through a hydraulic actuator. The load setup put all of the shear pockets under the same amount of horizontal load, as shown in Figures 87 and 88. The upper and lower limits of the fatigue load were determined in three steps.

Step 1: Calculate Stud Fatigue Resistance, Z_r . Using Equations 8 (Equation 6.10.10.2-1 (7)) and 9 (Equation 6.10.10.2-2 (7)) gives

$$Z_r = 7.53 \times 1.25^2 = 11.77 \text{ kip/stud}$$

Step 2: Calculate Vertical Shear Force, V_f .

$$V_{sr} = \frac{V_f Q}{I} \quad (15) \quad (\text{Equation 6.10.10.1.2-2 (7)})$$

where

V_f = vertical shear range due to fatigue load,

I = moment of inertia of the composite section,

Q = first moment of the area above the interface about the neutral axis, and

V_{sr} = shear flow range due to fatigue load at the interface, which can be determined by:

$$p \leq \frac{nZ_r}{V_{sr}} \quad (16) \quad (\text{Equation 6.10.10.1.2-1 (7)})$$

p = spacing of the studs = 24 in. or 48 in.,

n = number of studs in a cross section = 4 studs for $p = 24$ in., or 8 studs for $p = 48$ in.

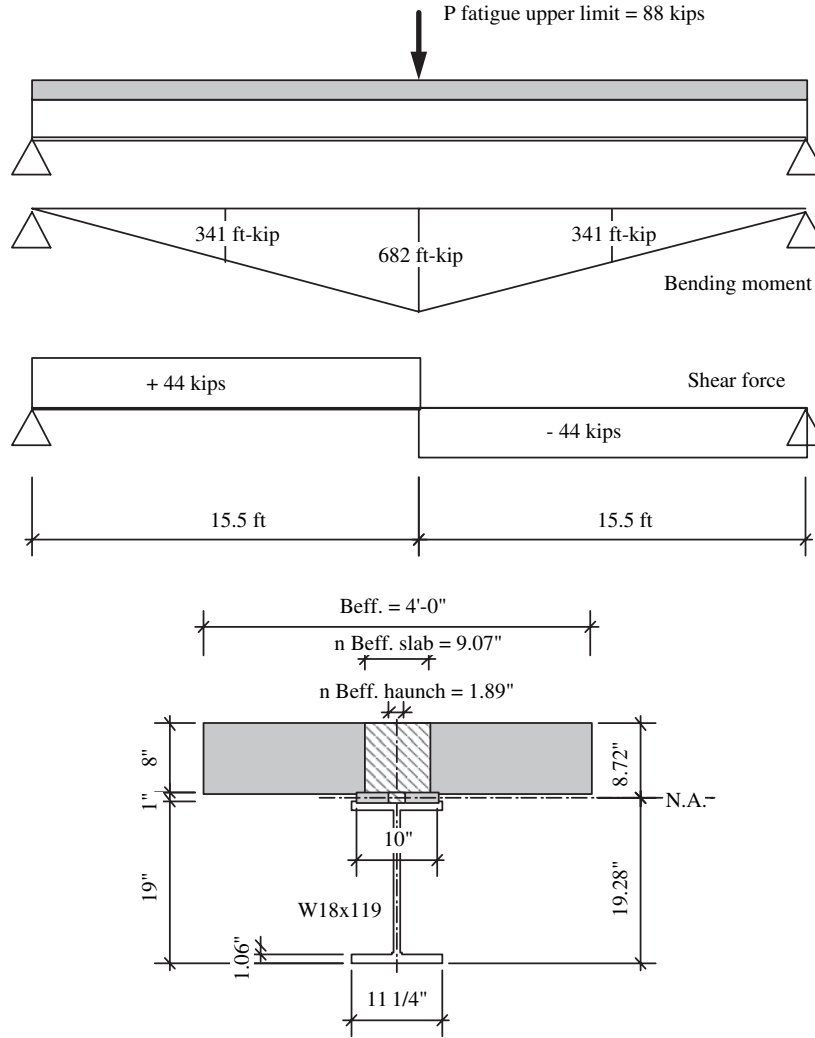


Figure 87. Elastic properties of the composite section.

I and Q were calculated as follows (see Figure 68):
 Effective slab width (LRFD specifications, Article 4.6.2.6.1):

$$B_{eff} = \text{least of} \left. \begin{array}{l} B = 4 \text{ ft} = 48 \text{ in.} \\ 12t_s + 0.5 \text{ girder flange} = 12 \times 8 + 0.5 \times 11.3 = 102 \text{ in.} \\ \frac{1}{4} \text{ span} = 0.25 \times 32 \text{ ft} = 8 \text{ ft} = 96 \text{ in.} \end{array} \right\} (17)$$

$$= 48 \text{ in.}$$

$$\text{Modular ratio, } n' = \frac{E_c}{E_s} = \frac{33,000 \times 0.150^{1.5} \sqrt{8.2}}{29,000} = 5,490 = 0.189$$

$$n' B_{eff} \text{ of the slab} = 0.189 \times 48 = 9.07 \text{ in.}$$

$$n' B_{eff} \text{ of the haunch} = 0.189 \times 10 = 1.89 \text{ in.}$$

Depth of the NA =

$$\frac{(9.07 \times 8)(4) + (1.89 \times 1)(8 + 0.5) + (35.1)(8 + 1.0 + 0.5 \times 19)}{(9.07 \times 8) + (1.89 \times 1) + (35.1)} = 8.75 \text{ in.}$$



Figure 88. Fatigue test setup.

$$I = \left[\frac{9.07 \times 8^3}{12} + (9.07 \times 8)(8.72 - 4)^2 \right] + \left[\frac{1.89 \times 1^3}{12} + (1.89 \times 1)(8.72 - 8 - 0.5)^2 \right] + \left[2,190 + (35.1)(8 + 1 + 0.5 \times 19 - 8.72)^2 \right] = 7,551 \text{ in}^4$$

$$Q = (9.07 \times 8)(8.72 - 4) + (1.89 \times 1)(8.72 - 8 - 0.5) = 342.9 \text{ in}^3$$

Substituting Equation 16 in Equation 15 yields

$$V_f = \frac{nZ_r I}{pQ} = \frac{4 \times 11.77 \times 7,551}{24 \times 342.9} = 43.2 \text{ kip}$$

$$P \text{ (concentrated load at midspan)} = 2 \times 43.2 = 86.4 \text{ kip}$$

To maintain stability of the test setup, a minimum load of 1.6 kip was provided as the lower limit of the fatigue load. Therefore, the upper limit of the fatigue load = $86.4 + 1.6 = 88 \text{ kip}$.

Step 3: Check Stresses at Midspan to Make Sure They Are Within the Elastic Range of Material

$$f_{\text{top surface of slab}} = -0.189 \frac{(682 \times 12)(8.72)}{7,551} = -1.79 \text{ ksi} < (0.4 f'_c = 0.4 \times 8.2 = 3.28 \text{ ksi})$$

$$f_{\text{bottom surface of slab}} = -0.189 \frac{(682 \times 12)(8.72 - 8)}{7,551} = -0.15 \text{ ksi}$$

$$f_{\text{top surface of steel beam}} = \frac{(682 \times 12)(8 + 1 - 8.72)}{7,551} = +0.30 \text{ ksi}$$

$$f_{\text{bottom surface of steel beam}} = \frac{(682 \times 12)(19.28)}{7,551} = +20.90 \text{ ksi} < (f_y = 50 \text{ ksi})$$

Strain gauges and vertical displacement measuring devices were installed at the quarter-point and midspan sections of

each beam. The upper limit of the fatigue load was applied as a static load, and the measurements were collected (pre-fatigue records); the beam was then exposed to 2,000,000 cycles of the fatigue load at 2,000,000 cycles/sec. Finally, the beam was loaded statically with the upper limit of the fatigue load, and the strain and displacement measurements were collected (postfatigue records).

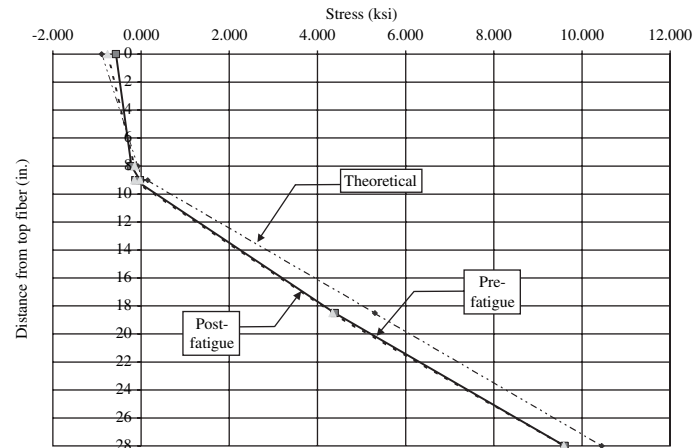
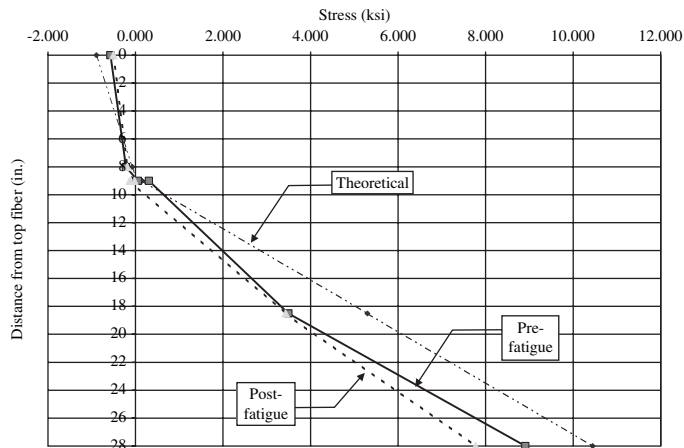
The testing scenario worked well with Beam 1. However, for Beam 2, the hydraulic system of the actuator needed to be repaired when the beam was exposed to about 1,000,000 cycles. The fatigue test was therefore stopped, the static load was applied, and the measurements were collected at 1,000,000 cycles. After the hydraulic system was repaired, the fatigue test was resumed. The measurements that were planned to be taken at 2,000,000 cycles were not, however, collected because the steel beam fractured as a result of fatigue load close to the midspan section at about 1,950,000 cycles, as shown in Figure 89. The fatigue fracture started at the bottom flange and propagated through the web, where it stopped close to the web/top flange junction. As a result of this unexpected failure, a $\frac{1}{2}$ in. (13 mm) separation between the haunch and the steel beam occurred over a distance of about 2 ft (610 mm) around the failure location. The beam was thoroughly inspected, and no other cracks or signs of distress were detected.

It was believed that the fatigue fracture failure occurred because the steel beam was previously subjected to 4,000,000 cycles of fatigue load when it was used for the full-scale bridge test. Also, welding and removing of the $2\frac{1}{2}$ in. (64 mm) diameter tubes that were needed in the full-scale bridge test resulted in residual stresses in that flange.

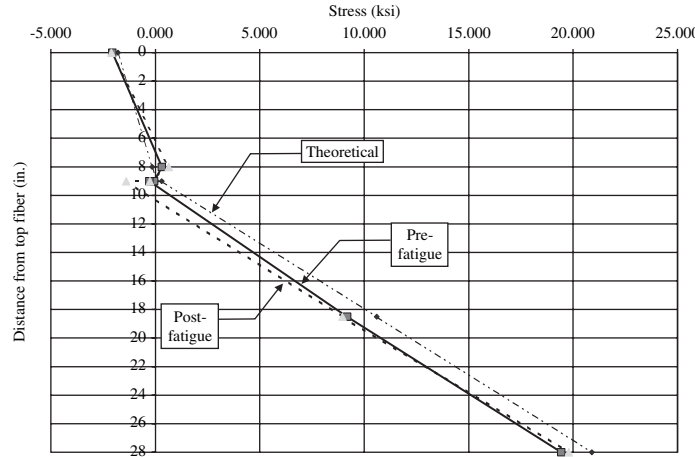
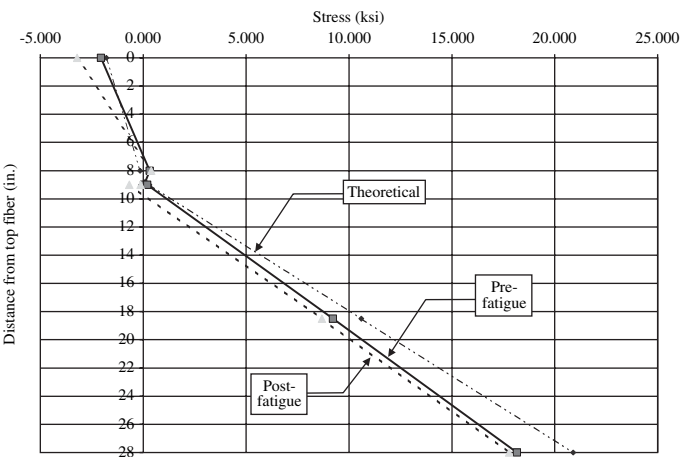
Figure 90 shows the pre- and post-fatigue stress distribution at the quarter-point and midspan sections of the beams and compares them with the stresses calculated by the elastic stress theory assuming full-composite action. Figure 91 shows the deflection of the beams at the quarter-point and



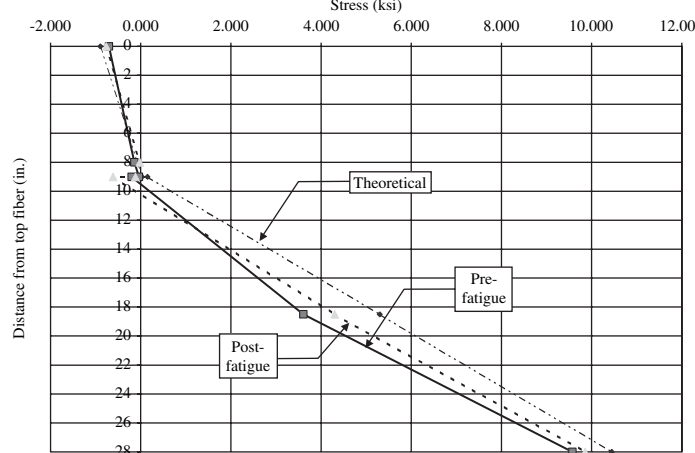
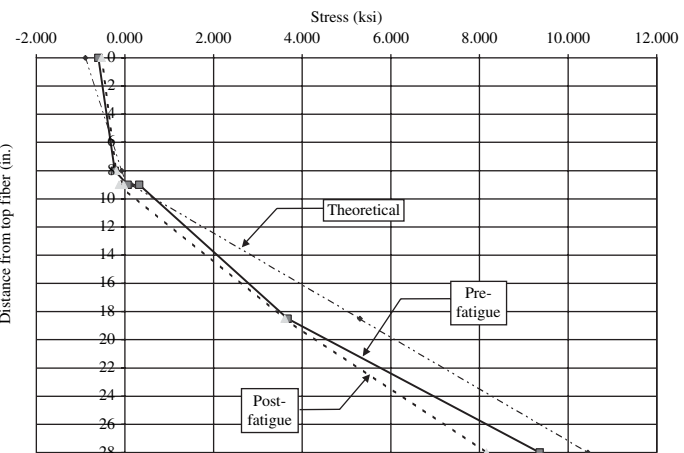
Figure 89. Fatigue fracture of the steel beam and separation between the haunch and the steel beam.



North side (Ties)



Midspan Section



South Side (Tube)

2-ft cluster spacing

4-ft cluster spacing

Figure 90. Composite section stresses (theoretical and pre- and post-fatigue).

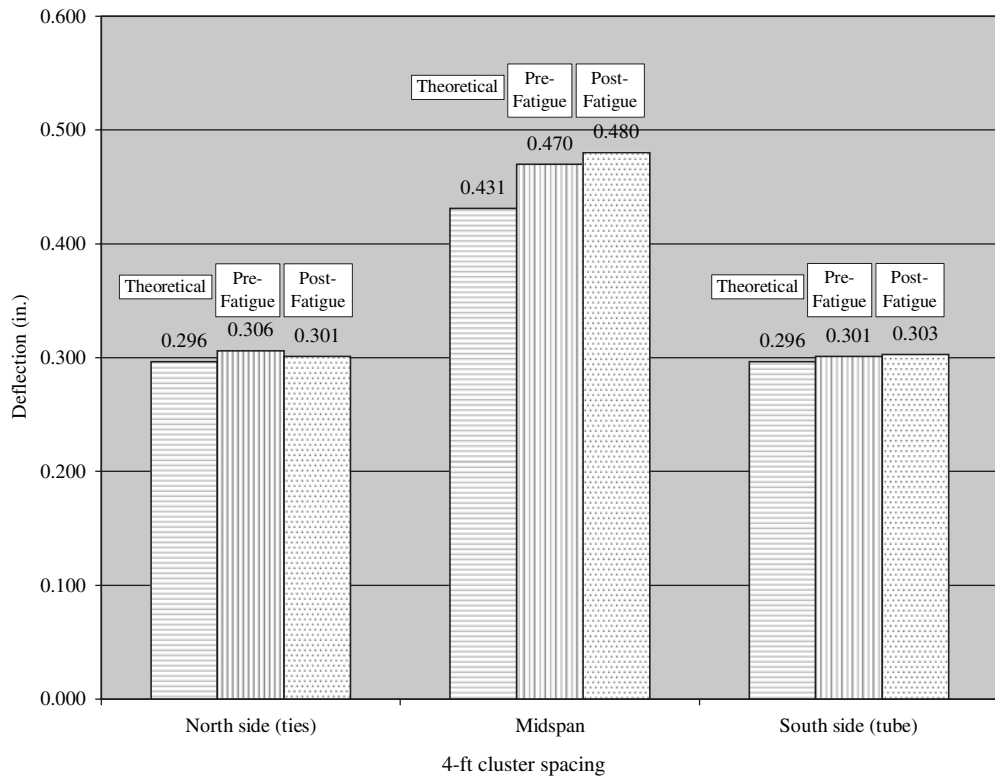
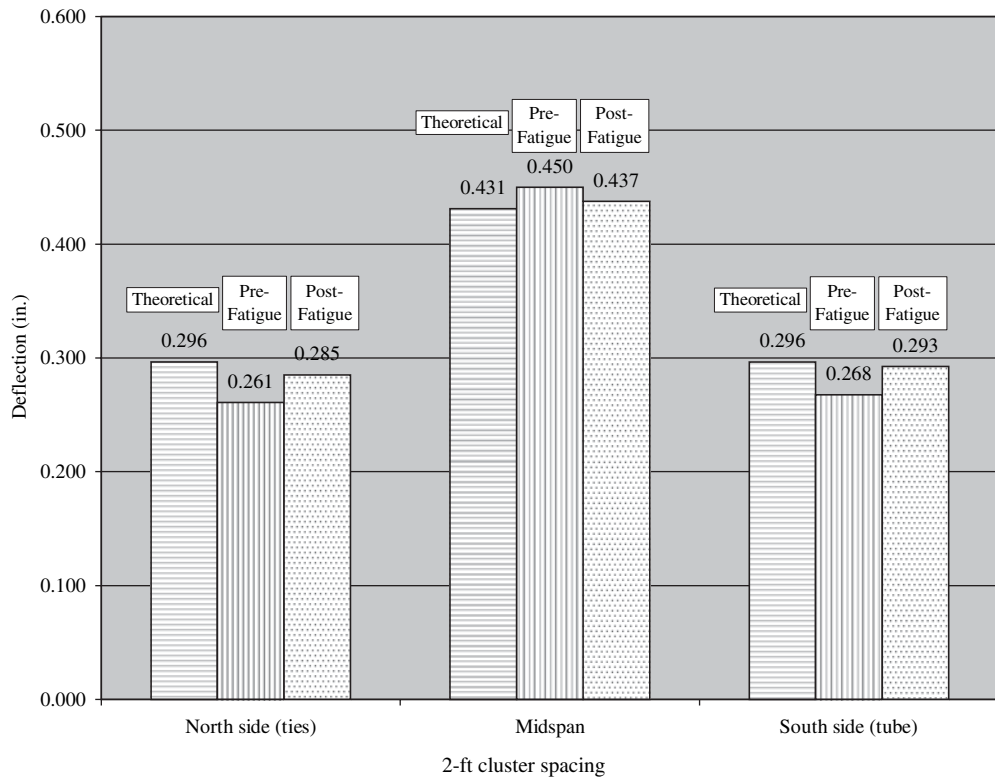


Figure 91. Composite section deflection (theoretical and pre- and post-fatigue).

midspan sections. The quarter-point and midspan sections were chosen because they were at the mid distance between two adjacent shear pockets, where it was highly expected that partial composite action would occur. An examination of these figures found the following:

- Regardless of the stud cluster spacing and the type of confinement:
 - At the quarter-point and midspan sections, pre- and post-fatigue stresses showed almost a linear distribution.
 - At the midspan section, pre- and post-fatigue stresses at extreme compression fiber of the composite beams were about 20% higher than the stresses calculated by the elastic stress theory. However, the opposite trend occurred at the quarter-point sections.
 - At the quarter-point and midspan sections, pre- and post-fatigue stresses at extreme tension fiber of the composite beams were about 20% less than the stresses calculated by the elastic stress theory.
 - At the quarter-point and midspan sections, pre- and post-fatigue stresses at extreme tension and compression fibers of the composite beams were within the elastic range of the material.
 - At the quarter-point and midspan sections, post-fatigue stresses and deflection showed almost no increase when compared with the prefatigue stresses. On the contrary, at some locations the postfatigue stresses were smaller than the prefatigue stresses.
 - The pre- and post-fatigue deflection levels were in close agreement with deflection calculated using the elastic stress theory.
- Regardless of the type of confinement provided around the stud clusters, the stress distribution and deflection measurements of Beam 1 and Beam 2 were almost identical.
- Regardless of the stud cluster spacing, the stress distribution and deflection measurements of the north side of the beam, where ties were used, were almost identical to the stress distribution and deflection measurements of the south side of the same beam, where tubes were used.
- Visual inspection of the composite beams before, during, and after applying the 2,000,000 cycles of fatigue load found
 - no cracks on the top surface of the concrete slab;
 - no separation between the concrete haunch and the steel beams, except the separation that occurred in Beam 2 around the location of the fatigue fracture failure;
 - no cracks or signs of distress in the haunch; and
 - no residual deflection at midspan after removing the load.

Based on these observations, the following conclusions were drawn:

- It is safe to use Equation 6.10.10.2-1 of the LRFD specifications (7) to determine the fatigue capacity of studs grouped in clusters and spaced as far as 48 in. (1220 mm) apart.
- Full composite action between precast concrete panels and steel beams can be maintained up to 48 in. (1220 mm) of spacing between clusters of studs.
- The two types of proposed confinement—closed ties and tubes—provide similar behavior due to fatigue load.

Ultimate Testing of the Full-Scale Beams

To individually investigate the ultimate capacity of the stud clusters for various types of confinement, the 32 ft (9.75 m) span of each beam was divided into two equal spans, as shown in Figures 92 and 93.

For Beam 1, an intermediate support was installed exactly at midspan. Then each beam half was tested as a 15.5 ft (4.72 m) simply supported beam under one concentrated load close to the midspan point of that span. This was done by removing the external support of the other half of the span, as shown in Figure 92. The applied concentrated load would thus provide horizontal shear forces at the interface only on the stud clusters that existed on the simply supported span. Although the weight of the cantilevered span would provide additional stresses on the studs of the simply supported span, careful checking of these stresses revealed that it would be about 2% of the stresses provided by the concentrated load, which could be ignored.

For Beam 2, two intermediate supports were added because the steel beam was fractured close to the midspan point. This arrangement resulted in two simply supported spans that each measured 11 ft (3.35 m) long. To make sure that no continuity existed between the two simply supported spans, the concrete slab was jackhammered at the same location where the steel beam was fractured to create a real hinge, as shown in Figure 92.

Each test setup used two hydraulic jacks, 300 kip (1334 kN) each, supported on a short spreader beam to apply the load as one concentrated load, as shown in Figures 92 and 93. Two modes of failure were checked to determine the possible mode of failure of each simply supported beam.

Flexural Capacity of the Composite Beam. The flexural capacity of the composite beam was determined in accordance with Article 6.10.7 of the AASHTO LRFD specifications (see Figure 94).

Assume that the neutral axis depth is less than the thickness of the slab, $D_p < 8$ in. Ignoring reinforcement in the longitudinal direction of the slab, equilibrium of forces at the plastic stage yields

$$(0.85 \times 8.2 \times 48)(D_p) = (50)(35.1)$$

$$D_p = 5.25 \text{ in.} < 8 \text{ in. (inside the concrete slab)}$$

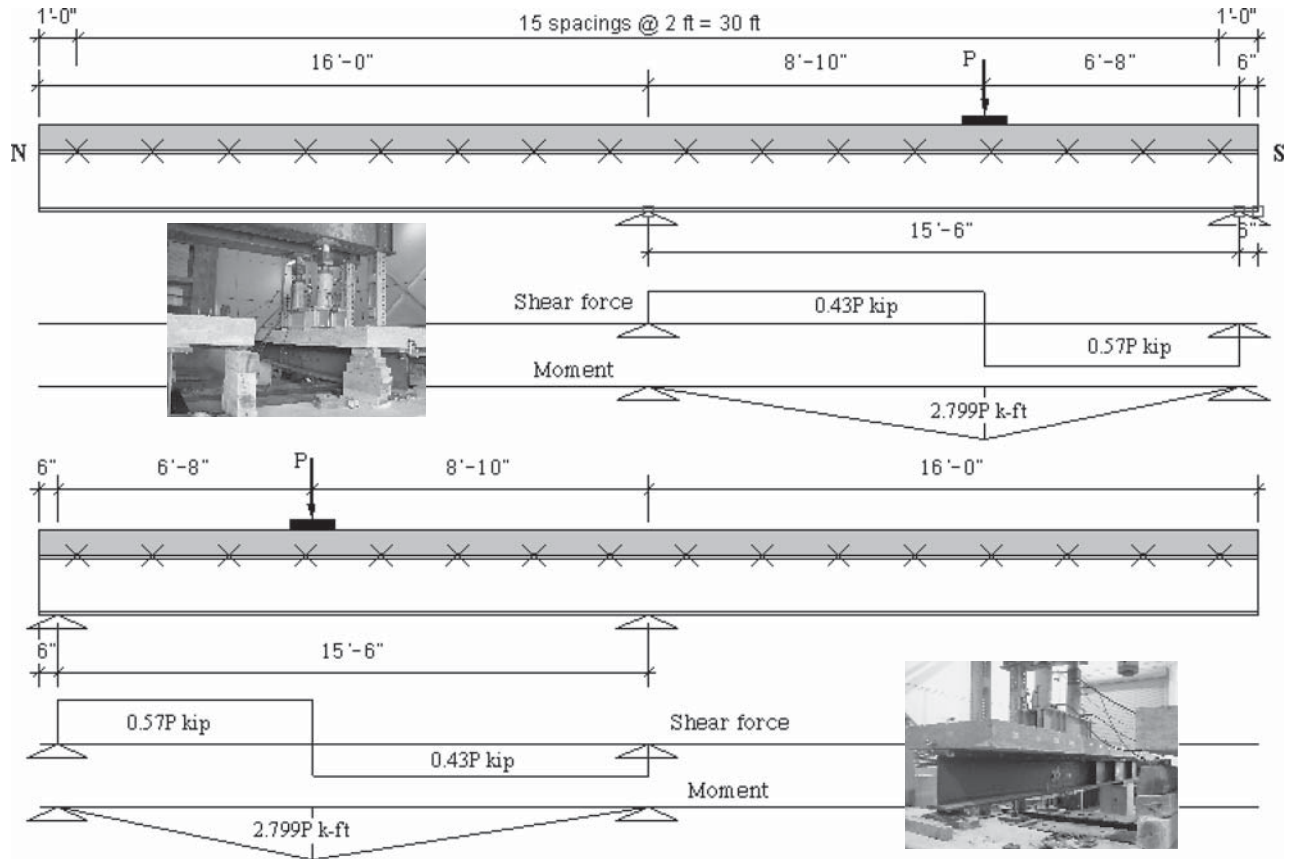


Figure 92. Ultimate test arrangement of Beam 1.

Classification of the composite section (compact versus noncompact):

$$\left(\frac{2D_{cp}}{t_w} = \frac{2 \times \text{zero}}{t_w} \right) \leq \left(3.67 \sqrt{\frac{E}{F_{yc}}} = 3.67 \sqrt{\frac{29,000}{50}} = 88.4 \right) \quad (18) \quad (\text{Equation 6.10.6.2.2-1 (7)})$$

where D_{cp} = depth of the web in compression at the plastic moment.

Therefore, the composite section was compact.

Since $D_p > [0.1D_t = 0.1(8 + 1 + 19) = 2.8 \text{ in.}]$ (Equation 6.10.7.1.2-1 (7)), where D_t = total depth of the composite section, therefore:

$$M_n = M_p \left(1.07 - 0.7 \frac{D_p}{D_t} \right) \quad (19) \quad (\text{Equation 6.10.7.1.2-2 (7)})$$

$$M_p = (0.85 \times 8.2 \times 48 \times 5.25)(8 + 1 + 0.5 \times 19 - 0.5 \times 5.25) = 27,883 \text{ kip-in.} = 2,324 \text{ kip-ft}$$

$$M_n = (2,324) \left(1.07 - 0.7 \frac{5.25}{8+1+19} \right) = 2,182 \text{ kip-ft}$$

Ductility can be checked as outlined in the LRFD specifications, Article 6.10.73:

$$[D_p = 5.25 \text{ in.}] < [0.42D_t = 0.42(8 + 1 + 19) = 11.76 \text{ in.}] \quad \text{OK}$$

Therefore, if the 15.5 ft (4.72 m) simply supported spans of Beam 1 were to fail in flexure, it would require a concentrated load $P = 2,182/3.799 = 574 \text{ kip}$, and, if the 11.0 ft (3.35 m) simply supported spans of Beam 2 were to fail in flexure, it would require a concentrated load $P = 2,182/2.588 = 843 \text{ kip}$, which was beyond the capacity of the hydraulic jacks.

Nominal Shear Resistance, Q_n . Using Equation 14 (Equation 6.10.10.4.3-1 (7)) where

$$A_{sc} = 1.23 \text{ in}^2,$$

$$E_c = 33,000 w_c \sqrt{f'_c} = 33,000(0.150)^{1.5} \sqrt{8.2} = 5,490 \text{ ksi, and}$$

$$F_u = 64 \text{ ksi}$$

$$Q_n = 0.5 \times 1.23 \sqrt{8.2 \times 5,490} = 130.5 \text{ kip/stud}$$

$$(1.23 \times 64 = 78.72 \text{ kip/stud}); \text{ therefore}$$

$$Q_n = 78.72 \text{ kip/stud}$$

$$= 78.72 \times 4 = 314.9 \text{ kip/four-stud cluster}$$

$$= 78.72 \times 8 = 629.8 \text{ kip/eight-stud cluster}$$

Therefore, if Beam 1 were to fail in horizontal shear at the interface, this would require failure of the four shear pockets between the concentrated load and the exterior support, as

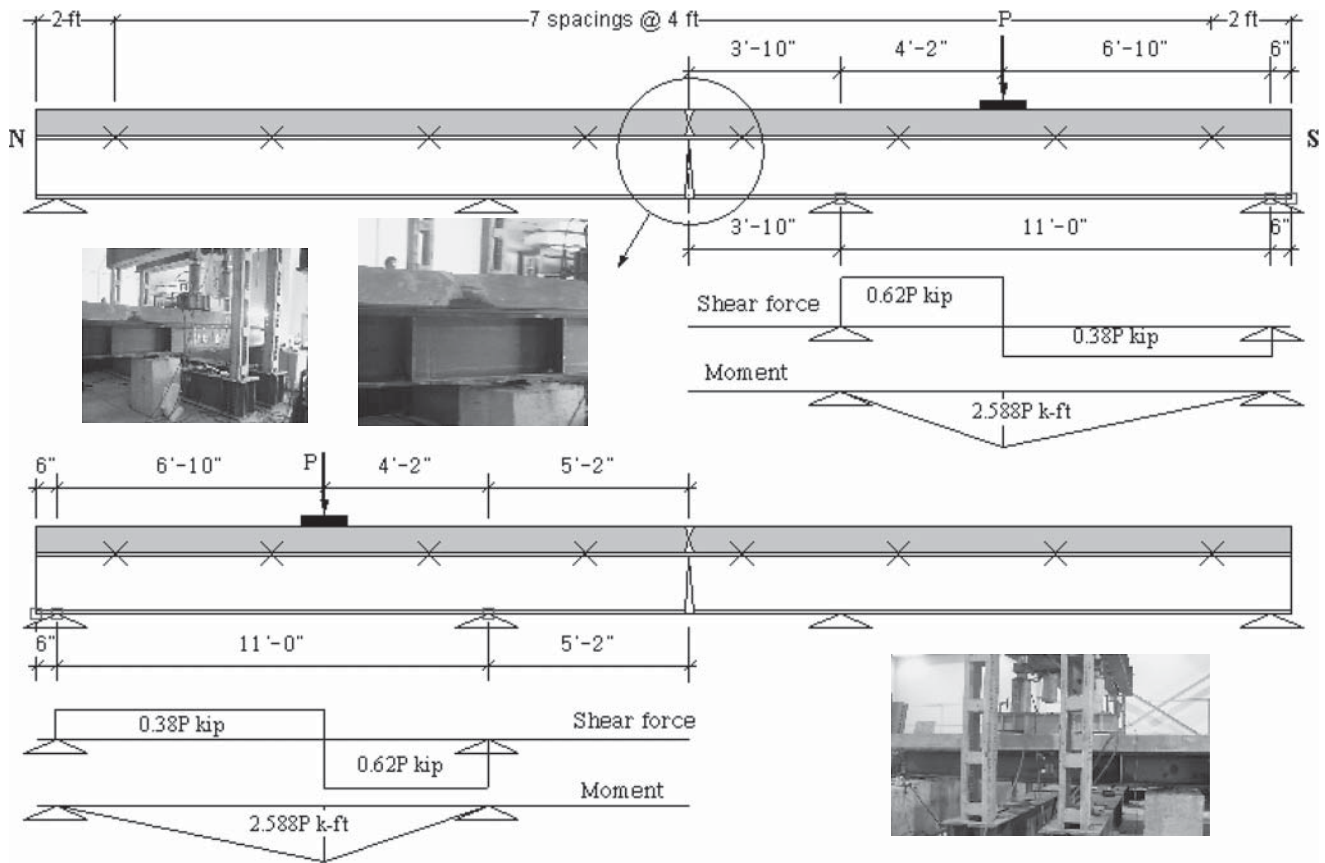


Figure 93. Ultimate test arrangement of Beam 2.

shown in Figure 92, and a horizontal shear force at the interface = $314.9 \times 4 = 1,259.6$ kip over this distance.

The height of the plastic neutral axis that is equivalent to this force

$$= \frac{1,259.6}{0.85 \times 8.2 \times 48} = 3.77 \text{ in.}$$

The corresponding plastic moment = $(1,259.6)(8 + 1 + 0.5 \times 19 - 0.5 \times 3.77) = 20,928$ kip-in. = 1,744 kip-ft.

The corresponding concentrated load = $1,744/3.799 = 459$ kip

Applying the same procedure for Beam 2, the concentrated load that would be required to cause horizontal shear failure at the stud cluster between the concentrated load and the interior support = 356.1 kip.

According to this analysis, it was expected that the four simply supported beams would fail in horizontal shear. Each simply supported beam was provided with one set of strain gauges and a deflection measurement device at the location of the applied concentrated load. The relative horizontal displacement between the slab and the steel beam was also recorded at the free end of each beam. The load was applied at 10 kip (44.5 kN) per second until failure occurred or until the hydraulic jacks' capacity of 600 kip (2669 kN) was reached, whichever came first.

Test Results

Beam 1-North and Beam 1-South failed in flexure where the top fiber of the concrete slab was crushed in compression, as shown in Figure 95. The applied load at failure was about 600 kip (2669 kN), which was equal to the maximum capacity of the hydraulic jacks combined. The flexural failure on Beam 1-North was accompanied with web buckling failure of the steel beam.

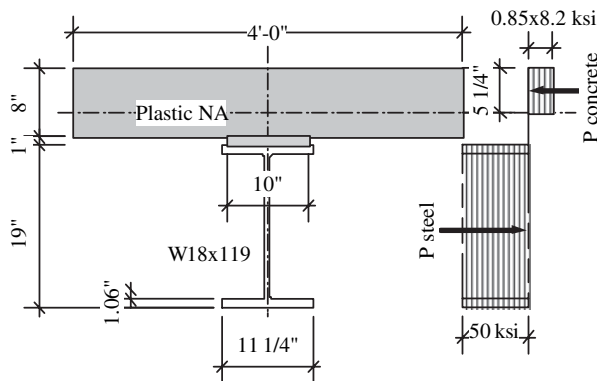
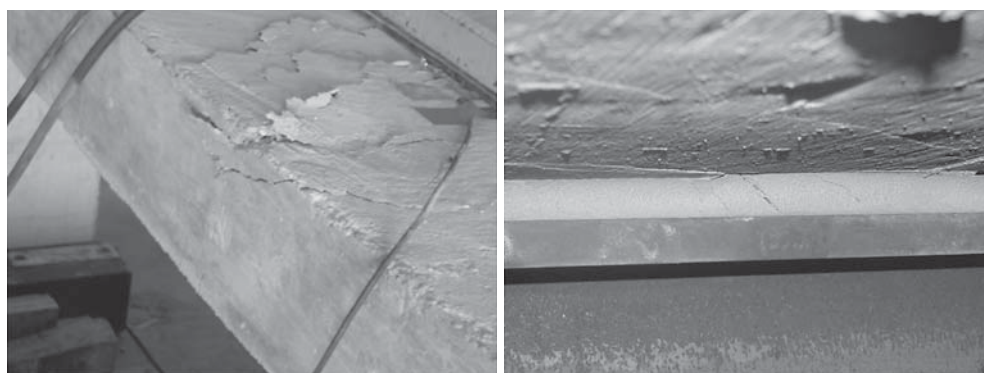


Figure 94. Stress distribution at plastic stage.



(a) Beam #1-North



(b) Beam #1-South



(c) Beam #2-North



(d) Beam #2-South

Figure 95. Failure modes of the full-scale beams.

Beam 2-North and Beam 2-South did not show any signs of failure in horizontal shear or flexure. Each beam was loaded up to the maximum combined capacity of the hydraulic jacks—namely, 600 kip (2669 kN).

Inspection of the top surface of the concrete slab showed that a longitudinal bursting hair crack was formed exactly over the web location of the steel beam, as shown in Figure 96. The crack covered almost the full length of Beam 1, which was made with 24 in. (610 mm) cluster spacing, while in Beam 2, which was made with 48 in. (1220 mm) cluster spacing, the crack covered only the midspan area of the north and south beams. The width of the crack of Beam 1 and Beam 2 was about 0.04 in. (1 mm) and 0.03 in. ($\frac{3}{4}$ mm), respectively. Due to the small width of these cracks, they were not detected

until the beams were removed from the supports and set on the ground. However, it is believed that these cracks started to form when the applied moment was about 70% of the plastic flexural capacity of the composite section, when a loud explosion was heard during testing of Beam 1-North and Beam 1-South.

Table 11 summarizes the failure mode and the maximum applied load.

Figures 97 and 98 show the load-deflection and load-horizontal slip relationships of the full-scale beams. To help in studying the structural behavior of the four beams, the load was replaced by the corresponding applied moment as a percentage of the plastic moment capacity of the composite section.

Figures 99 and 100 show the strain distribution of the full-scale Beam 1 and Beam 2, respectively, at various levels of applied load.

An analysis of these figures allowed the following conclusions to be drawn.

Appropriateness of Using the LRFD Specifications for Estimating the Horizontal Shear Capacity of Stud Clusters.

Regardless of the stud cluster spacing and the type of confinement, all beams were able to develop the stud ultimate capacity given by Equation 6.10.10.4.3-1 of the LRFD specifications (7).

The procedure in Article 6.10.7 of the AASHTO LRFD specifications gives a fair estimate of the ultimate flexural capacity of composite sections.

Deflection and Horizontal Slip (Figures 97 and 98). The slope of the load-deflection relationship, which is a measure of the composite beam stiffness, is almost the same for the four beams. This means that extending the stud cluster spacing to 48 in. (1220 mm) does not reduce the composite beam stiffness.

The beams where the stud clusters were confined with HSS tubes showed smaller deflection than the beams where the stud clusters were confined with closed ties. The difference is about 10%.

The beams made with 48 in. (1220 mm) cluster spacing showed about a 25% increase in deflection and horizontal slip compared with the beams made with 24 in. (610 mm) cluster spacing. The research team believes that this increase was due to the flexural fatigue failure at midspan that occurred during the fatigue test. This can be confirmed from Figure 97, where Beams 2-North and 2-South showed about 0.1 in. (2.54 mm) of deflection once a small amount of load was applied. Also, Figure 98 shows that these beams did not show any horizontal slip for the first period of applying the load (from zero to about 10%).

Stress Distribution (Figures 99 and 100). At the same ratio of applied moment-to-plastic flexural capacity, Beams 1 and 2 showed almost the same amount of stresses produced in the concrete slab and steel beam.

Beams made with HSS tube confinement showed almost the same amount of stresses as beams made with the closed-ties confinement.

Transverse Slab Reinforcement Required To Resist the Transverse Bursting Force. The horizontal shear force at the interface is transferred from the steel beam to the concrete slab by direct bearing of the grout volume on the precast panel. This mechanism is similar to the mechanism of transferring the bearing force of a posttensioned tendon to the end zone of a posttensioned concrete member. According to Article 5.10.9.3.6 of the LRFD specifications (7), the transverse bursting force is estimated using the following formula:

$$T_s = 0.2P_u \left(1 - \frac{a}{s}\right) \quad (20)$$

where

T_s = the bursting force,

P_u = the factored tendon load on an individual anchor (ultimate horizontal shear force generated by a cluster of studs),

a = the anchor plate width (width of the shear pocket), and

s = the anchorage spacing (stud cluster spacing).

For Beam 1 (2 ft spacing, four studs per cluster):

$$P_u = 478.7 = 314.8 \text{ kip}, a = 12 \text{ in.}, s = 24 \text{ in.}$$

$$T_s = 0.2 \times 314.8 \left(1 - \frac{12}{24}\right) = 0.2 \times 314.8 \times 0.5 = 31.48 \text{ kip/2ft} = 15.74 \text{ kip/ft}$$

Required conventional reinforcement:

$$A_s = \frac{T_s}{f_y} = \frac{15.74 \text{ kips}}{60 \text{ ksi}} = 0.26 \text{ in}^2/\text{ft}/2 \text{ layers}$$

For Beam 2 (4 ft spacing, eight studs per cluster):

$$P_u = 8 \times 78.7 = 629.6 \text{ kip}, a = 12 \text{ in.}, s = 48 \text{ in.}$$

$$T_s = 0.2 \times 629.6 \left(1 - \frac{12}{48}\right) = 0.2 \times 629.6 \times 0.75 = 94.44 \text{ kip/4ft} = 23.61 \text{ kip/ft}$$

Required conventional reinforcement:

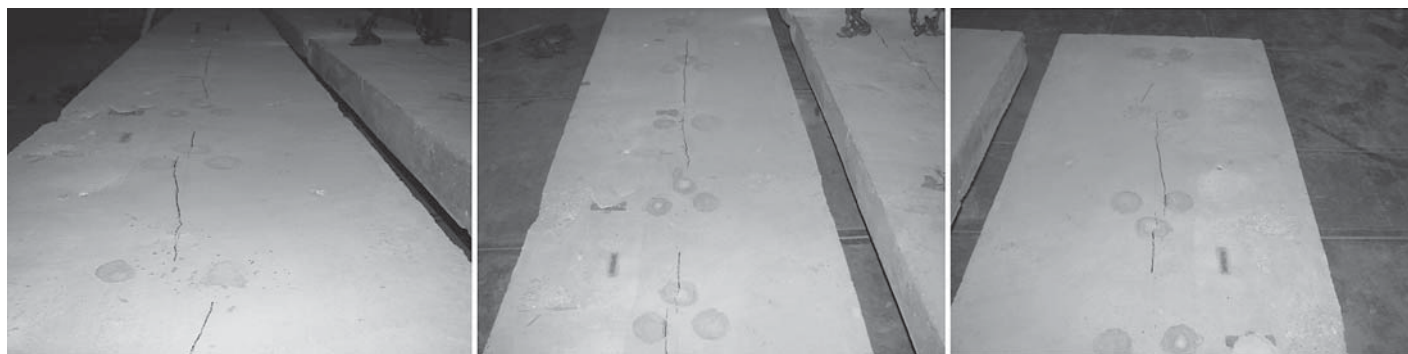
$$A_s = \frac{T_s}{f_y} = \frac{23.61 \text{ kips}}{60 \text{ ksi}} = 0.39 \text{ in}^2/\text{ft}/2 \text{ layers}$$

The required conventional reinforcement to resist the bursting force for Beam 1 or Beam 2 is smaller than the required reinforcement determined according to the empirical design method given in Article 9.7.2 of the LRFD specifications (7), which is $0.18 + 0.27 = 0.45 \text{ in}^2/\text{ft}/2 \text{ layers}$.

Removal of the Precast Panels of the Full-Scale Beams

The precast panels were removed by jackhammering the concrete around the shear pockets. The grout around the studs was then removed using a manual drill. Several observations on the condition of the shear studs and the grout surrounding them were made (see Figure 101).

- No air pockets were detected in the shear pockets or in the haunch.
- No grout crushing was detected at the base of the studs. Also, the grout was fully bonded to the studs.
- The studs were almost vertical. The maximum slope that was observed was about 5 degrees.
- No cracks were detected at the weld at the base of the studs.



Beam #1 (2-ft stud cluster spacing)



Beam #2 (4-ft stud cluster spacing)

Figure 96. Bursting longitudinal cracks on top surface of the slab.**Table 11. Summary of the full-scale beam ultimate test results.**

Beam	Stud Cluster Spacing (ft)	Confinement Type	Failure Mode	Maximum Applied Load (kip)	Load Required to Cause Flexural Failure (kip)	Load Required to Cause Horizontal Shear Failure (kip)
1-North	2	Ties	Flexural failure/ web buckling, Figure 95-a: Concrete crushing of the top fiber of the concrete slab at the concentrated load location. Also, a vertical crack formed at side surface of the slab at the section of the applied load. Four inclined cracks in the haunch at 45 degrees. One crack at each stud cluster located between the applied load and the exterior support. The web of the steel beam buckled at the exterior support.	588	574	459
1-South	2	Tube	Flexural failure, Figure 95-b: Concrete crushing of the top fiber of the concrete slab at the concentrated load location. Four inclined cracks in the haunch at 45 degrees. One crack at each stud cluster located between the applied load and the exterior support.	600	574	459
2-North	4	Ties	No failure occurred, Figure 95-c: The hydraulic jacks reached their maximum capacity.	600	843	356
2-South	4	Tube	No failure occurred, Figure 95-d: The hydraulic jacks reached their maximum capacity.	600	843	356

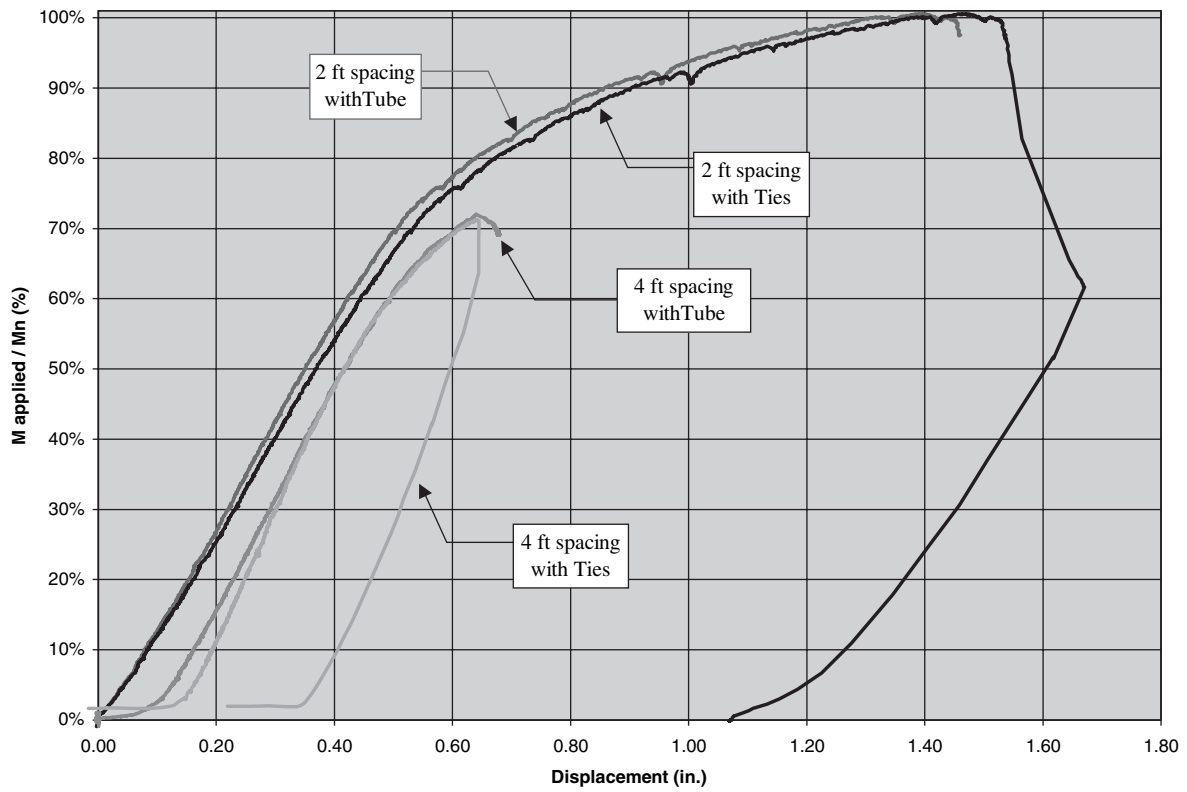


Figure 97. Load-deflection relationship of the full-scale beams.

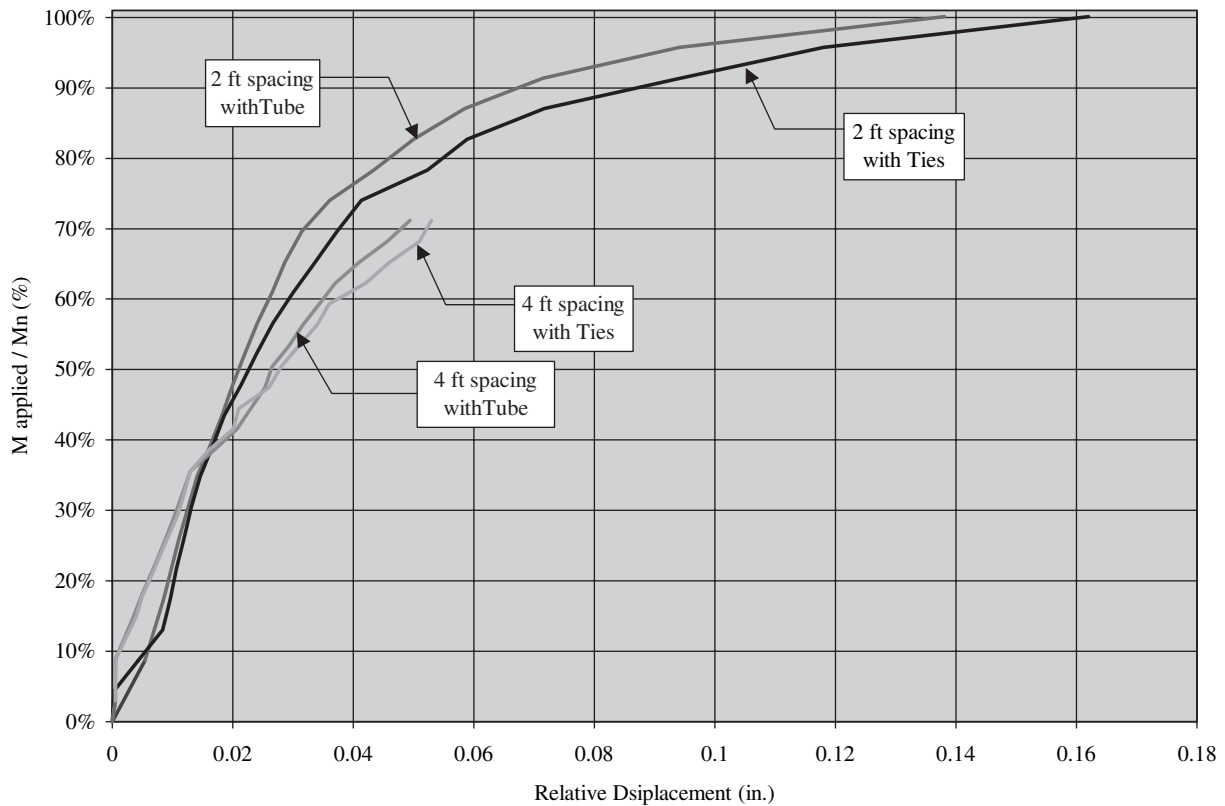


Figure 98. Load-horizontal slip relationship of the full-scale beams.

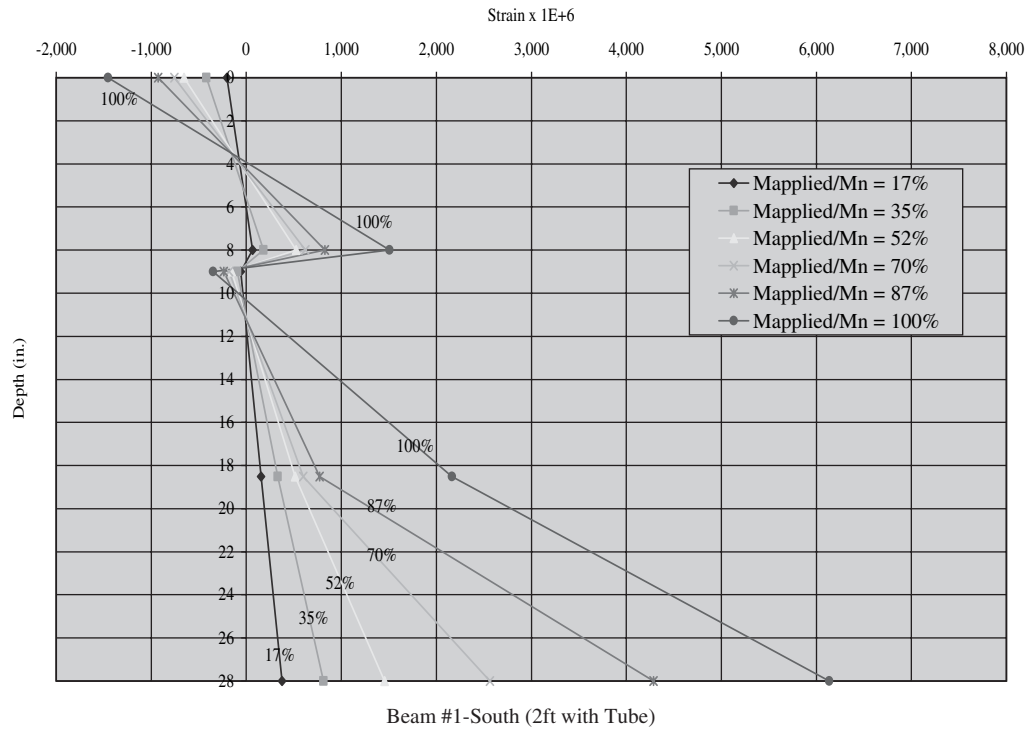
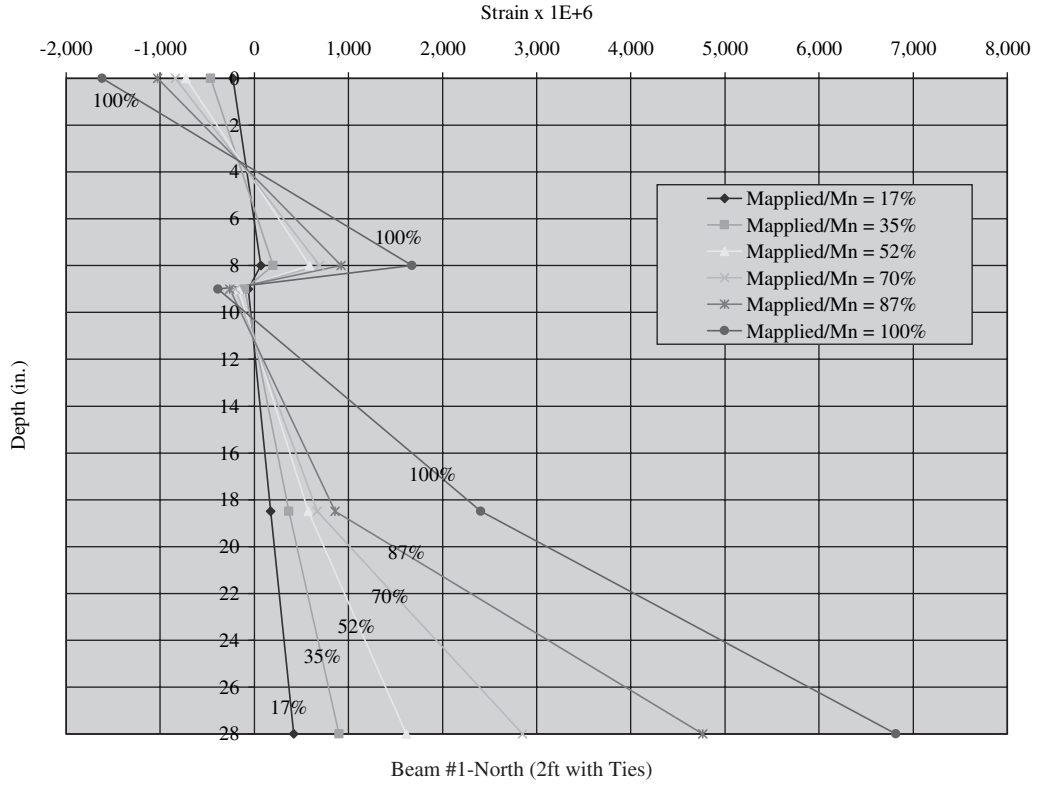


Figure 99. Strain distribution of the full-scale Beam 1.

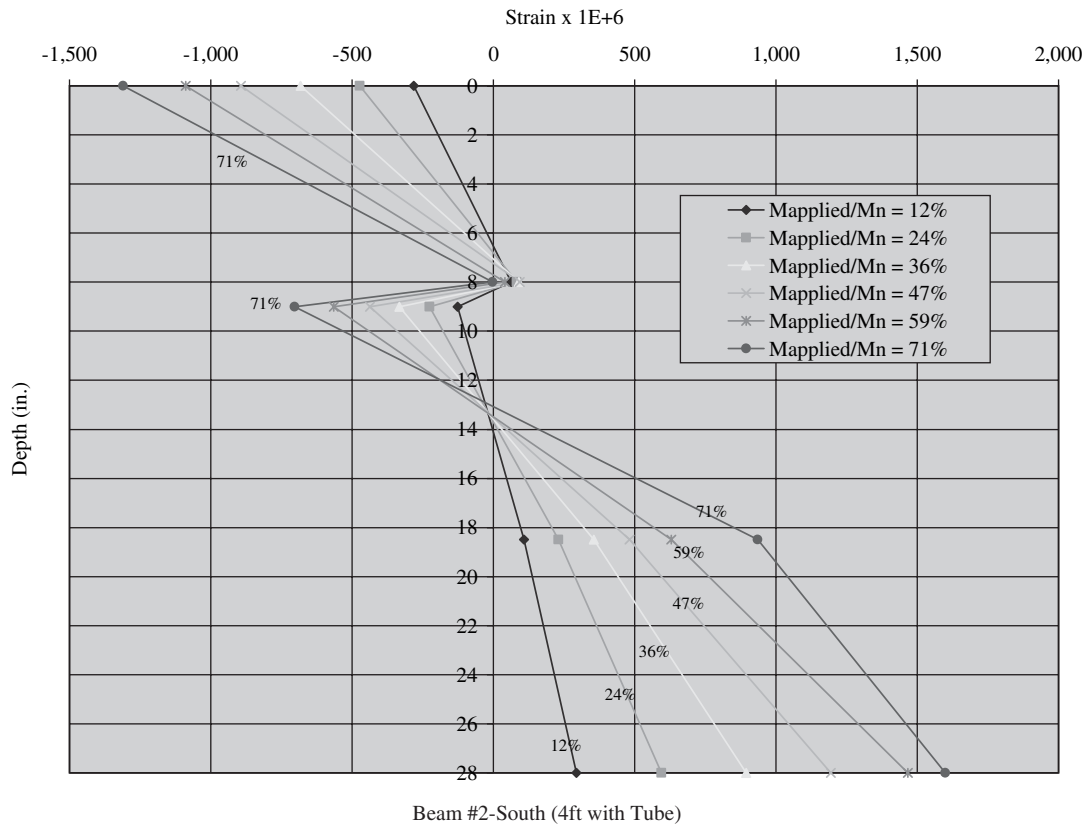
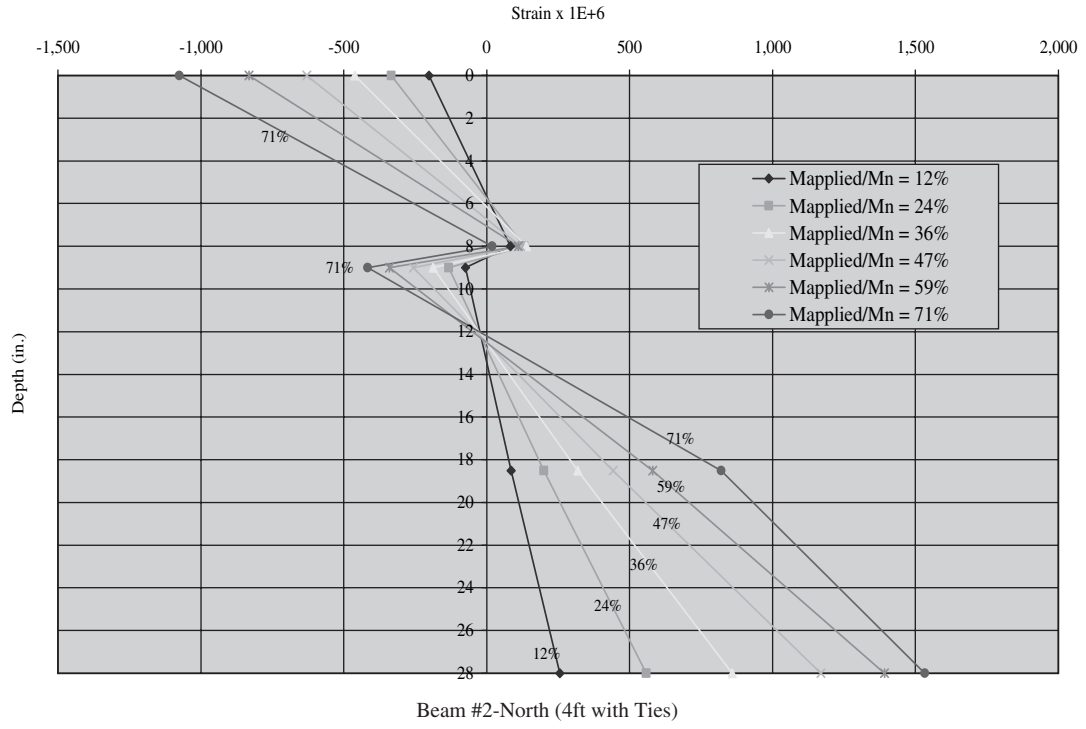


Figure 100. Strain distribution of the full-scale Beam 2.

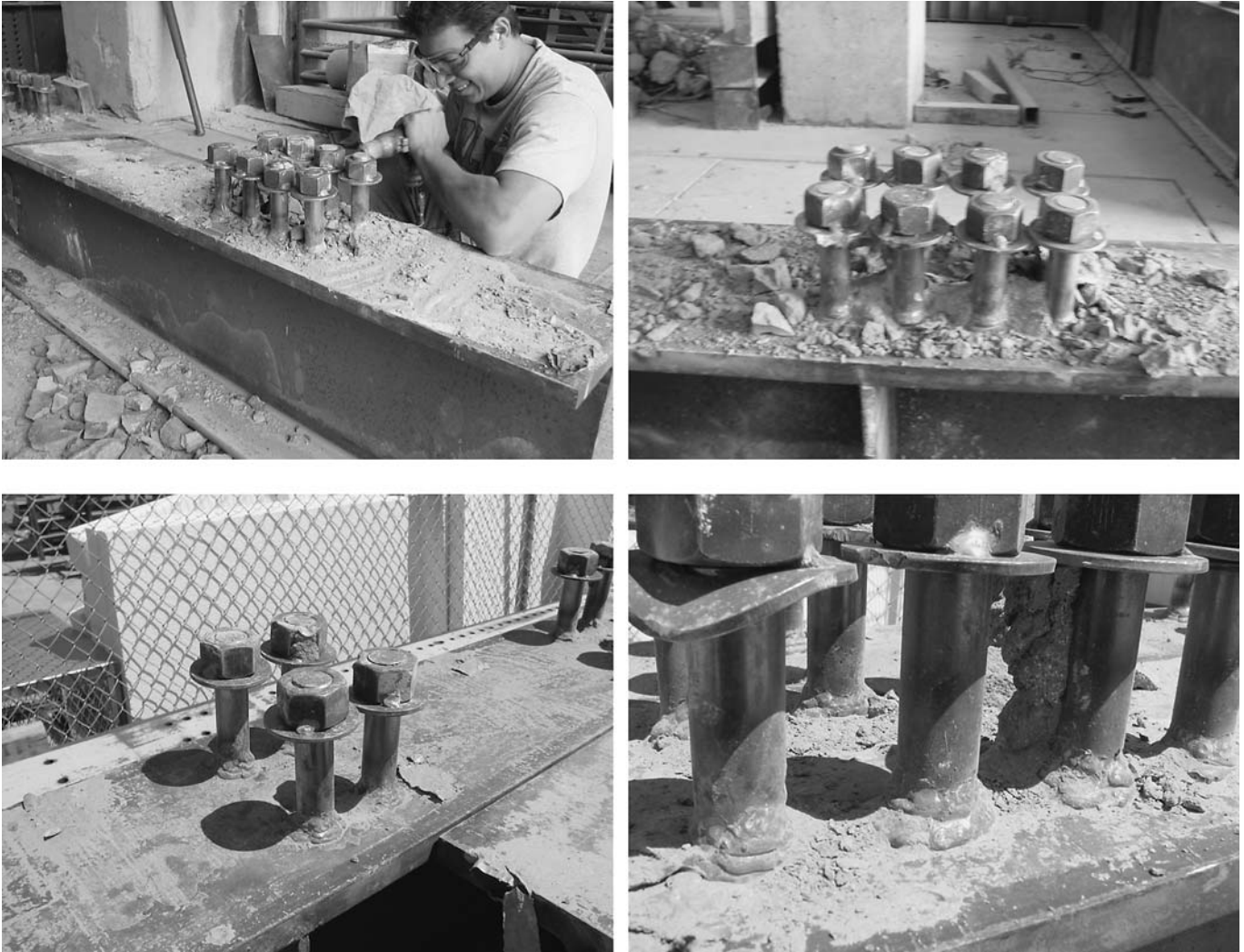


Figure 101. Shear studs after deck panel removal.

Guidelines for Design, Detailing, Fabrication, and Installation of Full-Depth, Precast Concrete Deck Panel Systems

Guidelines for the design, detailing, fabrication, and installation of full-depth precast concrete deck panel systems are given in Appendix C. The guidelines do not cover proprietary full-depth precast concrete bridge deck panel systems. Individual deck construction projects may have their own unique features and constraints, which may affect the design, fabrication, and construction process. The reader should

therefore evaluate the relevance of the provisions in accordance with the project requirements.

Proposed Revisions to AASHTO LRFD Specifications

Proposed revisions to Section 9 of the *AASHTO LRFD Bridge Design Specifications* (7) are given in Appendix D. The objective of the proposed revisions is to inform designers of the requirements pertaining to use of full-depth precast deck panel systems and thus promote use of these relatively new systems.

CHAPTER 4

Conclusions, Recommendations, and Suggested Future Research

Conclusions and Recommendations

Panel To Panel Connection Details Using Conventional Reinforcement

- Full-depth precast concrete panels can be effectively connected with conventional reinforcing bars.
- Bar splice length can be significantly reduced through use of HSS tubes, which effectively confine the grout surrounding the bars. In this research, two panel-to-panel connection details were successfully developed utilizing a 4 in. (102 mm) long cut of an HSS $4 \times 12 \times \frac{3}{8}$ in. ($102 \times 305 \times 10$ mm) tube, as follows:
 - The first connection detail requires threading a No. 6 (19) reinforcing bar, which extends about $7\frac{1}{2}$ in. (190 mm) outside the panel to be installed, into the old panel; this results in a 6 in. (152 mm) bar embedment length. The testing program has shown that this embedment distance is sufficient to develop the bar yield strength. However, accomplishing this connection requires that the panel to be installed be tilted during installation.
 - The second connection detail allows vertical installation of the new panels, where a No. 6 (19) bar is embedded 11 in. (280 mm) in the HSS tube, in each of the mating joints. After a new panel is installed, a 24 in. (610 mm) No. 6 (19) long splice bar is dropped through a vertical slot, which results in an 11 in. (280 mm) splice length. The testing program has shown that this splice length is adequate to develop the bar yield strength.
- The research provided a mathematical model to estimate the required development length of bars confined with an HSS tube. The model uses the development length formula currently used by the AASHTO LRFD specifications, modified for the type of confinement used in this research.
- The research provided a procedure to calculate the shear capacity of the reinforced joint and check it against the

LRFD specifications requirements. The procedure is based on the shear friction theory already covered in the LRFD specifications.

Panel to Concrete Girder Connection Detail

A new connection detail was developed, where clusters of three double-headed $1\frac{1}{4}$ in. (31.8 mm) studs are used. The clusters are spaced at 48 in. (1220 mm). This connection detail opens the way for using full-depth precast deck panels for concrete girders. Additional reinforcement was found to be necessary in the web to help reach the capacity of the studs and distribute the concentrated stud stresses into the beam. Article 5.8.4.1 of the AASHTO LRFD specifications can be used to determine the horizontal shear capacity of the new detail. A group of three $1\frac{1}{4}$ in. (31.8 mm) studs clustered at 48 in. (1220 mm) was found sufficient for bridges with spans up to 130 ft (39.6 m), with girder spacing up to 11 ft (3.35 m), and designed in accordance with the LRFD specifications.

Panel to Steel Girder Connection Detail

A new connection detail was developed, where clusters of eight $1\frac{1}{4}$ in. (31.8 mm) studs at 48 in. (1220 mm) spacing were used. HSS tubes or individual closed ties were shown to be effective in confining the grout surrounding the studs. Experimental and analytical investigation of the new connection detail found the following:

- The confinement provided by the HSS tubes or the closed ties was effective in distributing the shear force among the studs in each cluster and in protecting the grout at the base of each stud against crushing. If closed ties are used, the lowest tie should be placed as close to the top surface of the girder as possible.
- Equation 6.10.10.2-1 of the LRFD specifications, which is currently used to estimate fatigue capacity, does not require

modification for design of stud clusters at 4 ft (1220 mm) spacing.

- Equation 5.8.4.1-1 of the LRFD specifications may be used to estimate the ultimate capacity of stud clusters at 4 ft (1220 mm) spacing. Equation 6.10.10.4.3-1 should not be used for stud clusters at 2 ft (1220 mm) or greater spacing. This recommendation is expected to result in about a 30% increase in the required number of studs.
- The recommendation immediately above is based on the results of push-off testing of stud groups at 4 ft (1220 mm) spacing, which gave about 30% lower capacity than the current LRFD equation for single studs. The conclusion may be unnecessarily conservative as the authors do not believe that the push-off testing is as realistic in modeling beam behavior as is the actual beam test, which showed no reduction in capacity due to use of stud clusters. However, the authors believe that it is a conservative approach and it does not significantly affect the overall economy of bridges.

Recommended Guidelines for Full-Depth Precast Concrete Bridge Deck Panel Systems

Recommended guidelines for design, detailing, fabrication, and construction of full-depth precast concrete bridge deck panel systems were developed. The guidelines cover nonproprietary full-depth precast concrete bridge deck panel systems. Individual deck construction projects may have their own unique features and constraints, which may affect the design, fabrication, and construction process. The reader should therefore evaluate the relevance of the provisions in accordance with the project requirements.

Proposed Revisions to AASHTO LRFD Specifications

Proposed revisions to Section 9 of the AASHTO LRFD specifications were developed to help provide minimum design requirements. The revisions reflect the findings from the literature review, the national survey, and the experimental and analytical investigation conducted in this research. Explicitly covering precast full-depth panel systems in the LRFD specifications should help promote more extensive application of these relatively new systems.

Suggestions for Future Research

The recommendation to use Equation 5.8.4.1-1 of the AASHTO LRFD specifications, instead of Equation 6.10.10.4.3-1, to estimate the ultimate capacity of stud clusters at 4 ft (1220 mm) spacing is based on push-off specimen testing and may result in using as much as 30% more studs than in conventional single-stud applications. This recommendation may, however, be too conservative as full-scale composite beam testing revealed no reduction in fatigue or strength capacity as determined by current LRFD specifications for single-stud design. The authors believe that the push-off specimens are not as accurate as beams in modeling interface shear behavior in beams. The loading arrangement and the limited specimen size provide neither the true shear/flexure interaction nor the redundancy that exists in the more expensive beam testing. Therefore, the authors recommend additional full-scale beam testing if a less conservative approach than that recommended here is desired.

The authors recommend a follow-up study of an actual demonstration bridge project be used to implement the results of this research and to observe interaction of the various system components under actual field conditions.

References

1. Yamane, T., M. K. Tadros, S. S. Badie, and M. C. Baishya. Full-Depth Precast Prestressed Concrete Bridge Deck System. *PCI Journal*, Vol. 43, No. 3, May-June 1998, pp. 50–66.
2. Tadros, M. K., and M. C. Baishya. *NCHRP Report 407: Rapid Replacement of Bridge Decks*. TRB, National Research Council, Washington, D.C., 1998.
3. Badie, S. S., M. C. Baishya, and M. K. Tadros. NUDECK—An Efficient and Economical Precast Bridge Deck System. *PCI Journal*, Vol. 43, No. 5, Sept.-Oct. 1998, pp. 56–74.
4. Bassi, K. G., S. S. Badie, M. C. Baishya, and M. K. Tadros. Discussion: NUDECK—An Efficient and Economical Precast Bridge Deck System. *PCI Journal*, Vol. 44, No. 2, March-April 1999, pp. 94–95.
5. Badie, S. S., M. C. Baishya, and M. K. Tadros. Innovative Bridge Panel System A Success. *Concrete International*, Vol. 21, No. 6, June 1999, pp. 51–54.
6. Fallaha, S., C. Sun, M. D. Lafferty, and M. K. Tadros. High Performance Precast Concrete NUDECK Panel System for Nebraska's Skyline Bridge. *PCI Journal*, Vol. 49, No. 5, Sept.-Oct. 2004, pp. 40–50.
7. *AASHTO LRFD Bridge Design Specifications*, 3rd ed. American Association of State Highway and Transportation Officials, Washington, D.C., 2004, with 2005 and 2006 interim revisions.
8. *AASHTO LRFD Bridge Construction Specifications*, 2nd ed. American Association of State Highway and Transportation Officials, Washington, D.C., 2004, with 2006 interim revisions.
9. Anderson, A. R. *Special Report 132: Systems Concepts for Precast and Prestressed Concrete Bridge Construction*. HRB, National Research Council, Washington, D.C., 1972, pp. 9–21.
10. Biswas, M. Precast Bridge Deck Design Systems. *PCI Journal*, Vol. 21, No. 2, March-April 1986, pp. 40–94.
11. Babaei, K., A. Fouladgar, and R. Nicholson. Nighttime Bridge Deck Replacement with Full Depth Precast Concrete Panels at Route 7 Over Route 50, Fairfax County, Virginia. Presented at Transportation Research Board 80th Annual Meeting, Washington, D.C., 2001.
12. Culmo, M. P. Bridge Deck Rehabilitation Using Precast Concrete Slabs. Presented at 8th Annual International Bridge Conference, Pittsburgh, Penn., 1991.
13. Donnaruma, R. C. *A Review of the Development of System for Precast Deck Replacement for Composite I-Beam Bridges*. Report to the Research Committee. International Bridge, Tunnel & Turnpike Association, Chicago, Ill., Aug. 1974.
14. Donnaruma, R. C. Performance of Precast Concrete Bridge Deck Panels on the New York Thruway. Presented at Transportation Research Board 62nd Annual Meeting, Washington, D.C., 1983.
15. Farago, B., A. C. Agarwal, J. Brown, and K. G. Bassi. *Precast Concrete Deck Panels for Girder Bridges*. Special Report, Ministry of Transportation, Ontario, Canada, 1992.
16. Issa, M., A., et al. State-of-the-Art Report: Full Depth Precast and Precast, Prestressed Concrete Bridge Deck Panels. *PCI Journal*, Vol. 40, No. 1, Jan.-Feb. 1995, pp. 59–80.
17. Kropp, P. K., E. L. Milinski, M. J. Gulzwiller, and R. B. Lee. *Use of Precast Prestressed Concrete For Bridge Decks*. Joint highway research project conducted by Engineering Experiment Station, Purdue University, in cooperation with the Indiana State Highway Commission and the Federal Highway Administration. Final Report, July 1975, revised Dec. 1976.
18. Lutz, J. G., and D. J. Scalia. Deck Widening and Replacement of Woodrow Wilson Memorial Bridge. *PCI Journal*, Vol. 29, No. 3, May-June 1984, pp. 74–93.
19. Salvis, C. Precast Concrete Deck Modules for Bridge Deck Reconstruction. In *Transportation Research Record 871*, TRB, Washington, D.C., 1982, pp. 30–33.
20. Togashi, M., T. Ota, Y. Hiyama, T. Furumura, and T. Konishi. Application of Precast Slab and Sidewall to Construction of Bridge. *Journal of Prestressed Concrete, Japan Prestressed Concrete Engineering Association*, Vol. 35, No. 1, Jan.-Feb. 1993, pp. 22–32.
21. Nottingham, D. Joint Grouting in Alaska Bridges and Dock Decks. *Concrete International*, Vol. 18, No. 2, Feb. 1996, pp. 45–48.
22. Gulyas, R. J. Precast Bridge Decks: Keyway Grouting Data. *Concrete International*, Vol. 18, No. 8, Aug. 1996.
23. Issa, M., A., et al. Performance of Transverse Joint Grout Materials in Full-Depth Precast Concrete Bridge Deck Systems. *PCI Journal*, Vol. 48, No. 4, July-Aug. 2003, pp. 92–103.
24. Sprinkel, M. M. *Evaluation of Latex-Modified and Silica Fume Concrete Overlays Placed on Six Bridges in Virginia*. Report No. 01-R3. Virginia Transportation Research Council, Charlottesville, Va., Aug. 2000.
25. Sprinkel, M. M. High Performance Concrete Overlays for Bridges. Presented at Concrete Bridge Conference/PCI Annual Convention, Orlando, Fl., 2003.
26. Menkulasi, F., and C. L. Roberts-Wollmann. Behavior of Horizontal Shear Connectors for Full-Depth Precast Concrete Bridge Decks on Prestressed I-Girders. *PCI Journal*, Vol. 50, No. 3, May-June 2005, pp. 60–73.
27. *Standard Specifications for Highway Bridges*, 17th ed. American Association of State Highway and Transportation Officials, Washington, D.C., 2002.
28. Newmark, N. M., and C. P. Siess. Design of Slab and Stringer Highway Bridges. *Public Roads*, Vol. 23, No. 1, 1943.

29. Viest, I. M., and C. P. Siess. Composite Construction for I-Beam Bridges. In *Highway Research Board Proceedings*, Vol. 32, 1953.
 30. Viest, I. M., and C. P. Siess. Design of Channel Shear Connectors for Composite I-Beam Bridges. *Public Roads*, Vol. 28, No. 1, 1954.
 31. Issa, M. A., T. A. Patton, H. A. Abdalla, A. A. Youssif, and M. A. Issa. Composite Behavior of Shear Connections in Full-Depth Precast Concrete Bridge Deck Panels on Steel Stringers. *PCI Journal*, Vol. 48, No. 5, Sept.-Oct. 2003, pp. 76–89.
 32. Markowski, S. M., F. G. Ehmke, M. G. Oliva, J. W. Carter III, L. C. Bank, J. S. Russell, S. Woods, and R. Becker. Full-Depth, Precast, Prestressed Bridge Deck Panel System for Bridge Construction in Wisconsin. In *Proceedings of the PCI/National Bridge Conference*, Palm Springs, Calif., 2005.
 33. *Recording and Coding Guide for the Structure Inventory and Appraisal of the Nation's Bridges*. Report No. FHWA-PD-96-001. Federal Highway Administration, Washington D.C., 1995.
 34. Badie, S. S., M. K. Tadros, H. F. Kakish, D. L. Splittgerber, and M. C. Baishya. Large Studs for Composite Action in Steel Bridge Girders. *Journal of Bridge Engineering*, Vol. 7, No. 3, May-June 2002, pp. 195–203.
 35. *Bridge Design Manual*, 2nd ed. Precast/Prestressed Concrete Institute, Chicago, Ill., 2003.
 36. Tadros, M. K., S. S. Badie, and M.R. Kamel. A New Connection Method for Rapid Removal of Bridge Decks. *PCI Journal*, Vol. 47, No. 3, May-June 2002, pp. 2–12.
 37. *Standard Practice for Laboratory Testing of Bridge Decks*. ASTM D6275-2003, ASTM International, West Conshohocken, Pa., 2003.
 38. Saatcioglu, M., et al. Displacement-Based Design of Reinforcement Concrete Columns for Confinement. *ACI Structural Journal*, Jan.-Feb., 2002.
 39. Sun, C., A. Girgis, M. K. Tadros, and S. S. Badie. Structural Behavior of Flexural Member with High Strength Concrete. In *Proceedings of PCI/National Bridge Conference*, Atlanta, Ga., 2004.
 40. *Building Code Requirements for Structural Concrete and Commentary*. ACI 318-05, American Concrete Institute, Farmington Hills, Mich., 2005.
 41. Fallaha, S., C. Sun, M. D. Lafferty, and M. K. Tadros. High Performance Precast Concrete NUDECK Panel System for Nebraska's Skyline Bridge. *PCI Journal*, Vol. 49, No. 5, Sept.-Oct. 2004, pp. 40–50.
 42. Badie, S. S., A. Girgis, N. Nguyen, and M. K. Tadros. Development and Application of Large-Size Shear Studs to Steel Girder Bridges. *Engineering Journal*, Vol. 44, No. 2, 2007, pp. 79–90.
 43. Oehlers, D. J., and M. A. Bradford. *Elementary Behavior of Composite Steel and Concrete Structural Members*. Elsevier Science, United Kingdom, 2000.
 44. Oehlers, D. J., and M. A. Bradford. *Composite Steel and Concrete Structural Members, Fundamental Behavior*, 2nd ed. Elsevier Science, United Kingdom, 2004.
 45. Ollgaard, J. G., R. G. Slutter, and J. W. Fisher. Shear Strength of Stud Connectors in Lightweight and Normal Density Concrete. *Engineering Journal*, Vol. 8, 1971, pp. 55–64.
 46. Viest, I. M. Investigation of Stud Shear Connectors for Composite Concrete and Steel T-Beams. *American Concrete Institute Journal Proceedings*, Vol. 52, No. 4, April 1956, pp. 875–891.
 47. Badie, S.S., and M. K. Tadros. *I-Girder/Deck Connection for Efficient Deck Replacement*. Final Report, Project No. PR-PL-1(035)P516. Nebraska Department of Roads, Dec. 2000.
 48. Oehlers, D. J., and R. P. Johnson. The Strength of Stud Shear Connectors in Composite Beams. *The Structural Engineer*, 1987.
-

APPENDICES

The following appendices are not published herein but are available on the TRB website (<http://www.trb.org/TRBNet/ProjectDisplay.asp?ProjectID=354>):

- Appendix A, National Survey and Literature Review
 - Appendix B, Design Calculations of the Proposed System CD-1
 - Appendix C, Design, Detailing, Fabrication, and Installation Guide
 - Appendix D, Proposed AASHTO LRFD Specifications Revisions
 - Appendix E, Specifications of Selected Commercial Grout Material
 - Appendix F, Finite Element Analysis
-

Abbreviations and acronyms used without definitions in TRB publications:

AAAE	American Association of Airport Executives
AASHO	American Association of State Highway Officials
AASHTO	American Association of State Highway and Transportation Officials
ACI-NA	Airports Council International-North America
ACRP	Airport Cooperative Research Program
ADA	Americans with Disabilities Act
APTA	American Public Transportation Association
ASCE	American Society of Civil Engineers
ASME	American Society of Mechanical Engineers
ASTM	American Society for Testing and Materials
ATA	Air Transport Association
ATA	American Trucking Associations
CTAA	Community Transportation Association of America
CTBSSP	Commercial Truck and Bus Safety Synthesis Program
DHS	Department of Homeland Security
DOE	Department of Energy
EPA	Environmental Protection Agency
FAA	Federal Aviation Administration
FHWA	Federal Highway Administration
FMCSA	Federal Motor Carrier Safety Administration
FRA	Federal Railroad Administration
FTA	Federal Transit Administration
IEEE	Institute of Electrical and Electronics Engineers
ISTEA	Intermodal Surface Transportation Efficiency Act of 1991
ITE	Institute of Transportation Engineers
NASA	National Aeronautics and Space Administration
NASAO	National Association of State Aviation Officials
NCFRP	National Cooperative Freight Research Program
NCHRP	National Cooperative Highway Research Program
NHTSA	National Highway Traffic Safety Administration
NTSB	National Transportation Safety Board
SAE	Society of Automotive Engineers
SAFETEA-LU	Safe, Accountable, Flexible, Efficient Transportation Equity Act: A Legacy for Users (2005)
TCRP	Transit Cooperative Research Program
TEA-21	Transportation Equity Act for the 21st Century (1998)
TRB	Transportation Research Board
TSA	Transportation Security Administration
U.S.DOT	United States Department of Transportation